UNIVERSITY OF ILLINOIS
URBANA

AERONOMY REPORT NO. 103

THE TRANSPORT OF NITRIC OXIDE IN THE UPPER ATMOSPHERE BY PLANETARY WAVES AND THE ZONAL MEAN CIRCULATION

by
G. A. Jones
S. K. Avery

May 1, 1982

Library of Congress ISSN 0568-0581

Supported by
National Aeronautics and Space Administration
National Science Foundation

Aeronomy Laboratory
Department of Electrical Engineering
University of Illinois
Urbana, Illinois

UILU-ENG-82-2503

A E R O N O M Y R E P O R T

NO. 103

THE TRANSPORT OF NITRIC OXIDE IN THE UPPER ATMOSPHERE BY PLANETARY WAVES AND THE ZONAL MEAN CIRCULATION

by

G. A. Jones
S. K. Avery

June 1, 1982

Supported by
National Aeronautics and Space Administration
Grants NSG 7506 and NGR 14-005-181
National Science Foundation
Grants ATM 76-01773, ATM 79-09982 and
ATM 81-17440

Aeronomy Laboratory
Department of Electrical Engineering
University of Illinois
Urbana, Illinois

ABSTRACT

A time-dependent numerical model was developed to study the interaction between planetary waves, the zonal mean circulation, and the trace constituent nitric oxide in the region between 55 km and 120 km. The factors which contribute to the structure of the nitric oxide distribution were examined, and the sensitivity of the distribution to changes in planetary wave amplitude was investigated. Wave-induced changes in the mean nitric oxide concentration were examined as a possible mechanism for the observed winter anomaly.

Results obtained with the numerical model indicated that vertically-propagating planetary waves induce a wave-like structure in the nitric oxide distribution. This result was supported by an analysis of observational nitric oxide data. Model results also indicated that at certain levels, transports of nitric oxide by planetary waves could significantly affect the mean nitric oxide distribution. The magnitude and direction of these transports at a given level was found to depend not only on the amplitude of the planetary wave, but also on the loss rate of nitric oxide at that level.

The effects of both traveling waves and amplifying waves on the mean nitric oxide distribution were examined. The wave-induced changes in the mean concentration were significant, but were probably not large enough to result in the large increase of electron density associated with the winter anomaly phenomena.

TABLE OF CONTENTS

Page

LIST OF FIGURES

1. INTRODUCTION

1.1 *General Introduction*

Motions in the earth's upper atmosphere occur on a broad range of scales in both time and space. These motions range from small-scale acoustic fluctuations with time scales of hundredths of seconds and length scales on the order of millimeters, to large planetary scale motions with time scales on the order of weeks and length scales greater than 10^3 km. In general, these motions may be viewed as the motions of a compressible fluid on a rotating, gravitating sphere. However, it is not possible to obtain a general solution which spans this wide range of time and length scales. Instead, the equations of motion are examined in terms of a particular scale of motion, and terms which are unimportant at that scale are neglected.

In this work, planetary scale waves will be considered. Planetary waves are long-term, large-scale oscillations in the earth's atmosphere, which are observable in atmospheric parameters such as temperature, pressure, and wind velocity. These oscillations have periods on the order of days or weeks and wavelengths on the order of the earth's radius. Planetary waves result from the variation of the Coriolis force with latitude, and propagate westward relative to the mean zonal flow with a phase speed determined by the zonal and meridional wave numbers [HOLTON, 1972].

Planetary waves are analyzed by Fourier decomposition of meteorological variables about a latitude circle, and are represented by the first three zonal harmonics. Each wave can be described by a mode number, amplitude and phase, with the phase representing the longitudinal position of the maximum amplitude of the wave. Wave number 0 represents the mean

value about a particular latitude, while wave number 1 has one maximum and one minimum about a latitude circle.

Planetary waves are divided into two groups: stationary and traveling. The stationary waves have periods on the order of months, while traveling waves have periods on the order of days or weeks. Stationary waves are forced primarily by sea-level temperature differentials, as well as by zonal wind flow over topography. Traveling waves are thought to be generated by fluctuations in the mean flow, or by variations in forcing mechanisms. They may also represent resonant modes of the atmosphere.

Stationary planetary waves play a large role in the overall circulation in the stratosphere and mesosphere. VAN LOON et al. [1973] state that for the month of January, at 10 mb and 65°N, planetary waves 1 and 2 accounted for 99.9% of the deviation of temperature and geopotential height from their mean values.

In modeling studies of stationary waves, the background atmosphere through which the wave propagates is called the basic state or the mean state. The basic state is characterized by zonal mean quantities, where the zonal mean is an average value around a latitude circle. In time-independent studies, the zonal mean state is assumed to be constant in time. In the actual atmosphere, an interaction exists between the planetary waves and the zonal mean variables. Wave transports of energy and momentum can cause significant changes in the zonal mean state. In order to study this effect, a time-dependent model which includes the effect of the wave-mean interaction must be used.

There has recently been great interest in the question of the transport of trace chemical constituents in the earth's atmosphere. These transports are carried out mainly by zonal mean and planetary wave winds

in the stratosphere. In the mesosphere, the transport effects of smaller scale motions must also be considered. In particular, the transport of nitric oxide is of interest in connection with the catalytic destruction of ozone in the stratosphere. In the mesosphere, change in the mean nitric oxide concentration due to transport effects has been suggested as a possible mechanism for the winter anomaly [GELLER and SECHRIST, 1971]. This phenomenon, which is characterized by periods of increased radio wave absorption at mesospheric heights, results from an increase in electron density that could be due to an increase in the local nitric oxide concentration. Since planetary waves can have large amplitudes in this region, they may contribute significantly to the changes in mean nitric oxide concentration thought to be responsible for the winter anomaly.

1.2 *Statement of the Problem*

The object of this research is to determine the effects of planetary waves and the zonal mean circulation on the nitric oxide distribution in the 55 to 120 km region. A time-dependent numerical model will be used to calculate planetary wave and zonal mean winds, which will then be used to determine the resulting structure of the nitric oxide distribution. The variations in transports due to time-dependent wave forcings will be investigated, and the effect of the wave-mean interaction on the overall nitric oxide concentration will be determined. Planetary wave-zonal mean transports will also be investigated in connection with the winter anomaly

In the next chapter, a review of the topics to be covered in this work will be presented. A derivation of the wave, mean, and nitric oxide equations is presented in Chapter 3, and a method of solution is outlined. Chapter 4 presents the results of an observational analysis which were used as inputs for the time-independent study of stationary planetary wave

nitric oxide transports presented in Chapter 5. The results obtained using the time-dependent model are presented in Chapter 6, and Chapter 7 contains a summary and suggestions for future work.

2. REVIEW OF LARGE-SCALE ATMOSPHERIC MOTIONS AND NITRIC OXIDE CHEMISTRY

This chapter provides a review of the topics outlined in Chapter 1. Sections 1 and 2 deal with some of the observed and theoretically predicted characteristics of stationary and traveling planetary waves. Sections 3 and 4 discuss the zonal mean circulation and wave-mean interactions in the Eulerian framework, and Section 5 provides a review of the studies of nitric oxide and the winter anomaly. Lastly, Section 6 provides a brief discussion of Lagrangian versus Eulerian viewpoints, and Section 7 provides a summary of the chapter.

2.1 *Stationary Planetary Waves*

Planetary wave structure is obtained by a Fourier decomposition of meteorological data. This data is obtained from various sources. Below 30 km, conventional data obtained from rawinsondes and radiosondes is used [HIROTA and SATO, 1969; VAN LOON et al., 1973]. Above 30 km, various satellite devices such as the pressure modulation radiometer (PMR) [HIROTA and BARNETT, 1977] and the limb radiance inversion radiometer (LRIR) [GILLE et al., 1977] provide global coverage. Rocket experiments also can provide some data on planetary wave structure up to 60 km but the absence of a complete zonal coverage prevents detailed analysis. Correlations between ionospheric and stratospheric data [BROWN and WILLIAMS, 1971] and wave-like behavior in certain ionospheric parameters [CAVALIERI et al., 1974] indicate that planetary waves are present up to at least 120 km.

Figure 2.1a,b shows some typical wintertime planetary wave structures for the northern hemisphere. VAN LOON et al. [1975] performed a Fourier decomposition on geopotential height data covering the seven years from 1964 to 1970. Shown in Figure 2.1 are the first two zonal harmonics which resulted from that decomposition. Wave number 1 maximizes near 45-50° N

(a)

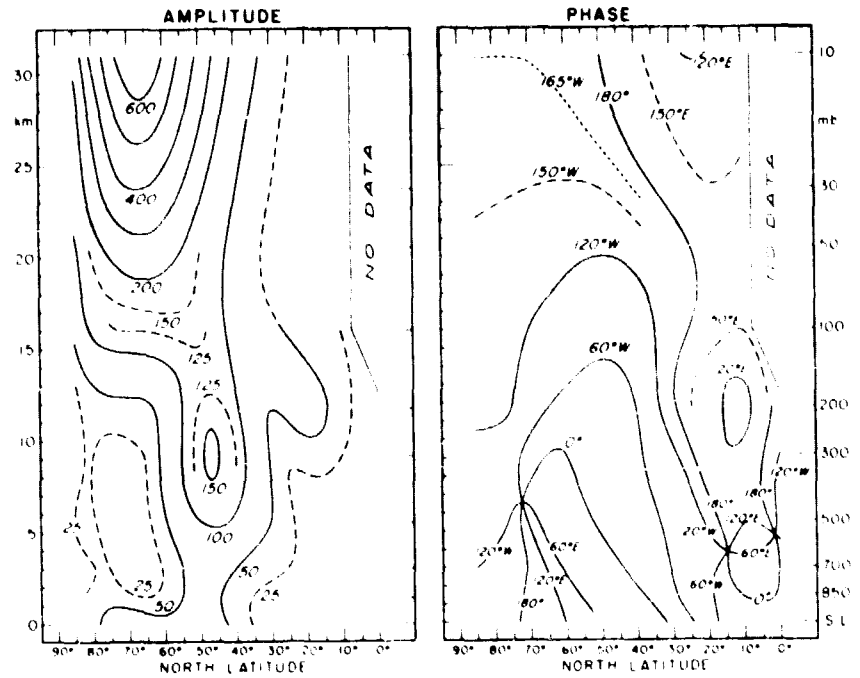

(b)

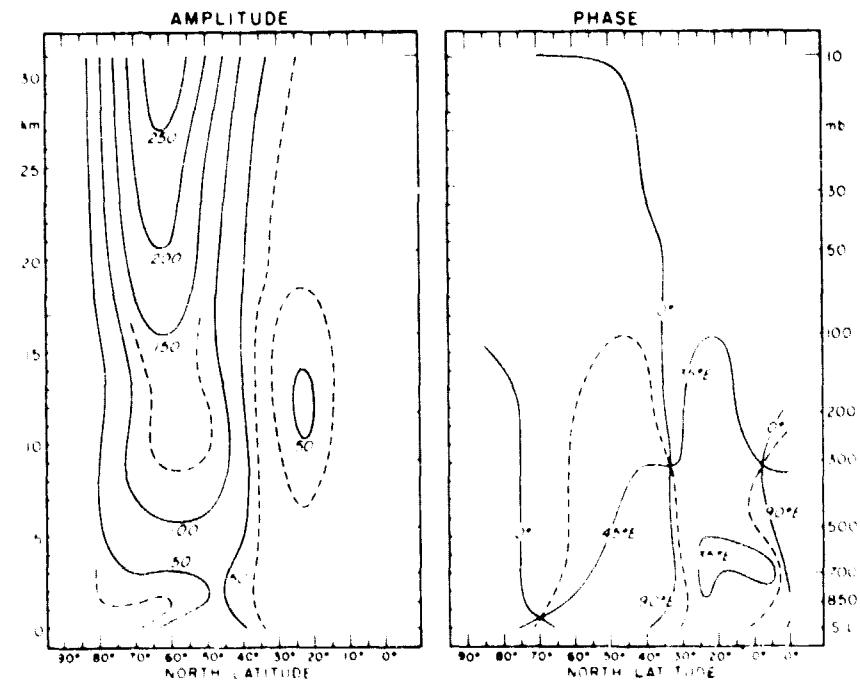

Figure 2.1 Monthly mean vertical structure for January. (a) Zonal harmonic number one; (b) zonal harmonic number two [VAN LOON et al., 1973].

latitude in the troposphere. The location of this maximum gradually shifts northward with height, reaching 65°N at 30 km. The maximum amplitude of both wave number 1 and 2 occurs near the latitude of the polar night jet, while the minimum occurs near the latitudes of the weak subtropical westerlies. Thus, planetary wave strength is closely related to zonal wind values. The phase lines, which represent the longitude of the amplitude maximum at each level, tilt westward with height, indicating upward energy propagation [ELIASSEN and PALM, 1961].

This westward tilt of phase with height was also observed by MUENCH [1965] in an analysis of January, 1958 data. He also observed that the amplitudes of wave numbers 1 and 2 increased with height, while wave numbers 3 and 4 had lower amplitudes and did not increase as rapidly with height. He noted that the lower the wave number, the greater the westward phase tilt with amplitude, indicating that the longer wavelengths were the major source of vertical energy propagation.

Figure 2.2, from VAN LOON et al. [1973], shows the monthly mean vertical structure of zonal harmonic number one for July. The July results are based on the same seven year data set used to obtain the results in Figure 2.1. The amplitude of this wave decreases rapidly with height above 15 km, and the phase lines tilt eastward with height. This indicates that planetary waves do not readily propagate vertically in the summer.

One other important characteristic of planetary waves is that they exhibit a great deal of variability in amplitude and phase from year to year. Figure 2.3, also from VAN LOON et al. [1973], shows the structure of wave number 1 and 2 with height at constant latitude for five different Januarys. Both wave numbers vary greatly from year to year, with the maximum and minimum amplitudes for wave number 1 differing by as much as a

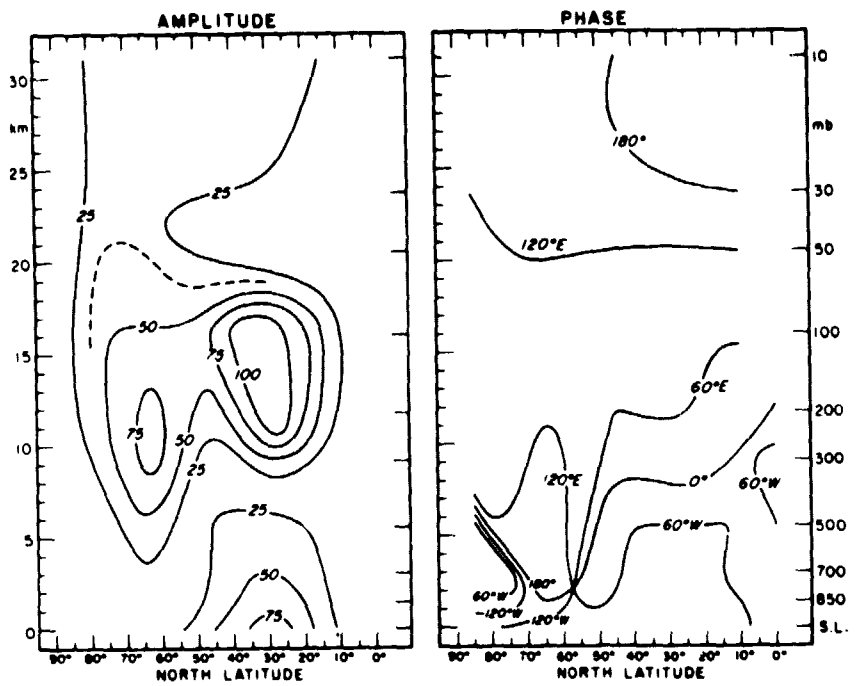

Figure 2.2 Monthly mean vertical structure for July, zonal harmonic number one [VAN LOON et al., 1973].

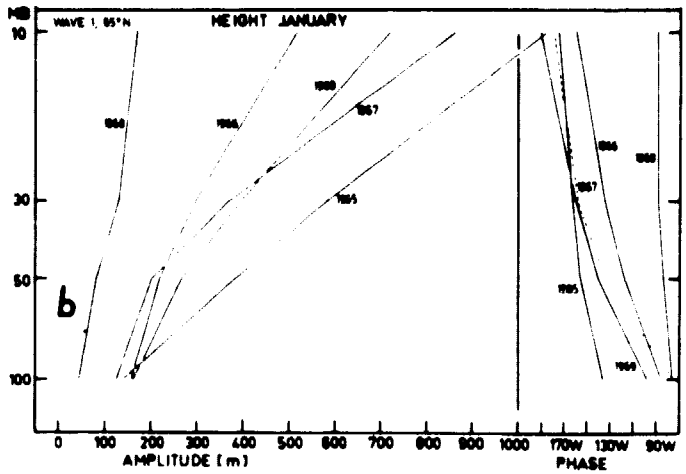

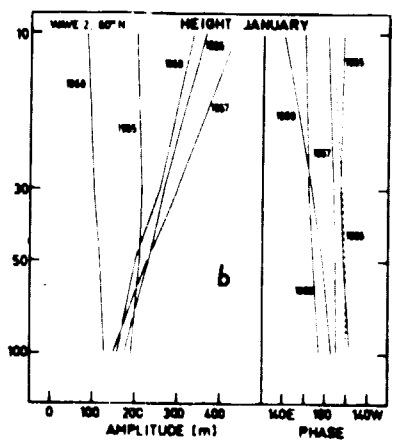

Figure 2.3 Monthly mean wave structure of zonal harmonics one and two, shown at constant latitude during January from 100 mb to 10 mb for five different years [VAN LOON et al., 1973].

factor of 10 at 10 mb. This variability was also noted by SATO [1974]. He suggested that the variability in the wave structure from year to year could be due to variations in the strength of the polar night jet.

While most of the previously mentioned studies have involved the use of conventionally obtained meteorological data, more recent studies have involved the use of satellite data. The PMR data used by HIROTA and BARNETT [1977] allowed them to obtain planetary wave structures up to as high as 85 km. Their analysis indicated that planetary waves one and two have significant amplitudes up to at least 85 km, and show a westward tilt of phase with height. The maximum amplitude for wave number 1 occurred at 65 km and 60° north latitude.

Theoretical studies of planetary wave propagation date back to CHARNEY and DRAZIN [1961], who studied the propagation of planetary waves in a simplified model atmosphere. Their model predicted that planetary waves would propagate vertically only if the mean zonal wind was westerly and less than a cutoff velocity of 40 m/sec. Since the mean zonal wind in the summer is westward, the Charney and Drazin model correctly predicted that planetary waves would not propagate in the summer. However, the cutoff velocity of 40 m/sec implied that vertical wave propagation would be greatest during the equinoxes, which contradicted observations showing maximum wave amplitude in January. DICKINSON [1968a] extended the work of Charney and Drazin by removing some of the unrealistic assumptions of their model. By using a realistic Coriolis parameter and allowing for vertical wind shears in the basic state, he found that the cutoff velocity for vertical propagation was much greater than 40 m/sec. This provided an explanation for the presence of planetary waves in the stratosphere in winter, when westerly winds were strong. DICKINSON [1968b, 1969a]

included a Newtonian cooling damping mechanism in the model which parameterized the energy loss to space due to infrared emission by carbon dioxide and to a lesser extent, water vapor. He found that this damping could strongly attenuate vertically propagating planetary waves in the presence of weak westerly winds, which could account for the small amplitude of planetary waves observed during the equinoxes.

DICKINSON [1968b] also advanced the wave guide theory of planetary wave propagation. Using a model with spherical geometry and latitudinally varying winds, he predicted that planetary waves could be ducted to the north and south of a midlatitude westerly jet. Figure 2.4 illustrates this scheme. Wave energy flow from the troposphere into the stratosphere is split by the strong westerly jet. Part of the wave propagates up the polar wave guide, being reflected by the pole to the north and the strong midlatitude westerlies to the south. The remainder of the wave energy travels into the equatorial wave guide, where it is absorbed by the zero wind line and converted into zonal mean momentum.

MATSUNO [1970] obtained planetary wave solutions numerically using a linear model in a realistic, spherical atmosphere forced at the lower boundary by observed 500 mb planetary wave geopotential height. Wave number 1 results compared fairly well to observations, but wave number 2 amplitudes were too small compared to those observed by MUENCH [1965]. Matsuno attributed the difference to the neglect of nonlinear effects.

SCHOEBERL and GELLER [1976] improved upon Matsuno's model by using height dependent static stability and damping parameters. If a parcel of air is displaced adiabatically from equilibrium, the static stability provides a measure of how readily the parcel will return to its equilibrium position. They found that the stratospheric wave structure was

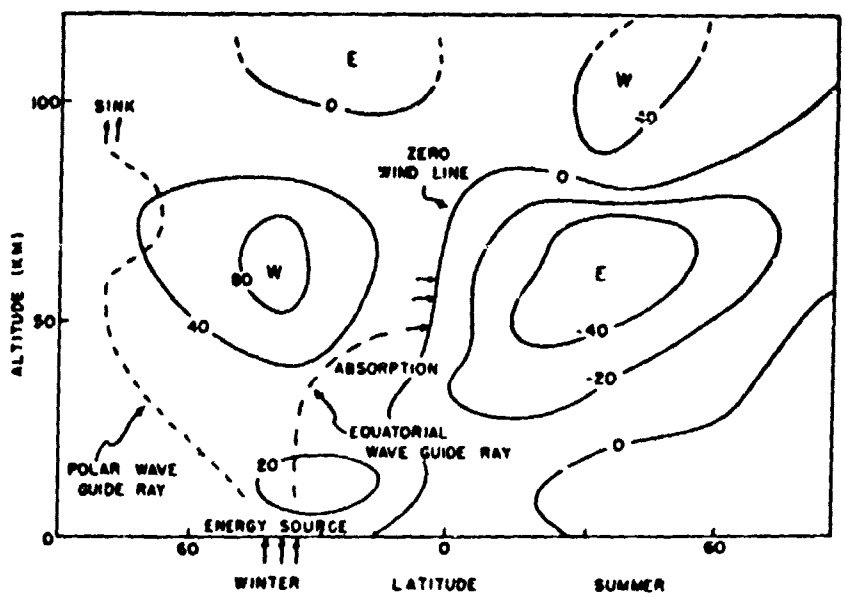

Figure 2.4 Ducting of wave energy by a strong westerly (W) jet [DICKINSON, 1968b].

insensitive to static stability changes, but was quite sensitive to changes in the basic zonal wind state, particularly to changes in the strength of the polar night jet. This sensitivity provided a possible explanation for the difference of Matsuno's results from observations. Matsuno's calculated waves used an average basic state from several years, while the observations he compared to were from January, 1967. The discrepancy between calculations and results could have been due to changes in the basic state.

The studies mentioned previously have all dealt with the vertical propagation of planetary waves. Other studies concentrate primarily on forcing of waves by topography and diabatic heating. CHARNEY and ELIASSEN [1949] considered topographical forcing and determined that planetary waves were a result of the forced ascent of westerly winds over the continents. SMAGORINSKY [1953] was the first to include a prescribed tropospheric heating function. He concluded that the observed distribution of sea level pressure could be attributed to heating effects, while topographical forcing became more important at higher altitudes. SALTZMAN [1965], using a different heating profile, concluded that thermal forcing could also be responsible for stratospheric wave structure.

RATES [1977] incorporated both the propagation and forcing aspects of planetary waves into a one-dimensional model. He concluded that thermal forcing dominated in the troposphere, while topographic and thermal forcing were equally important in the upper stratosphere. The fact that the model was one dimensional, however, limited the results obtained. More recently, AVERY [1978] developed a linear, quasi-geostrophic, steady-state planetary-wave model which included the effects of both thermal and topographical forcing. The effects of thermal forcing and topographical

forcing were considered separately and together. Planetary wave structure and propagation properties appeared to be sensitive to the vertical distribution of the heating. Three separate heating profiles with maximum heating at different levels were studied, and each appeared to excite different planetary wave modes having different vertical propagation characteristics. The thermally generated waves dominated the structure in the troposphere for both wave numbers 1 and 2. At higher altitudes, the two forcings produced an equal response for wave number 2, but for wave number 1, the thermally forced component still dominated. When both forcing mechanisms were applied together, the thermally and topographically forced waves joined together to produce a vertical energy flux greater than the flux produced from either forcing mechanism individually.

2.2 *Traveling Planetary Waves*

Traveling planetary waves having a variety of periods have been observed in the middle atmosphere. The most commonly observed periods are near 5 and 16 days. Observational studies of traveling wave structure and period date back to DELAND [1964]. In an analysis of six months of mid-latitude data at 500 mb, he obtained evidence of westward propagating wave number 1 and 2 disturbances with periods from 2 1/2 days to 6 days. More recent studies by ELIASSEN and MACHENHAUER [1969]; MADDEN and JULIAN [1972]; and ROGERS [1976] have also indicated the presence of large-scale 5-day traveling waves. Other observational studies by HIROTA [1968]; SATO [1977]; and MADDEN [1978] have indicated the presence of westward propagating, wave number 1 waves with periods of 14-16 days.

There is some disagreement as to the observed vertical structure of these traveling waves. These waves are coherent over a broad height range MADDEN [1978], so stratospheric structure can be deduced from tropospheric

studies. DELAND [1973b], in an analysis of Nimbus III satellite data, concluded that the phase of the westward traveling waves exhibited a westward tilt with height. This tilt was also observed by HIROTA [1968] and ELIASSEN and MACHENHAUER [1969] in their study of the 14- to 16-day wave. The westward tilt of phase with height is a property of an internal planetary wave, as opposed to a free resonant mode. HIROTA and SATO [1969] attempted to explain this 14-day traveling wave in terms of an interaction between topographically forced planetary waves and the zonal mean flow. They noted that an increase in upward propagation of wave energy was associated with periods of weakened westerly winds, and suggested that a coupling existed between the two phenomena. This wave-mean flow interaction will be discussed more fully in a later section. SATO [1977], in an analysis of pressure-height data from the winters of 1965-1966 and 1966-1967 in the northern hemisphere, also observed the westward tilt of phase with height. He also determined that the wave amplitude increased with height, resulting in a much stronger wave in the lower stratosphere than in the troposphere.

A comprehensive study of the properties and structure of the 5- and 15-day westward propagating traveling waves is presented by MADDEN [1978]. He analyzed 73 years of sea level pressure data and nine years of geopotential height data for large-scale traveling waves. He found a 5-day wave was present at all seasons south of 50°N latitude, while a 16-day wave was present north of 50° during winter and spring. The 16-day wave was seen to be coherent in the vertical, and exhibited little phase shift with height, which is typical of a free Rossby wave mode. The amplitude of the 16-day wave maximized between 60° and 70° N, increased with height, and had an amplitude of 100 geopotential meters (gpm) at 100 mb. The

5-day wave also exhibited little change in phase with height, typical of a free Rossby wave mode. The amplitude of the 5-day wave increased with height, but the amplitude attained at 30°N and 100 mb was 10 gpm.

Theoretical modeling attempts have increased the understanding of these large-scale traveling waves. These waves are treated either as a result of a wave-mean interaction, a topic discussed in Section 2, or as a free Rossby oscillation of the atmosphere. GEISLER and DICKENSON [1976] used a numerical model to determine the sensitivity of the 5-day wave to various basic state atmospheres. By varying the frequency of wave forcing at the lower boundary, they were able to determine the free modes which were allowed. The effects of temperature gradients at the lower boundary and sensitivity to background winds on the 5-day wave were seen to be small, except during the summer solstice, when a wave cavity is formed in the mesosphere and amplification of the wave results. The results of this theoretical study agreed well with the observations of MADDEN and JULIAN [1972].

More recently, SCHOEBERL and CLARK [1980] have done a theoretical study concerning the resonant modes which could be responsible for the 15-day wave. They found that the 15-day wave, unlike the 5-day wave, could be reflected and distorted by the polar night jet. The amplitude of the calculated 5-day wave in the winter hemisphere increased with height up to 35 km. Above that level, the amplitude dropped off steadily, illlustrating the trapping effect of the strong westerly polar night jet. This rapid decrease with height in the presence of strong winds is consistent with the idea of the CHARNEY and DRAZIN [1961] cutoff velocity. This trapping does not occur in the summer hemisphere, where the mean zonal wind is easterly. The model results agreed fairly well at high latitudes

to observations by MADDEN [1978], but the agreement at low latitudes was poor. The lack of agreement was attributed to noise due to non-resonant modes generated at the lower boundary, which could mask the resonant solution at low latitudes.

A comprehensive review of the theoretical and observational evidence for traveling planetary waves is presented in WALTERSCHEID [1980]. He indicates that westward traveling waves with periods in the range of 3-7 days (the "5-day wave") and in the range of 10-20 days (the "16-day wave") are discussed most frequently in the literature. He indicates that although both the 5-day and 16-day wave seem to be connected with free Rossby wave modes, the observational evidence for that fact, especially regarding the 16-day wave, is not conclusive.

2.3 *The Zonal Mean Circulation*

The circulation of the middle and upper atmosphere can be characterized in terms of a zonally averaged mean state, and deviations from that mean. The discussion up to this point has been concerned with the large-scale deviations from that mean, namely, planetary waves. The structure of these waves is sensitive to the zonal mean state, and the propagation characteristic of the waves are strongly dependent on the structure and strength of the zonal mean wind. This section will discuss the observed features of the zonal mean circulation and will review the role of the planetary waves in maintaining that circulation. Several theoretical models of the zonal mean will also be discussed.

A general picture of the zonal mean wind and temperature at the solstices is shown in Figure 2.5 [MURGATROYD, 1969]. In the absence of planetary waves, the circulation is driven by differential heating due to absorption of solar ultraviolet energy by ozone and the emission of

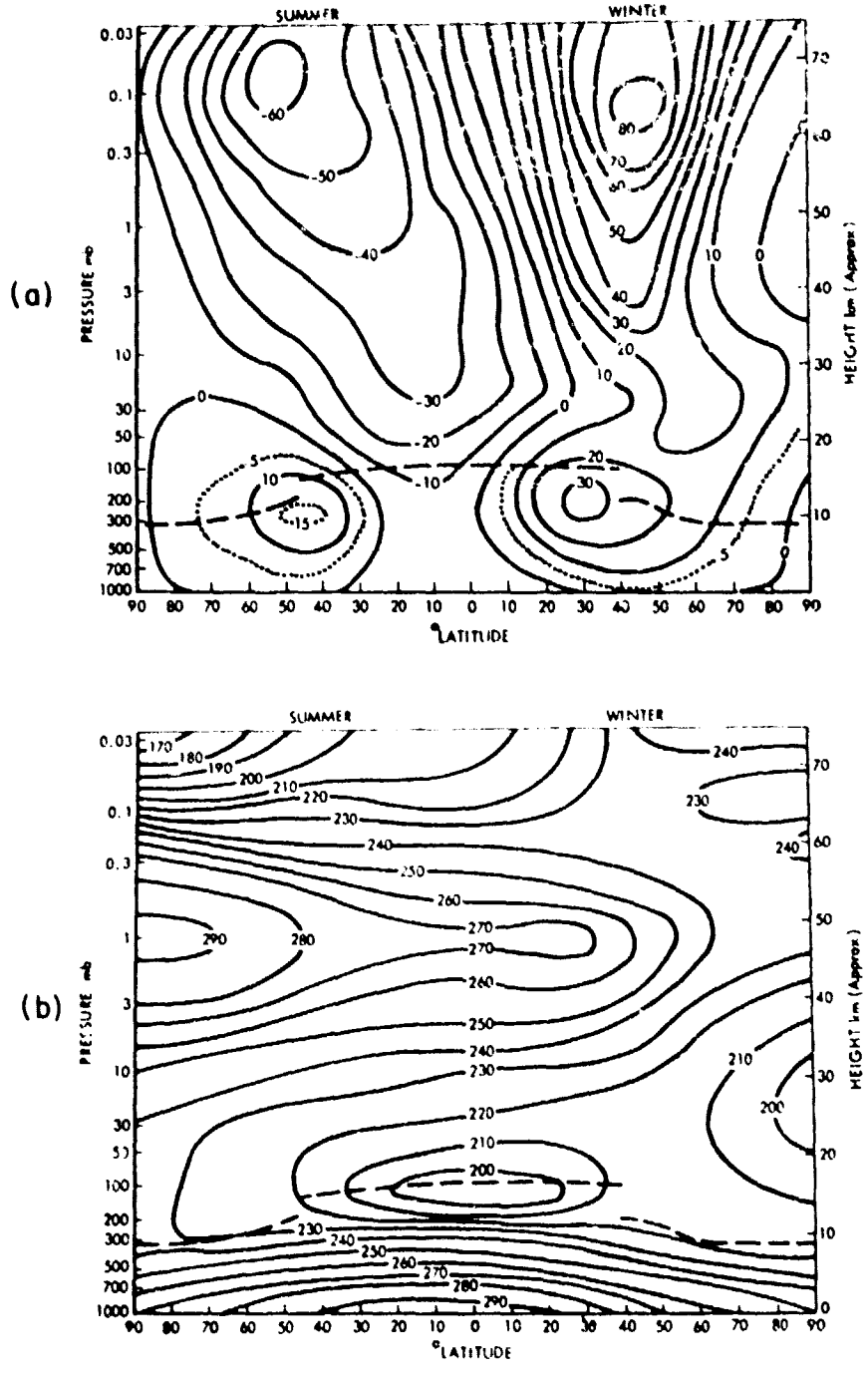

Figure 2.5 Latitude-height section of (a) zonal mean wind (m/sec) and (b) temperature (°K) [MURGATROYD, 1969].

infrared radiation to space by carbon dioxide and water vapor. The net effect is heating near the summer pole and cooling near the winter pole, which produces an overall meridional motion towards the winter pole, with rising motion near the summer pole and sinking motion near the northern pole. The Coriolis force acting on the meridional flow produces the westward flow in the summer hemisphere and an eastward flow in the northern hemisphere. The temperature structure resulting from this differential heating is in approximate balance with this circulation, with temperatures generally increasing from the winter to summer hemisphere.

Planetary wave fluxes modify this thermally direct circulation in several significant ways. DOPPLICK [1971] determined that the zonal mean circulation in the winter lower stratosphere was markedly influenced by planetary waves propagating in the troposphere. The convergence of planetary wave heat and momentum fluxes tends to drive a secondary meridional circulation opposite in direction to the thermally direct circulation due to differential heating. In the lower stratosphere, this secondary circulation dominates, so that the winter hemisphere meridional circulation is thermally indirect, that is, rising motion near the winter pole and a gradual equatorward motion.

The ozone layer is centered in the upper stratosphere, near 50 km, and the effect of solar heating is greatest in this region. The secondary circulation driven by the planetary waves at and above these heights is not as strong as it is in the lower stratosphere, and hence the circulation in the upper stratosphere and mesosphere is thermally direct. This thermally direct, summer pole to winter pole circulation in the mesosphere gives rise to the warm winter mesopause [SCHOEBERL and STROBEL, 1978].

Techniques of measuring the wind in the middle atmosphere are summarized in Figure 2.6 from GAGE [1981]. In the 30-80 km range, rocket experiments have provided most of the measurements, while above 80 km, wind data can be obtained through various radar techniques. One of the most widely used techniques for obtaining mesospheric winds involves the use of vaporized meteor trails [BARNES, 1972]. Other radar measurement methods include the coherent scatter radar techniques [COUNTRYMAN and BOWHILL, 1979; BALSLEY and GAGE, 1980], and the partial reflection drifts experiment [GREGORY et al., 1979]. In addition to these ground-based experiments, satellite measurements of geopotential height and temperature up to .4 mb (55 km) are also available on a daily or weekly basis. Wind fields can be determined from these data if a thermal wind balance is assumed. The thermal wind equation allows a calculation of wind shears if latitudinal temperature gradients are known.

Several mean wind and temperature profiles based on experimental data are available for use in theoretical modeling. OORT and RASMUSSON [1971] have determined a wind and temperature profile for below 50 mb based on five years of experimental data. Above 50 mb, zonal mean wind and temperature profiles extending into the thermosphere are available in the CIRA [1972, 1975] reference atmospheres. These atmospheres are based on a compilation of many data sources. Other profiles are also available, such as the one given in BELMONT et al. [1975], which is based on meteorological rocket network data below 65 km.

Figure 2.7 shows a wind model used by SCHOEBERL and GELLER [1976] in their study of stationary planetary waves. This model is based on the CIRA [1975] standard reference atmosphere, and is quite similar below 65 km to the profile presented in BELMONT et al. [1975]. The wind profile

Middle atmosphere wind measurement
Summary of *in situ* techniques

TECHNIQUE	ALTITUDE RANGE	HEIGHT RESOLUTION	ACCURACY (1 MIN AVE)	EXTENT OF USE	COMMENTS
AIRCRAFT	0-20 KM	<100 M	~1 M/S	INTER-MITTENT	USED FOR MESOSCALE RESEARCH
BALLOON	0-40 KM	300 M	~1-5 M/S	ROUTINE	ACCURACY DEPENDS ON TRACKING SYSTEM & DEGRADES WITH RANGE
SMOKE TRAILS	0-60 KM	<100 M	~0.1 M/S	INTER-MITTENT	USED FOR SMALL-SCALE WINDSHEAR
ROCKET SONDE	10-70 KM	300M-3KM	~3 M/S	ROUTINE	RESOLUTION VARIES WITH FALL RATE
FALLING SPHERE	30-80 KM	300M-3KM	~3M/S	ROUTINE	RESOLUTION VARIES WITH FALL RATE
CHAFF	45-95 KM	2KM	~5 M/S	INTER-MITTENT	NO LONGER IN COMMON USE
CHEMICAL RELEASE	70-100 KM+	1KM	~1M/S	INTER-MITTENT	USUALLY RESTRICTED TO NIGHTTIME & TWILIGHT

Middle atmosphere wind measurement
summary of optical and acoustic methods

TECHNIQUE	ALTITUDE RANGE	HEIGHT RESOLUTION	ACCURACY	EXTENT OF USE	COMMENTS
SATELLITE/ CLOUD WINDS	1-12 KM	LIMITED TO ONE LEVEL	4 M/S	ROUTINE	MOSTLY USED OVER OCEANS
STELLAR SCINTILLATION	0-15 KM	3-5 KM	5 M/S	NOT IN CURRENT USE	CLOUD-FREE, NIGHTTIME
AIRGLOW	95-100 KM	5 KM	5 M/S	ROUTINE	CLOUD-FREE, NIGHTTIME
LIDAR	—	GOOD	—	INTERMIT USE IN BOUNDARY LAYER	UNDER DEVELOPMENT
ACOUSTIC PROPAGATION	STRATOSPH. & LOWER THERMOSPH	LIMITED TO ONE LEVEL	3-5 M/S	ROUTINE	ACOUSTIC REFLECTION LEVEL UNCERTAIN, TEMP MUST BE KNOWN AT REFL. LEVEL
ROCKET GRENADE	30-80KM	5 KM	~20%	NOT IN CURRENT USE	ERROR DEPENDS ON ARRAY GEOMETRY

Middle atmosphere wind measurement
summary of radio (radar) technique

TECHNIQUE	ALTITUDE RANGE	HEIGHT RESOLUTION	ACCURACY	EXTENT OF USE	COMMENTS
METEOR TRAILS	80-100 KM	4 KM	3 M/S	ROUTINE	DAY & NIGHT OBSERVATIONS
DOPPLER RADAR (MST)	0-100 KM	100 M-5 KM	1 M/S	ROUTINE	MESOSPH. WINDS OBSERVABLE ONLY DURING DAYTIME
SPACED ANTENNA DRIFTS (PRD)	60-100 KM	1 KM	5-10 M/S	ROUTINE	MESOSPH. WINDS OBSERVABLE ONLY DURING DAYTIME
INCOHERENT SCATTER	65-100 KM	500 M	1-3 M/S	INTER-MITTENT	RECENTLY DEMONSTRATED AT THESE ALTITUDES LIMITED TO DAYTIME OBSERVATIONS

Figure 2.6 Summary of wind measurement techniques in the middle atmosphere, from GAGE [1981].

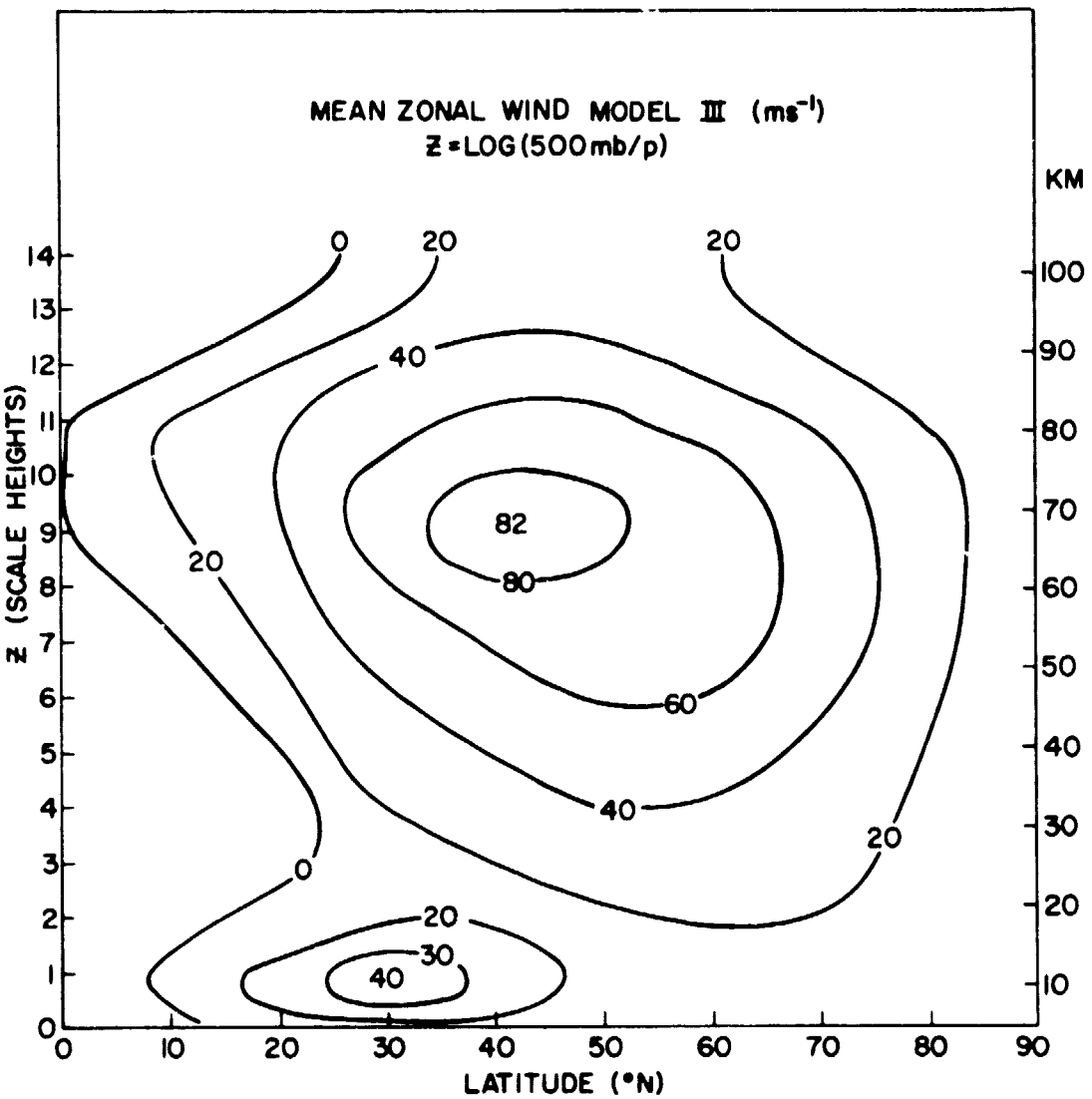

Figure 2.7 Model of the zonal mean wind (m/sec) used by SCHOEBERL and GELLER [1976].

shown in Figure 2.7 has a strong polar night jet, with a maximum of 82 m/sec, centered at 40° latitude and 70 km. The tropospheric jet has a maximum amplitude of 40 m/sec centered at 10 km and 30°N. Note the location of the zero wind line, which acts as an absorber of planetary wave energy near the equator. Figure 2.8 shows the temperature distribution obtained from the wind model in Figure 2.7 by using the thermal wind relationship and a CIRA vertical temperature profile. Note the warm winter mesopause, the gradual temperature increase from pole to equator in the 30 to 60 km region, and the midlatitude temperature maximum in the lower stratosphere.

Although detailed information on the amount of planetary wave energy converted to zonal mean energy in the upper stratosphere and mesosphere is sparse, theoretical models have been fairly successful in calculating the zonal mean circulation. LEOVY [1964] obtained a realistic zonal and meridional circulation with his model of the thermally driven mesospheric circulation. He parameterized the divergences of eddy heat and momentum fluxes as functions of perturbation temperature and velocity. Using radiative heating by ozone and a parameterized cooling, he obtained a summer pole to winter pole meridional circulation which accounted for the polar night jet, and cool summer mesosphere, and the warm winter mesosphere.

Later, SCHOEBERL and STROBEL [1978] used a numerical model to solve a zonal mean equation similar to Leovy's. However, they included an explicit calculation of planetary wave fluxes, instead of a parameterization as Leovy had used. Advances made by DICKINSON [1973] in the infrared cooling parameterization and by PARK and LONDON [1974] in the calculation of differential solar heating were also included. The one adjustable parameter in the model was the Rayleigh friction, which was varied until agreement

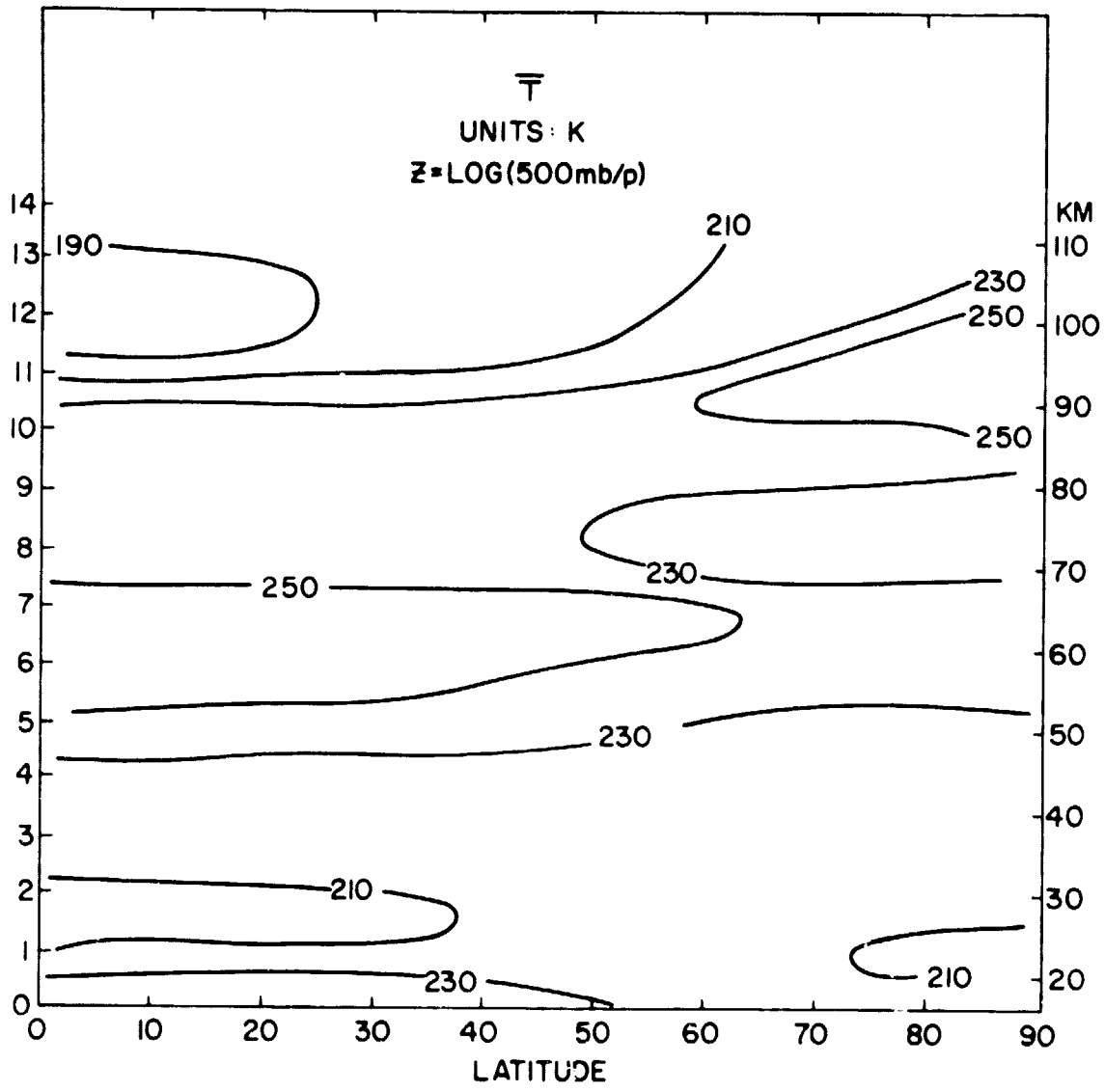

Figure 2.8 Distribution of zonal mean temperature (°K) as calculated by SCHOEBERL and GELLER [1976].

with observations was attained. With their model, Schoeberl and Strobel were able to simulate the main features of the zonal mean circulation, i.e., the cold summer mesosphere, the warm winter mesosphere, and the polar night jet. In order to obtain realistic results, they determined that the Rayleigh friction coefficient needed to increase exponentially with height. This produced a thermally direct meridional circulation in the mesosphere, and a polar night jet with an amplitude of 85 m/sec. The zonal mean circulation produced by their model when exponential damping was being used is shown in Figure 2.9a. The polar night jet in the winter hemisphere maximizes around 50°N latitude and 60 km. Figure 2.9b shows the distribution of zonal mean temperature. Note the warm winter mesosphere and cold summer mesosphere. Figures 2.9c,d and represent the meridional and vertical components of the zonal mean wind. The circulation is generally poleward and downward in the winter hemisphere.

The Rayleigh friction coefficient used by SCHOEBERL and STROBEL [1978] is supposed to simulate the effects of smaller scale waves and turbulence on the zonal mean circulation. There is no self-consistent theory that can be used to estimate its value, however, and in general a value is chosen which is small at low levels and increases rapidly with height. Schoeberl and Strobel used a damping which increased exponentially with height above the stratopause, where the time constant was about 10 days. HOLTON and WEHRBEIN [1980b], however, used a value that was constant below 80 km, with a time constant of 80 days. Above the 80 km level, the time constant decreased rapidly, reaching a minimum of about 2 days at 90 km. This rapid decrease in time constant was intended to simulate the effect of damping due to the turbulent breakdown of gravity waves in this region.

While the choice of the damping parameter appears to be somewhat

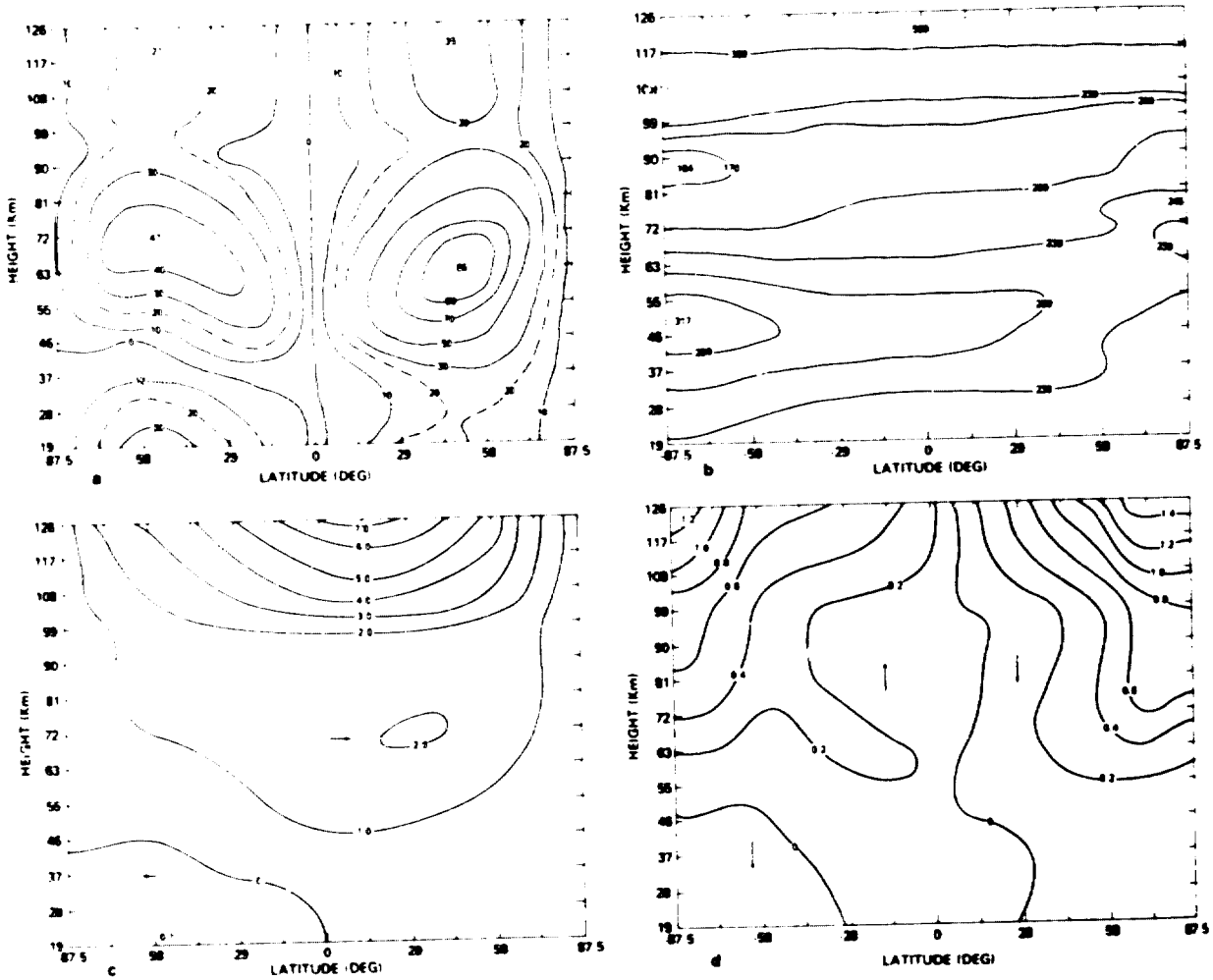

Figure 2.9 Mean distributions obtained by SCHOEBERL and STROBEL [1978]: (a) zonal wind (m/sec), (b) meridional wind (m/sec), (c) temperature (°K), and (d) vertical wind (cm/sec).

arbitrary, a reasonable approximation to the zonal mean wind structure was obtained in each of the two previously-mentioned studies. However, more investigation into the nature of the damping process is needed, especially in light of the recent observational results of NASTROM et al. [1982]. These results indicate mean meridional flows of 10-15 m/sec in the summer hemisphere near 90 km, in contrast to values of 1 m/sec in this region as obtained from the numerical model of SCHOEBERL and STROBEL [1978].

Observational evidence in the regions above the mesosphere is, in general, too sparse to provide a complete picture of the mean circulation. However, certain localized data exist to which theoretical modeling efforts can be compared. The zonal mean circulation in the thermosphere has been calculated by DICKINSON et al. [1977]. This circulation is primarily driven by a strong solar heating, in addition to a high latitude heat source, which is the result of joule heating in the auroral zone. Figure 2.10a shows the zonal mean circulation obtained from this thermospheric model. Note that the thermospheric jet is much stronger than that obtained by Schoeberl and Strobel. This is because the heating distribution of Schoeberl and Strobel did not include the effects of atmospheric absorption of solar extreme ultraviolet radiation $\lambda < 1025$ Å. This EUV heating is small below 100 km, but becomes increasingly important with increasing height. Note that a relative minimum in zonal mean wind velocity occurs in both models near 100 km. Figure 2.10b shows the perturbation temperature at thermospheric heights. Below 150 km, the thermal wind equation is approximately satisfied by the wind and temperature fields. Note that the temperature near the winter pole is unrealistically low. This is attributed to difficulties with the lower boundary conditions used in the model. Figures 2.10c and 2.10d show the meridional and

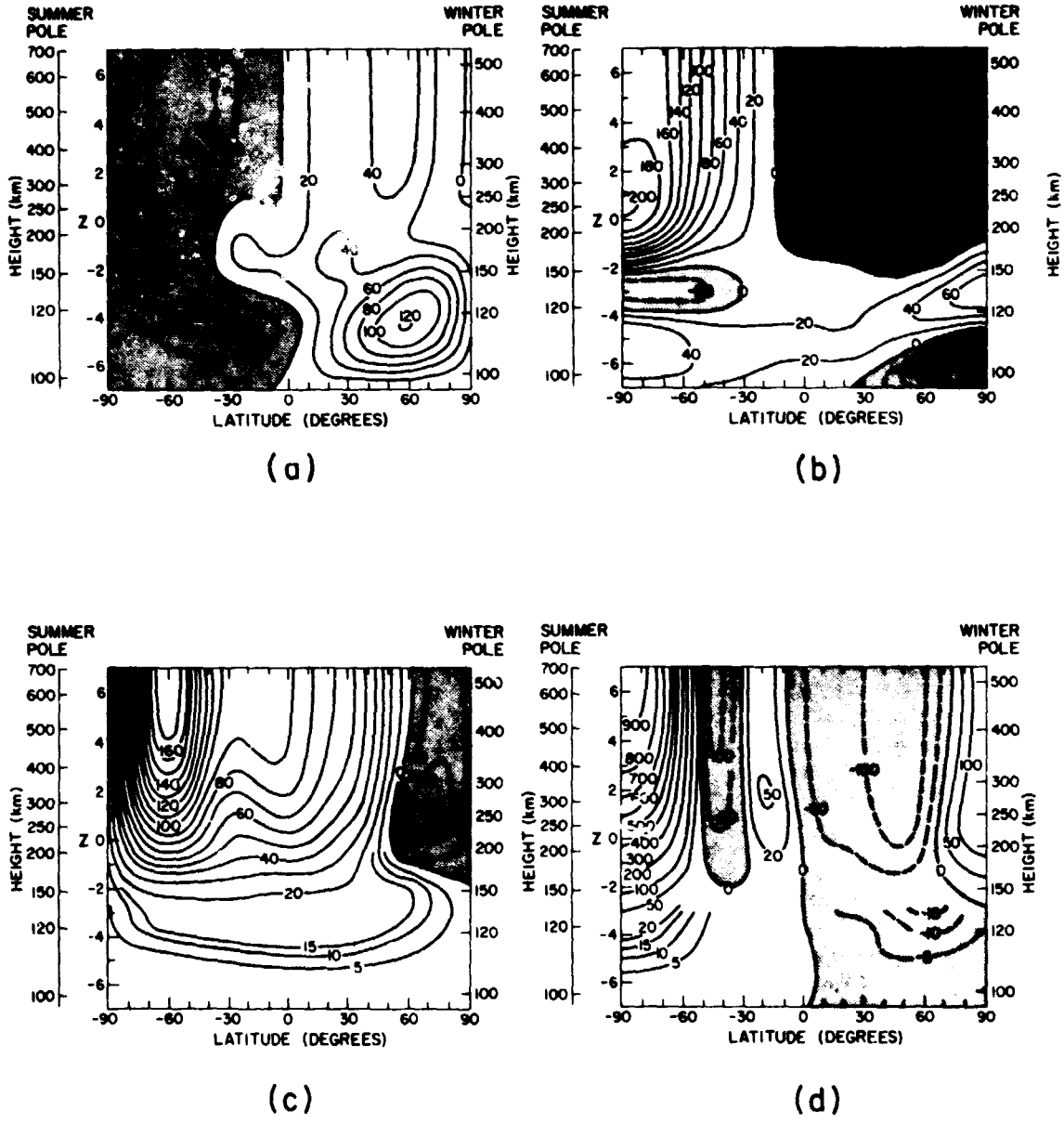

Figure 2.10 Mean distributions obtained by DICKINSON et al. [1977]: (a) zonal wind (m/sec), (b) meridional wind (m/sec), (c) temperature (°K), and (d) vertical wind (cm/sec).

vertical velocities, respectively. These values below 120 km are in reasonable agreement with those from Schoeberl and Strobel, Figures 2.9c and 2.9d. This indicates that a model similar to that of SCHOEBERL and STROBEL [1973] extending upward to 150 km, could provide a reasonable approximation of the zonal mean circulation at the base of the thermosphere.

2.4 *Wave-Mean Interactions and Stratospheric Warmings*

In the previous sections, planetary waves and the zonal mean circulation were discussed as two interrelated quantities. The fact was mentioned that planetary wave structure can be strongly dependent on the basic state winds, and also that the zonal circulation is determined in part by planetary wave momentum and heat fluxes. The modeling studies cited in the previous sections, however, have dealt with steady state and time-independent effects. This section will deal with some of the time-dependent theoretical considerations of wave-mean interactions, and will discuss the natural phenomena of the stratospheric warming, which can be explained using these considerations.

One of the fundamental considerations of wave-mean interaction theory is the fact that, in the absence of critical layers, dissipation, and transience, planetary waves have no effect on the zonal mean circulation. The secondary meridional circulation generated by the waves exactly cancels the effect of the planetary wave fluxes on the zonal mean. This phenomenon is referred to as the noninteraction theorem. The noninteraction theorem has been discussed for certain special cases by ELIASSEN and PALM [1960]; CHARNEY and DRAZIN [1961]; DICKINSON [1969b]; and HOLTON [1974], and was generalized by ANDREWS and MCINTYRE [1976a] and BOYD [1976]. In the actual atmosphere, the conditions required for noninteraction are often not satisfied, and hence theories treating these cases

have been developed.

DICKINSON [1969b] showed that the presence of singular lines and planetary wave damping was necessary if the planetary waves were to have an effect on the zonal mean circulation. The planetary wave forcing essentially modifies the equilibrium mean flow, and maintains that part of the zonal mean flow which is not due to solar heating sources. A planetary wave incident on a critical level is absorbed there; i.e., the wave amplitude decreases rapidly and the wave energy flow vanishes above the critical level. The resulting sharp gradient in heat flux results in an increased temperature below the critical level, and results in an induced meridional circulation. This mechanism will be discussed further in connection with MATSUNO's [1971] model of the stratospheric warming.

URYU [1974] discusses the case of a transient planetary wave packet propagating upwards through a motionless basic state. In this simplified case, the result was an acceleration of the zonal mean flow at the leading edge of the wave packet, and a corresponding deceleration at the trailing edge.

Numerical models which attempt to simulate the interaction between wave and mean have been developed. Already discussed was the model by SCHOEBERL and STROBEL [1978], which simulated the zonal mean circulation using solar ozone heating and planetary wave fluxes. A time-dependent model developed by HOLTON and WEHRBEIN [1980a] was used to simulate the zonal mean circulation to a first approximation by including only diabatic heating. Since the effects of planetary wave fluxes were absent, this model failed to reproduce the thermally indirect circulation of the lower stratosphere. The addition of wave number 1 fluxes in an extension of this model [HOLTON and WEHRBEIN, 1980b] removed this discrepancy in the

lower stratosphere. In the upper stratosphere and mesosphere, Holton and Wehrbein found that the addition of the wave fluxes made little difference in the mean meridional circulation, although the strength of the polar night jet was reduced.

One of the most dramatic demonstrations of the interaction between planetary waves and the zonal mean circulation occurs during a stratospheric warming event. Just prior to the warming, a large enhancement of the vertical flux of wave energy occurs. This increased flux is sometimes due to wave number 1, sometimes to wave number 2. After a period of a week or two, the results of this increased flux are seen in the stratosphere. The temperatures in the polar region may increase by as much as 50°C, reversing the meridional temperature gradient and changing the mean zonal wind from westerly to easterly. If this wind reversal occurs early enough in the winter season, the westerly circulation will be restored. If the warming occurs late in winter, however, it is called a final warming, and marks the onset of a summer circulation pattern. These warmings occur sporadically, and are not observed every winter.

MATSUNO [1971] suggested that the warming phenomenon was due to the interaction of planetary waves and the mean flow at critical levels. Matsuno's explanation of the stratospheric warming is pictured in Figure 2.11 as taken from SCHOEBERL [1978]. An anomalous increase in planetary wave flux and the resulting increase in northward heat flux due to the wave leads to a warming of the polar regions. This results in a meridional circulation with rising motion in the polar region and sinking motion at low latitudes as shown in the figure. This flow, acted on by Coriolis torques, generates an easterly flow which serves to decelerate and eventually reverse the normal westerlies at high latitudes. This wind

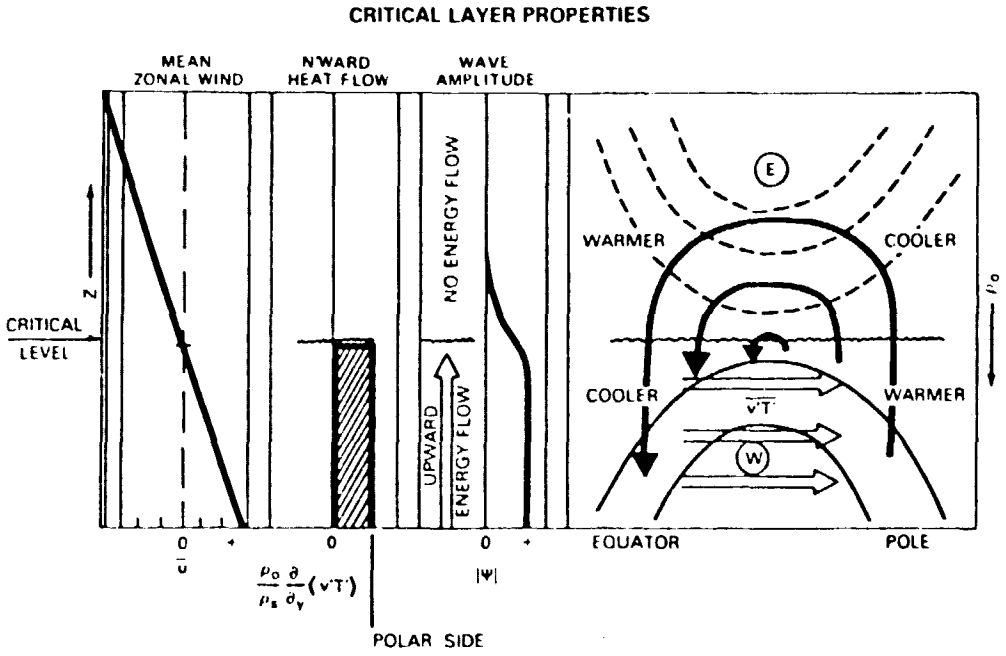

Figure 2.11 Idealized critical layer properties during a stratospheric warming, from SCHOEBERL [1978].

reversal causes a line of zero zonal wind, i.e., a critical layer, and a region of easterlies through which the planetary waves cannot penetrate. Figure 2.11 shows the situation after the critical layer has developed. The inability of the planetary wave to penetrate the critical level causes a discontinuity in the amount of the heat transported northward by the wave at that level. This produces even more net heating at high latitudes with an enhancement of the pole to equator meridional circulation and a strengthening of the easterlies above the level. Thus, the stratospheric warming is seen to be a result of wave-mean flow interactions. This mechanism for the warming was also modeled and verified by HOLTON [1976].

Numerous observational and theoretical studies have been performed since the introduction of MATSUNO's [1971] theory. QUIROZ et al. [1975] have classified stratospheric warmings according to the behavior of temperature perturbations prior to the warming. LABITZKE [1977] has classified warmings according to the behavior of planetary waves one and two prior to the warming, shown in Figure 2.12 from SCHOEBERL [1978]. A type A warming is characterized as follows: wave number 2 amplitude increases two weeks before the warming, followed by an increase in wave number 1 and a weakening of wave number 2. Wave number 1 maximizes one week before the warming, and falls off in amplitude after the warming, in conjunction with an increase in wave number 2 amplitude. A type B warming is typified by an increase in both waves 1 and 2 prior to the warming, with wave number 1 dominating. Both wave amplitudes fall off after the warming occurs, and then wave number 2 intensifies again about one week later. The type A warming occurs most frequently. Complete reviews of recent developments in the theory and observations of stratospheric warmings are given by SCHOEBERL [1978]; and HOLTON [1980a].

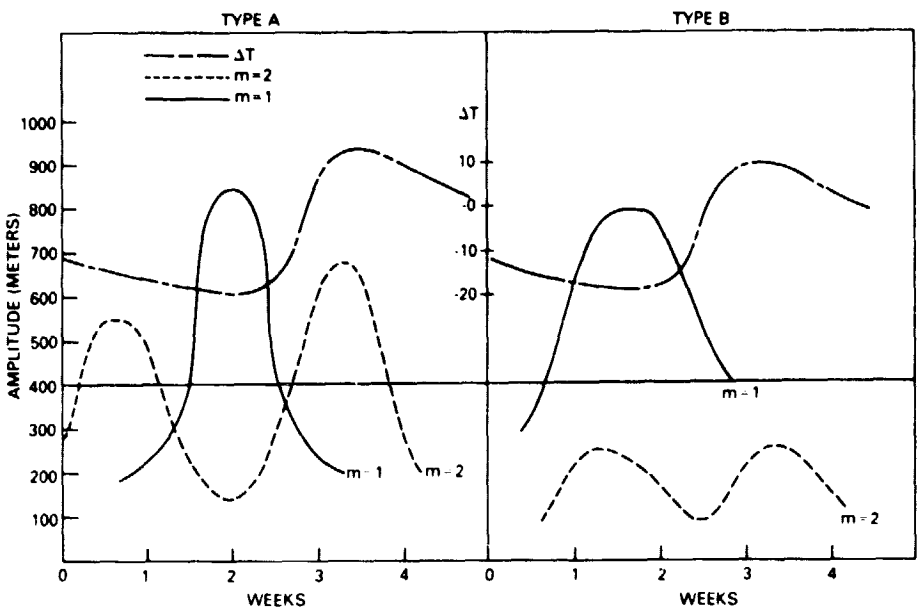

Figure 2.12 Stratospheric warmings classified according to the behavior of planetary waves one and two prior to the warming event, from SCHOEBERL [1978].

A second observed phenomenon that could be the result of a wave-mean interaction is the vacillation in atmospheric parameters observed by MCGUIRK and REITER [1976]. They observed a vacillation in the northern hemisphere atmospheric energy parameters with a 24-day period. A similar vacillation with a period of 18-23 days was also observed in the southern hemisphere stratosphere by WEBSTER and KELLER [1975]. Vacillations in sea level pressure data and tropospheric and stratospheric geopotential height data with periods of 5 days and 16 days have been observed by MADDEN [1978]. The cause of these vacillations is uncertain. They could be due to fluctuations in planetary wave forcing mechanisms. HUNT [1978], using a general circulation model, reproduced vacillations with an approximate 20 day period. The vacillation occurred in the eddy energies, and also in the forcing terms. However, HOLTON and MASS [1976], using a two-dimensional, time-dependent model, were able to simulate vacillations without varying the basic state forcing. MADDEN [1978] proposed that vacillations are due to a quasi-resonance formed by the interaction of stationary and traveling planetary waves. The works of SCHOEBERL and GELLER [1976] and AVERY [1978] indicate that changes in the reflective properties of the stratosphere and troposphere may lead to vacillations due to the interaction of waves and mean flow.

2.5 *Nitric Oxide and the Winter Anomaly*

Although nitric oxide can be characterized as a trace constituent in the earth's atmosphere, it engages in certain chemical reactions which have great importance to life on the surface of the earth. In the stratosphere, nitric oxide is the result of the combination of N_2O with ground state oxygen, as follows: $O\ (^1D) + N_2O \rightarrow 2NO$. Stratospheric nitric oxide has been identified as an efficient catalyst in reactions which serve as a

sink for ozone [CRUTZEN, 1970]. Stratospheric ozone absorbs certain harmful wavelengths of ultraviolet radiation, which would otherwise reach the surface. The emission of NO from SST aircraft and the effect of this increase in NO on the ozone layer was first discovered by CRUTZEN [1971] and JOHNSTON [1971], and the controversy which arose sparked a great deal of interest in the structure and properties of NO. In the upper stratosphere and mesosphere, NO is thought to play a role in another atmospheric phenomenon, the winter anomaly [SECHRIST, 1967]. This subject will be discussed in detail later in this section.

Although there are hundreds of reactions involving nitrogen, oxygen, and other constituents that take place in the thermosphere and mesosphere, a general picture of NO chemistry can be obtained by examining a few of the more important reactions. In the stratosphere, the reaction mainly responsible for the production of NO is the reaction of excited state atomic oxygen with N_2O as follows

$$O(^1D) + N_2O \rightarrow 2NO \tag{2.1}$$

Nitric oxide is lost in this region due to the combination with ground state nitrogen

$$N(^4S) + NO \rightarrow N_2 + O \tag{2.2}$$

The catalytic destruction of ozone in the stratosphere can be expressed as follows

$$NO + O_3 \rightarrow NO_2 + O_2 \tag{2.3}$$

$$NO_2 + O \rightarrow NO + O_2 \tag{2.4}$$

In the upper mesosphere, the production of NO is dominated by the reaction of excited state atomic nitrogen with molecular oxygen, as follows

$$N(^2D) + O_2 \rightarrow NO + O \qquad (2.5)$$

The loss process involves the reaction of NO with ground state nitrogen, as in the stratosphere (see equation 2.2). Thus, according to this highly simplified scheme, the concentration of NO is determined by the relative amounts of ground state and excited state atomic nitrogen [RUSCH and BARTH, 1975]. There are several sources for atomic nitrogen in this region, as follows;

$$NO^+ + e^- \rightarrow N + O \qquad (2.6)$$

$$N_2^+ + O \rightarrow NO^+ + N \qquad (2.7)$$

$$N_2^+ + e^- \rightarrow N + N \qquad (2.8)$$

The last source of atomic nitrogen involves the collision of molecular nitrogen with fast photoelectrons

$$e^-(fast) + N_2 \rightarrow N + N + e^- \qquad (2.9)$$

These equations suggest that the auroral zone should be an important source of NO in the upper mesosphere and thermosphere. The primary auroral electrons colliding with the earth's atmosphere will produce ionization electrons necessary for equations 2.6-2.8, and fast secondary electrons necessary in equation 2.9. Thus, the auroral region provides a source for atomic nitrogen, which, if in the excited state, reacts with molecular oxygen to form NO.

An interesting result can be obtained by examination of equation 2.6. This reaction is the principal loss mechanism for both ground state atomic nitrogen and nitric oxide. In the polar region, the density of nitric oxide exceeds that of atomic nitrogen [RUSCH and BARTH, 1975]. Thus, if

the production rate of $N(^4S)$ is small, reaction 2.6 will soon deplete the $N(^4S)$, with the result that the NO lifetime will be quite long, on the order of several days or more. This long lifetime for nitric oxide has also been noted by STROBEL [1971b, 1972]; ORAN et al. [1975], and OGAWA and SHIMAZAKI [1975]. The long lifetime at mesospheric heights makes nitric oxide a particularly good candidate for transport by meridional and vertical winds due to planetary waves.

Early theoretical studies of nitric oxide were primarily one-dimensional and involved simplified chemistry. STROBEL et al. [1970] investigated the sensitivities of the nitric oxide distributions to different chemical schemes. STROBEL [1971a] used simplified chemistry, vertical eddy diffusion, and a downwards NO flux at the mesopause to theoretically calculate a vertical NO profile that showed adequate agreement with observations of BARTH [1966a] and MEIRA [1971]. He concluded that a strong downward flux was necessary at the upper boundary in order to simulate the observed vertical NO distribution. This flux represents one of the main sources of NO in the mesosphere. Many one-dimensional studies using molecular and eddy diffusion as a vertical transport mechanism have been performed [ROBLE and REES, 1977; REES and ROBLE, 1979; and GERARD and RUSCH, 1979]. These model studies all indicate that nitric oxide densities will gradually increase with time due to production in the auroral zone. The time required for the nitric oxide to reach a new equilibrium distribution is found to be large, on the order of 10^6 sec after the aurora is switched on.

Observational results have indicated that although the concentration of mesospheric nitric oxide is relatively constant with time south of 40°N latitude [RUSCH, 1973], the nitric oxide distribution in the polar region

shows a great deal of variability [RUSCH and BARTH, 1975]. This change in variability with latitude led to the development of two-dimensional, time-dependent numerical models which were used to study the effects of horizontal transport on NO distributions in the auroral zone. ROBLE and GARY [1979] included advection of NO by mean meridional winds in their study of the effects of transport on auroral NO densities. They found that horizontal transport spreads out the buildup of NO obtained in the one-dimensional models, reducing the peak density obtained by one-third. More recently, SOLOMON [1981] has included the effects of chemistry and transport by mean winds and eddy diffusion in a single numerical model. Solomon finds that the transport of NO from the auroral zone can be a significant source of NO in the polar winter stratosphere.

Observations of nitric oxide concentrations can be obtained through satellite measurements [CRAVENS and STEWART, 1978] or with rocket experiments [SWIDER and NARCISI, 1977]. In the lower thermosphere, nitric oxide has a latitudinal gradient, with the concentration in polar regions being 2 to 5 times higher than the concentration at the equator. The horizontal and vertical structure of the observed nitric oxide concentration will be discussed in greater detail in Chapter 4.

The ion chemistry of the D region, i.e., from 60 to 90 km, is very complex. This is illustrated by the fact that both positive and negative ions are present in significant amounts. The negative ion chemistry involves primarily the reaction of O_2^- with various minor gases. Positive ion chemistry is not well understood, and so it is difficult to identify electron loss processes. The main source of ionization in the D region is the ionization of nitric oxide by solar Lyman α radiation. This ionization, which can be detected by various ground-based experiments,

shows a strong diurnal variation, disappearing almost completely at night due to a lack of incoming solar radiation. The amount of ionization also shows a seasonal effect due to variations in the solar zenith angle. On some winter days, there is an anomalous enhancement in the electron concentration at heights above 65 km, which shows up in ground-based measurements as a period of increased atmospheric absorption. This phenomenon is known as the winter anomaly.

Figure 2.13 shows the results of some absorption measurements as reported by SCHWENTEK [1971]. These measurements were made over Germany, and were taken at constant solar zenith angle. This absorption can be characterized as the sum of a long-term seasonal trend (the "normal" winter anomaly) and shorter term peaks superimposed on this trend. In this work, references to the winter anomaly refer to these short-term peaks. Figure 2.13 indicates that these short periods of high absorption occur quite frequently throughout the winter. In another observational study, SCHWENTEK [1974] determined that the amplitude and duration of the anomaly decreased with latitude. He also noted that the winter anomaly in 1971-1972 seemed to occur with a periodicity of about seven days. By comparing measurements made in Germany and Spain, he also determined that the region of increased absorption was coherent over a distance of at least 1900 km. Figure 2.14, from GELLER and SECHRIST [1971], presents an idealized picture of the vertical structure of the electron concentration for normal versus anomalous conditions. This figure is based on rocket data obtained by SECHRIST et al. [1969]. Figure 2.14 indicates that the electron concentration from 60 to 90 km is enhanced on anomalous days by as much as a factor of 10.

There have been many suggestions as to the origin of the winter

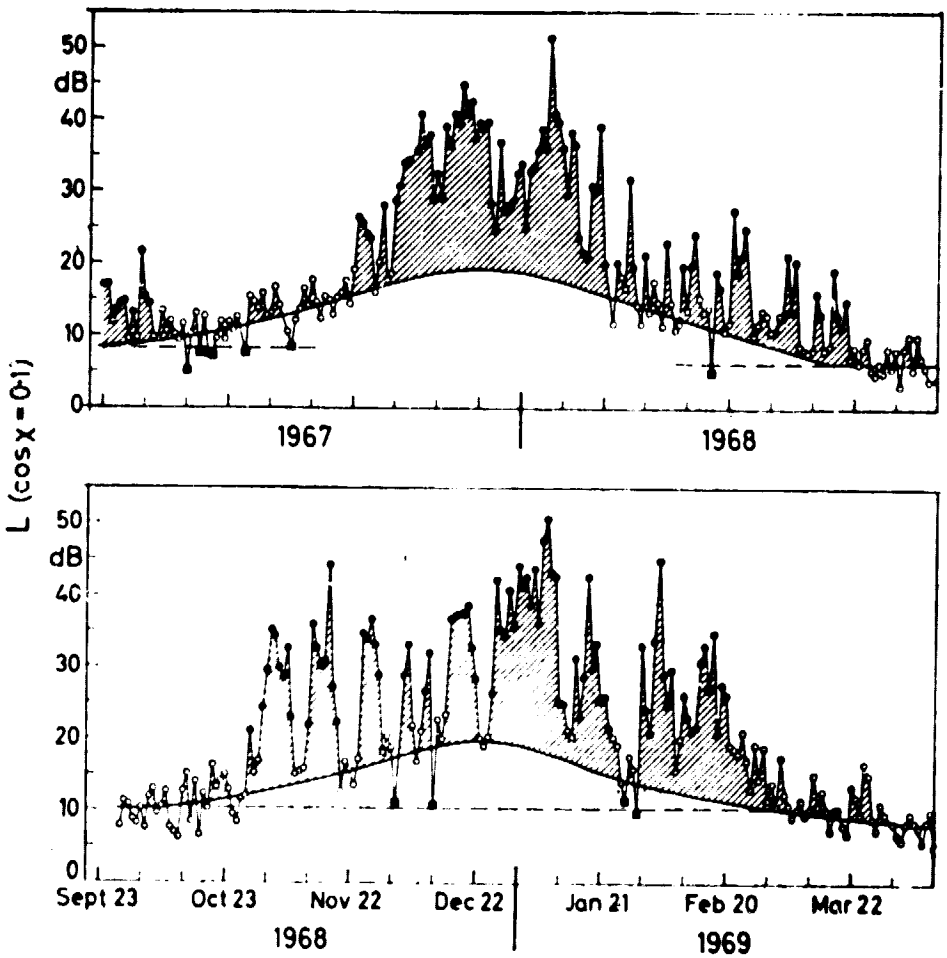

Figure 2.13 Absorption measurements made over Germany for two winters, as reported in SCHWENTEK [1971].

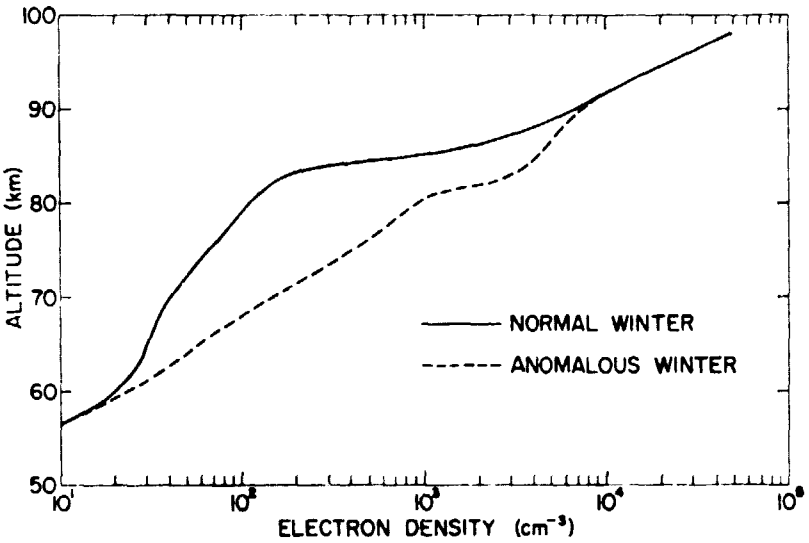

Figure 2.14 Idealized electron-density profiles characteristic of winter normal conditions and winter anomalous conditions, from GELLER and SECHRIST [1971].

anomaly, but the actual mechanism which causes the increase in electron concentration is still uncertain. OFFERMANN [1979] in his recent review paper, has summarized the possible causes of enhanced electron density as follows:

(1) Increase of electron production rate,

(2) Decrease of effective electron loss rate.

Both of these effects may be brought about by:

(1) Vertical and/or horizontal transports of minor atmospheric constituents with low ionization potential or with the ability to enter relevant chemical reactions.

(2) Temperature variations affecting neutral and/or ion chemistry.

In our study, we will primarily be concerned with the possibility of an increase of electron production rate due to vertical and/or horizontal transport of nitric oxide.

Most free electrons in the D region are a result of the ionization of NO by Lyman α radiation, as follows

$$NO + h\nu(1216\text{Å}) \rightarrow NO^{+} + e^{-} \qquad (2.10)$$

Thus, changes in the NO concentration could affect the electron concentration. GREGORY [1965] suggested that changes in the atmospheric circulation could affect the distribution of ionization in the mesosphere. SECHRIST [1967] proposed that the increase in electron concentration was due to an increase in the nitric oxide concentration. He proposed that a temperature increase in the D region would increase the equilibrium concentration. However, GEISLER and DICKINSON [1968] indicated that NO was not in photochemical equilibrium in the region due to the lack of atomic nitrogen. They suggested that the change in concentration of NO could be accomplished by transport due to transient planetary waves.

CHRISTIE [1970] proposed that the transport of NO through the mesopause was similar to the transport of ozone through the tropopause. MANSON [1971] suggested that equatorward flow could transport NO from the auroral zone where it is produced to midlatitudes, where it would enhance the electron concentration due to ionization by increasing Lyman α. This idea was also expressed by GELLER et al. [1976]. HESS and GELLER [1978] showed a correlation between southward winds and electron densities during winter at D region heights. In a similar study, MEEK and MANSON [1978] found some evidence of transports, but they could not determine if the effect was large scale or localized.

LABITZKE et al. [1979] have analyzed atmospheric data from various sources obtained during the Western European Winter Anomaly Campaign. An attempt was made to correlate wind velocity and direction, temperature, and electron concentration at about 85 km. The analysis was performed for two locations, one in Germany, and one in Spain. Some results of this study are shown in Figure 2.15. Note that on 31 Dec. 1975 and 28 Jan. 1976, advection from the northwest was associated with periods of high absorption at both sites, but that on 21 Jan. 1976, only low or moderate absorption was observed. Also, note that on 4 Feb., 14 Jan., and 21 Jan. 1976, upward motion was associated with low absorption over Germany. However, on 6 Jan., upward motion was associated with excessive absorption. LABITZKE et al. [1979] concluded that no clear correlation existed between temperature of the region and the enhancement of absorption. They did note, however, that horizontal advection from the north during periods of low temperature seemed to lead to high absorption. Also, upward motion could possibly produce low absorption in spite of high temperatures. They concluded that both the winds and temperatures associated with planetary

DATE	NORDDEICH LINDAU (NL) LARGE SCALE CIRCULATION	CH, 3000 [mW/]	ABSORPTION [dB]	ARANJUEZ-BALERMA (AB) LARGE SCALE CIRCULATION	CH, 3000 [mW/]	ABSORPTION [dB]
31 DEC 1975	ADVECTION FROM NORTHWEST.	COLD, 37	HIGH, +19	ADVECTION FROM NORTHWEST.	COLD, 34	HIGH, +15
	NL AND AB BELONG TO THE SAME AIR FLOW WITH HORIZONTAL ADVECTION FROM THE NORTHWEST. VERTICAL MOTIONS ARE WEAK. UNDISTURBED TEMPERATURE PROFILES CAN BE ASSUMED IN THE MESOSPHERE, WITH MESOPAUSE TEMPERATURES BELOW – 100 C AT ABOUT 80 KM.					
28 JAN. 1976	ADVECTION FROM NORTHWEST.	COLD, 37	EXCESSIVE, +24	ADVECTION FROM NORTHWEST.	COLD, 35	EXCESSIVE, +28
	NL AND AB BELONG TO THE SAME AIR FLOW WITH HORIZONTAL ADVECTION FROM THE NORTHWEST, SIMILAR TO 31 DECEMBER 1975, VERTICAL MOTIONS ARE WEAK.					
7 JAN 1976	FLOW FROM EAST, ANTICYCLONE DUE TO STRATWARM DOWNWARD MOTION ON 7 JAN.	5-6 JAN. COLD, 34 7-8 JAN. WARM, 40	LOW, +1/+5 HIGH +15/+19	STRONG WIND FROM WNW, WEAK UPWARD MOTION	6 JAN. COLD, 34 8 JAN. WARM, 38	EXCESSIVE, +26 LOW, +4
	IT SCHOULD BE NOTED THAT ON 5/6 JAN. THE MESOSPHERE REGION WAS COLD DUE TO THE INTENSE STRATOSPH. WARMING, THIS REGIME MOVED TO THE EAST AND THE MESOPAUSE REGION WARMED ON 7/8 JAN.			IN CONTRAST TO CONDITIONS OVER CENTRAL EUROPE SPAIN REMAINED IN A FLOW FROM THE WESTNORTH-WEST.		
4 FEB 1976	FLOW FROM NORTH, STRONG UPWARD MOTION	COLD, 37	LOW, 1	FLOW FROM NORTH-EAST, WEAK DOWNWARD MOTION.	COLD, 34	LOW +1
	GENERAL FLOW FROM NORTH OR NORTHEAST OVER EUROPE, DUE TO INTENSE RIDGE OVER THE ATLANTIC CAUSED BY STRATOSPH. WARMING, (COMP. SECTION 3).					
14 JAN. 1976	FLOW FROM NORTH, UPWARD MOTION	13 JAN. WARM, 41	LOW, +1	FLOW FROM NORTH-WEST.	13 JAN. WARM, 38	HIGH, +13
	DESPITE HORIZONTAL ADVECTION FROM THE NORTH AND WARM MESOPAUSE REGION, LOW ABSORPTION. IT IS SUGESTED THAT THIS IS DUE TO UPWARD MOTIONS.			WARM MESOPAUSE REGION FAVOURABLE FOR HIGH ABSORPTION.		
21 JAN 1976	FLOW FROM NORTH-WEST, UPWARD MOTION	WARM, 40	LOW, +4	FLOW FROM NORTH-WEST, WEAK UP-WARD MOTION	WARM, 38	MODERATE, +6
	SIMILAR TO 14 JANUARY			SIMILAR TO 14 JANUARY		

Figure 2.15 Comparison of large-scale circulation, temperature of the mesopause region, and ionospheric absorption over NW Germany and SW Spain, as presented in LABITZKE et al. [1979].

wave activity need to be considered to gain an understanding of the behavior of absorption at a particular location in winter.

2.6 *Eulerian Versus Lagrangian Mean Viewpoints*

The modeling studies presented in later sections are performed using an Eulerian framework; i.e., particle motions are measured relative to a fixed coordinate system. In this framework, transports due to both the zonal mean motion and the wave motion must be considered. Convergences of heat and momentum fluxes associated with a propagating planetary wave induce a secondary meridional circulation which tends to cancel out the effect of wave motions. In fact, in the absence of dissipation and critical levels, this cancellation is complete, and the wave has no net effect on the zonal mean circulation. This result is known as the non-interaction theorem, and was first introduced by CHARNEY and DRAZIN [1961]. A comprehensive theory of the noninteraction of waves and mean flow in the Eulerian framework is presented in BOYD [1976].

When considering the transport of trace constituents in the upper atmosphere, this tendency for cancellation of wave and mean transport exists even though dissipation is present. In an Eulerian calculation, care must be taken to include not only the effects of the planetary wave transports themselves, but also the transports due to the wave-induced circulation. A consideration of zonal mean or wave transports independently could lead to erroneous conclusions. Discussions of the transport of trace constituents in the stratosphere are given in MAHLMAN and MOXIM [1978] and HOLTON [1980b].

An alternative to the use of the Eulerian framework in the study of tracer transports has arisen with the development of the Lagrangian mean theory by ANDREWS and MCINTYRE [1976, 1978a,b]. In this framework,

motions are viewed as the displacement of the center of mass of an ensemble of particles from an original equilibrium position. This ensemble, in the absence of wave activity, can be characterized as a tube of material extending around the globe at a particular latitude and height. In order for transport to occur, the center of mass of this tube must be displaced from its original equilibrium position; this displacement is measured in terms of Lagrangian coordinates, and the displacement velocity is called the Lagrangian mean velocity.

The effect of wave motion on this material tube has been discussed by ANDREWS and MCINTYRE [1978a] and DUNKERTON [1978]. Andrews and McIntyre consider the situation of a string of fluid parcels which are connected by "elastic bands" to an imaginary "massless rod". The massless rod is constrained to be parallel to a latitude circle, and the effect of the wave is to displace the particles from their initial position along the rod. These individual displacements are measured in Lagrangian coordinates, and the average of the individual particle motions over the entire rod is equivalent to the Lagrangian mean motion. For a small amplitude wave in the absence of critical levels and dissipation, this average motion is zero, which is simply a manifestation of the noninteraction theory as viewed in the Lagrangian framework [ANDREWS and MCINTYRE, 1976].

In the actual atmosphere, the effects of critical levels and dissipation must be considered. In cases where the criteria for non-acceleration are violated, the effect of the wave on the individual air parcels is such that the ensemble average is non-zero, and hence an acceleration of the center of mass of the particles and a motion of the massless rod results. Several examples of this effect are discussed by MCINTYRE [1980], and a

review of Lagrangian theory in relation to nonacceleration is given by DUNKERTON [1980].

The mean motions in Lagrangian and Eulerian frameworks can be related through the use of the Stokes drift, which is essentially a measure of the effect of wave fluxes on the mean motion. The relation between Lagrangian ($\vec{v}_L$) and Eulerian ($\vec{v}_E$) velocities can be expressed as

$$\vec{v}_L = \vec{v}_E + \vec{v}_s$$

where $\vec{v}_s$ represents the Stokes drift, which is a function of the wave amplitude. In the case where the non-acceleration theorem is valid, the Stokes drift is exactly cancelled by the wave-induced secondary mean circulation. In this case, the Lagrangian circulation is just equal to the thermally-driven diabatic circulation, a fact noted by DUNKERTON [1978] in his study of the stratospheric Lagrangian circulation. When the conditions for nonacceleration are not met, such as at a critical level, the wave contribution to the Lagrangian mean motion through the Stokes drift may be large. MATSUNO and NAKAMURA [1979] have used a numerical model to investigate this critical layer effect in a study of the Lagrangian flow during a sudden stratospheric warming. They determined that the effect of the Stokes drift is large, giving rise to large differences in the Eulerian and Lagrangian circulations. SCHOEBERL [1981] also performed a numerical study which indicated that the Lagrangian mean flow resulting from damped planetary waves in the stratosphere was nearly twice as strong as the diabatic circulation. Thus, for cases in which realistic winds and damping are considered, planetary waves do make a significant contribution to the Lagrangian circulation.

The theoretical implications of the Lagrangian mean formalism have been investigated by DUNKERTON [1978] and PLUMB [1979]. In the Eulerian

framework, the effects of both the Eulerian mean circulation and wave motions on the tracer concentration must be considered. In the Lagrangian framework, however, tracer motion can be determined from the Lagrangian mean velocities only. Thus, the Lagrangian framework would appear to be the more natural choice for a discussion of tracer motion. A review of the Lagrangian approach to tracer transport in the stratosphere is presented by MATSUNO [1980].

Unfortunately, the Lagrangian equations do not readily lend themselves to numerical simulation, especially in the case of large amplitude waves and non-conservative tracers. For large amplitude waves, computational difficulties may arise from the large particle displacements from equilibrium over a long period of time. With a non-conservative tracer, sources and sinks for the tracer exist within the modeling region. Thus, not only the average position of the ensemble is important, but also the position of the individual parcels with respect to the source and sink regions. In these situations, which include the one we will attempt to model in later chapters, an Eulerian approach may allow a simpler model to be used. The Eulerian approach has been used effectively by HARTMANN and GARCIA [1979] and KURZEJA [1981] in studies of transport of ozone by planetary waves, and by SOLOMON [1981] in a study of nitric oxide transport by mean meridional winds and diffusion.

The effects of transience and sinks on transport by small amplitude waves have been investigated theoretically by PLUMB [1979]. For a steady wave and conservative tracer, he found that transport was due simply to advection by the Lagrangian mean flow. For a conservative tracer and growing wave, the Lagrangian eddy flux could be represented as the sum of advective and diffusion-like terms. He obtained a similar result for the

case of a steady wave and non-conserved tracer; however, the rate of "diffusion" in the second case was dependent on the loss rate in the sink regions. This implies that tracers having different loss rates will be transported at different rates. A second implication of his study is that the eddy fluxes of a conservative tracer are not necessarily down gradient, but can in fact be upgradient for a decaying wave.

In this section, a discussion of Lagrangian and Eulerian frames of reference was presented. The Lagrangian formalism provides a simple theoretical explanation of the noninteraction theorem, and has important applications concerning the transport of conservative tracers by small scale waves. The Eulerian approach has been more widely used in numerical modeling because of difficulties associated with the Lagrangian formalism. Calculations made in either framework should be consistent; however, calculations can be more easily made using the Eulerian approach. In our studies, the Eulerian framework will be used, but reference will be made at times to certain aspects of the Lagrangian formalism if a result can be clarified.

2.7 *Summary*

In this chapter, a review of the topics relevent to the thesis problem was presented. In Section 2.1, stationary planetary waves were discussed. They represent a major source of motion in the upper atmosphere, and the convergences of planetary wave momentum and heat fluxes can significantly affect the zonal mean circulation. The amplitude of these waves was seen to increase with height, and the phase exhibited a westward tilt with height in regions where the wave was propagating energy vertically. The wave structure was seen to have a strong dependence on the zonal mean wind profile.

In Section 2.2, traveling planetary waves were considered. These waves can be classified by period into two groups, the 5-day wave and the 16-day wave. Although the evidence is not conclusive, these waves appear to be free Rossby wave modes, that is, resonant modes of the atmosphere exhibiting no phase tilt with height. However, there is some evidence to indicate a westward phase tilt with height for the 16-day wave, which is typical of a forced planetary wave model.

In Section 2.3, the zonal mean circulation was examined. In the winter hemisphere, the wind structure is typified by a tropospheric and an upper stratospheric jet, the polar night jet. The strength of the polar night jet typically ranges from 60 to 85 m/sec from the west (westerly). The wind structure is determined both by asymmetries in solar heating and by inputs of energy into the zonal mean from planetary wave momentum and heat flux convergences. The interrelation between wave and mean is discussed in Section 2.4, where it is seen that wave inputs can significantly affect the zonal mean circulation, such as during a stratospheric warming phenomenon. The results of attempts at modeling this complex interactive system are discussed, and the results of these modeling studies are examined in light of observational results.

In Section 2.5, a review of nitric oxide chemistry is presented. Although the complete chemistry of the middle atmosphere is quite complex, the important reactions affecting the nitric oxide distribution are summarized with only a few reactions. The role of nitric oxide in the winter anomaly phenomenon is also examined, and studies concerning transport of nitric oxide by winds and wave motions are briefly discussed.

In Section 2.6, the question of Eulerian versus Lagrangian frameworks is discussed, and the Lagrangian theory is presented in a simplified

manner. Although the transport of a conservative trace constituent is simplified when viewed in a Lagrangian framework, reasons for performing numerical modeling in the Eulerian framework were presented.

In future chapters, we hope to tie the preceding subjects together by determining the effect of planetary wave winds on the nitric oxide concentration in the upper atmosphere. Initially, studies will be performed using stationary planetary waves and a time-independent meridional circulation and nitric oxide concentration. Then, the steady-state restriction will be removed, and the effects of the waves on the nitric oxide concentration will be considered in a time-dependent framework. A time-dependent numerical model will be used to calculate the effects of changes in wave structure and wave-induced changes in the meridional circulation on the nitric oxide distribution.

3. NUMERICAL MODEL

This chapter discusses the model used to study the transport of nitric oxide by zonal mean and planetary wave winds. Section 1 discusses the various approaches that could be used in studying this problem. Section 2 presents the zonal mean equations used, while Section 3 deals with the planetary wave propagation equation. Section 4 discusses the numerical scheme used to solve these equations, and Section 5 describes the method of calculating changes in the nitric oxide concentration due to transports by zonal mean and planetary wave winds. Section 6 ties these various modeling sections together by outlining the operation of the model. Some limitations are also discussed.

3.1 *Zonal Mean Circulation*

The equations used to describe the zonal mean circulation are similar to those used by SCHOEBERL and STROBEL [1978] in their study of the zonal mean circulation. In this model, the zonal mean circulation is driven not only by solar heating (and radiative cooling), but also by terms which represent the convergences of planetary wave momentum and heat fluxes. The scaling arguments which lead to these equations are presented in LEOVY [1964] and are also discussed in HOLTON [1975].

In the following development, an overbar represents a zonally-averaged quantity, determined as follows:

$$\overline{(\ )} = \frac{1}{2\pi} \int_0^{2\pi} (\ )\, d\lambda$$

$(\ )'$ represents a perturbation from the zonal mean, and $\langle\ \rangle$ represents a global (latitude and longitude) average. This definition of overbar is slightly different from that used by SCHOEBERL and STROBEL [1978], and results in a slightly modified set of equations. Also, we retain the

Eulerian time derivatives used by LEOVY [1964]. The resulting momentum and thermodynamic equations are as follows:

$$(\frac{\partial}{\partial t} + \beta_p)\bar{u} + 2\Omega\ \bar{v}\ \sin\theta = -\frac{1}{a\cos^2\theta}\frac{\partial}{\partial\theta}\ \overline{u'v'}\ \cos^2\theta \tag{3.1}$$

$$\frac{\partial}{\partial t}\ (R\bar{T}) + \frac{1}{a\cos\theta}\frac{\partial}{\partial\theta}\ \overline{v'\phi_z'}\ \cos\theta + (2\Omega a)^2\ s\bar{\omega}$$

$$= R[\bar{H} - \langle H\rangle - \alpha_0\ (\bar{T} - \langle T\rangle)] \tag{3.2}$$

The continuity equations in log pressure coordinates are given by

$$\frac{1}{a\cos\theta}\frac{\partial}{\partial\theta}\ \bar{v}\ \cos\theta + \bar{\omega} - \frac{\partial\bar{\omega}}{\partial z} = 0 \tag{3.3}$$

The geostrophic balance and hydrostatic balance equations are expressed as

$$2\Omega\ \bar{u}\ \sin\theta = -\frac{1}{a}\frac{\partial\bar{\phi}}{\partial\theta} \tag{3.4}$$

$$R\bar{T} = \frac{\partial\bar{\phi}}{\partial z} \tag{3.5}$$

Equations 3.4 and 3.5 can be combined to produce the thermal wind equation,

$$\frac{1}{a}\frac{\partial\bar{T}}{\partial\theta} = -\frac{f}{R}\frac{\partial\bar{u}}{\partial z} \tag{3.6}$$

This equation relates the horizontal temperature gradient to the vertical wind shear. In equations 3.1-3.6, we have used the following notations.

λ longitude

θ latitude

p pressure

p_0 reference pressure

a mean radius of the earth

Ω angular rotation frequency of the earth

z = log pressure height defined as $\ln(p_0/p)$

ω = dz/dt, vertical velocity in log pressure coordinates

u, v eastward (zonal), northward (meridional) velocity

β_r Rayleigh friction coefficient

a_0 Newtonian cooling coefficient

g acceleration due to gravity

ϕ geopotential

R gas constant for dry air

T temperature

c_p specific heat at constant pressure

k R/c_p

s static stability, given by $s = \frac{R}{(2\Omega a)^2}\left(k\overline{T} + \frac{\partial \overline{T}}{\partial z}\right)$

H heating rate per unit mass in degrees Kelvin/day

β_r in equation 3.1 is the Rayleigh friction coefficient, and is a parameterization of the nonlinear effects of small-scale waves and turbulence on the zonal mean circulation. Although there is no theoretical method for calculating the value of β_r, studies by SCHOEBERL and STROBEL [1978] and HOLTON and WEHRBEIN [1980a] have indicated that this parameterized damping is necessary in order to adequately simulate the observed zonal mean circulation. The damping used in our model will be similar to that used by SCHOEBERL and STROBEL [1978].

In equation 3.2, $\overline{H} - \langle H \rangle$ represents the differential heating due to incoming solar radiation absorbed at a particular level. The variation of heating with latitude is primarily due to earth-sun geometry. The differential heating used in SCHOEBERL and STROBEL [1978] was obtained through a self-consistent calculation based on a parameterization scheme for the absorption of solar radiation by ozone introduced by LINDZEN and WILL [1973].

Our model does not include a calculation of differential heating;

instead, we will use the differential heating as given in SCHOEBERL and STROBEL [1978]. The a_0 in equation 3.2 represents the Newtonian cooling parameterization, which represents cooling to space due to the emission of infrared radiation by CO_2 and water vapor. This cooling serves to relax the atmospheric temperature back to its equilibrium value. Again, we will use the Newtonian cooling profile as given in SCHOEBERL and STROBEL [1978] which is based on calculations by DICKINSON [1973].

The derivation of the zonal mean propagation equation proceeds as follows. Equations 3.1 and 3.2 are solved for $\bar{v}$ and $\bar{\omega}$ respectively, and the result is substituted into equation 3.3, the continuity equation. After some manipulation, an equation for the zonal mean circulation in terms of the geopotential ϕ is obtained, as follows:

$$\left(\frac{\partial}{\partial t} + \beta_r\right) \frac{\sin^2\theta}{\cos\theta} \frac{\partial}{\partial\theta} \frac{\cos\theta}{\sin^2\theta} \frac{\partial\bar{\phi}}{\partial\theta} + \left(\frac{\partial}{\partial t} + a_0\right)\left(\sin^2\theta\, e^z \frac{\partial}{\partial z} \frac{e^{-z}}{s} \frac{\partial\phi}{\partial z}\right)$$

$$+ \frac{\partial a_0}{\partial z} \frac{\sin^2\theta}{s} \frac{\partial\bar{\phi}}{\partial z} = \sin^2\theta\, e^z \frac{\partial}{\partial z} \frac{e^{-z}}{s} R(\bar{H} - \langle H\rangle + a_0 \langle T\rangle)$$

$$+ 2\Omega \frac{\sin^2}{\cos} \frac{\partial}{\partial\theta} \frac{1}{\cos\theta\sin\theta} \frac{\partial}{\partial\theta} \overline{u'v'} \cos\theta$$

$$- \frac{\sin^2}{a\cos\theta} e^z \frac{\partial}{\partial z} \frac{e^{-z}}{s} \frac{\partial}{\partial\theta} \overline{v'\phi'}_z \cos\theta \qquad (3.7)$$

If the time step chosen (ΔT) is small enough, the Eulerian time derivative can be expressed as

$$\frac{\partial\phi}{\partial t} = \frac{\phi^t - \phi^{t-1}}{\Delta t} \qquad (3.8)$$

Making this substitution, we can eventually reduce the equation for the zonal mean circulation to the form

$$A \frac{\partial^2\psi}{\partial z^2} + B \frac{\partial\psi}{\partial z} + C \frac{\partial^2\psi}{\partial\theta^2} + D \frac{\partial\psi}{\partial\theta} + E\psi = F \qquad (3.9)$$

where

$$A = \frac{a_0^t}{\beta_r^t}$$

$$B = \frac{1}{\beta_r} \frac{\partial a_0^t}{\partial z} - \frac{a_0^t}{\beta_r^t} \left(1 + \frac{1}{s} \frac{\partial s}{\partial z}\right)$$

$$C = \frac{s}{\sin^2\theta}$$

$$D = -\frac{(1 + \cos^2\theta)s}{\sin^3\theta \cos\theta}$$

$$E = 0$$

$$F = \text{Heat} + \text{Flux} + \text{Time}$$

Here we have used the following expressions

$$a_0^t = a_0 + 1/\Delta t \tag{3.10}$$

$$\beta_r^t = \beta_r + 1/\Delta t \tag{3.11}$$

$$\text{Heat} = \frac{s}{\beta_r^t} e^z \frac{\partial}{\partial z} \frac{e^{-z}}{s} \left(R\bar{H} - \langle H \rangle + a_0 \langle T \rangle\right) \tag{3.12}$$

$$\text{Flux} = \frac{s}{\beta_r^t \cos\theta} \left[\frac{\partial}{\partial\theta} \frac{2\Omega}{\cos\theta\sin\theta} \frac{\partial}{\partial\theta} \overline{u'v'} \cos^2\theta - \frac{e^z}{a} \frac{\partial}{\partial z} \frac{e^{-z}}{s} \frac{\partial}{\partial\theta} \overline{v'\phi_z'} \cos\theta\right] \tag{3.13}$$

$$\text{Time} = \frac{s}{\beta_r^t \Delta t} \left(\frac{1}{\cos\theta} \frac{\partial}{\partial\theta} \frac{\cos\theta}{\sin^2\theta} \frac{\partial}{\partial\theta} + e^z \frac{\partial}{\partial z} \frac{e^{-z}}{s} \frac{\partial}{\partial z}\right) \phi^{t-1} \tag{3.14}$$

With the equation in this form, it can be solved using a numerical scheme outlined in LINDZEN and KUO [1969]. This numerical scheme will be discussed in detail in Section 3.3.

3.2 *Planetary Wave Model*

The planetary wave propagation model that will be used in this research is based on a equation derived from the linearized thermodynamic and vorticity equations. The variables in these equations are expressed as the sum of a zonal mean and a perturbation from the mean. The two equations are combined, retaining only the first order terms. The perturbation terms are then expressed in terms of the perturbation geopotential ϕ'. The result is an equation containing ϕ' and other variables representing the basic state, which is considered to be a known quantity. The solution is then obtained numerically, as outlined in Section 3.3.

The equation for quasi-geostrophic planetary wave motions on a spherical earth was given by SCHOEBERL and GELLER [1977] and solved for stationary waves. The equation was modified by AVERY [1978] to include steady-state forcing by topographical and thermal sources. The time dependence in the thermodynamic and momentum equations will be retained in order to derive a time-dependent planetary wave equation, which will be coupled with the time-dependent zonal mean equaton outlined in the previous section.

The derivation of the the time-dependent equation begins with the linearized perturbation vorticity and thermodynamic equations

$$\left(\frac{\partial}{\partial t} + \tilde{u}\,\frac{\partial}{\partial \lambda} + \beta_r\right)\xi' + \frac{v'}{a}\,\frac{\partial \bar{z}}{\partial \theta} - 2\Omega \sin\theta\, e^{z}\,\frac{\partial}{\partial z}\, e^{-z}\,\omega' = 0 \qquad (3.15)$$

$$\left(\frac{\partial}{\partial t} + \tilde{u}\,\frac{\partial T'}{\partial \lambda} + \frac{v'}{a}\right)\frac{\partial \bar{T}}{\partial \theta} + \omega'\left(\frac{\partial \bar{T}}{\partial z} + k\bar{T}\right) = H' - a_0 T' \qquad (3.16)$$

where the new variables introduced are as follows:

$\tilde{u}$ angular speed of basic zonal flow,

ξ' vertical component of vorticity $= \dfrac{\partial v'}{a\cos\theta\ \partial\lambda} - \dfrac{1}{a}\dfrac{\partial u'}{\partial \theta}$

H' = longitudinally asymmetric heating rate per unit mass in degrees Kelvin/day.

As before, an overbar denotes a zonally averaged quantity, and a prime denotes a perturbation from that average.

Using the perturbation hydrostatic relation:

$$RT' = \frac{\partial \phi'}{\partial z} \tag{3.17}$$

and the thermal wind equation 3.6, T' and $\partial \overline{T}/\partial\theta$ can be eliminated from equations 3.15 and 3.16. Then the geostrophic approximation is applied, so that u' and v' can be expressed in terms of ϕ', as follows:

$$u' = -\frac{1}{2\Omega a \sin\theta} \frac{\partial \phi'}{\partial \theta} \tag{3.18}$$

$$v' = \frac{1}{2\Omega a \cos\theta \sin\theta} \frac{\partial \phi'}{\partial \lambda} \tag{3.19}$$

A small non-geostrophic component must be added to v' in order to preserve energetic consistency [MATSUNO, 1970], giving

$$v' = \frac{1}{2\Omega a \sin\theta} \left[\frac{1}{\cos\theta} \frac{\partial \phi'}{\partial \lambda} - \frac{1}{2\Omega \sin\theta} \left(\frac{\partial}{\partial t} + \tilde{u} \frac{\partial}{\partial \lambda}\right) \frac{\partial \phi'}{\partial \theta}\right] \tag{3.20}$$

Equation 3.16 is solved for ω', and the expressions for u', v', and ω' are substituted into the vorticity equation 3.16. This results in a single equation in ϕ', the perturbation geopotential.

$$\left(\frac{\partial}{\partial t} + \tilde{u} \frac{\partial}{\partial \lambda} + \beta_r\right) \frac{\sin^2\theta}{\cos\theta} \frac{\partial \phi}{\partial \theta} \frac{\cos\theta}{\sin^2\theta} \frac{\partial \phi'}{\partial \theta} + \frac{1}{\cos^2\theta} \frac{\partial^2 \phi'}{\partial \lambda^2}$$

$$+ \left(\frac{\partial}{\partial t} + \tilde{u} \frac{\partial}{\partial \lambda} + a_0\right) \sin^2\theta \, e^z \frac{\partial}{\partial z} \frac{e^{-z}}{s} \frac{\partial \phi'}{\partial z} + \frac{1}{\cos\theta} \frac{\partial \phi'}{\partial \lambda} \frac{\partial \overline{q}}{\partial \theta}$$

$$+ \frac{\sin^2\theta}{s} \frac{\partial a_0}{\partial z} \frac{\partial \phi'}{\partial z} = \sin^2\theta \, e^z \frac{\partial}{\partial z} \frac{e^{-z}}{s} R J' \tag{3.21}$$

where $$\frac{\partial \overline{q}}{\partial \theta} = \cos\theta \left[2(\Omega + u) + 3\tan\theta \frac{\partial \tilde{u}}{\partial \phi} - \frac{\partial^2 u}{\partial \theta^2} - \sin^2\theta \, e^z \frac{\partial}{\partial z} \frac{e^{-z}}{s} \frac{\partial \tilde{u}}{\partial z}\right]$$

In order to solve this equation, we assume that the perturbation

quantities can be expanded in a Fourier series in longitude and a Fourier integral in time as outlined in SCHOEBERL and GELLER [1976]

$$( )' = \sum_{m=-\infty}^{\infty} e^{im\lambda} \frac{1}{2\pi} \int_{-\infty}^{\infty} e^{i\sigma t} ( )'_{m,\sigma} \, d\sigma \tag{3.22}$$

where

$$( )'_{m,\sigma} = \frac{1}{2\pi} \int_0^{2\pi} e^{-im\lambda} \int_{-\infty}^{\infty} e^{-i\sigma t} ( )' \, dt \, d\lambda$$

Here σ is the frequency, and m is the zonal wave number. The frequency can be complex; however, an imaginary σ causing the disturbance to grow with time could eventually invalidate the assumptions of linearity upon which equations 3.15 and 3.16 are based. In our iterative model, we will consider only those cases in which the growth of the perturbation with time is small or equal to zero. In this way, the scaling assumptions made in order to obtain the planetary wave equation will not be violated. Scaling arguments presented in SCHOEBERL and GELLER [1976] indicate that the planetary wave equation is valid over the height range under consideration for values of m and σ such that $m \leq 2$ and $\frac{2\pi}{\sigma} > 10$ days.

Using the form as given in equation 3.22 for the primed variables, we can evaluate the time and longitudinal derivatives in equation 3.21. We also make the substitution

$$\psi_{m,\sigma}(\theta,z) = \frac{e^{-z/2}}{\sqrt{s}} \phi_{m,\sigma}(\theta,z) \tag{3.23}$$

After some manipulation, we obtain the equation

$$\frac{\sin^2\theta}{\cos\theta} \frac{\partial}{\partial\theta} \frac{\cos\theta}{\sin^2\theta} \frac{\partial\psi_{m,\sigma}}{\partial\theta} + Q_{m,\sigma} \psi_{m,\sigma} + \frac{\nu_1}{\nu_0} \frac{\sin\theta}{s} \frac{\partial^2\psi_{m,\theta}}{\partial z^2}$$

$$- \frac{i\sin^2}{\nu_0} \frac{\partial z_0}{\partial z} \frac{1}{s} \frac{\partial\psi_{m,\sigma}}{\partial z} = -i \, \zeta_{m,\sigma} \tag{3.24}$$

where $\nu_0 = \sigma + \tilde{u}m - i\beta_r$

$$\nu_1 = \sigma + \tilde{u}m - ia_0$$

$$Q_{m,\sigma} = \frac{m\frac{\partial q}{\partial \theta}}{\cos\theta\ \nu_0} + \frac{\nu_1}{\nu_0}\frac{\sin^2\theta}{s}\tau$$

$$- \frac{i\sin^2\theta}{\nu_0}\frac{\partial a_0}{\partial z}\frac{1}{2s}\left(1 + \frac{1}{s}\frac{\partial s}{\partial z}\right) - \frac{m^2}{\cos^2\theta} \qquad (3.25)$$

$$\tau = -\frac{3}{4}\frac{1}{s^2}\left(\frac{\partial s}{\partial z}\right)^2 - \frac{1}{2s}\left(\frac{\partial s}{\partial z} - \frac{\partial^2 s}{\partial z^2}\right) - \frac{1}{4}$$

and $$G_{m,\theta} = \frac{\sin}{\sqrt{s}\ \nu_0} e^{z/2}\frac{\partial}{\partial z}\frac{e^{-z}}{s} RH'_m$$

Also, an expression for ω' in terms of ϕ' can be obtained from the thermodynamic equation by evaluating the longitudinal and time derivatives in equation 3.16 and by using the thermal wind and hydrostatic balance equations, as follows:

$$\omega' = \frac{RH' - i\nu_1\frac{\partial \phi'}{\partial z} + 2\Omega a\ \sin\theta\cos\theta\ \nu'\frac{\partial \tilde{u}}{\partial z}}{(2\Omega a)^2 s} \qquad (3.26)$$

The final step in the derivation of the planetary wave equation involves making the following change of variables, which somewhat simplifies the equation:

$$\psi'_{m,\sigma}(\theta,z) = \frac{e^{-z/2}}{\sqrt{s}}\phi'_{m,\sigma}(\theta,z) \qquad (3.27)$$

After some manipulation, equation 3.24 can be expressed in a form similar to that of the zonal mean equation 3.9. The subscripts σ and m have been omitted, but from now on $(\ )'$ will represent a single Fourier component in longitude and time, with the form $e^{i(m\lambda + \sigma t)}$. After making the change of variable, and assuming that the perturbation heating rate H' is zero, we

obtain

$$A \frac{\partial^2 \psi}{\partial z^2} + B \frac{\partial^2 \psi}{\partial z} + C \frac{\partial^2 \psi}{\partial \phi^2} + D \frac{\partial \psi}{\partial \theta} + E\psi = F \tag{3.28}$$

where

$$A = \frac{\nu_1}{\nu_0}$$

$$B = - \frac{i}{\sqrt{0}} \frac{\partial a_0}{\partial z}$$

$$C = \frac{s}{\sin^2 \theta}$$

$$D = \frac{-s(1 + \cos^2 \theta)}{\sin^3 \theta \cos \theta}$$

$$E = \frac{s}{\sin^2 \theta} Q_m^t$$

$$F = 0$$

In this form, the planetary wave propagation equation is a two-dimensional elliptical differential equation in latitude, θ, and log pressure height z.

By expressing the differentials in finite difference form and applying the numerical technique outlined in LINDZEN and KUO [1969], solutions as a function of latitude, longitude and height may be obtained. The solutions are in the form of an amplitude and phase at each point on a latitude-height grid. The method of solution will be outlined in Section 3.3.

Equation 3.28 represents a generalized planetary wave propagation equation for a wave of zonal wave number m and frequency σ. The planetary waves and winds obtained from the solution of equation 3.28 will be used as inputs to the zonal mean equation, which was described in Section 3.1.

By alternating the calculation of the zonal mean and the planetary waves, the interaction between the two can be determined. The effects of this wave-mean interaction on the nitric oxide distribution in the upper atmosphere can then be investigated.

3.3 *Numerical Method*

The method of solution of the zonal mean and the planetary wave equation is described in LINDZEN and KUO [1969]. The use of this method for planetary wave equations has been outlined in SCHOEBERL and GELLER [1976], and AVERY [1978]. Both the zonal mean and planetary wave equations have been written in the form

$$A \frac{\partial^2 \psi}{\partial z^2} + B \frac{\partial \psi}{\partial z} + C \frac{\partial^2 \psi}{\partial \theta^2} + D \frac{\partial \psi}{\partial \theta} + E\psi = F \tag{3.29}$$

where ψ either represents the mean geopotential or is related to the perturbation geopotential as given in equation 3.27. The coefficients A-F are complex quantities in the wave equation, and are real quantities in the zonal mean equation. Hence, the planetary wave equation is more difficult and costly to solve.

The solution of the generalized equation 3.29 proceeds as follows. The equation is first written in finite difference form using a five-point scheme, resulting in

$$(\bar{\bar{A}}_j + \Delta z\, \bar{\bar{B}}_j/2)\, \bar{\psi}_{j+1} + (\Delta z^2\, \bar{\bar{R}}_j - 2\bar{\bar{A}}_j)\, \bar{\psi}_j + (\bar{\bar{A}}_j - \Delta z\, \bar{\bar{B}}_m/2)\, \psi_{j-1} = \Delta z^2\, \bar{F}_j \tag{3.30}$$

Here $z = j\Delta z$, $\theta = k\Delta\theta$. $\bar{\bar{A}}$, $\bar{\bar{B}}$, and $\bar{\bar{R}}$ are square k_T by k_T matrices, where k_T is the number of meridional grid points. ψ_j is a column matrix of dimension k_r, with elements ψ_k^j. The elements of matrices $\bar{\bar{A}}$, $\bar{\bar{B}}$, and $\bar{\bar{R}}$ are as follows:

$$a^j_{k,k} = A(k\Delta\theta, j\Delta z)$$

$$b^j_{k,k} = B(k\Delta\theta, j\Delta z)$$

$$r^j_{k,k+1} = C(k\Delta\theta, j\Delta z)/\Delta\theta^2 + D(k\Delta\theta, j\Delta z)/2\Delta\theta$$

$$r^j_{k,k} = E(k\Delta\theta, j\Delta z) - 2C(k\Delta\theta, j\Delta z)/\Delta\theta^2$$

$$r^j_{k,k-1} = C(k\Delta\theta, j\Delta z)/\Delta\theta^2 - D(k\Delta\theta, j\psi\theta)/2\Delta\theta$$

All other elements are zero. $\overline{F}_j$ is a column vector, with elements $F(k\Delta\theta, j\Delta z)$. Next we assume, as indicated by LINDZEN and KUO [1969], that ψ_j can be expressed as follows:

$$\overline{\psi}_j = \overline{\overline{\Omega}}_j \overline{\psi}_{j+1} + \overline{B}_j$$

Here, $\overline{\overline{\Omega}}_j$ is an unknown square k_T by k_T matrix, and $\overline{B}_j$ is an unknown column matrix. We can eliminate ψ_{j-1} in equation 3.30 using 3.31, and obtain a recursion relation for $\overline{\overline{\Omega}}_j$ and $\overline{B}_j$.

$$\overline{\overline{\Omega}}_{j+1} = -[\Delta z^2 \overline{\overline{R}}_{j+1} - 2\overline{\overline{A}}_{j+1} + (\overline{\overline{A}}_{j+1} - \Delta z\, \overline{\overline{B}}_{j+1}/2)\overline{\overline{\Omega}}_j]^{-1}$$
$$(A_{j+1} + \Delta z\, \overline{\overline{B}}_{j+1}/2) \qquad (3.32)$$

$$\overline{B}_{j+1} = -[\Delta z^2 \overline{\overline{R}}_{j+1} - 2\overline{\overline{A}}_{j+1} + (\overline{\overline{A}}_{j+1} - \Delta z\, \overline{\overline{B}}_{j+1}/2)\overline{\overline{\Omega}}_j]^{-1}$$
$$((\overline{\overline{A}}_{j+1} - \Delta z\, \overline{\overline{B}}_{j+1}/2)\overline{B}_j - \overline{G}_j) \qquad (3.33)$$

At the lower boundary, ψ is specified by observations for both the zonal mean and the planetary wave case. These observations are discussed in Chapter 4. In order to match this boundary condition at level $j = 0$, we see from equation 3.31 that

$$\overline{\psi}_0 = \overline{B}_0 \text{ and } \overline{\overline{\Omega}}_0 = 0$$

Using these values of ψ_0 and B_0 and the recursion relations 3.32 and 3.33,

we can obtain values of $\bar{\bar{\psi}}_0$ and $\bar{\beta}_0$ at all levels. At the upper boundary, the planetary wave and zonal mean cases are treated separately.

A sponge layer boundary condition is applied at the upper boundary for the planetary wave by assuming $\psi' = 0$ at $z = z_{Top}$ [JONES and HOUGHTON, 1971]. This is accomplished by providing a region of increased damping called the sponge layer just below the upper boundary. The planetary wave amplitudes in the region of interest will not be affected by the sponge layer if the upper boundary lies sufficiently above the region of interest.

The upper boundary value for the zonal mean geopotential was determined from a postulated wind profile at the upper boundary. The mean geopotential at the equator was estimated for equilibrium conditions, and the geostrophic balance equation was used to fit the variation of mean geopotential with latitude to the postulated wind structure. Although this method is only approximate, the effect of the boundary condition is felt only near the upper level. Hence, if the upper boundary is chosen high enough, the effect on the region of interest will be minimal.

The horizontal boundary conditions, although not explicitly required by the numerical scheme, enter into the calculation of the coefficients of equation 3.30. The calculation of the matrix elements of $\bar{\bar{R}}$ requires a knowledge of the behavior of the wave function at the equator and pole. Since the zonal mean wind in this model approaches zero at the equator, it represents a critical level for the planetary wave. Thus, we have the condition $\psi' = 0$ at the equator. The fact that $u' = 0$ at the pole implies $\psi' = 0$ there also. The fact that the zonal mean wind $\bar{u}$ approaches zero at the equator and pole imposes the condition $\frac{\partial \Phi}{\partial \theta} = 0$ for the zonal mean geopotential at the latitudinal boundaries.

The calculations are performed on a 17 x 45 latitude height grid, extending from equator to pole and from 55 km to 150 km. The horizontal grid spacing ($\Delta\theta$) is 5° latitude, while the vertical grid size Δz is about 2 km. The time step ΔT is one hour for the zonal mean calculations.

3.4 *Nitric Oxide Equations*

The equations for transport of a trace constituent were first outlined in LINDZEN and GOODY [1965], and have been used by CLARK and ROGERS [1979] and HARTMANN and GARCIA [1979] to study the transport of ozone by planetary waves. They have also been used by PLUMB [1979] in his study of transport of conservative tracers by small amplitude waves. We will employ a similar set of equations to study the transport of nitric oxide by planetary waves in the upper mesosphere.

If n_m is the molecular number density of air, the approximate continuity equation can be written:

$$\frac{dn_m}{dt} + n_m \nabla\cdot\vec{v} = 0 \tag{3.34}$$

where $\frac{d}{dt}$ is the substantive derivative, and v is the velocity. Likewise, for the trace constituent, n_i, we can write

$$\frac{dn_i}{dt} + n_i \nabla\cdot\vec{v} = P_i \tag{3.35}$$

where P_i is the net rate of production of n_i. Solving 3.34 for $\nabla\cdot\vec{v}$, and substituting into 3.35, we obtain

$$\frac{dn_i}{dt} + \frac{n_i}{n_m}\frac{dn_m}{dt} = P_i \tag{3.36}$$

with the substitution $\gamma = \frac{n_i}{n_m}$, where γ = mixing ratio, we obtain

$$\frac{d\gamma}{dt} = P_i/n_m$$

where in log pressure coordinates,

$$\frac{d}{dt} = \frac{\partial}{\partial t} + \frac{u}{a\cos\theta}\frac{\partial}{\partial \lambda} + \frac{v}{a}\frac{\partial}{\partial \theta} + \omega \frac{\partial}{\partial z} \tag{3.37}$$

We now express γ in terms of a zonal mean and perturbation from that mean, i.e., $\gamma = \bar{\gamma} + \gamma'$. Taking a zonal average, and using the continuity equation, we obtain an equation for the time rate of change of $\bar{\gamma}$.

$$\frac{\partial \bar{\gamma}}{\partial t} + \frac{\bar{v}}{a}\frac{\partial \bar{\gamma}}{\partial \theta} + \bar{\omega}\frac{\partial \bar{\gamma}}{\partial z} + \frac{1}{a\cos\theta}\frac{\partial}{\partial \theta}\overline{v'\gamma'}\cos\theta + \left(\frac{\partial}{\partial z} - 1\right)\overline{\omega'\gamma'} = \frac{\bar{r}}{n_m} \tag{3.38}$$

Subtracting the zonal mean equation from the total equation, and linearizing, we obtain an equation for the perturbation mixing ratio, γ'.

$$\frac{\partial \gamma'}{\partial t} + \frac{\bar{u}}{a\cos\theta}\frac{\partial \gamma'}{\partial \lambda} + \frac{\bar{v}}{a}\frac{\partial \gamma'}{\partial \theta} + \frac{v'}{a}\frac{\partial \bar{\gamma}}{\partial \theta} + \omega'\frac{\partial \bar{\gamma}}{\partial z} + \bar{\omega}\frac{\partial \gamma'}{\partial z} = \frac{r'}{n_m} \tag{3.39}$$

Equations 3.7, 3.21, 3.38, and 3.39 represent a closed set of equations, which allow the calculation of transports of nitric oxide by the zonal mean and planetary wave winds.

A second method of calculating transport involves the use of a parameterization which ideally represents transport by all scales of motion other than the zonal mean motion. The first method involved an explicit calculation of the effects of large-scale planetary waves. The second method uses an eddy diffusion coefficient to parameterize the transport due to all scales of wave motion, including tides and gravity waves. This technique was employed by ROBLE and GARY [1979] to approximate the vertical transport of nitric oxide in the auroral zone. A transport calculation involving strictly planetary waves represents only one part of the total transport picture. EBEL [1980] has modeled eddy diffusion in the mesosphere, and has determined values of the coefficients based on studies of wind variance and potential temperature. He used an analysis which was essentially an extension of REED and GERMAN's [1965] study of the

stratosphere. The transport equations are as follows [EBEL, 1980].

The continuity equation for a trace constituent is as before

$$\frac{\partial n}{\partial t} + \nabla F = r \tag{3.40}$$

Here, F represents fluxes due to the zonal mean, represented as $\bar{n}\,\bar{v}$, and fluxes due to eddy motion, as in $\overline{n'v'}$. By using the eddy diffusion coefficients, the eddy fluxes can be related to the gradients of the mean concentration, as follows:

$$\begin{aligned}\overline{n'v'} &= -\bar{\rho}\, k \cdot \nabla(\bar{n}/\bar{\rho}) \\ &= -\bar{\rho}\, k \cdot \nabla\bar{\gamma}\end{aligned} \tag{3.41}$$

Thus, the contribution of wave fluxes to the zonal mean concentration can be obtained from a knowledge of the coefficient values and the gradient of the mean distribution. The parameterization allows for a determination of wave effects on the zonal mean concentration without a calculation of the actual wave amplitudes. EBEL's [1980] eddy diffusion coefficients have been used by SOLOMON [1981] in a two-dimensional photochemical model. The results of our calculations will be compared to the results from that model.

3.5 *Summary*

In this chapter, we have presented the various parts of the model that will be used to investigate the transport of nitric oxide by planetary waves. The model involves three main parts, the zonal mean circulation, the planetary waves, and the nitric oxide concentrations. Ideally, the model would be run with a one-hour time step. Starting with an initial zonal mean equilibrium state and a prescribed planetary wave forcing function, the planetary wave amplitude and momentum and heat fluxes could be calculated using this initial zonal mean state. The effect of the

combined zonal mean and planetary wave winds on an initial nitric oxide distribution would be determined and the nitric oxide concentration at time $T + \Delta T$ could be calculated. This procedure involves assuming that the zonal mean and planetary wave winds change little during the one-hour time period, and indeed this is the case. The divergences of eddy momentum and heat flux calculated at $T = T_0$ would then be used to calculate the zonal mean state at time $T + \Delta T$. Then, a new wave structure at time $T + \Delta T$ could be calculated. At this point, the whole cycle is repeated. Unfortunately, cost limitations prevent a calculation of the planetary wave structure every hour. Instead, the wave amplitude is calculated once every 24 hours. For a stationary wave calculation, this presents no problem, since the wave amplitudes are constant with time. For a traveling wave with constant angular velocity, the phase of the wave may shift with time but the products $\overline{v'T'}$ and $\overline{u'v'}$ remain constant. Thus, the effect of the traveling wave on the zonal mean circulation also remains constant in time. The quantities v' and ω' needed for the hourly calculation of NO and NO′ can be obtained by shifting the phase of the values of v' and ω' by $\sigma\Delta T$ each hour.

The main problem arises with an exponentially growing or decaying wave. Here, the effect is two-fold. First, the zonal mean circulation may not change as much as it should over one day, and secondly the transports due to v' and ω' will be underestimated. Test calculations have shown however, that if the growth rate of the planetary wave is restricted to 10%/day or less, the effect of the 1-hour vs. 24-hour time step is small.

In conclusion, the planetary wave amplitudes and fluxes are calculated every 24 hours. The zonal mean winds and nitric oxide calculations are

determined once every model hour. In the standing wave and constant frequency traveling wave cases, this poses no problem, and the error in the growing wave case is minimized if the growth ir amplitude is less than 10%/day.

4. OBSERVATIONAL ANALYSIS

In this chapter, we will present the results of an analysis of some observational geopotential height and nitric oxide concentration data. The geopotential height data is from the National Meteorological Center (NMC), and is in the form of a weekly averaged geopotential height map at .4 mb (55 km). These maps were analyzed for weekly and monthly averaged planetary wave structures. The nitric oxide data used was presented in CRAVENS and STEWART [1978], and was obtained from measurements made by the Atmospheric Explorer C (AE-C) satellite at 105 km. This data was also analyzed for wave-like structures. Although the nitric oxide and geopotential height data were taken at different height levels, they do cover the same time period (Winter, 1974-1975).

4.1 Geopotential

Northern Hemisphere Maps of .4 mb geopotential height were obtained for the 9 weeks of January 2 through February 27. These maps give the actual height in meters of the .4 mb pressure surface averaged over a one-week period. Values of geopotential height were read off at each point of a latitude-longitude grid, having grid increments of 5° latitude and 10° longitude. A Fourier decomposition was then performed at each latitude, resulting in values of zonal mean geopotential and planetary waves 1, 2, and 3 for each weekly data set. Wave and mean geopotential values were also obtained using monthly and seasonally averaged data sets. The results of this analysis served as guidelines for the lower boundary forcings needed in the theoretical model.

Figure 4.1a shows the wave number 1 results for the five weeks of January, 1975, obtained from the Fourier decomposition of geopotential height data. There is a considerable amount of variability from week to

(a)

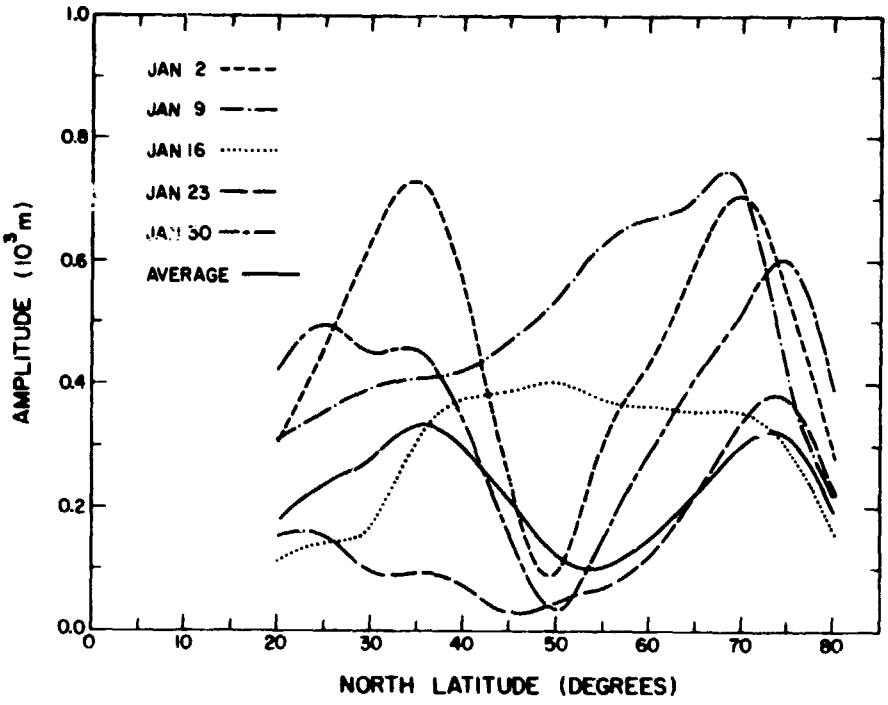

(b)

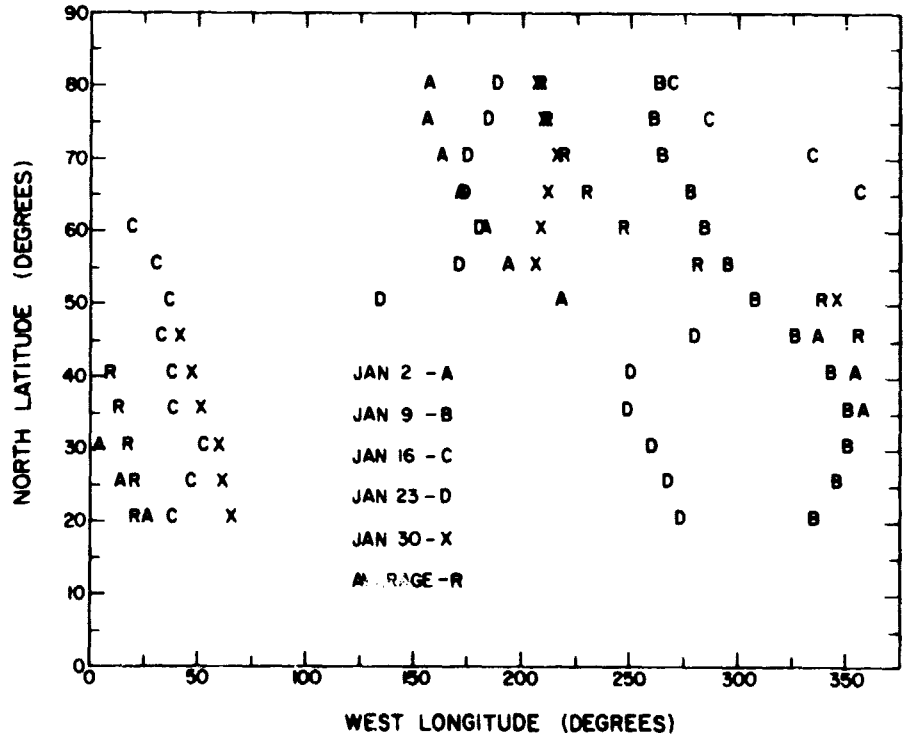

Figure 4.1 Planetary wave number one in January: (a) amplitude in meters and (b) phase in degrees west longitude.

week, indicating the presence of large-scale transient disturbances. A double-peaked maximum of about 700 geopotential meters (gpm) is observed during the week of January 2, with the peaks centered at 35° and 70°N latitude. The phase structure for that week (Figure 4.1b) shows a nearly 180° shift in phase from 60° to 40° latitude. A minor warming occurred during early January [LABITZKE, 1977], and this splitting of wave energy is possibly due to ducting around a region of reduced zonal winds. Although no warming occurred then, this double-peaked structure is observed again during the week of January 30. During this week, the phase also shows a pronounced shift in midlatitudes. This shift is also observed to a lesser extent during the week of January 23. The difference in phase between low latitude and high latitude regions could result from the splitting of wave energy by the polar night jet into these two regions having different transmission characteristics.

The planetary wave structure for the weeks of January 9 to January 16 show a gradual increase in amplitude from low to midlatitudes. The amplitude for January 9 continues to increase with latitude, reaching a maximum of about 750 gpm at about 65° latitude. The phase during these weeks is coherent across midlatitudes, showing a gradual shift to the east with increasing latitude. This gradual shift has also been observed by LABITZKE [1977] in her study of large-scale planetary waves.

Figure 4.2a shows the wave number 2 amplitudes for January. Again, there is a great deal of variability from week to week, with the largest amplitude, about 780 gpm, being reached during the week of January 23. An examination of the phases indicates that wave number 2 is fairly coherent across latitude. Again, the phase lines (Figure 4.2b) in general show a gradual eastward shift with increasing latitude. Note also that with the

(a)

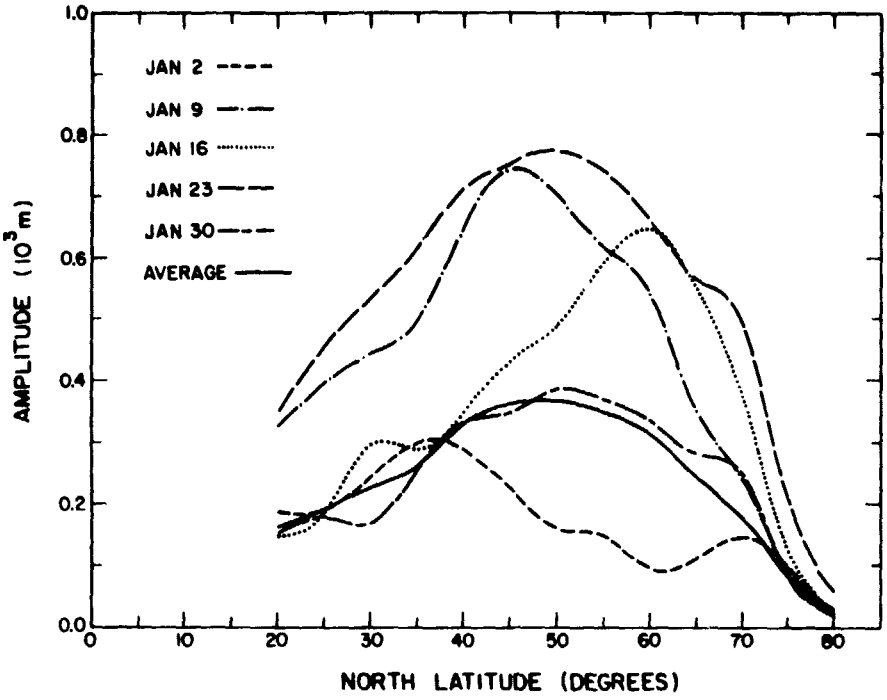

(b)

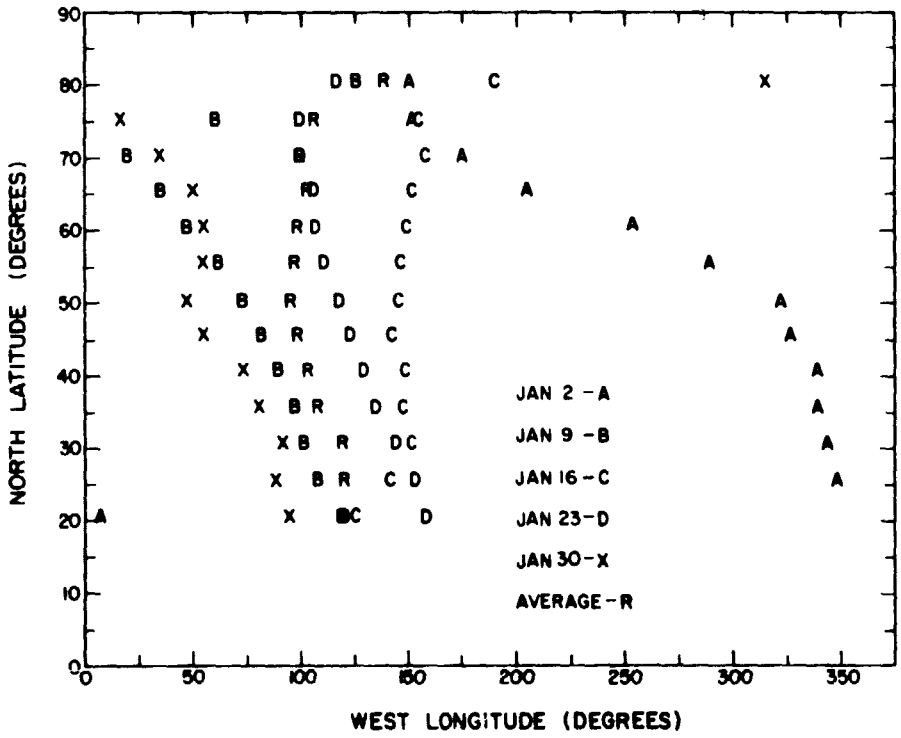

Figure 4.2 Planetary wave number two in January: (a) amplitude in meters and (b) phase in degrees west longitude.

exception of the week of January 2, the variations in wave number 2 are primarily in amplitude, with the phase showing far less variation from week to week than the wave number 1 phases. This would tend to indicate that the large-scale transient waves were primarily wave number 1 disturbances.

Figure 4.3a,b shows the wave number 3 amplitudes and phases for January. Note that with the exception of the week of January 16, the wave number 3 amplitudes are all below 200 gpm. The phase changes greatly from week to week, and again coherence in the phases with latitude is poor. Since the amplitude of wave number 3 is small, its effects on the nitric oxide concentration, especially at upper mesospheric heights, will be negligible. Hence, from now on we will consider only waves 1 and 2.

Figure 4.4 shows the mean geopotential obtained for the month of January. If we assume geostrophic wind balance, we can use the latitudinal gradient of the mean geopotential as an indicator of the zonal mean wind. Note that although the planetary wave activity was ranging greatly from week to week, the effect on the zonal mean wind velocity was small, as evidenced by the small changes in the latitudinal gradient of mean geopotential. The largest change in zonal mean geopotential occurred poleward of 70°, primarily during the two weeks when wave number 1 showed a two-peaked character. However, the zonal mean wind velocity is so small in this region, that the actual net change in magnitude is slight.

Figure 4.5a,b shows the wave number 1 results for the four weeks in February, 1974. This was an especially interesting time period in that a major stratospheric warming occurred near the end of the month [LABITZKE, 1977]. With the exception of the week of February 20, the $m = 1$ amplitudes were about the same as they were in January, with the

(a)

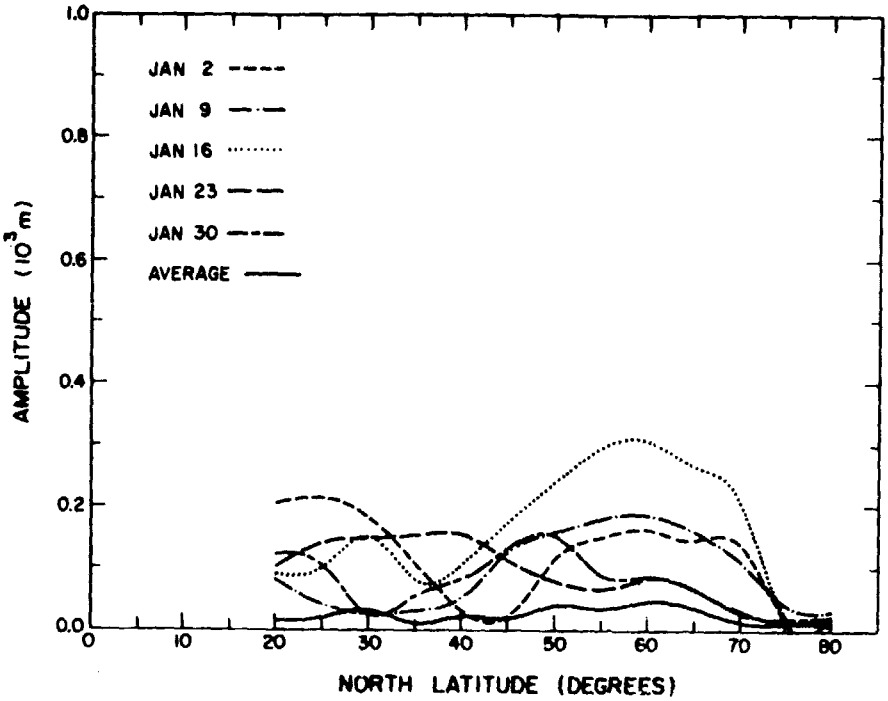

(b)

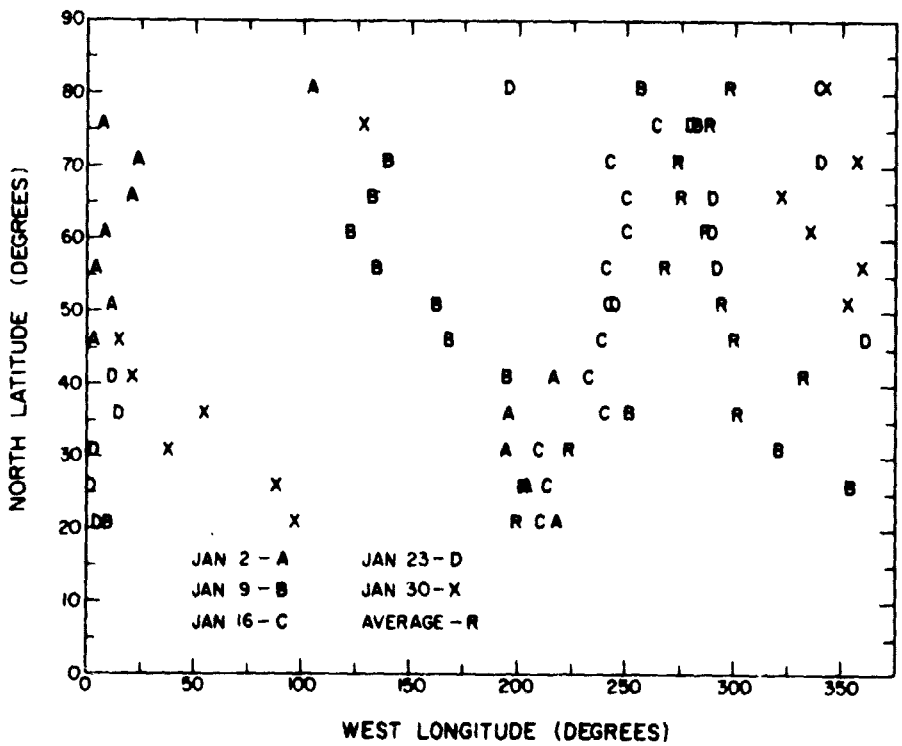

Figure 4.3 Planetary wave number three in January: (a) amplitude in meters and (b) phase in degrees west longitude.

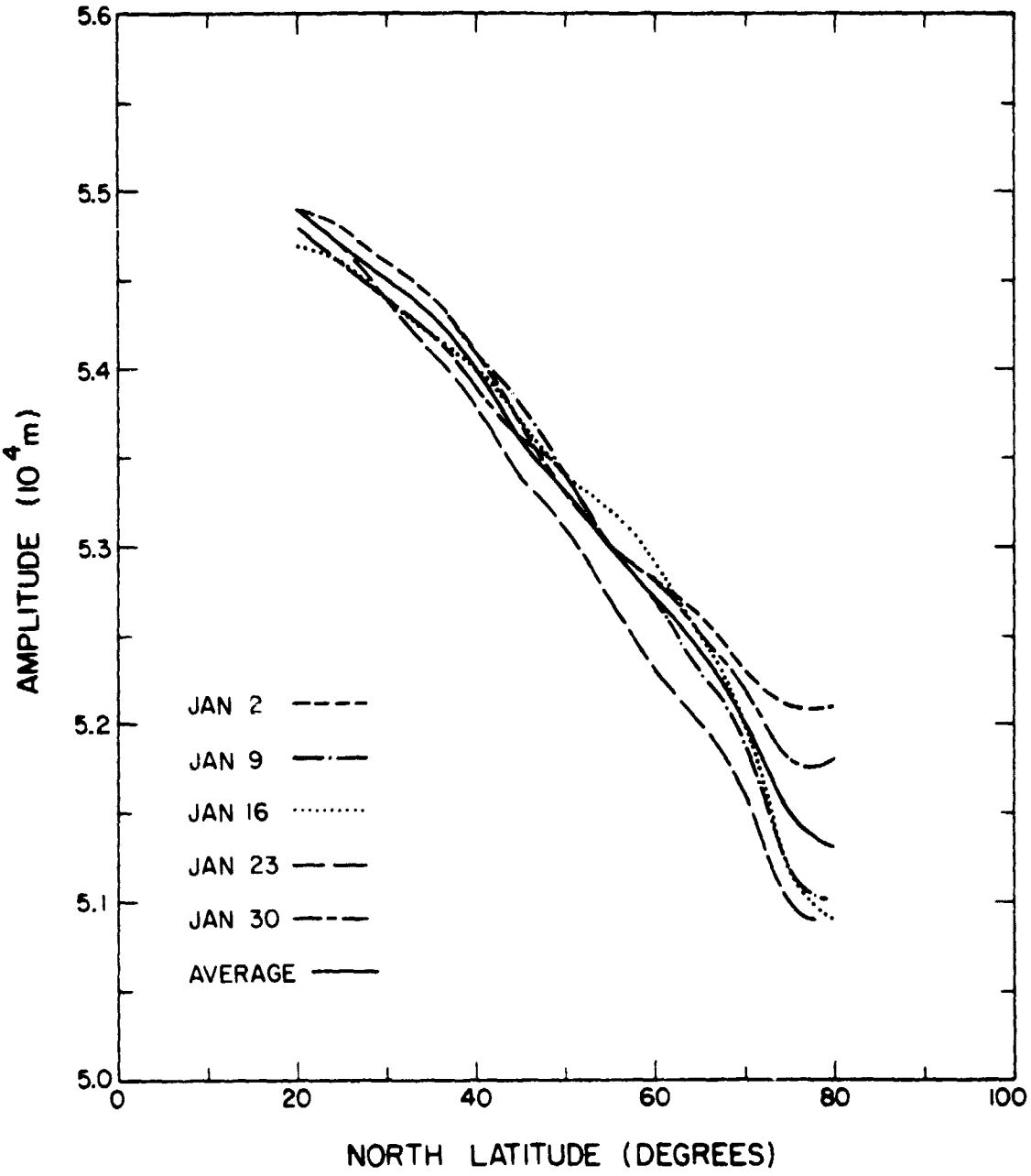

Figure 4.4 Zonal mean geopotential height (m) in January.

(a)

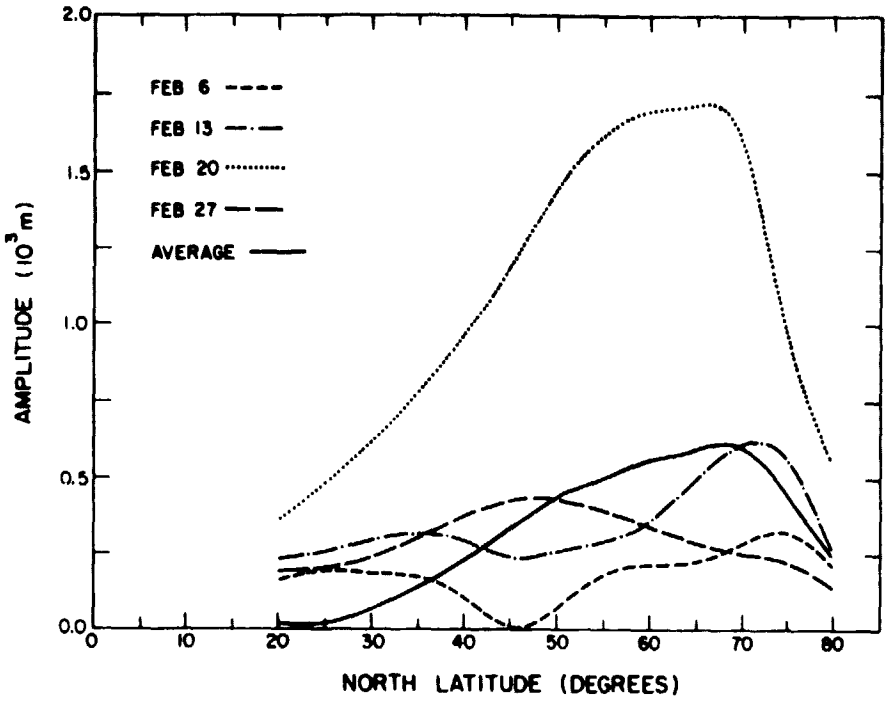

(b)

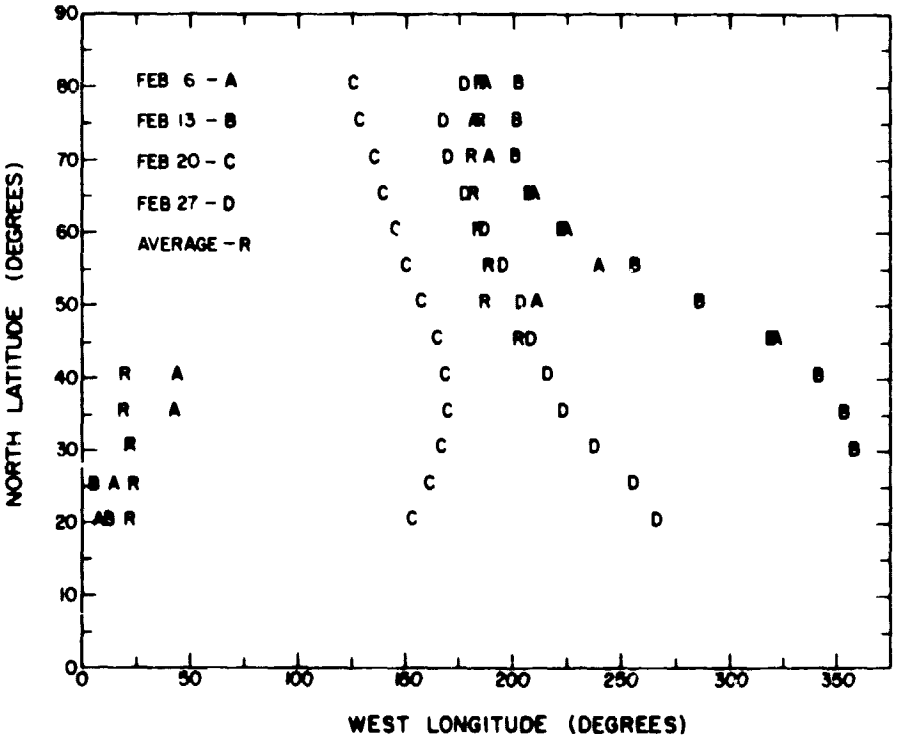

Figure 4.5 Planetary wave number one in February: (a) amplitude in meters and (b) phase in degrees west longitude.

maximum amplitude of about 700 gpm at 70°N latitude occurring during the week of February 13. The large increase of planetary wave number 1 amplitude during the week of February 20 occurred just prior to the stratospheric warming event. Note that the phase associated with this large amplitude shows very little variation with latitude, in contrast to the other February weeks. Note also that the double-peaked behavior observed in the January months recurred with lesser amplitude during the week of February 6. Once again, there is a large phase shift across midlatitudes associated with this double maxima.

The amplitudes and phases presented in Figure 4.6a,b represent the $m = 2$ values for February. The events associated with the stratospheric warming are clearly visible in this figure also. The wave number 2 amplitudes up to the week of February 27 are much smaller than the wave number 2 amplitudes in January. The maximum value obtained during the first three weeks was about 300 gpm, which was reached during the week of February 13. The large amplitude that occurred during the week of February 27 followed the large wave number 1 amplitude observed during the week of February 20, which is typical of a type A warming. Notice that the phase for the week of February 27 again shows little variation with latitude. The maximum amplitude for wave number 2 is 600 meters at about 45°N. The phase diagram indicates that the location of this maximum occurs near 165°W longitude ($\lambda_{max} = \phi_{max}/m$) which is roughly the location of the $m = 1$ maximum the previous week.

Figure 4.7 shows the zonal mean geopotential values obtained for February. Again, the effect of the warming is clearly seen. The latitudinal gradient of mean geopotential becomes less negative during the week of February 20, and finally becomes zero or positive poleward of about 50°

(a)

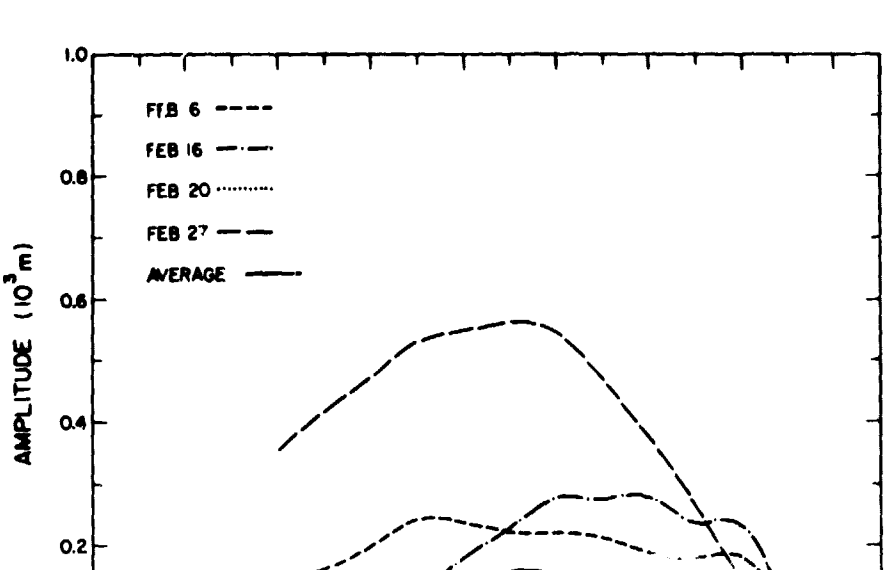

(b)

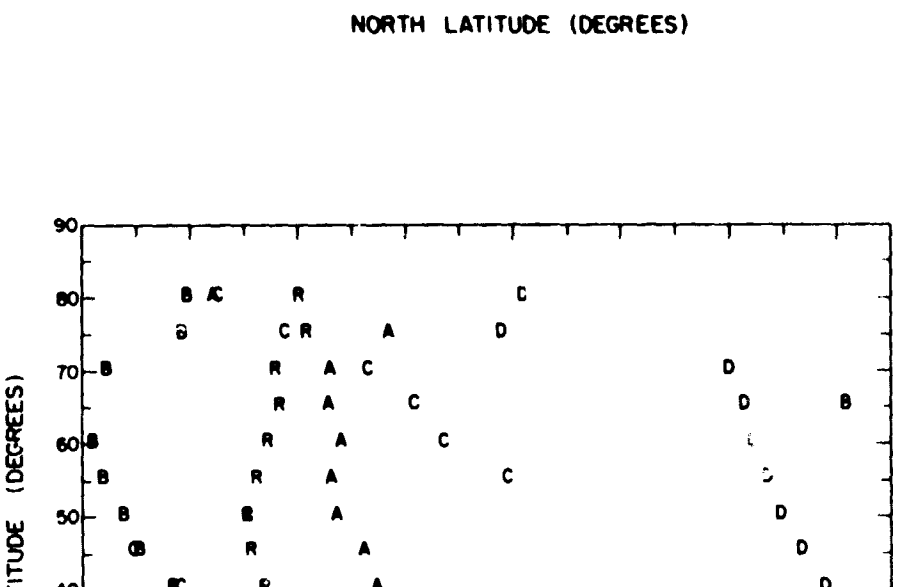

Figure 4.6 Planetary wave number two in February: (a) amplitude in meters and (b) phase in degrees west longitude.

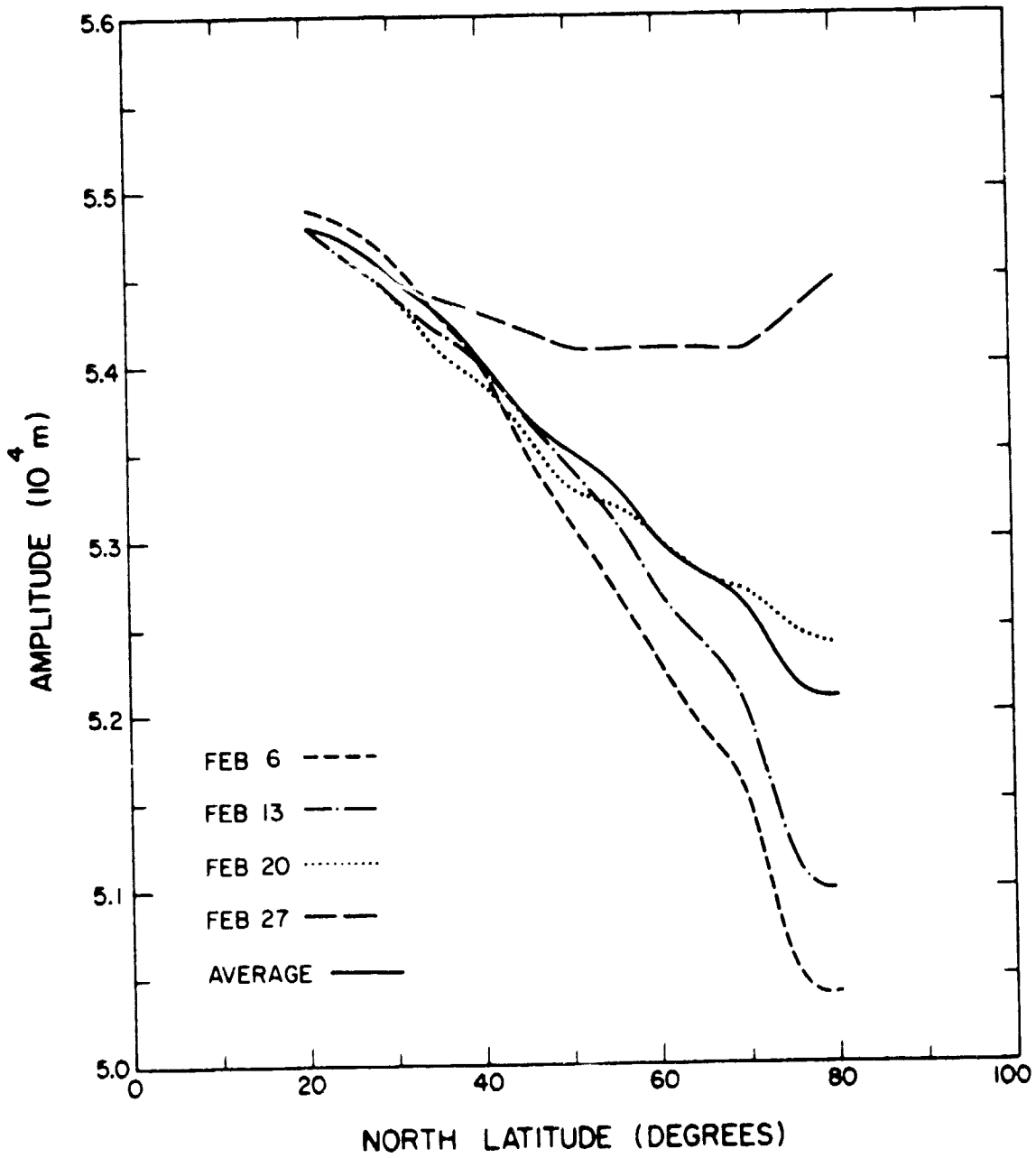

Figure 4.7 Zonal mean geopotential height (m) in February.

longitude during the week of February 27. This indicates that the zonal mean wind weakened and finally reversed during the last week of the month, due to the effects of the enhanced planetary wave amplitude during the weeks of February 20 and 27.

There is obviously a great deal of transient activity present at the .4 mb level, as seen in the large variability of planetary wave amplitudes from week to week. In order to eliminate some of these short term effects, a Fourier analysis was performed on average data sets from January and February, and also on a combined data set from all nine weeks which we call the Winter Average Set. The results of the Fourier decompositions of these average data sets served as guidelines for the lower boundary forcings required by the numerical model.

The results of the Fourier decomposition of the averaged data sets for wave number 1 are shown in Figure 4.8a,b. Note that the dominant feature in January is the double maximum structure, having a maximum amplitude of about 350 gpm at both 35° and 70°N. Consistent with the bifurcated wave amplitude, the phase experiences a rapid change between 40° and 60°N latitude. The strong wave number 1 amplitude present during the stratospheric warming dominates the average wave structure for February. It reaches a maximum of about 600 gpm near 70° latitude. The phase of the February average $m = 1$ wave is nearly constant with latitude, again reflecting the effect of the February 20 weekly values on the overall monthly average. For the winter averaged results, the double maximum structure has nearly disappeared, with the main maximum of 400 gpm occurring near 70°N latitude. A smaller relative maximum occurs at low latitudes, and the shift in phase is still evident at 40° in the winter average case.

(a)

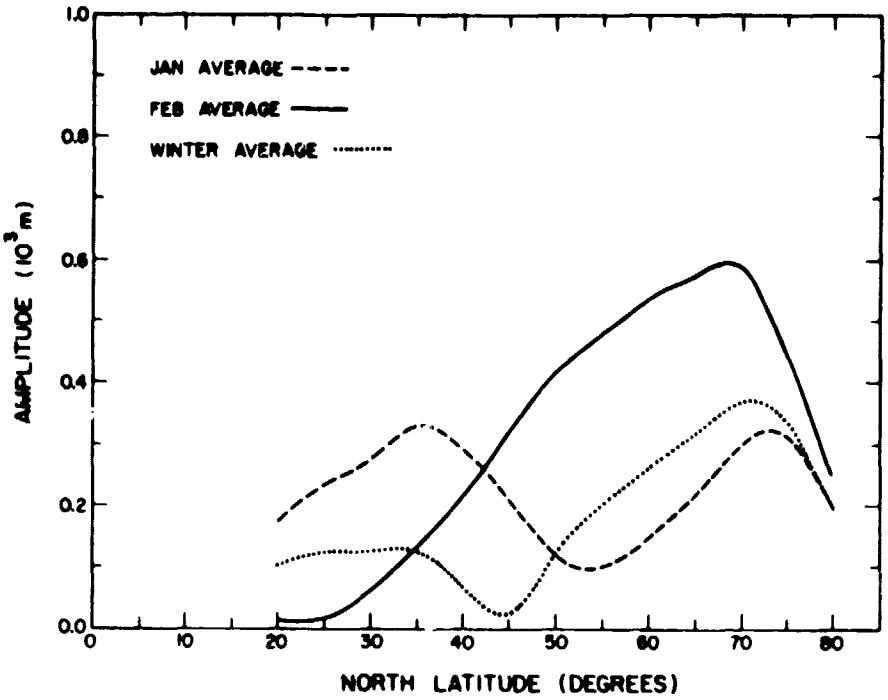

(b)

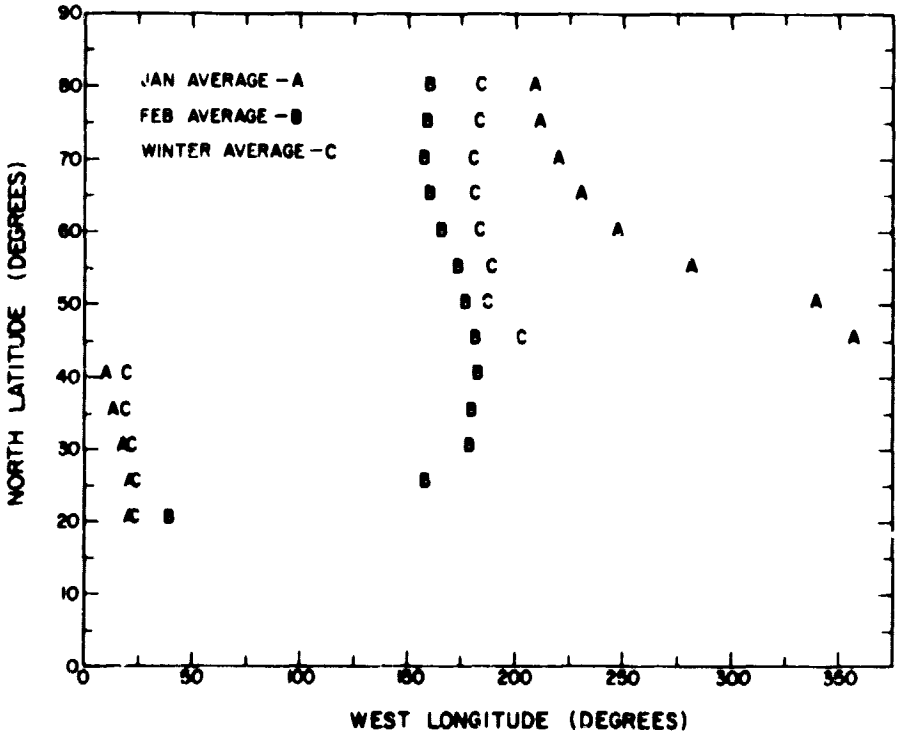

Figure 4.8 Planetary wave number one from the averaged data sets: (a) amplitude in geopotential meters and (b) phase in degrees west longitude.

The wave number 2 average results are shown in Figure 4.9a,b. Even though the $m = 2$ amplitude appeared to be enhanced during the week of February 27, the amplitude during that week was still smaller than most of the January amplitudes. This is seen in the relatively large $m = 2$ amplitude for the January average case. The January maximum reaches nearly 400 gpm at 50°N latitude, while the February average value at that latitude is only about 150 gpm. The phases for both the January and February average are relatively coherent with latitude, and the positions of the actual maxima for January and February occur within about 50° longitude of each other at nearly all latitudes. The stronger $m = 2$ values in January dominate the winter average pictures.

The zonal mean geopotential obtained from the averaged data sets is shown in Figure 4.10. South of 40° latitude, the three averages are nearly identical. Poleward of 40°, the January average falls off faster with latitude, which indicates a stronger zonal mean wind. The less steep latitudinal gradient of mean geopotential for February reflects the effects of the reversal of the zonal mean westerlies which occurred late in that month. Notice that the main height of the .4 mb surface varies by about 3 km from 20° to 80°N latitude.

4.2 *Nitric Oxide*

The nitric oxide concentrations to be used in this study are based on results presented in CRAVENS and STEWART [1978]. They presented the results of an ultraviolet nitric oxide experiment [BARTH et al., 1973] which was on the Atmospheric Explorer C satellite (AE-C). The results of this experiment were analyzed to obtain the nitric oxide concentration at 105 km for three time periods in 1974; group A, from day 21 to day 46 group B, from day 212 to day 249, and group C, from day 258 to day 275.

(a)

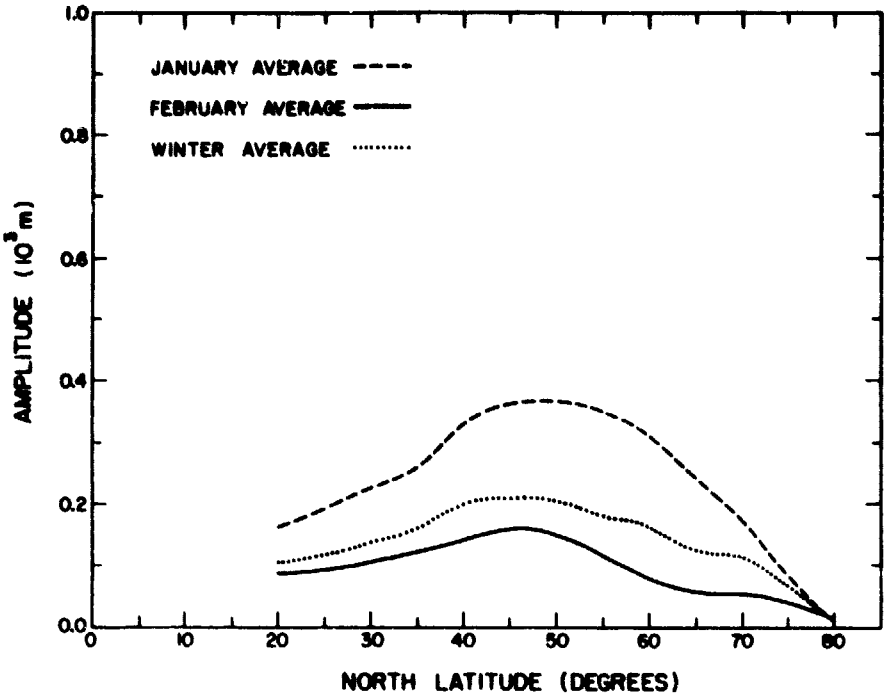

(b)

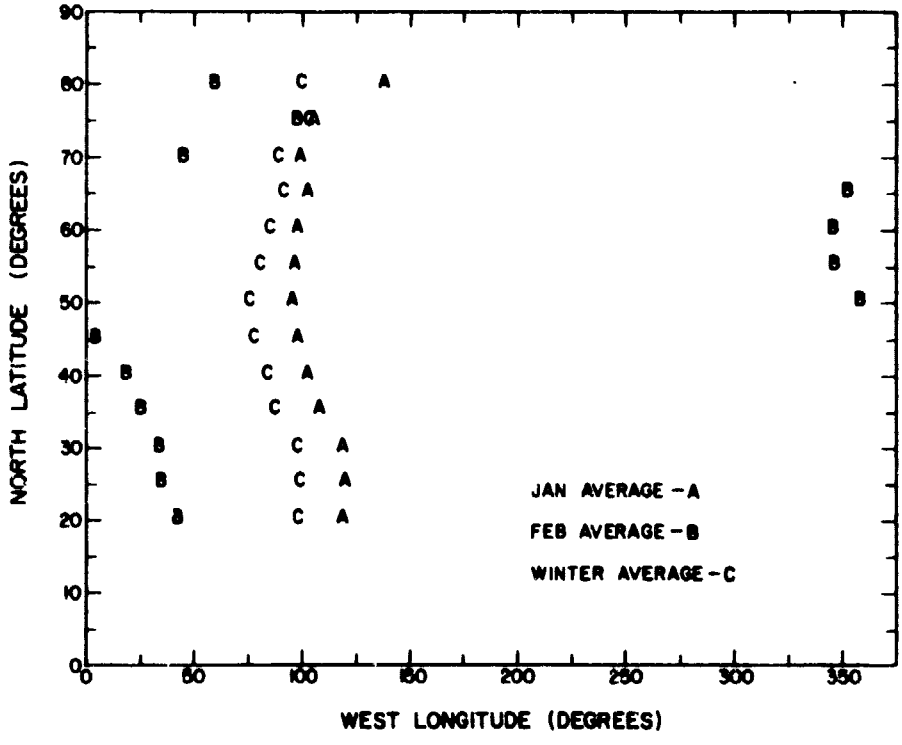

Figure 4.9 Planetary wave number two from the averaged data sets: (a) amplitude in geopotential meters and (b) phase in degrees west longitude.

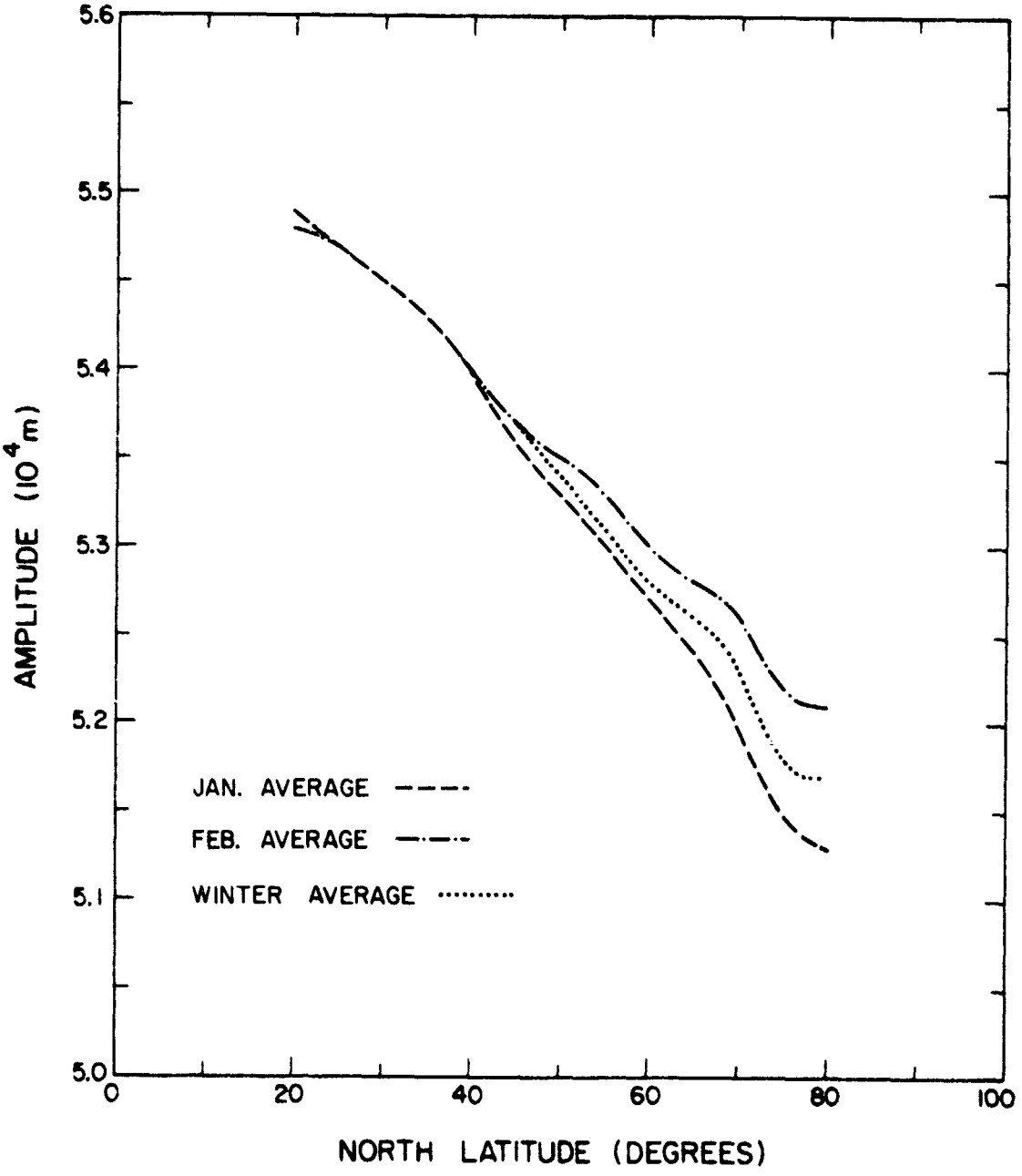

Figure 4.10 Zonal mean geopotential height (m) obtained from the averaged data sets.

Thus, group A represents a winter situation, group B a summer situation, and group C a fall situation. Although the observations were all made at the same height, unfortunately they could not be taken during periods of equal magnetic activity. The average value of the planetary index A_p was 20 for group A and 23 for group B; however, for group C, the average planetary index was 38. Thus, the seasonal changes in the nitric oxide distributions obtained from the satellite data cannot be attributed entirely to seasonal changes in transports.

Figure 4.11a,b shows the distribution of NO for the winter and summer seasons as presented in CRAVENS and STEWART [1978]. Figure 4.11a contains the distribution for the northern hemisphere in winter. Note that the maximum concentration of almost $1.0 \times 10^8/cm^3$ occurs near 90° west longitude and between 50° and 70° latitude. There is a marked asymmetry about the pole, which is probably due in part to the geographical asymmetric production of nitric oxide in the auroral zone. However, part of this asymmetry could be due to the transport effects of large-scale planetary waves. The relatively symmetric situation which occurs during summer months in the northern hemisphere when planetary waves are not present also suggests the importance of transport on the nitric oxide distribution.

The results as presented in Cravens and Stewart were used as a basis for initial NO concentration required by the numerical model. A spacial Fourier decomposition was performed on values of nitric oxide concentration at 105 km obtained from the results presented in Cravens and Stewart. The results of this decomposition for the winter northern hemisphere are shown in Figure 4.12a,b. Shown are the mean concentration, and the first two spacial harmonics. Due to the lack of resolution in the data, higher order harmonics were quite noisy. The zonal mean concentration, $m = 0$,

(a)

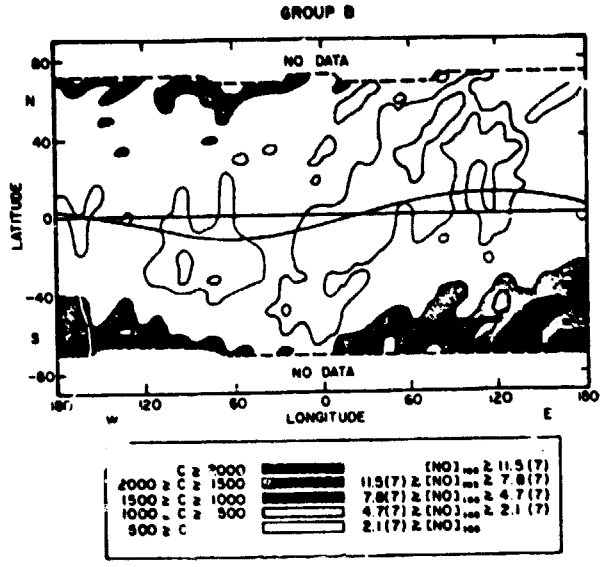

(b)

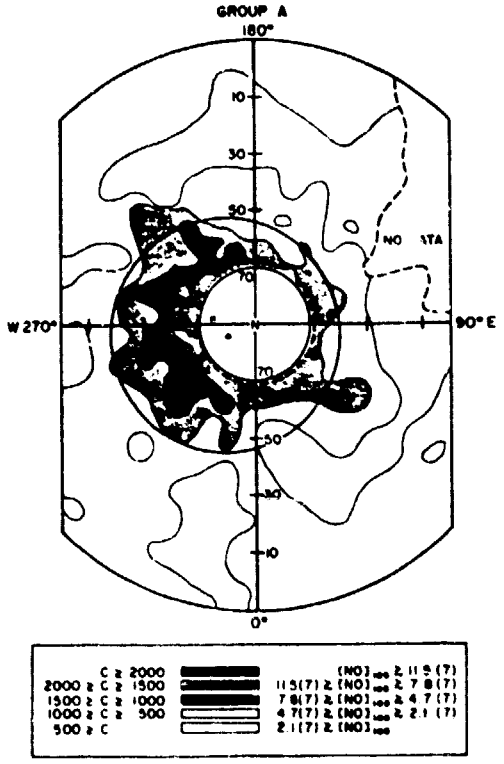

Figure 4.11 (a) Map of nitric oxide concentration during mid-January through mid-February, 1974, (b) map of nitric oxide concentration (molec/cm^3) measured during August, 1974 [CRAVENS and STEWART, 1978].

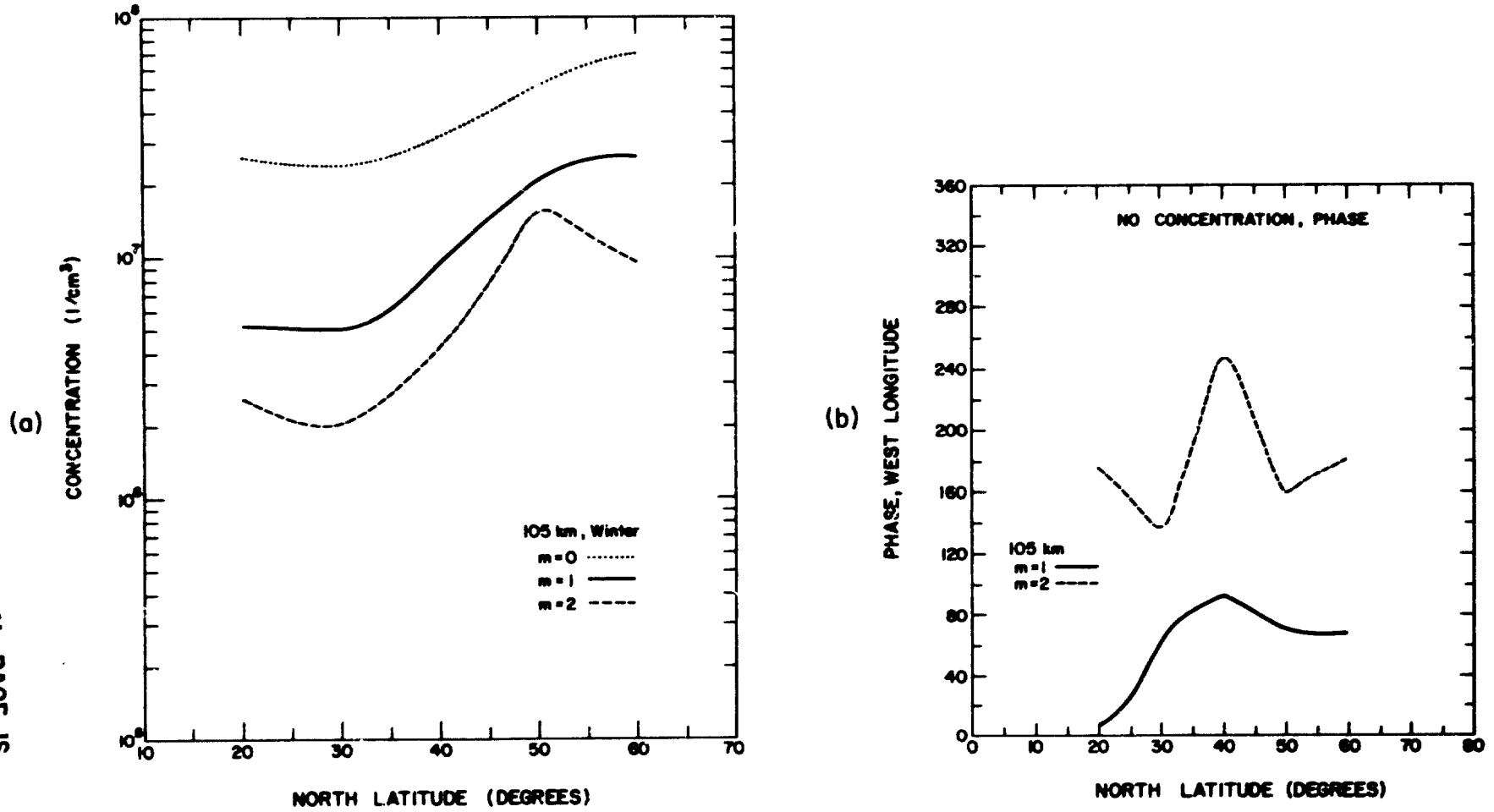

Figure 4.12 Results of a Fourier decomposition of winter Northern Hemisphere nitric oxide concentrations at 105 km. (a) amplitude ($1/cm^3$) and (b) phase (°W).

shown in Figure 4.12a agrees well with the mean concentration presented in CRAVENS and STEWART [1978]. The $m = 1$ amplitude maximized at $2.1 \times 10^7/cm^3$ at 60°N, while the $m = 2$ amplitude reached a maximum of $1.6 \times 10^7/cm^3$ at 50° latitude. Figure 4.12b shows the phase values in degrees west longitude for wave numbers 1 and 2. The longitudinal position of the maximum for a wave number, m, is given by ϕ/m, where ϕ is the phase in degrees west longitude. The $m = 1$ maximum is centered around 80°W longitude north of 30°, while the $m = 2$ maximum is centered near 100°W longitude, although it varies significantly with latitude.

In this study, we hope to show that the nitric oxide distribution is a function of both the asymmetric production in the auroral zone and of transports due to zonal mean and planetary wave circulations. Since planetary waves are absent in the summer mesosphere, we would not expect to see much higher order wave-like structure in the summer NO distribution. A $m = 1$ structure would be expected due to the asymmetric production, however. A Fourier decomposition performed on the summer data supports this hypothesis, as seen in Figure 4.13a,b. The summer zonal mean distribution again agreed quite well with that presented in CRAVENS and STEWART [1978].

The $m = 1$ summer amplitude is largest at 60°, and falls off rapidly to the south. This is consistent with the idea of the asymmetric auroral nitric oxide source. The phase of this $m = 1$ distribution occurs near 90°W longitude, and varies little with latitude. The $m = 2$ amplitude is quite small, even at high latitudes, and the phase is very noisy. This indicates the absence of any major planetary wave effect during the summer months. The results of the $m = 1$ winter decomposition are shown for comparison. Notice that the perturbation concentration as obtained from

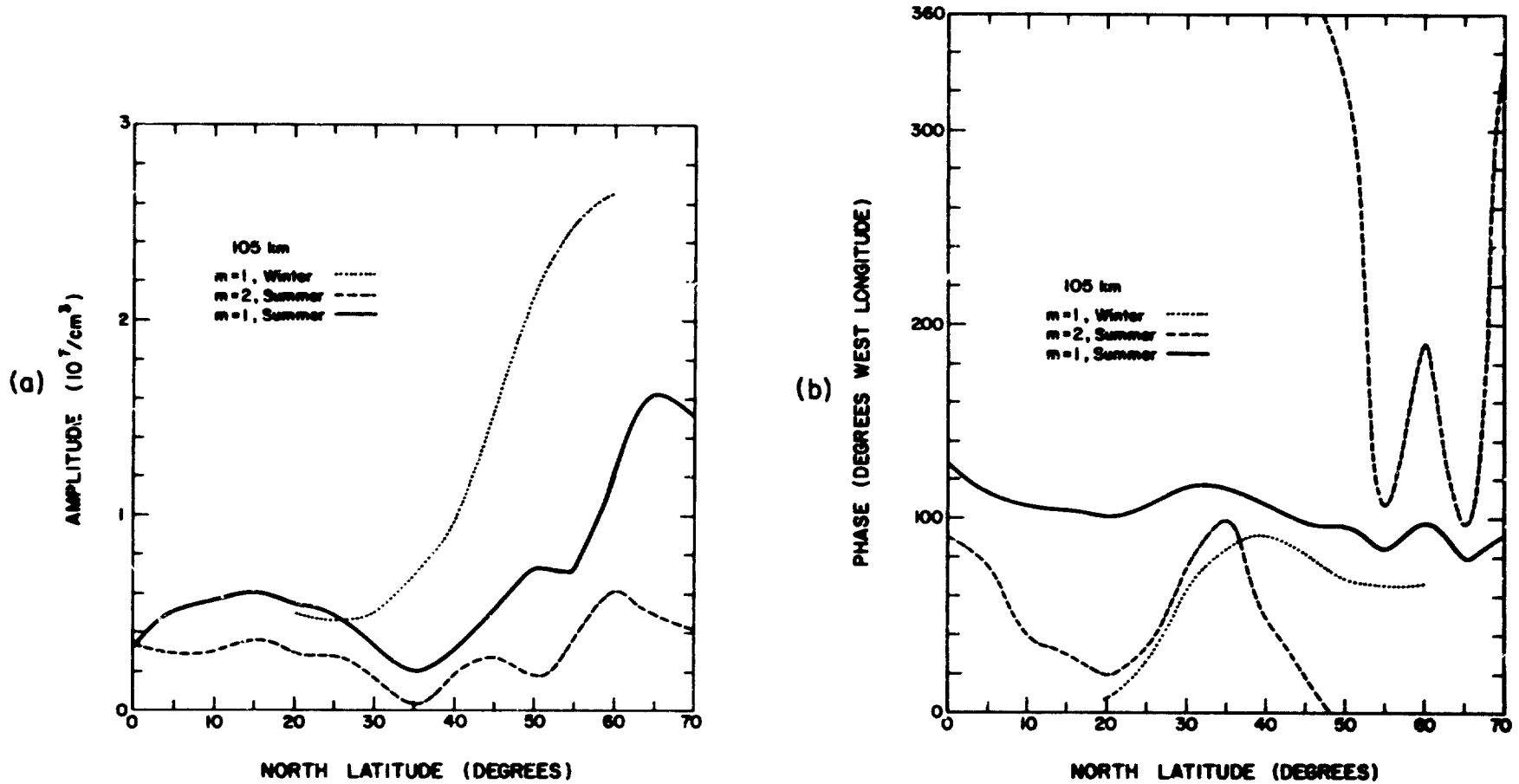

Figure 4.13 Comparison of perturbation nitric oxide concentrations for winter and summer at 105 km. (a) amplitude (1/cm^3) and (b) phase (°W).

the data is considerably larger in winter, when planetary wave amplitudes are at a maximum.

Since the numerical model requires an initial two-dimensional nitric oxide profile, we have coupled the latitudinal distributions of NO just presented with a postulated vertical profile shown in Figure 4.14. This profile is based on a combination of profiles presented in BAKER et al. [1977] and BARTH [1966b]. The 105 km maximum is due to the strong production of NO at that level, which is then transported downwards to the sink region for NO which occurs around 80 km.

4.3 *Summary*

The observational results presented in this chapter will be used to guide the choice of boundary forcings and initial states needed by the numerical model. The geopotential height analysis provides an estimation of the magnitude of planetary wave activity at the lower boundary of the region of concern. The mean geopotential and also the wind structure at the lower boundary are also obtained from this analysis.

The seasonal variation of the nitric oxide distribution at 105 km indicates that distribution of nitric oxide is a result of both asymmetric production and transport by zonal mean and planetary wave winds. The winter distribution provides the initial NO state required by the numerical model, and the effects of model calculated zonal mean and planetary wave winds on this distribution will be studied in upcoming chapters.

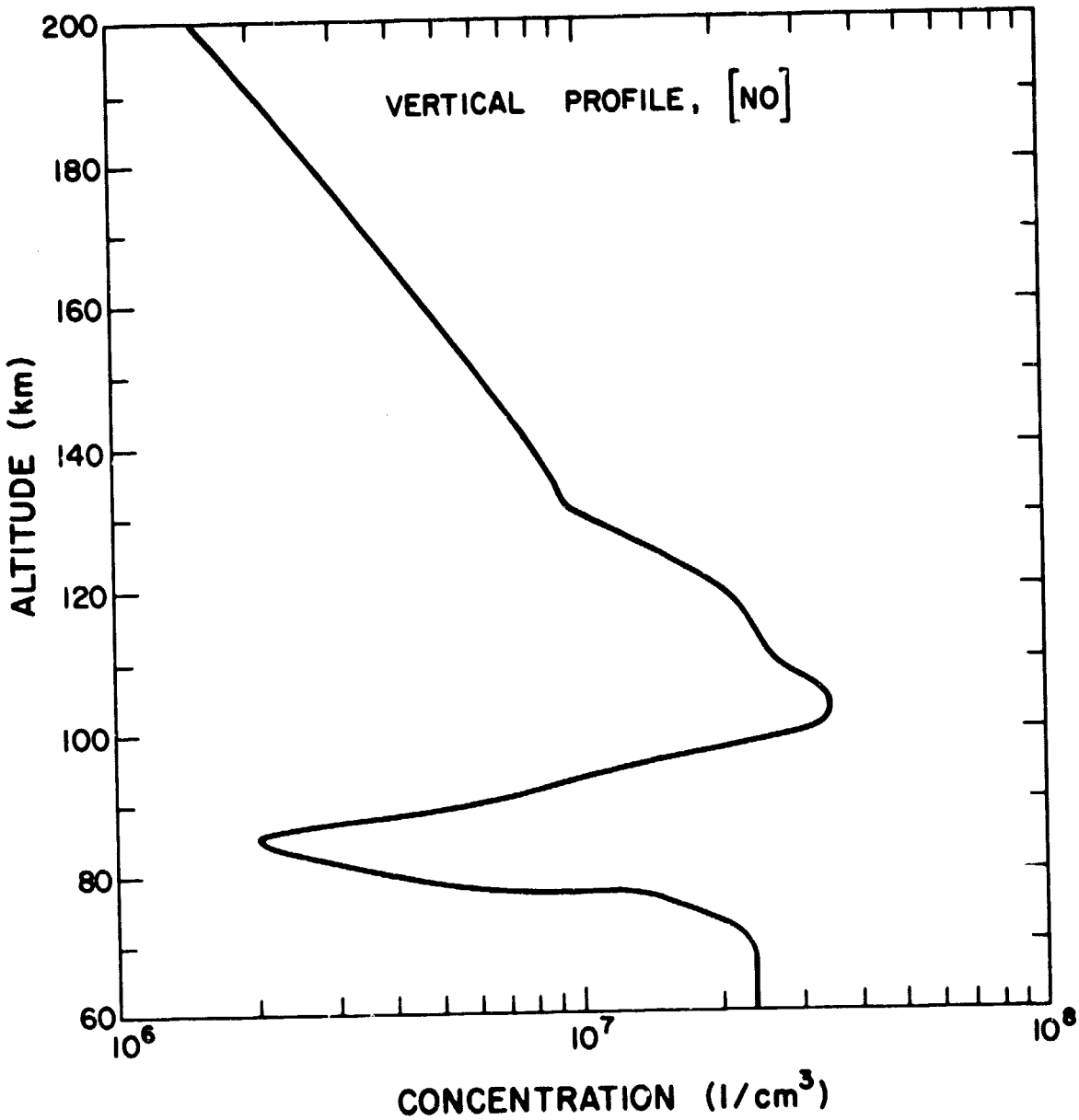

Figure 4.14 Postulated vertical nitric oxide profile.

5. STEADY-STATE CALCULATIONS

Results of transport calculations using the previously discussed nitric oxide and gepotential height data are discussed in this chapter. The transports calculated in this chapter are due to planetary wave winds only. The effects of the zonal mean meridional circulation which arise from diabetic heating and wave fluxes are ignored. The transports due to the planetary wave-induced secondary circulation tends to partially cancel the transports due to the waves themselves; hence, the results in this chapter should be regarded as an upper bound on the effects of planetary wave transports on the zonal mean nitric oxide distribution. Transports due to both planetary wave winds and the zonal mean circulation will be studied in Chapter 6.

5.1 *Planetary Wave Structure*

The planetary wave winds used to calculate the transports in this study were obtained using the time-independent planetary wave model. This model required as input both the mean zonal wind structure, and the amplitude and phase of the planetary wave at the lower boundary. The mean zonal wind profiles used in this study are shown in Figure 5.1a,b. The polar night jet in each case is similar in structure and position to that presented in SCHOEBERL and STROBEL [1978]. The thermospheric jet was modeled after the circulation above 100 km as presented in DICKINSON et al. [1977]. The values of mean geopotential height from the observational study were used to estimate the mean zonal wind at 55 km for the months of January and February. The polar night jet strength was adjusted to agree with the observational results, thus giving a separate wind profile for each month. In the January wind model, Figure 5.1a, a maximum in the polar night jet amplitude of 80 m/sec occurs at 45°N latitude and 70 km in

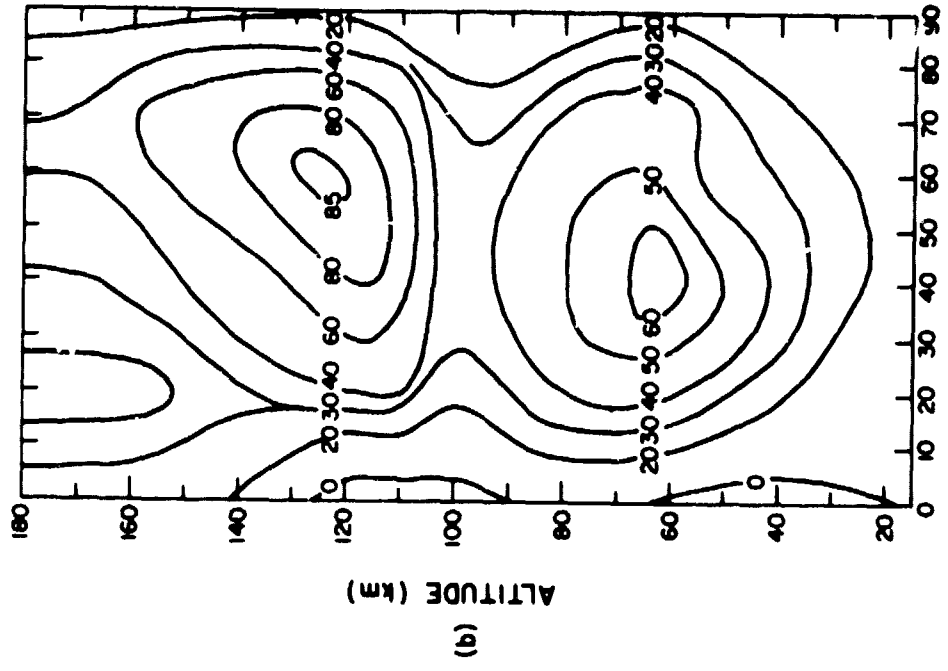

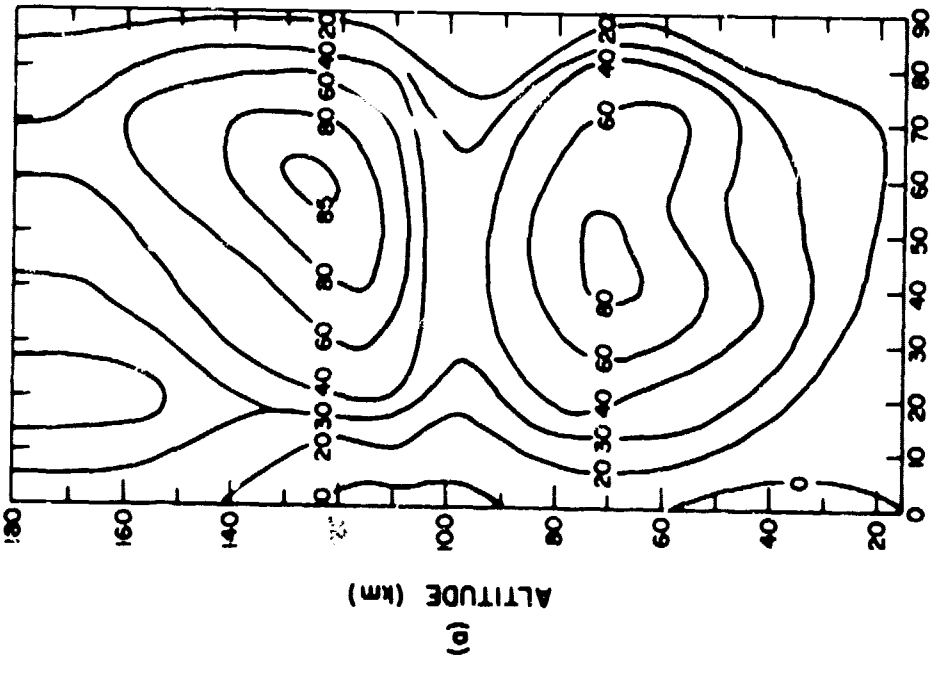

Figure 5.1 Contours of zonal mean wind (m/sec) for (a) January and (b) February.

height. For February, Figure 5.1b, the maximum of 60 m/sec occurs near 40°N latitude and 63 km. These differences are consistent with changes from January to February in the latitudinal gradient of zonal mean geopotential height, as obtained from observational data.

The planetary wave structure obtained from the numerical model depends not only on the zonal mean wind, but also on the structure of the wave at the lower boundary. The lower boundary level was set at 55 km, so that the results of the spacial Fourier decomposition of geopotential height data as presented in Chapter 4 could be used. In order to filter out the effects of transient waves, only the monthly averaged boundary forcings were considered. Thus, planetary wave structures for each month and wave number could be calculated using the appropriate boundary forcing and wind model.

The calculated values of geopotential amplitude and phase are shown in the next several figures. Figure 5.2 shows the calculated geopotential for the January $m = 1$ case, obtained using the January average $m = 1$ forcing at 55 km and the January wind model. Figure 5.2a contains contours of geopotential height, while the contours in Figure 5.2b represent the phase. The January average forcing (see Figure 4.8a) had two maxima, and this double maxima structure persists up to $z = 8$. Above $z = 8$, the structure is dominated by a single maximum located in midlatitudes. The position of this maximum gradually shifts northward with height. The phase structure (Figure 4.8b) shows a westward tilt with height, indicating vertical energy propagation. Note the rapid change in phase with height at high latitudes below $z = 11$, indicating the ducting of wave energy poleward of the strong January polar night jet [DICKINSON, 1968a].

Figure 5.3 shows the calculated wave amplitude and phase for the

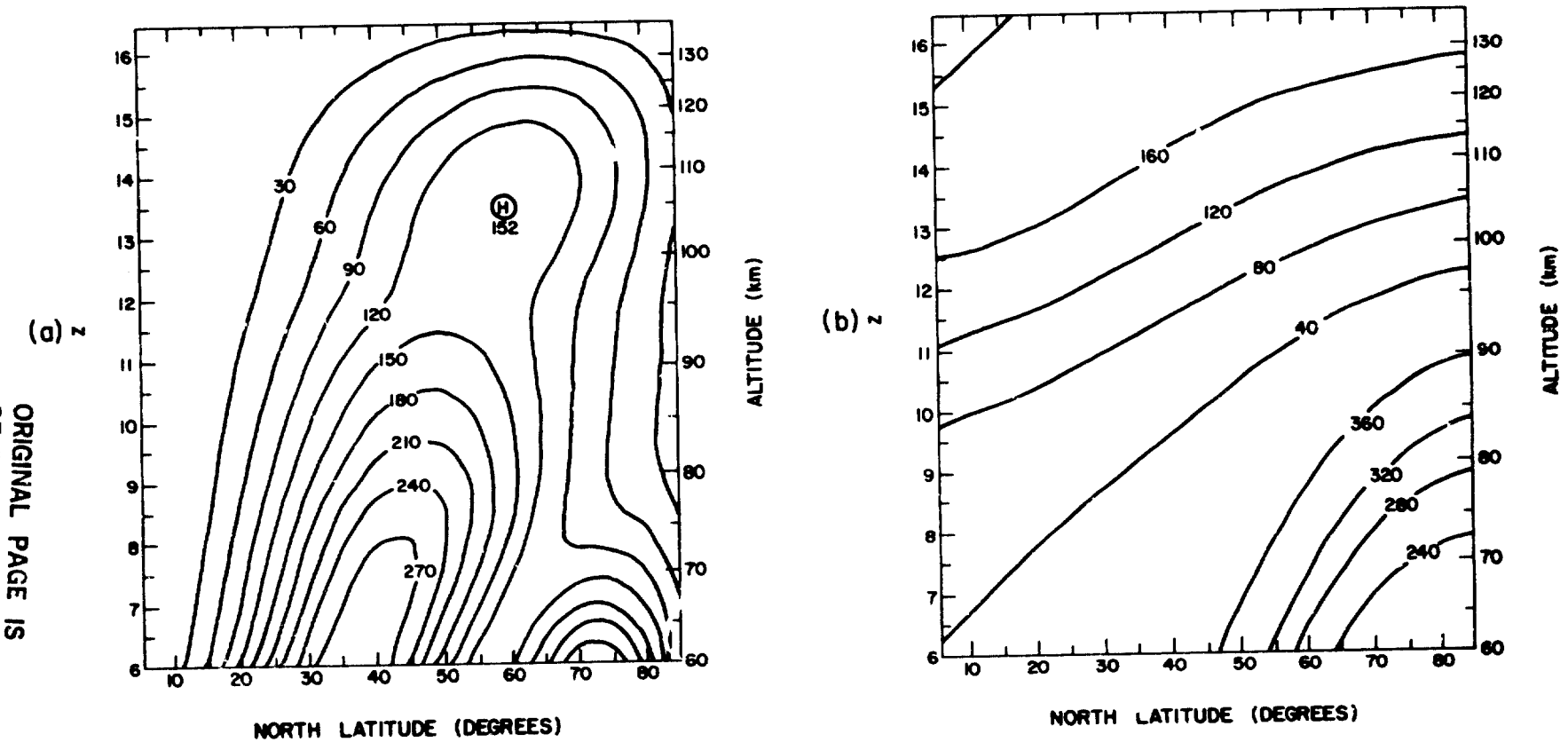

Figure 5.2 Calculated structure for wave number one in January: (a) amplitude in meters and (b) phase in degrees west longitude.

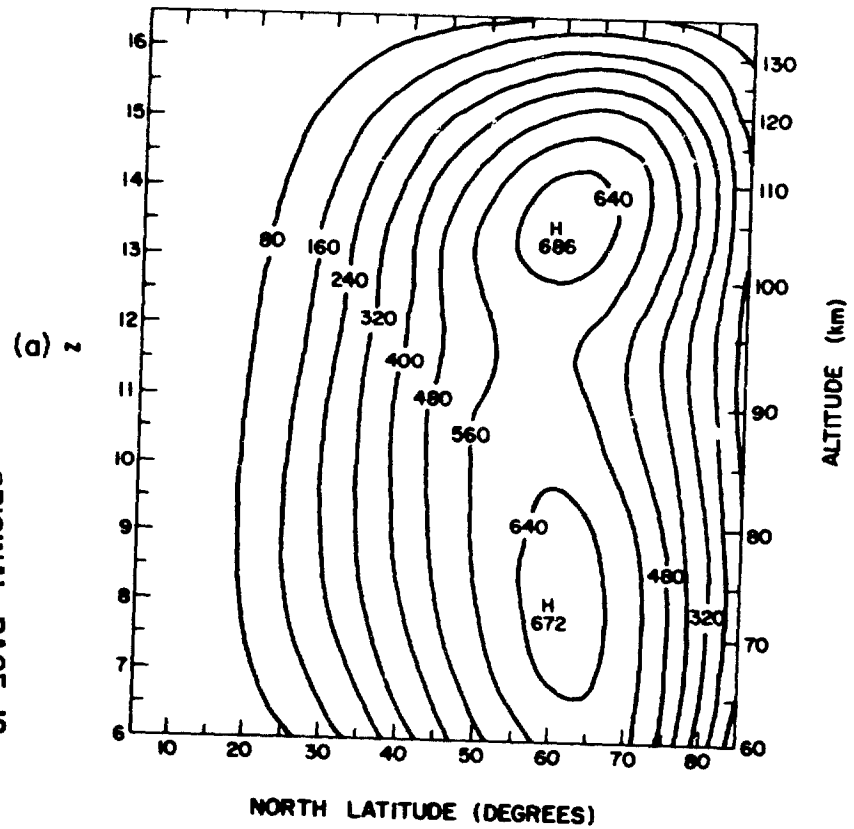

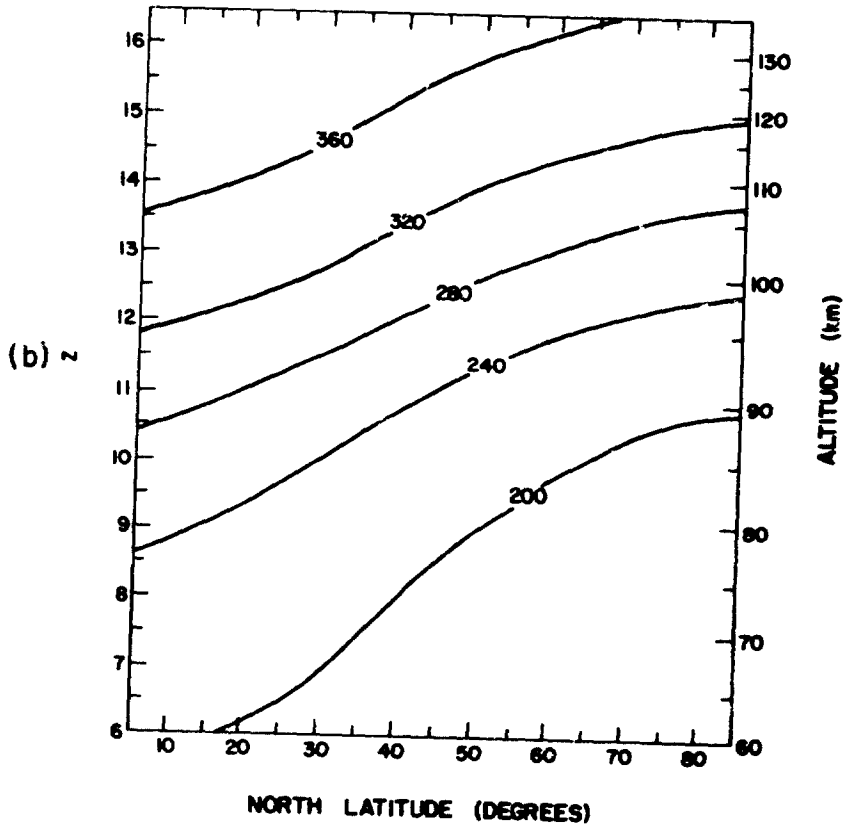

Figure 5.3 Calculated structure for wave number one in February: (a) amplitude in meters and (b) phase in degrees west longitude.

February $m = 1$ case. The $m = 1$ forcing in the February average case was much stronger than that in January, mainly due to the contribution of the strong $m = 1$ amplitude which preceded the stratospheric warming in late February. As a result, the calculated wave amplitude for February (Figure 5.3a) is much larger than that for January. Note that the February $m = 1$ amplitude peaks at $z = 8$ at 672 gpm, and again at $z = 13.5$ at 686 gpm. This is very different from the amplitude in January, which only reached 152 gpm at $z = 13.5$. The February amplitude maxima at $z = 13.5$ is situated just below the thermospheric jet maximum, and could be the result of reflection of wave energy by that maximum. In Figure 5.3b, the phase lines for February show a westward tilt with height, indicating vertical energy propagation; however, the phase change at lower levels is not nearly so rapid with height as the January case. This is due both to the difference in wind structure and forcing between months. Note that at $z = 13.5$, the phase for January is 110°W, while the phase for February is almost 290°W. This 180° shift in phase results in markedly different values of nitric oxide flux and transport for January and February.

Figure 5.4 shows the $m = 2$ results for January. Recall that the maximum $m = 2$ amplitude for January was larger than the $m = 1$ maximum (see Figure 4.2). This results in larger low level geopotential amplitudes for the January $m = 2$ case. In Figure 5.4a, a maximum amplitude of 366 gpm is reached at 50°N latitude and $z = 7$. The $m = 2$ wave dies out much more rapidly with height than the $m = 1$ wave however, and at $z = 13.5$, the $m = 2$ amplitude has decreased to about 100 gpm at 50°N latitude. Although the phase lines in Figure 5.4b show westward tilt with height, the small amplitude of the wave indicates that not much vertical energy propagation occurs due to $m = 2$ at this level.

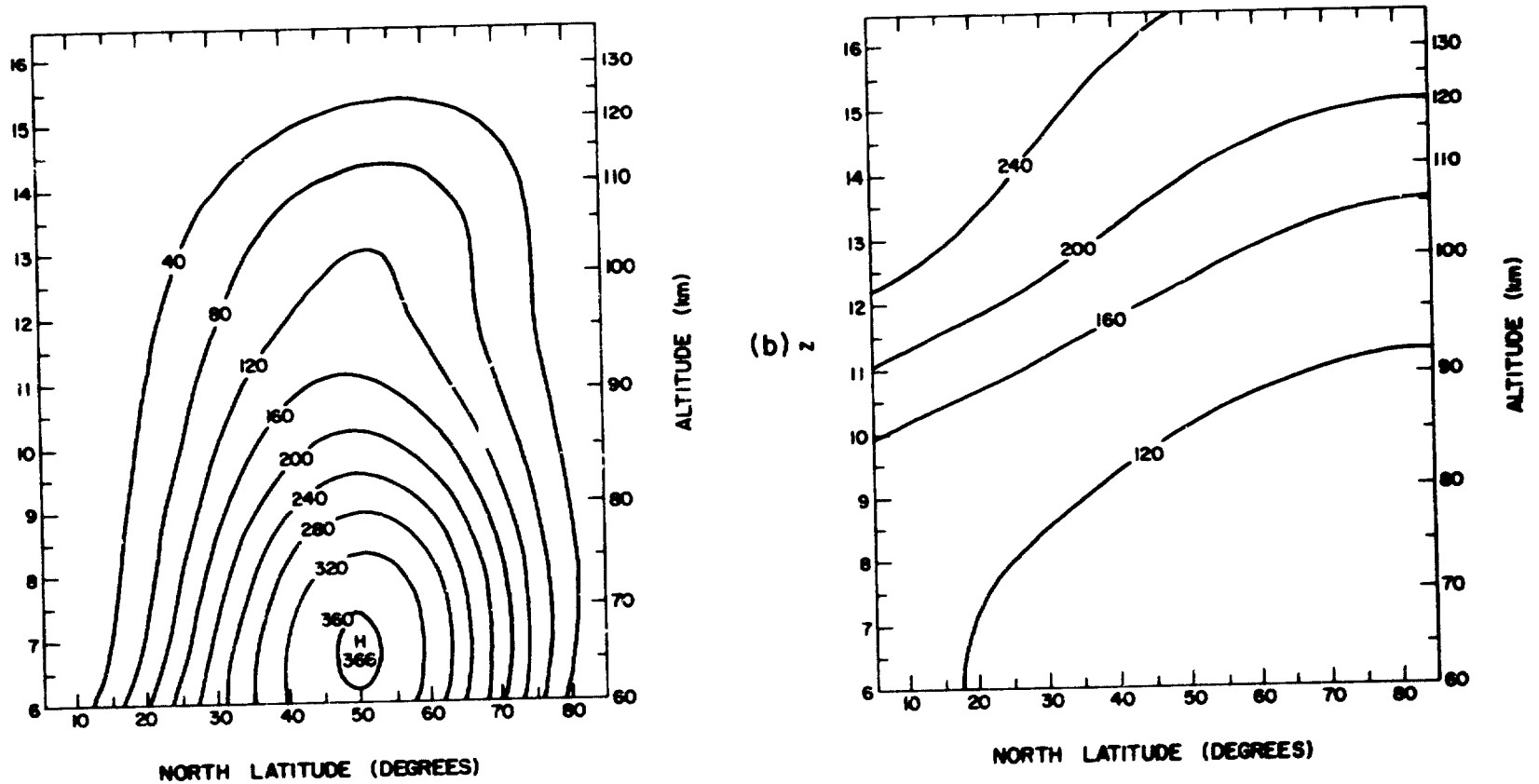

Figure 5.4 Calculated structure for wave number two in January: (a) amplitude in meters and (b) phase in degrees west longitude.

Figure 5.5 shows the results of the February $m = 2$ calculations. The boundary forcing for this case had a small amplitude and this results in a maximum value of only 140 gpm at $z = 7$ as indicated in Figure 5.5a. This $m = 2$ wave also dies out rapidly with height, having a maximum of only 60 gpm at $z = 13.5$. Thus, the transport effects of the $m = 2$ February case are small. Note that at 50° latitude and $z = 13.5$, the phase for $m = 2$ (Figure 5.4b), January is about 180°, while the phase for $m = 2$ (Figure 5.5b), February is about 110°. This difference in phase, as well as the difference in amplitude, results in significantly different transports from month to month.

5.2 *Horizontal Flux and Transport*

In this section we will discuss the horizontal fluxes and transports which result from the steady state planetary waves presented in the previous section. In the absence of a mean meridional circulation and loss coefficient equation 3.38 can be reduced to

$$\frac{\partial \bar{\gamma}}{\partial t} + \frac{1}{a\cos\theta}\frac{\partial}{\partial \theta}\overline{v'\gamma'}\cos\theta + \left(\frac{\partial}{\partial z} - 1\right)\overline{w'\gamma'} = 0$$

The second term on the left-hand side represents the north-south transport due to planetary waves, and the third term on the left-hand side will be referred to as the vertical transport. The horizontal flux is given by $\overline{v'\gamma'}$, while the vertical flux is given by $\overline{w'\gamma'}$. Here, the over-bar represents a zonally averaged quantity. The perturbation concentration is assumed to be constant with time, and therefore equal for the months of January and February. The fluxes and transports for each month and wave number are calculated using geopotential values from the numerical model coupled with the perturbation nitric oxide distribution at 105 km as obtained from CRAVENS and STEWART [1978]. Since the data used in obtaining

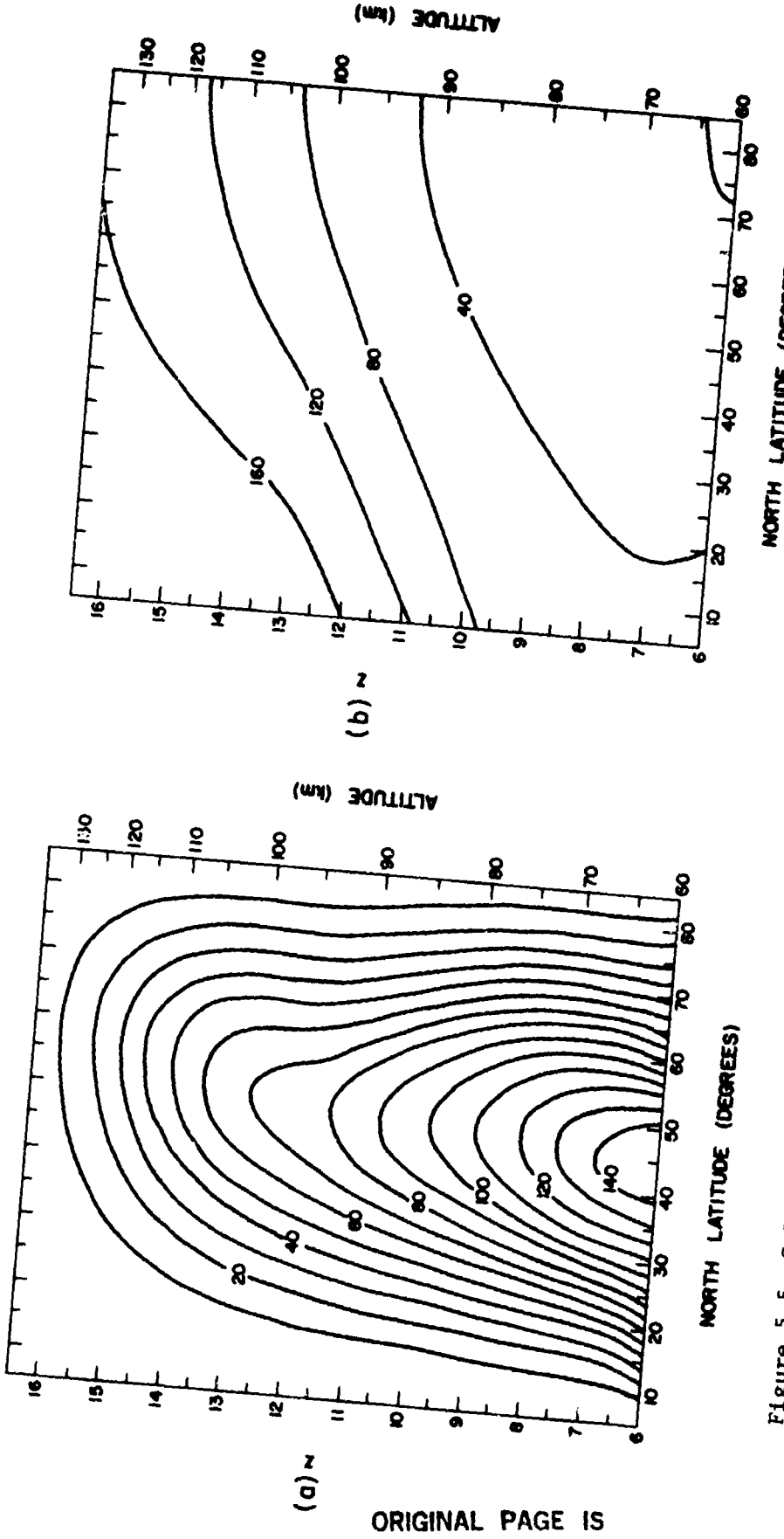

Figure 5.5 Calculated structure for wave number two in February: (a) amplitude in meters and (b) phase in degrees west longitude.

the perturbation distribution was taken at 105 km (z = 13.5), we will confine our discussion of transports and fluxes to that level.

Figure 5.6 shows the zonally-averaged horizontal flux of nitric oxide for both wave numbers in January and February. The numbers and scales represent the magnitude of the fluxes, while the arrows indicate the direction of the flux. An upward pointing arrow represents a northward flux, and a downward arrow, a southward flux. In January, the flux at 105 km due to horizontal planetary wave winds was southward at all latitudes, with a maximum of 7.5×10^{-4} (cm/sec) at 60°N latitude. In February, however, the fluxes have reversed direction and increased in magnitude. The flux in February is directed northwards at all latitudes, and maximizes at 3.6×10^{-4} cm/sec at 60°N. This reversal in flux direction is due to the 180° phase difference in the calculated geopotential from January to February. The February maximum amplitude is almost five times greater than the January maximum, and is a result of the strong $m = 1$ wave component present in February.

The fluxes due to the $m = 2$ waves also show a shift in direction from month to month, due again to the shift in geopotential phase at 105 km from January to February. At 50° latitude, the $m = 2$ flux for January is southward with a magnitude of 4.6×10^{-4} cm/sec, while in February, the flux is northward, with a magnitude of 3.2×10^{-4} cm/sec. The flux directions north of 60° latitude do not change from month to month; however, the amplitudes at a given latitude do vary widely. This is again due to the variation in the geopotential structure from month to month. Note also that $m = 1$ fluxes are, in general, larger than the $m = 2$ fluxes at 105 km. This is a result of the rapid decay with height of $m = 2$ geopotential amplitude.

ZONALLY AVERAGED HORIZONTAL FLUX AT 105 KM

$\overline{v'[\gamma]'}$

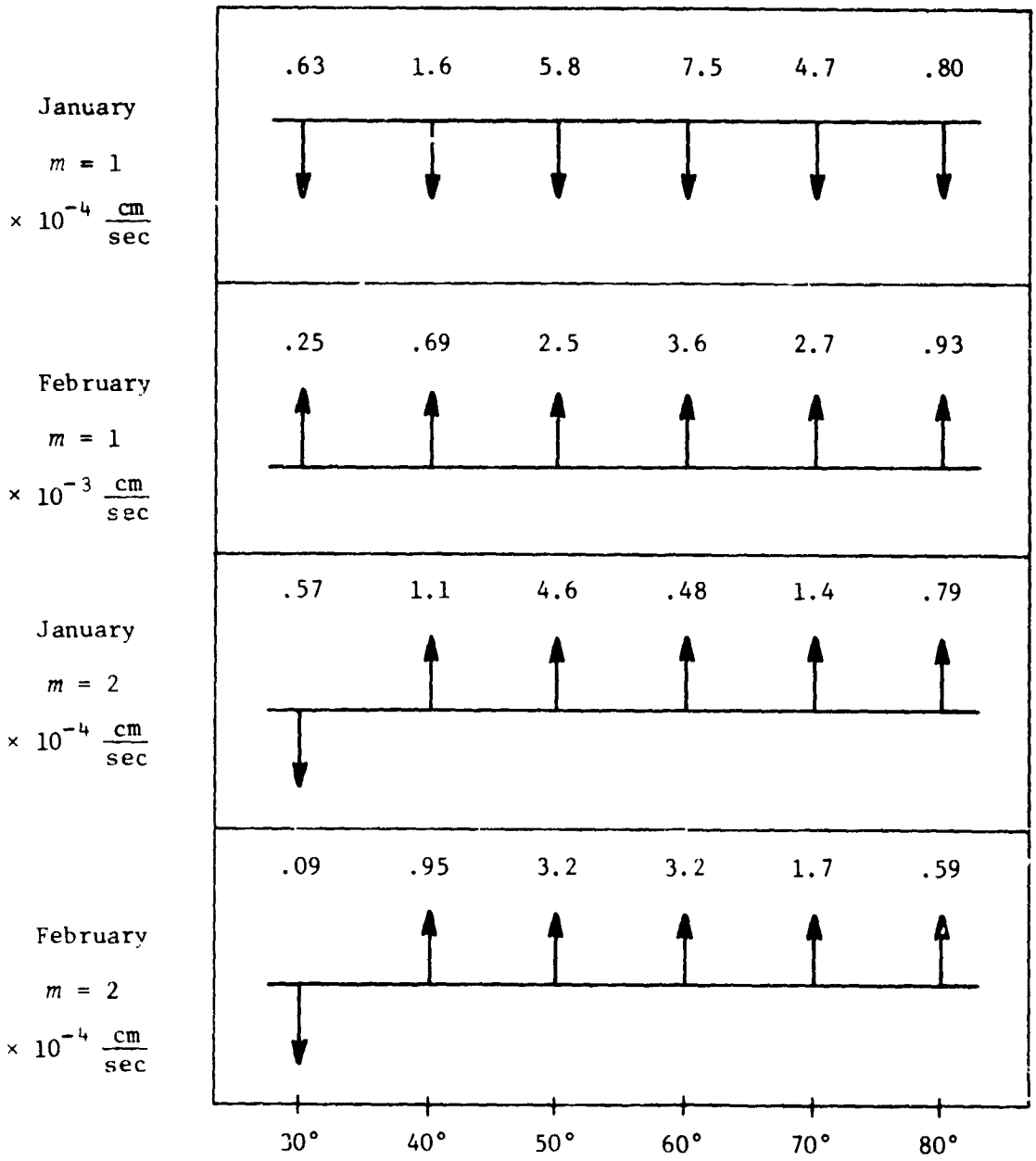

$$\frac{\partial \overline{[\gamma]}}{\partial t} + \frac{1}{a\cos\theta}\frac{\partial}{\partial \theta}\left(\overline{v'[\gamma]'}\cos\theta\right) + \frac{\partial}{\partial z}\left(\overline{w'[\gamma]'}\right) - \overline{w'[\gamma]'} = \overline{P} - \overline{L}$$

Figure 5.6 Zonally averaged horizontal nitric oxide flux ($\overline{v'\gamma'}$) due to planetary waves.

Planetary wave transports, expressed as a percentage change in the zonally mean nitric oxide mixing ratios, are shown in Figure 5.7. The $m = 1$ transports in January (Figure 5.7a), result in a 3% increase in $\overline{NO}$ per day at 105 km at 45°N, and a 4% decrease per day at 75°N. The January $m = 1$ flux was southward, indicating that nitric oxide is being transported southward out of the polar regions and into the midlatitudes. In February, the situation is reversed. A strong northward flux of nitric oxide exists, resulting in a decrease in $\bar{\gamma}$ of 13% per day at 45°N, and an increase of 26% per day at 80°N. Thus, different planetary wave structures for the months of January and February result in significantly different changes in the zonal mean nitric oxide concentration.

The large percent change per day associated with the $m = 1$ wave in February is probably not realistic, in that the assumption of equilibrium of $\bar{\gamma}$ is probably violated. For transports of this magnitude, it is incorrect to assume that the perturbation concentration remains unchanged with time. These results more accurately represent an upper limit on the changes in the zonal mean nitric oxide concentration that could occur as a result of transport by planetary waves. In the next chapter, a time-dependent calculation should provide a more realistic assessment of the effects of planetary wave transport.

The January $m = 2$ flux arrows in Figure 5.6 indicate a convergence between 40° and 50° latitude, and a divergence of flux between 30° and 40°, and 50° and 60°. The $m = 2$ results in Figure 5.7b indicate that this flux convergence produces a 4.8% per day increase in $\bar{\gamma}$ at 45°N latitude. The results of flux divergence show up as two regions of decreasing $\overline{NO}$ centered at 35°N and 55°N. The February $m = 2$ transport shows a 2.25% decrease per day at 40°N, and a 1.5% increase at 80°N. This is accomplished

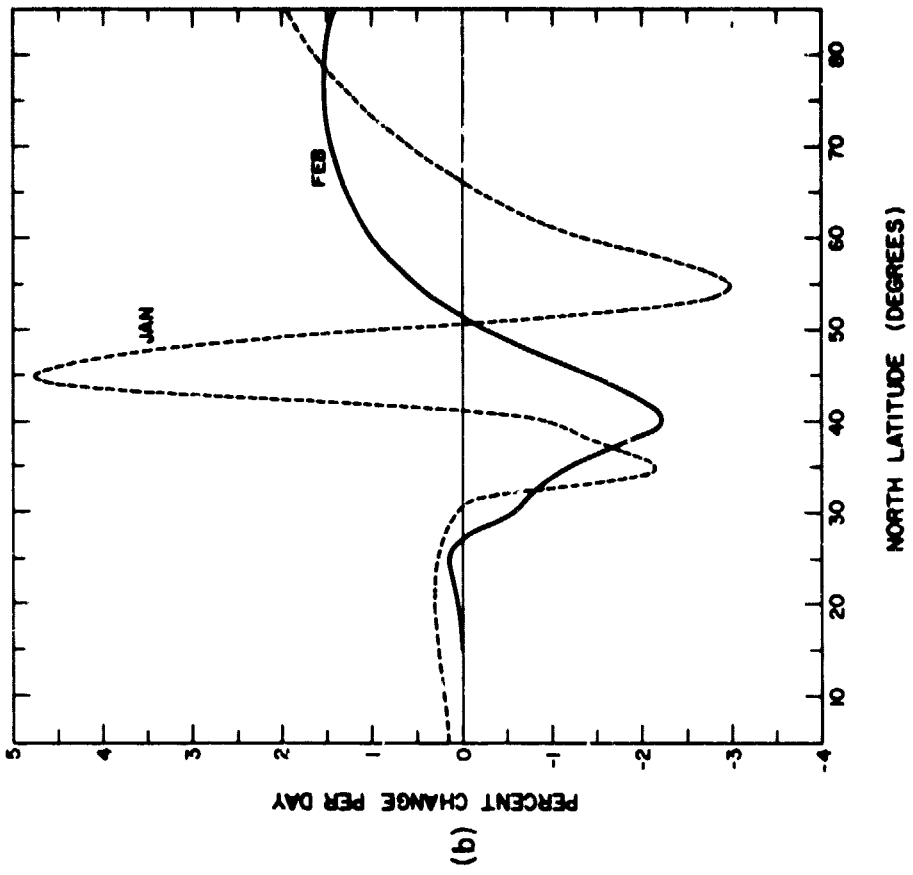

Figure 5.7 Percent change in zonal mean nitric oxide mixing ratio due to north-south planetary wave transport: (a) wave number one and (b) wave number two.

by a flux of nitric oxide from the south toward the polar regions, as seen in Figure 5.6.

5.3 *Vertical Flux and Transport*

An analysis similar to that in the preceding section can also be performed for the vertical transports. Figure 5.8 shows the results of flux calculations for $m = 1$ and $m = 2$, January and February. Here, an upward-pointing arrow represents an upwards flux, and a downward-pointing arrow represents a downwards flux. North of 30°, the $m = 1$ flux in January is upwards, with the maximum occurring at 70°. In February, the situation is reversed, with downward flux poleward of 30°. The February flux again is much larger than that in January, having a maximum amplitude of three times the January maximum. This is again due to the large $m = 1$ wave amplitude in January.

The $m = 2$ vertical fluxes are an order of magnitude smaller than the $m = 1$ fluxes, due to the diminished amplitude of the $m = 2$ wave. The flux for both January and February is basically upwards. The flux in January maximizes at 6.3×10^{-13}/sec at 60°N, while the flux in February has a maximum of 6.7×10^{-13}/sec at 50°N.

Figure 5.9 shows the results of the vertical transport calculations. For the January $m = 1$ case in Figure 5.9a, $\bar{\gamma}$ shows an increase at all latitudes, with a maximum of about 4% per day occurring at 65°N latitude. This increase is the result of transport of nitric oxide into the region from below. For $m = 1$ in February, $\bar{\gamma}$ shows a decrease at all latitudes, with a maximum decrease of about 2% per day occurring near 70° latitude. This is the result of flow of nitric oxide downward out of the region. These transports due to vertical winds are about an order of magnitude larger than those calculated by KURZEJA [1981] in his study of wave

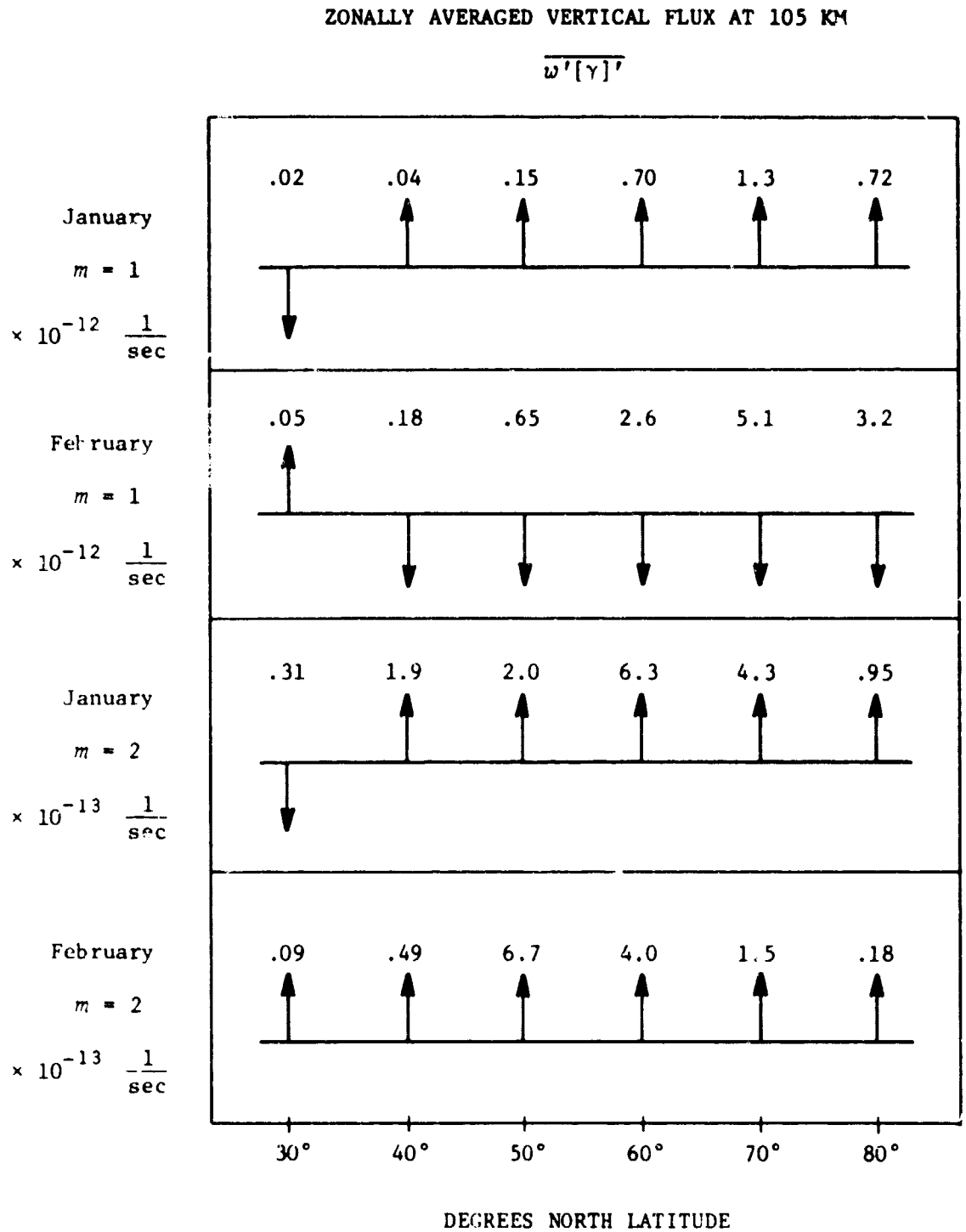

$$\frac{\partial\overline{[\gamma]}}{\partial t} + \frac{1}{a\cos\theta}\,\frac{\partial}{\partial\theta}\left(\overline{v'[\gamma]'}\cos\theta\right) + \frac{\partial}{\partial z}\left(\overline{w'[\gamma]'}\right) - \overline{w'[\gamma]'} = \overline{P} - \overline{L}$$

Figure 5.8 Zonally averaged vertical nitric oxide flux $\overline{w'\,\gamma'}$ due to planetary waves.

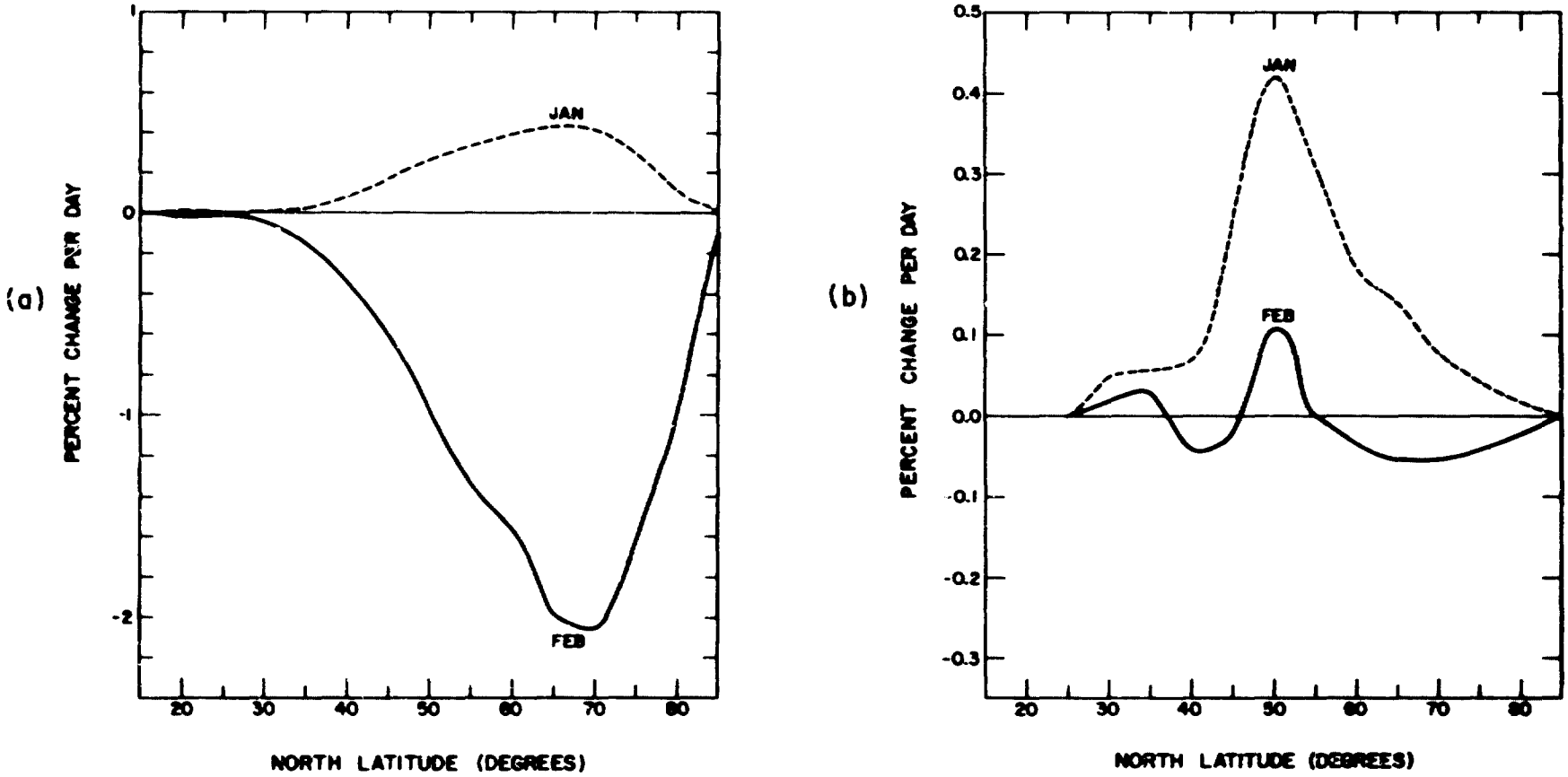

Figure 5.9 Percent change in zonal mean nitric oxide mixing ratio due to vertical planetary wave transport: (a) wave number one and (b) wave number two.

effects on the stratospheric ozone distribution. This is due to the fact that wave amplitudes and hence planetary wave winds increase rapidly with height.

The effect of the $m = 2$ vertical transports on $\bar{\gamma}$ is small, as seen in Figure 5.9b. The maximum increase obtained for January was about .4% per day at 50°N latitude. This was the result of transport into the region from below. The $m = 2$ wave amplitude in February was very small, and this is reflected in the almost insignificant change in $\bar{\gamma}$ produced by the vertical $m = 2$ transports for that month.

5.4 *Conclusions*

In this study, stationary planetary waves were coupled with a time-independent nitric oxide perturbation mixing ratio in order to calculate the effect of planetary wave winds on the zonal mean nitric oxide concentration. The planetary wave structures were obtained using a numerical model forced at the lower boundary by planetary wave observational data. The perturbation mixing ratio $\bar{\gamma}$ was also based on observational data taken during approximately the same time period as the geopotential height data.

Fluxes of nitric oxide due to planetary waves were seen to be strongly dependent on wave amplitude and phase. The transports calculated for February were nearly opposite those obtained for January. Figure 5.10 shows the net transport due to $m = 1$ for January and February. The net transport represents the sum of both north-south and vertical transports; however, the dominating terms are the north-south values. The changes due to vertical transport are at least an order of magnitude smaller than the changes due to north-south motion. In January, $\bar{\gamma}$ shows an increase of about 3% per day at 45°N, and a decrease of about 4% per day at 75°N.

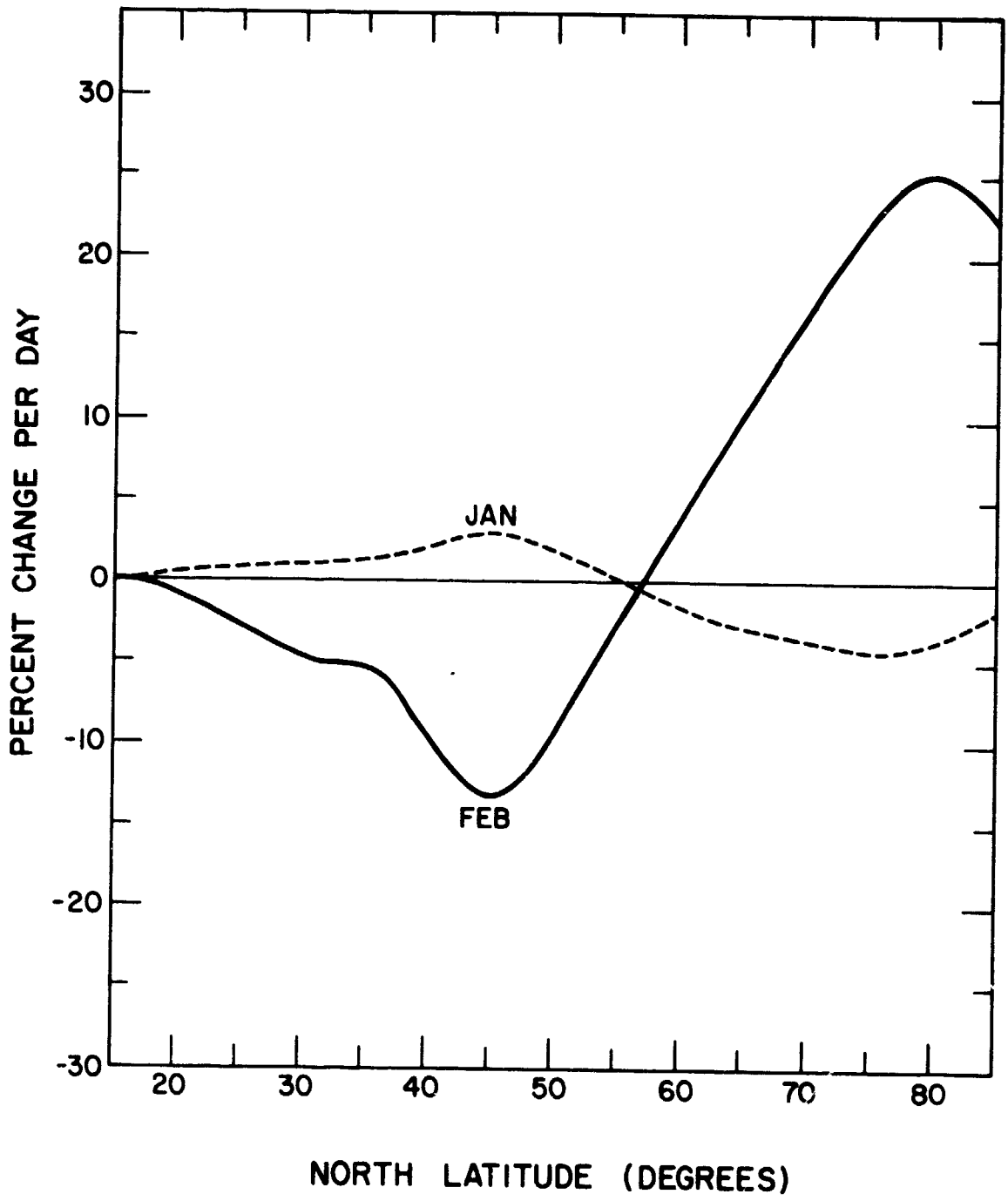

Figure 5.10 Percent change in zonal mean nitric oxide mixing ratio due to both vertical and horizontal wave number one transport.

This is due mainly to motion of nitric oxide from the south toward the north. In January, for $m = 1$, the flux at 105 km is southward and upward; in February, the fluxes are much greater and are northward and downward. This northward flux in February results in a decrease of 13% per day at 45°N, and an increase of 25% per day at 80°N. Thus, depending on the planetary wave forcing, the polar regions may experience either an increase or a decrease in mean concentration.

The changes which occurred as a result of the large $m = 1$ amplitude in February would certainly invalidate the assumption of constant $\bar{\gamma}$ if this persisted for several days. Thus, a model which calculates time-dependent changes in $\bar{\gamma}$ and γ' is necessary to adequately study the problem of transport by planetary waves. Also omitted in this steady-state study was the effect of the zonal mean circulation, which is driven by both diabatic heating and planetary wave fluxes. The secondary circulation generated by planetary waves tends to cancel the effect of the waves themselves; this is the result of the non-interaction theorem. A time-dependent study will be presented in Chapter 6, which will include the effects of changes in and transports due to the mean meridional circulation. The results presented in Chapter 5 should be regarded as an upper limit on the effects of planetary wave transports on the mean nitric oxide distribution.

6. TIME-DEPENDENT CALCULATIONS

In this chapter, results obtained using the time-dependent model will be discussed. In Section 6.1, the interaction between wave and mean flow as evidenced by trial runs of the model is discussed. Section 6.2 will discuss the relative importance of various transport mechanisms present in the upper atmosphere. In Sections 6.3 and 6.4, the results of equilibrium atmosphere studies will be presented. Sections 6.5 and 6.6 will contain traveling and amplifying wave studies and Section 6.7 will present results and conclusions.

6.1 *Zonal Mean Circulation - Contributing Factors*

6.1.1 *Diabatic circulation.* This section will discuss the elements responsible for the zonal mean circulation in the upper atmosphere, namely diabatic heating and dissipation. The effect of planetary wave momentum and heat fluxes on the mean circulation will be discussed in Section 6.1.2

Atmospheric heating results primarily from absorption of solar radiation by ozone in the middle atmosphere, while cooling is a result of infrared emission by CO_2. Since the infrared emission is a function of temperature, an equilibrium temperature is achieved in which heating and cooling are balanced. This balance can be modified by eddy fluxes of heat and momentum, and in the stratosphere, both effects are of equal importance. However, in our region of concern, the mesosphere, planetary wave fluxes are only a second order effect in most cases.

Due to the earth-sun geometry and seasonal variations in the ozone profile, the atmospheric heating rate is hemispherically asymmetric. This hemispheric asymmetry is known as the diabatic heating, and is responsible for driving the mesospheric mean circulation. A meridional circulation is

established to restore thermal balance, and Coriolis torques acting on this meridional circulation force the zonal mean circulation. Figure 6.1 shows the diabatic heating rate for solstice conditions as presented in SCHOEBERL and STROBEL [1978], which was obtained using the LINDZEN and WILL [1973] parameterization. In the mesosphere, this heating results in a rising motion over the summer hemisphere, and sinking in the winter hemisphere, with strong westerlies in the northern hemisphere generated by the Coriolis force acting on the direct pole to pole circulation cell.

Using a diabatic heating similar to that in Figure 6.1, the numerical model can be used to generate the diabatic circulation in the absence of planetary wave fluxes. We assume that the diabatic heating remains constant, and hence the equilibrium circulation can be obtained by setting FLUX = 0 and TIME = 0 in equation 3.9.

The mean meridional circulation which results from the calculation described above is shown in Figure 6.2. Figures 6.2a and 6.2b show the northward and vertical winds in the northern hemisphere as driven by the imbalance between the diabatic heating and radiative cooling. The net heating deficit near the winter pole drives a northwards and downwards meridional circulation. The meridional wind at 105 km maximizes at about 5 m/sec near the equator, and gradually falls off poleward. The vertical wind is strongest in the polar regions, having a value of almost 2 cm/sec at 105 km and 85° north.

An examination of equations 3.1-3.5 indicates that the steady-state zonal mean wind in the absence of planetary wave fluxes is a function of the meridional circulation $\overline{v}$ and the Rayleigh friction β_r. In the absence of Rayleigh friction, the meridional circulation vanishes in the steady state, and the diabatic heating and Newtonian cooling are in

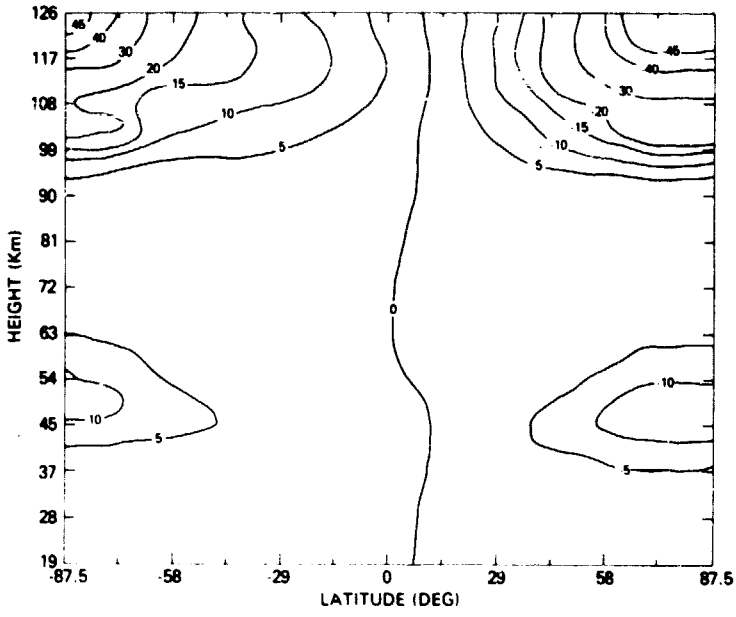

Figure 6.1 Perturbation diabatic heating rate from SCHOEBERL and STROBEL [1978] for solstice conditions. Contours are in °K/day.

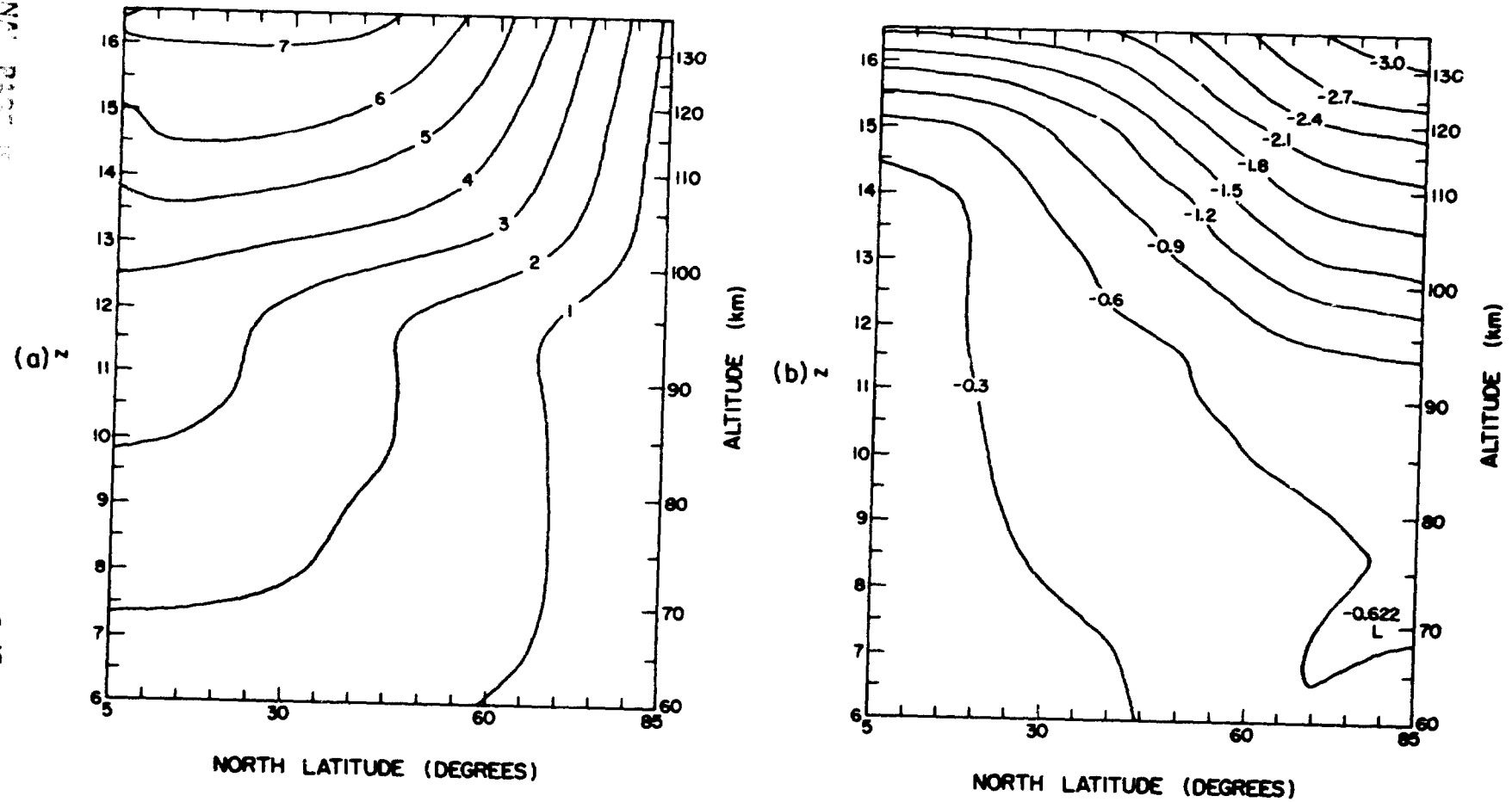

Figure 6.2 Mean circulation resulting from the diabatic heating: (a) meridional winds (m/sec) and (b) vertical winds (cm/sec).

balance everywhere. This results in a strong temperature decrease from equator to pole, and a corresponding increase in zonal mean wind with height at all levels. This situation is contrary to observational evidence, however, and hence, a non-zero β_r must be used in order to simulate the observed wind structure. The Rayleigh friction coefficient represents viscous damping due to the nonlinear effects of smaller scale waves; however, there is no fundamental theoretical method of calculating its value. The Rayleigh friction profile used in this study increases exponentially with height, and is taken from a study of the zonal mean circulation by SCHOEBERL and STROBEL [1978].

The zonal mean circulation which results from the use of the exponential β_r is shown in Figure 6.3a. The wind profile contains a strong polar night jet with a maximum of 85 m/sec centered at 55 km and 47° north latitude. A smaller jet is present in the lower thermosphere having a maximum of about 42 m/sec. The strength and location of the polar night jet agree well with observations presented in CIRA [1975]. However data for the lower thermospheric circulation are sparse. DICKINSON et al. [1977] in a modeling study of the thermosphere have obtained thermospheric jet velocities or 80 to 120 m/sec at 120 km and 60°N. These values are larger than those obtained in this study, and can be attributed to differences in the heating profile above 120 km.

The associated temperature profile is shown in Figure 6.3b. In the lower mesosphere, the temperature gradually increases poleward, consistent with the zonal mean wind through the thermal wind equation. At mesopause heights, the temperature gradient is reversed, producing a temperature maximum of 196° in the polar mesopause. This warm winter mesopause is consistent with the CIRA [1972] atmosphere, although our maximum of 196°K

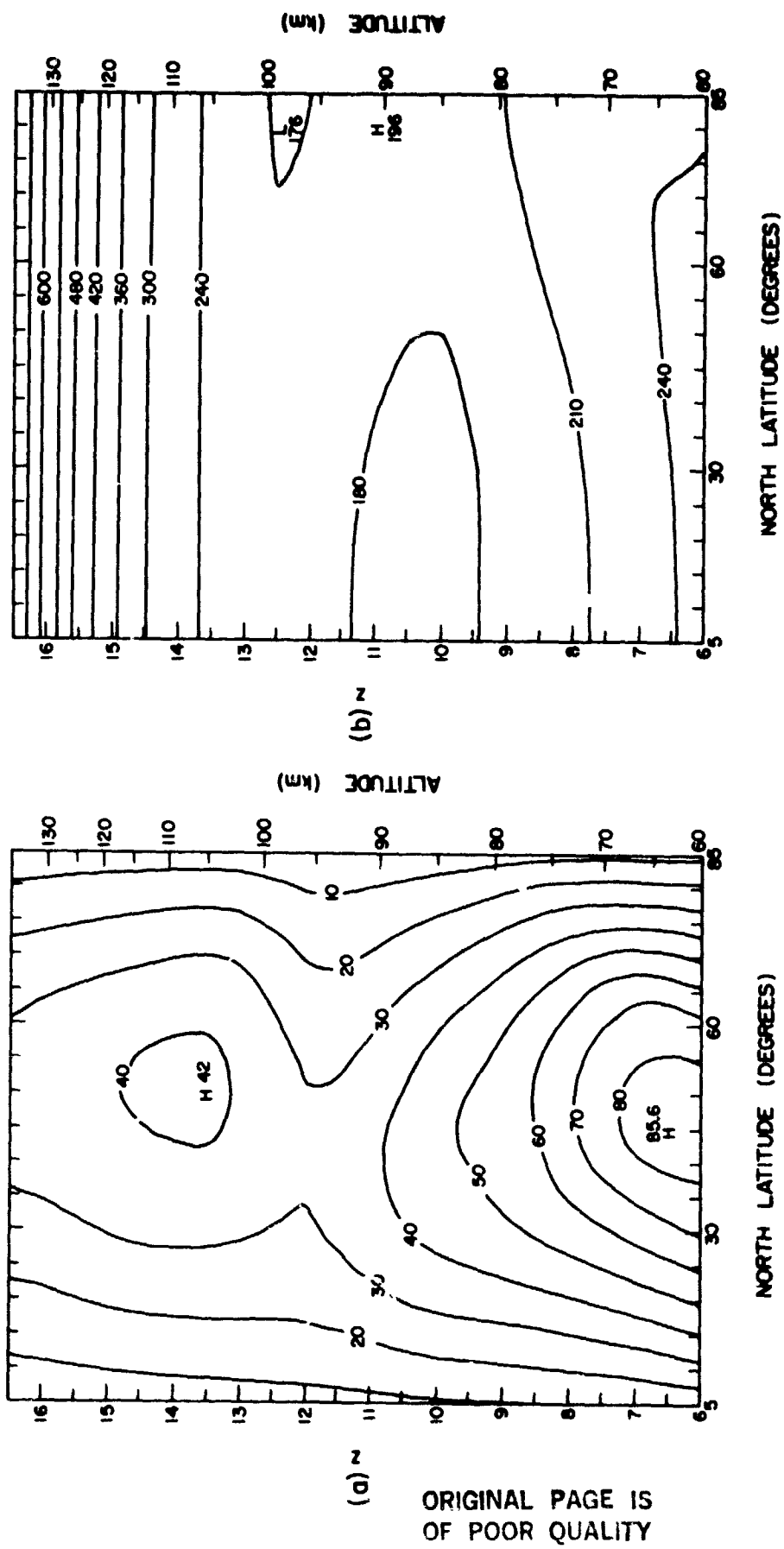

Figure 6.3 (a) Zonal mean wind (m/sec) and (b) zonal mean temperature (°K) resulting from diabatic heating. A positive mean wind implies a westerly (eastward) flow.

is smaller than the CIRA [1972] January maximum of 211°K at 70°N and 85 km. The calculated temperature profile at other levels is in good general agreement with the CIRA [1972] atmosphere.

Thus, using the diabatic heating and β_r profiles as presented in SCHOEBERL and STROBEL [1978], a mean meridional circulation can be calculated using the time-dependent model. The mean circulation obtained provides an adequate representation of the main observational features of the winter upper atmosphere, namely, the poleward and downward meridional circulation, the strong polar night jet and weaker thermospheric jet, and also the warm winter mesopause. These results also closely resemble those of SCHOEBERL and STROBEL [1978], and indicate that the model is working properly.

6.1.2 *Non-interaction and reduced Eulerian formalism.* In this section, the effects of planetary wave fluxes on the zonal mean circulation will be considered. A vertically-propagating planetary wave will transport heat northward, resulting in a planetary wave induced meridional circulation, with rising motion in the polar regions. In the absence of dissipation, transience, or critical levels, this induced circulation will exactly balance the effect of the wave fluxes, resulting in no net mean zonal flow acceleration. This result is known as the non-interaction theorem, as introduced by CHARNEY and DRAZIN [1961].

If the criteria for nonacceleration are not met, then the wave can have an effect on the zonal mean. The wave-induced circulation will tend to reduce the mean meridional circulation, with the corresponding decrease in the zonal mean wind. If the planetary wave fluxes become large enough, as in a stratospheric warming, this thermally indirect wave-induced circulation may dominate, causing a complete reversal of the zonal mean

wind and the formation of an associated critical level.

The differences between the Eulerian and Lagrangian viewpoints were briefly discussed in Chapter 3. It was pointed out that the role of planetary waves in the zonal mean circulation is difficult to assess because of the wave-induced circulation which partially cancels the effect of the wave fluxes. An alternative method of analyzing wave effects was introduced by ANDREWS and MCINTYRE [1976], who defined a residual circulation as that part of the mean meridional circulation which was not balanced by the divergence of its horizontal eddy heat flux. Using the notation introduced in Chapter 3, we can define the residual circulation v_R and ω_R as

$$\omega_R = \bar{\omega} + \frac{1}{(2\Omega a)^2 s} \frac{1}{a\cos\theta} \frac{\partial}{\partial\theta} \overline{v' \frac{\partial \phi'}{\partial z}} \cos\theta \tag{6.1}$$

$$v_R = \bar{v} + \frac{1}{(2\Omega a)^2 s} \left(1 - \frac{\partial}{\partial z}\right) \frac{\overline{v' \frac{\partial \phi'}{\partial z}}}{s} \tag{6.2}$$

The terms on the far right represent the contribution of the wave to the reduced circulation. Note that the continuity equation also applies to the residual mean winds. DUNKERTON [1978] has indicated that the reduced circulation is more appropriate for use in the study of chemical trace transport than the Eulerian mean circulation. In this section, we will study the effects of various planetary wave amplitudes on the zonal mean circulation from both the Eulerian and reduced Eulerian points of view.

If the expressions for the reduced circulation are substituted into equations 3.1 and 3.2, the following equations result.

$$\left(\frac{\partial}{\partial t} + \beta_r\right)\bar{u} - f v_r$$

$$= -\frac{1}{a\cos^2\theta} \frac{\partial}{\partial\theta} \overline{u'v'} \cos^2\theta - \frac{f}{(2\Omega a)^2} \left(1 - \frac{\partial}{\partial z}\right) \frac{1}{s} \overline{v' \frac{\partial \phi'}{\partial z}} \tag{6.3}$$

$$(\frac{\partial}{\partial t} + a_o)\phi_z + (2\Omega a)^2 s\ \omega_R = \overline{Q} \qquad (6.4)$$

where $\overline{Q}$ = diabatic heating.

In this framework, the residual circulation results from an imbalance between the diabatic heating and Newtonian cooling terms in equation 6.4. As before, the zonal mean wind arises due to the Coriolis torque on the meridional velocity. The right-hand side of equation 6.3 represents the sum of the eddy momentum flux divergence and the vertical gradient of the eddy heat flux, and is equivalent to the potential vorticity flux. Thus, in this framework, accelerations of the mean flow result from a non-zero potential vorticity flux, but not necessarily from non-zero heat or momentum fluxes. In fact, for a wave in a non-dissipative medium, the potential vorticity flux goes to zero, which indicates a zero mean flow acceleration consistent with the non-interaction theorem. Note also that in the absence of planetary wave activity, the reduced Eulerian and Eulerian circulations are equivalent.

6.1.3 *Model results: planetary wave effects on the zonal mean.* In this section, we will present the results of studies using the time-dependent model. Two different planetary wave forcings were applied at the lower boundary, and the model was run until an equilibrium was attained. The Eulerian meridional circulation which resulted was then compared to the circulation which existed in the absence of waves.

In the first test run, the February averaged forcing that was discussed in Chapter 5 was used as the lower boundary condition. The model was then allowed to run until changes in the mean state were less than 2%, which in this case took seven days of model time. The wave structure after this seven-day run is shown in Figure 6.4a,b. The maximum amplitude

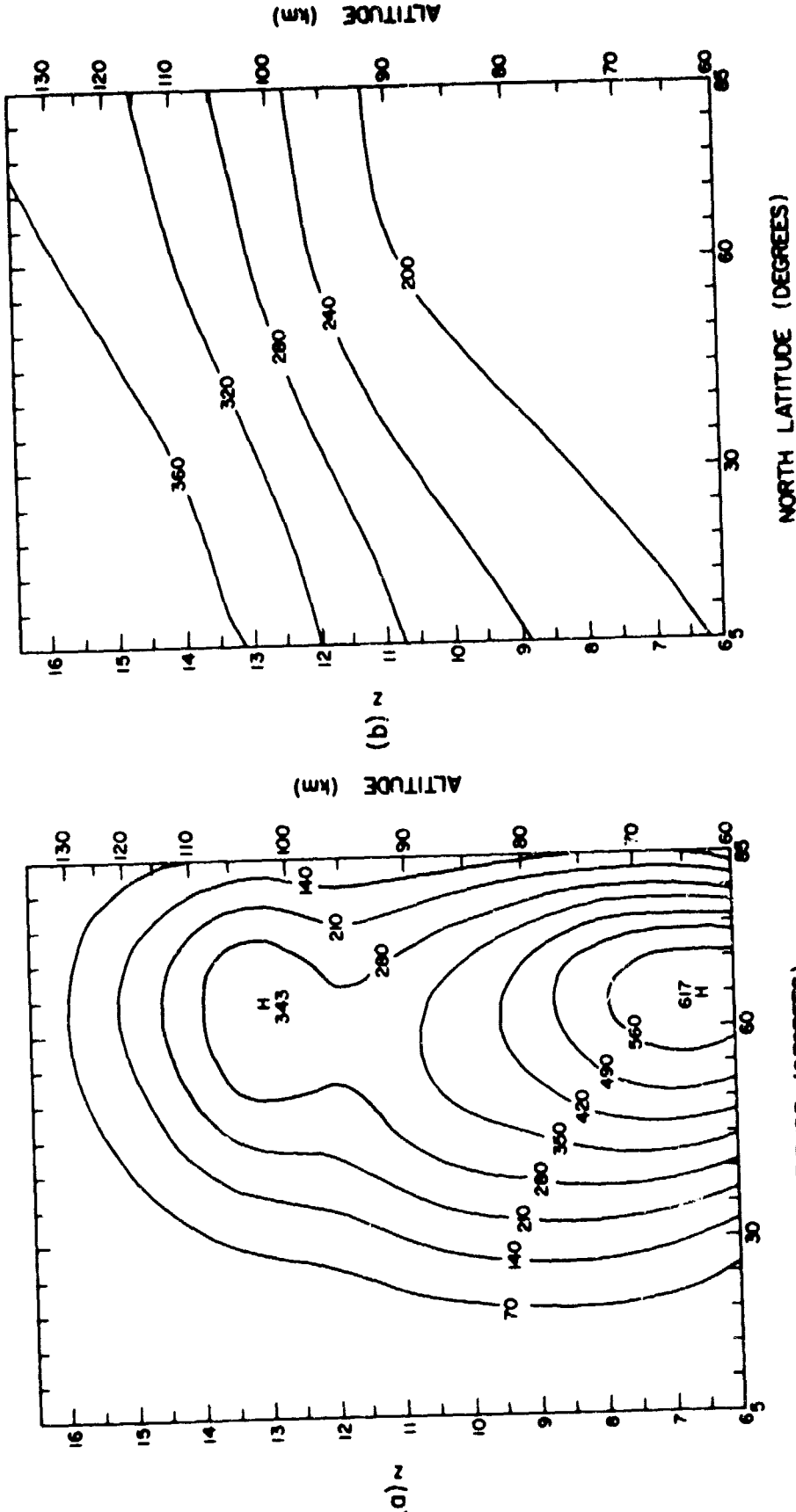

Figure 6.4 Planetary wave number one structure obtained using FEBAVE forcing: (a) amplitude in meters and (b) phase in degrees west longitude.

of about 615 geopotential meters occurs near the lower boundary of the model and is centered at about 65°N latitude. A secondary maximum exists at about 100 km and 60°N. The phase structure indicates that the wave is propagating vertically, and the changes in phase occur more rapidly with increasing height due to the effects of increased dissipation.

The wind structure at this point is shown in Figure 6.5. The wind structure is similar to that calculated without wave fluxes (Figure 6.3a), which indicates that a wave of this amplitude has little effect on the mean flow. Figure 6.6a,b shows the change in $\bar{v}$ and $\bar{\omega}$ that occurred during the seven-day period due to the planetary wave fluxes. The meridional circulation set up by the waves reduced the meridional circulation by a maximum of .58 m/sec at 105 km and 65°N. This was associated with a reduction in the downward flow (increase in the upward flow) as indicated in Figure 6.6b.

The largest change in $\bar{v}$ also occurred near 100 km in the polar regions. This is due to the fact that the potential vorticity flux and hence the effect of the wave on the mean maximizes in that region. Figure 6.7a,b shows the changes in $\bar{u}$ and $\bar{T}$ after seven days. The thermospheric jet has been reduced by a maximum of 6.8 m/sec in the polar regions around 100 km, consistent with the reduction of $\bar{v}$ in that region. The effect of the wave fluxes on temperature is shown in Figure 6.7b. The temperature in the polar regions shows a decrease above 100 km and an increase below the 100 km level due to the readjustment of temperature to achieve thermal balance. This effect will be discussed in greater detail in the next section.

In the second test run, the amplitude of the lower boundary forcing was doubled. Initially, this has the effect of doubling the wave ampli-

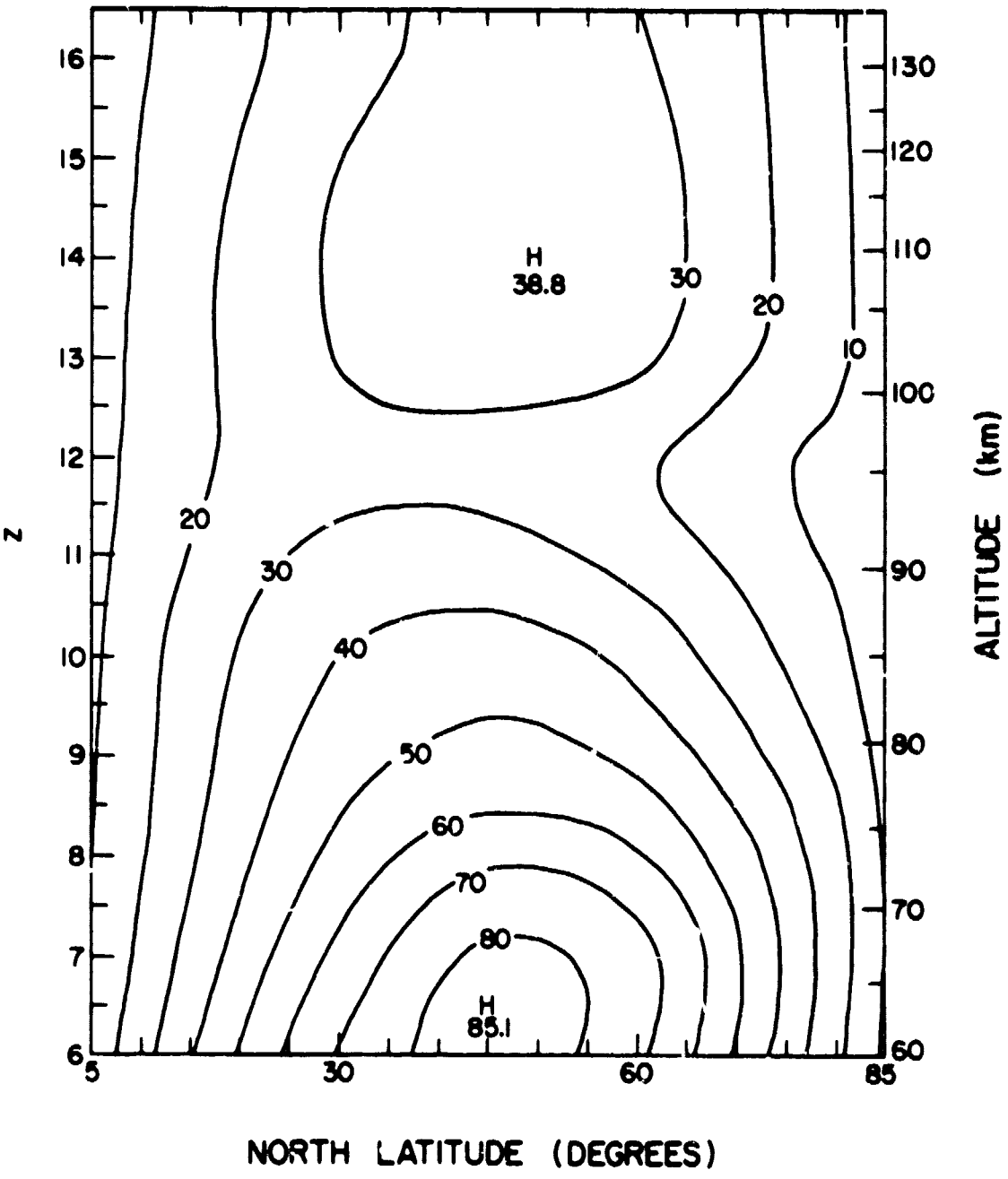

Figure 6.5 Zonal mean wind contours (m/sec) obtained after one week of FEBAVE forcing.

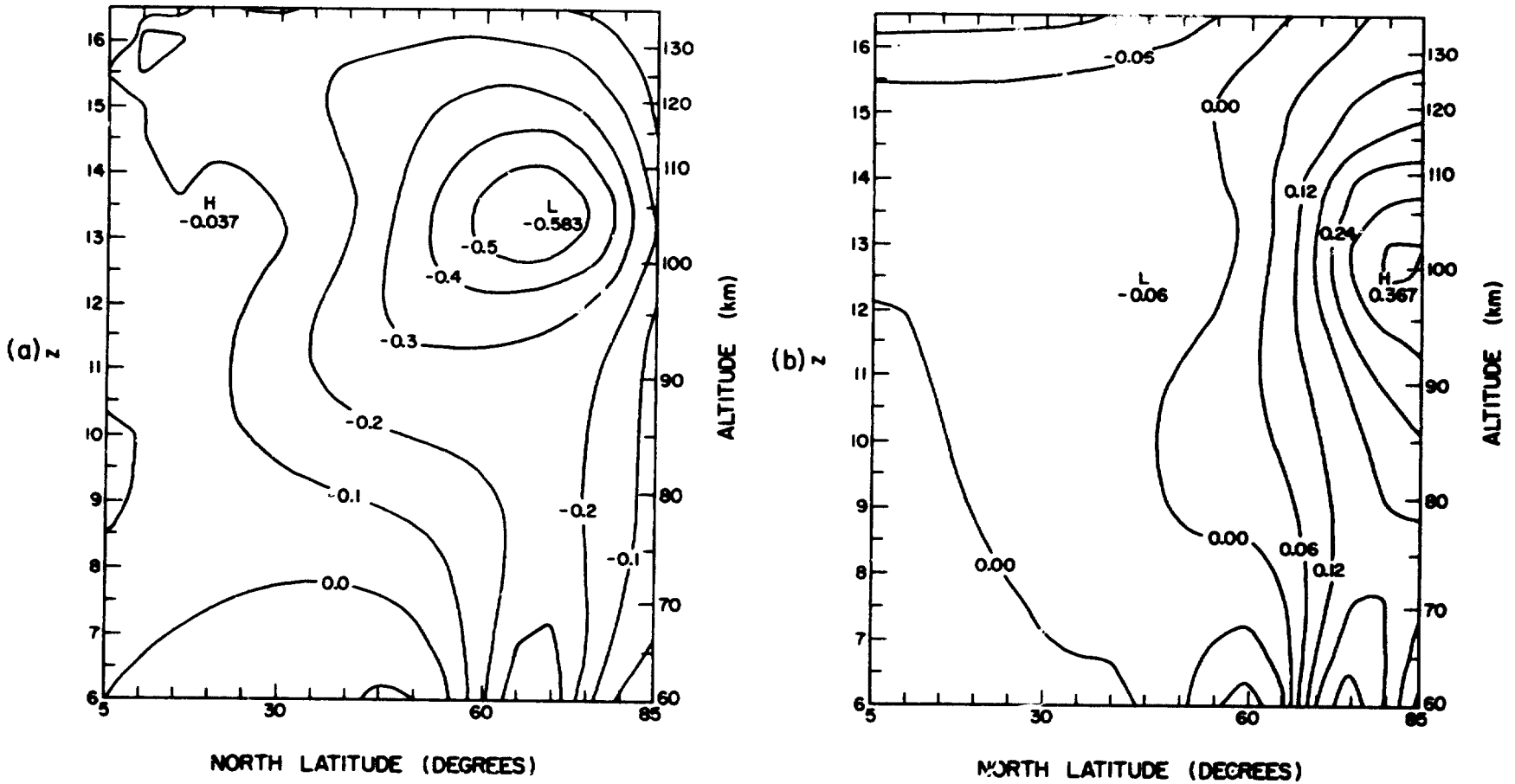

Figure 6.6 Changes in (a) mean meridional wind (m/sec) and (b) mean vertical wind (cm/sec) after one week of FEBAVE forcing.

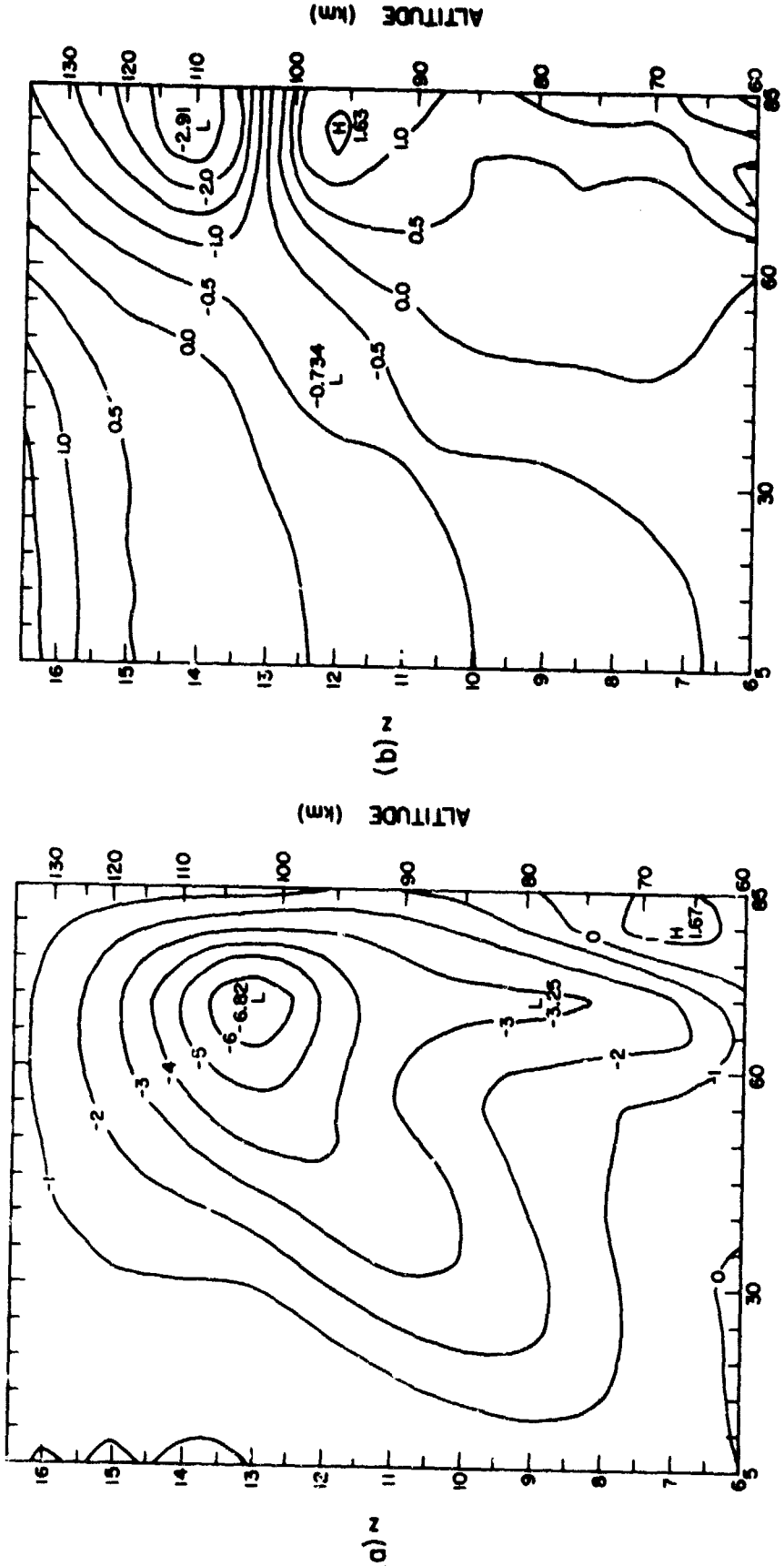

Figure 6.7 Changes in (a) zonal mean wind (m/sec) and (b) mean temperature (°K) after one week of FEBAVE forcing.

tude everywhere, but as time progresses, the wave and mean interact and a new zonal mean state is obtained. This run was terminated after 14 days, and at that point the changes that were occurring were less than 5% per day.

The wave amplitude and phase obtained with the FEBAVE*2 forcing are shown in Figure 6.8a,b. The wave amplitude maximizes at about 1200 gpm at 60 km and 65°N latitude, and has a secondary maximum of about 345 gpm near 105 km and 60°N latitude. Note that although the wave amplitude is nearly double that of the FEBAVE case, the wave amplitudes for the two cases are nearly equal at 105 km. The planetary wave fluxes in the FEBAVE*2 case have caused a shift in the zonal mean wind structure such that the wave is attenuated more rapidly than in the FEBAVE case. Thus, a doubling in the forcing does not necessarily mean that the amplitude of the wave structure will double.

The phase structure of the wave is shown in Figure 6.8b. The phase lines exhibit a westward tilt with increasing height but near the 100 km level, $z = 13$, the phase lines are nearly constant with latitude. This indicates that at this level, the eddy momentum flux vanishes, and that the effect of the wave on the mean is through the eddy heat flux only.

Figure 6.9 shows the wind structure after the 14-day integration. The thermospheric jet intensity has been reduced by about 7 m/sec, and the winds in the $z = 8$ to $z = 14$ region have been greatly reduced. A smaller region of easterlies has formed in the polar regions near $z = 11$, but the planetary wave amplitudes were of insufficient strength to cause a more widespread wind reversal. This general reduction of wind throughout the region is responsible for the reduced planetary wave amplitudes at high

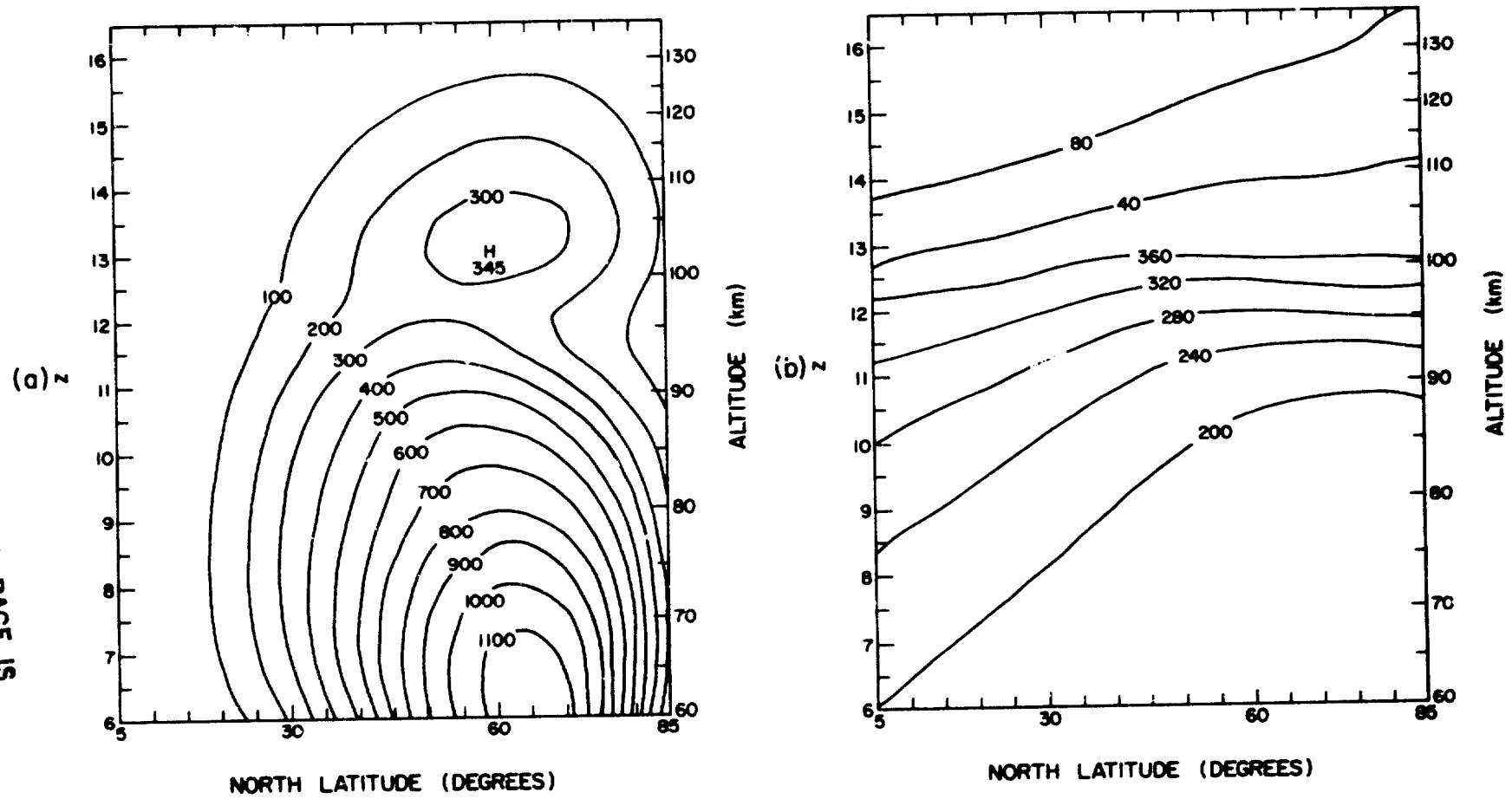

Figure 6.8 Planetary wave number one structure obtained using FEBAVE*2 forcing: (a) amplitude in meters and (b) phase in degrees west longitude.

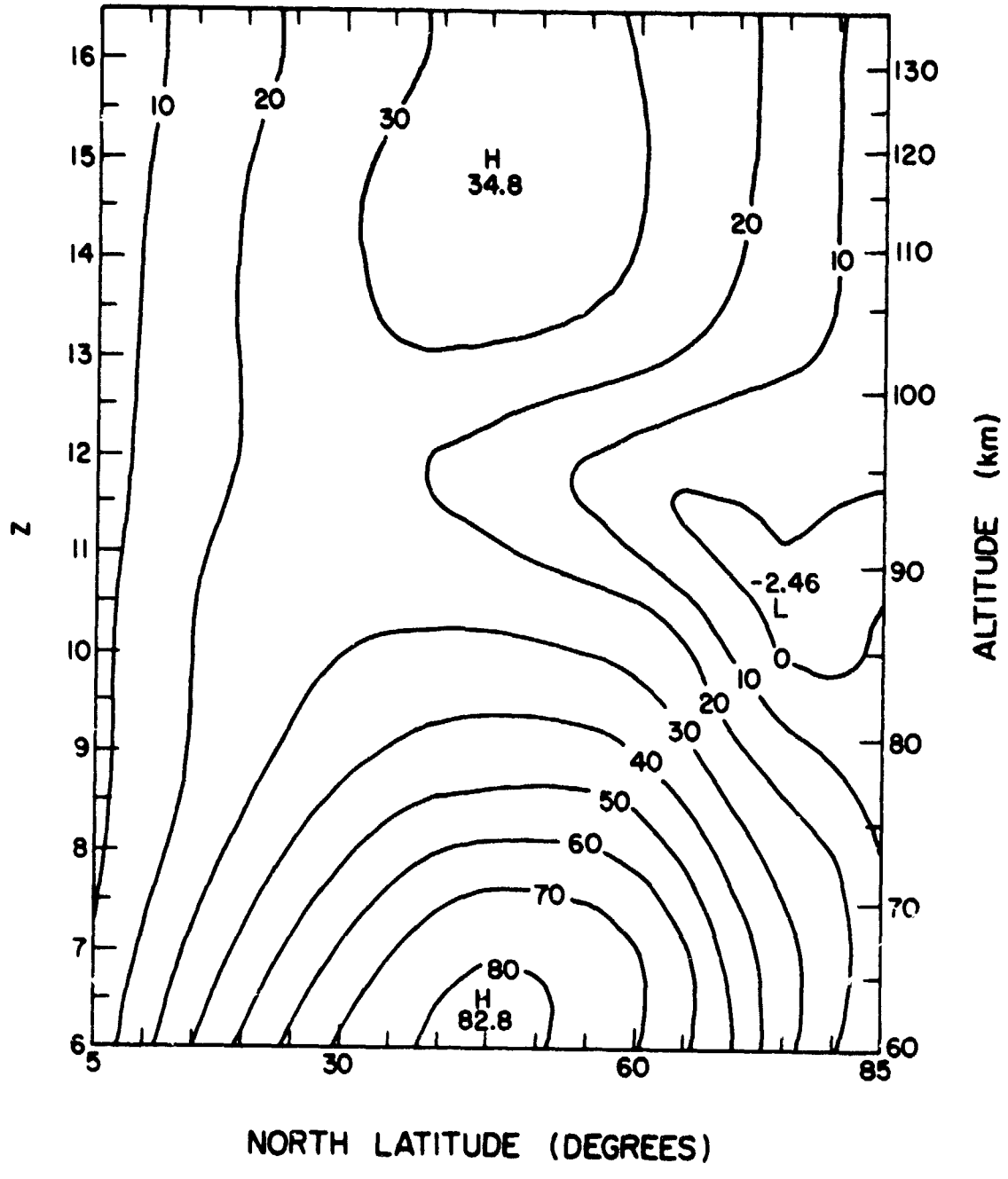

Figure 6.9 Zonal mean wind (m/sec) after two weeks of FEBAVE*2 forcing.

levels, due to a reduction in the ducting of wave energy by the zonal mean structure [DICKINSON, 1968b].

Figure 6.10 shows the changes in the zonal mean state expressed as the difference between the final and initial states. In Figure 6.10a, the reduction in $\bar{u}$ is easily seen. The maximum reduction occurred around $z = 11.0$ (90 km), where the wind was reduced by 23.5 m/sec. It is in this region that the wind reversal occurred. The changes in temperature shown in Figure 6.10b are similar to those observed in a minor stratospheric warming [SCHOEBERL, 1978]. A maximum temperature increase of about 8° occurs around $z = 9$ (80 km) in the mesosphere, with corresponding temperature reductions in the upper mesosphere polar regions and low altitude equatorial regions. Figure 6.11a shows the associated change in $\bar{v}$, with the maximum reduction of 1.3 m/sec occurring around $z = 12.0$ and 55°N. Figure 6.11b shows the reduction in $\bar{\omega}$. Again, the change in $\bar{\omega}$ was greatest in the polar regions at around $z = 12.0$, and results in a lessening of the downward motion.

As a result of these two studies, we have seen that the interaction between wave and mean must be considered if an accurate picture of the zonal mean circulation is to be obtained. If the waves are small enough, little effect on the zonal mean circulation will be seen, as evidenced by the calculations using FEBAVE forcing. However, as the wave amplitude increases, the interaction between wave and mean becomes increasingly important, and large errors could result from assuming that the interaction was negligible for large waves. This finding probably does not significantly affect the results presented in Chapter 5, which ignored the wave mean interaction, because the FEBAVE wave amplitude was the largest forcing used in that study.

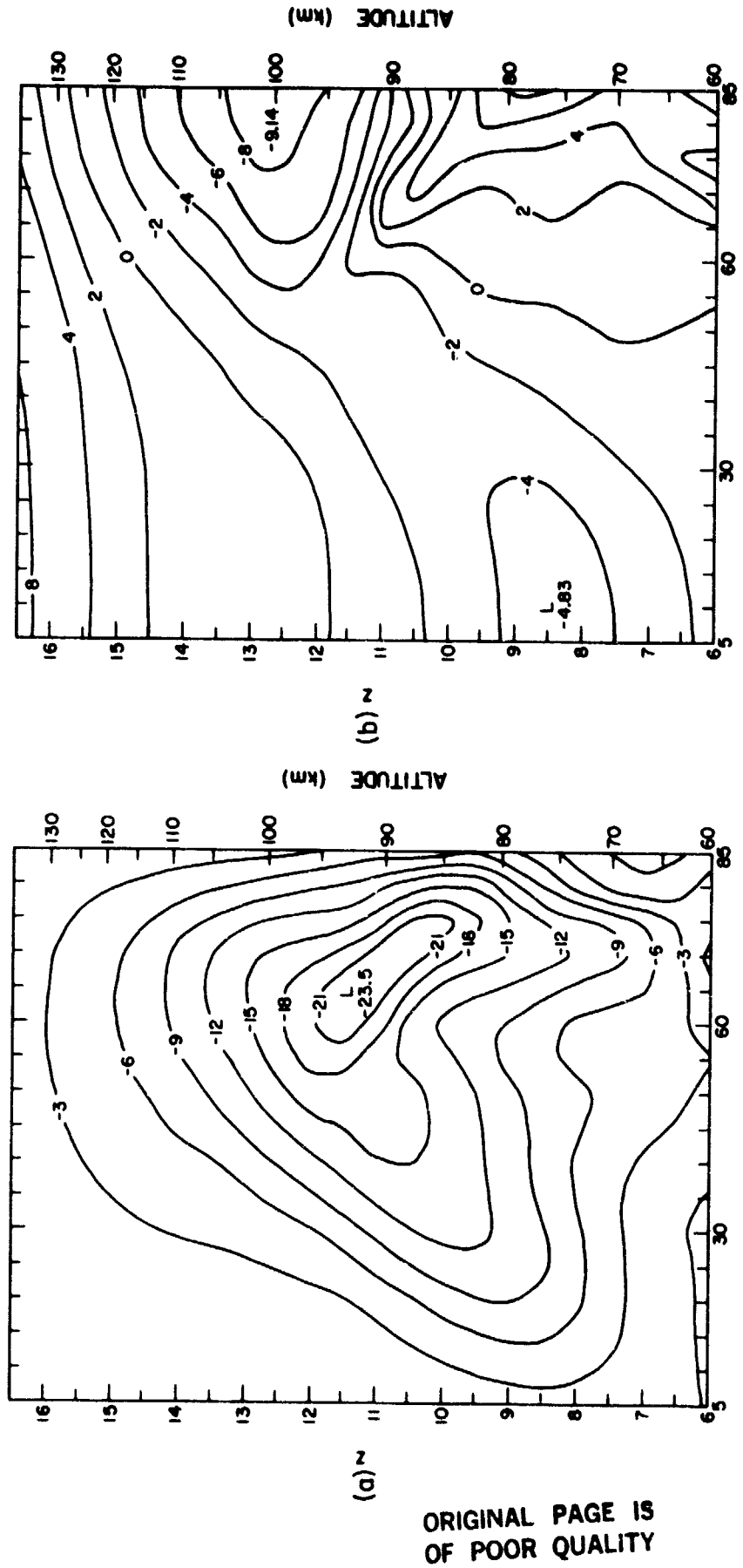

Figure 6.10 Changes in (a) zonal mean wind (m/sec) and (b) zonal mean temperature (°K) after two weeks of FFBAVE*2 forcing.

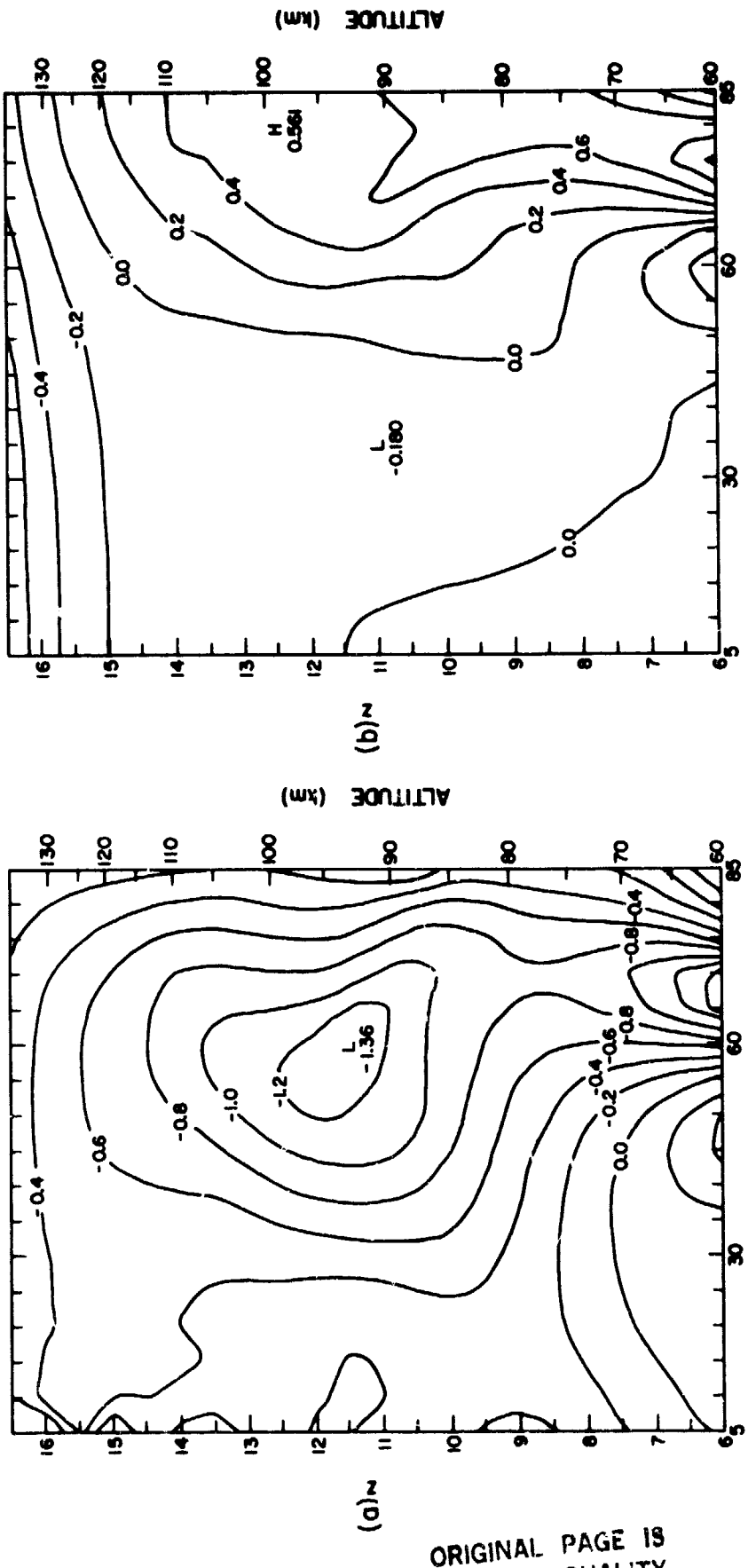

Figure 6.11 Changes in (a) mean meridional wind (m/sec) and (b) mean vertical wind (cm/sec) after two weeks of FEBAVE*2 forcing.

6.1.4 *Model results: reduced Eulerian framework.* In this section, we will discuss the interaction between wave and mean in terms of the reduced Eulerian framework, which was briefly discussed in a previous section. We will concern ourselves only with the FEBAVE*2 forcing case, as the wave-mean interaction in the FEBAVE case was small.

In Section 6.1.2, the residual circulation was defined in terms of the zonal mean circulation and a contribution from a term involving the eddy heat flux. We will for this discussion express the reduced circulation as

$$\omega_R = \bar{\omega} + \omega_{wave}$$

$$v_R = \bar{v} + v_{wave}$$

where ω_{wave} and v_{wave} represent the last term on the right-hand side of equations 6.1 and 6.2. The right-hand side of equation 6.3, which is approximately the quasi-geostrophic potential vorticity flux, will be represented as $\bar{p}$. In this framework, $\bar{p}$ determines the effect of the wave on the mean, and $\bar{v}_R$ and $\bar{\omega}_R$ are the velocities which are most appropriate for tracer transport. In our notation,

$$p = \text{eddy momentum flux divergence} - f\, v_{wave}$$

where f is the Coriolis parameter $2\Omega\sin\theta$.

Figure 6.12a,b contains plots of the two terms that contribute to the potential vorticity flux as calculated on day 14 of the FEBAVE*2 case. The eddy momentum flux divergence (Figure 6.12a) is greatest at high latitudes in the lower mesosphere. However, this effect is partially cancelled by the $-f\, v_{wave}$ term (Figure 6.12b) which is large negatively in that same region. For a steady wave propagating in a non-dissipative region, this cancellation would be complete. Both terms are small south of about 40°N latitude, but a large imbalance occurs in high latitudes

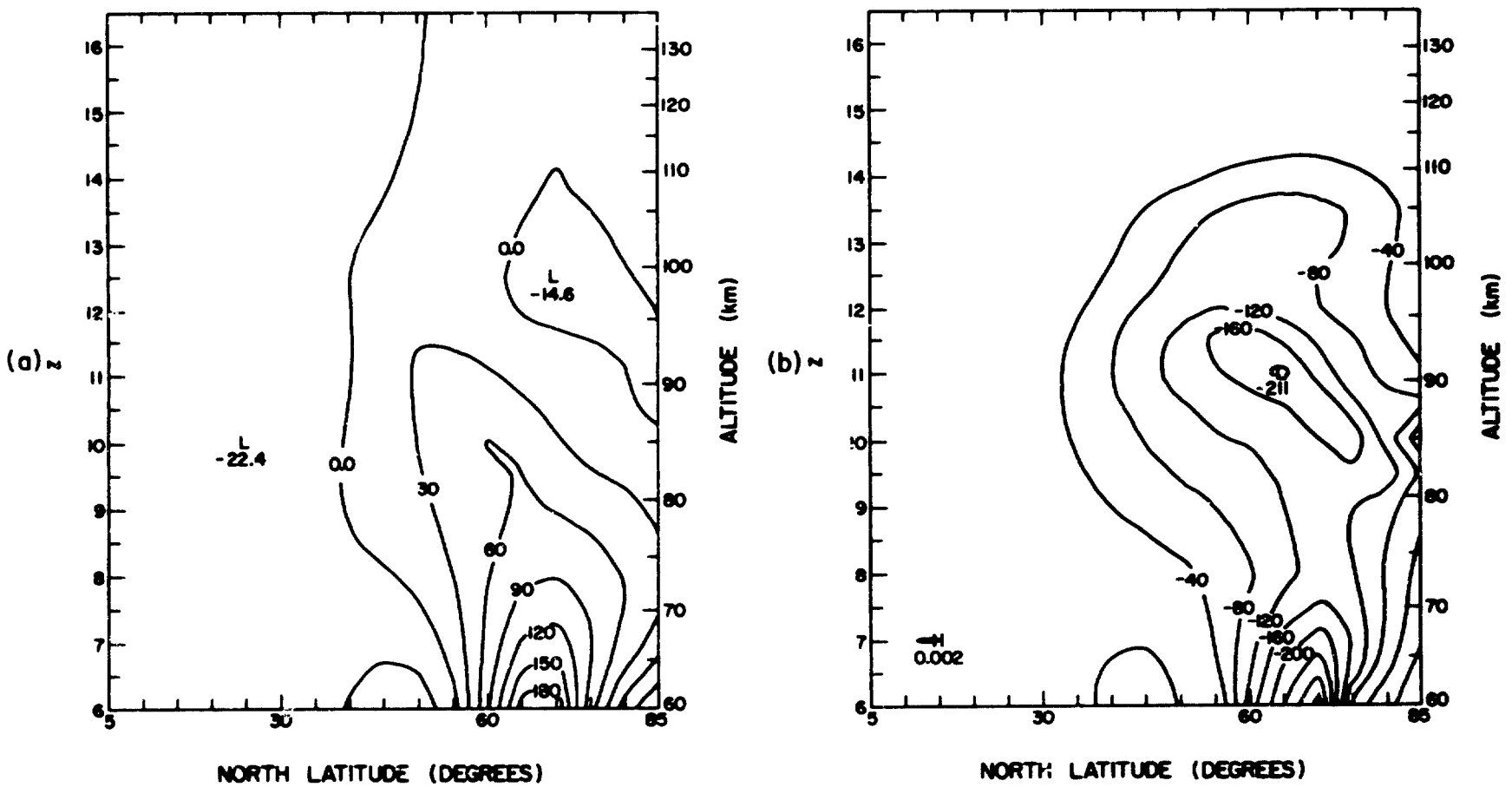

Figure 6.12 Terms which contribute to the potential vorticity flux: (a) eddy momentum flux divergence (cm/sec^2) and (b) the $-f v_{wave}$ term (cm/sec^2).

around z = 11 (90 km). This imbalance results from a violation of the conditions of the non-interaction theorem, which holds only in the absence of critical layers and dissipation. The eddy momentum flux divergence in this region is small (consistent with the horizontal phase lines in that region (Figure 6.8b)) but the $-f\, v_{wave}$ term is large in that region.

These imbalances are more easily seen in Figure 6.13, which gives the potential vorticity flux on day 14. The large negative values of $\overline{p}$ in the upper mesosphere result in a deceleration of the zonal mean wind in that region (see Figure 6.10a), with corresponding changes in $\overline{T}$ (Figure 6.11b). The negative value of $\overline{p}$ partially balances the Coriolis torque on the residual meridional velocity, allowing for a reduced zonal mean wind. In order to maintain balance through the thermal wind equation, adjustments in the temperature structure result.

A calculation of the residual mean winds v_{wave} and ω_{wave} on day 14 provides some interesting results, which are shown in Figure 6.14a,b. The v_{wave} term maximizes around z = 11 and 70°, with a maximum amplitude of about 1.6 m/sec. A second maximum of about 2.1 m/sec exists near the lower boundary at about 70°N latitude. The ω_{wave} term shown in Figure 6.14b is negative north of 50° latitude, and has a maximum of -.6 cm/sec at z = 10.5 and 70°N. A second relative maximum of -1.2 cm/sec exists at 70°N near the lower boundary.

A comparison of Figures 6.14a,b with Figures 6.10b and 6.11a indicates that the wave-induced winds tend to counteract the changes which occur in the zonal mean meridional and vertical winds $\overline{v}$ and $\overline{\omega}$. Although the $\overline{v}$ and $\overline{\omega}$ components of the residual circulation decreased, increases in the v_{wave} and ω_{wave} components compensated for that effect and reduced the changes occurring in the residual circulation. Even though a very large wave

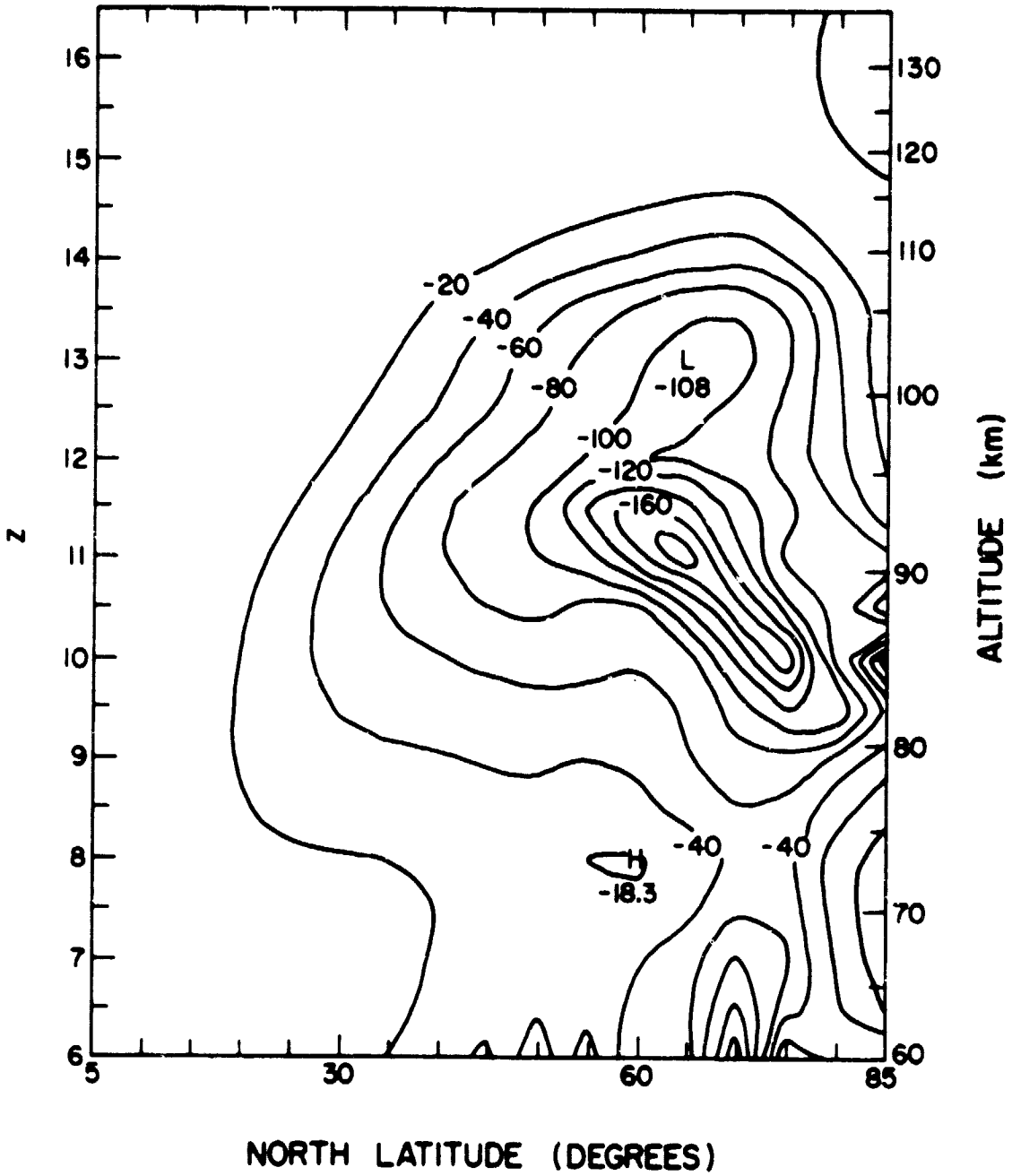

Figure 6.13 Potential vorticity flux (cm/sec^2) after two weeks of FEBAVE*2 forcing.

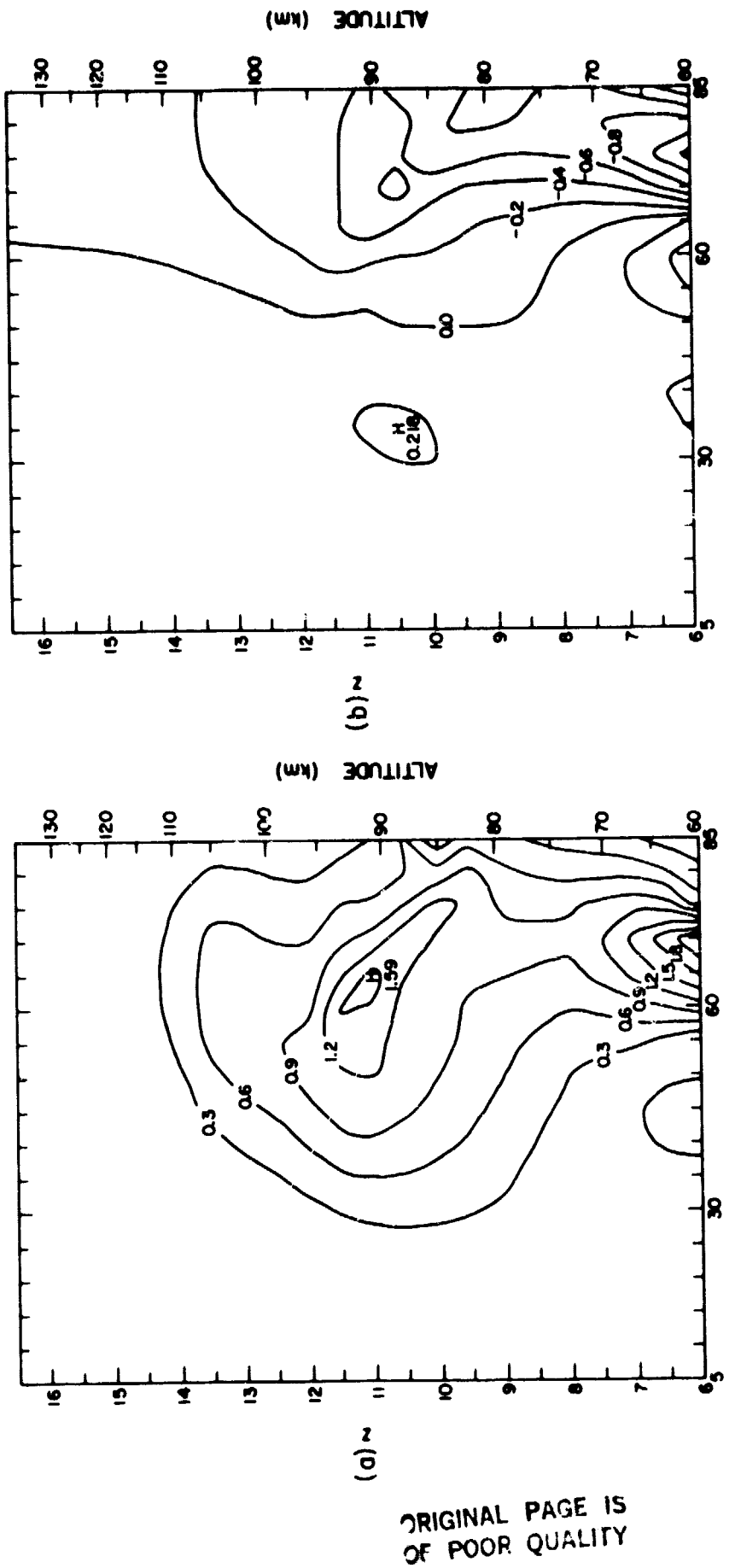

Figure 6.14 Residual mean winds after two weeks of FEBAVE*2 forcing: (a) meridional wind (m/sec) and (b) vertical wind (cm/sec).

amplitude was present and large changes in $\bar{v}$ and $\bar{\omega}$ occurred, changes in the residual circulation were not nearly so large.

6.2 *Zonal Mean Nitric Oxide Concentration - Contributing Factors*

The various factors which contribute to the structure of the zonal mean nitric oxide concentration will be discussed in this section. The effects of diffusion, winds, and sink regions will be examined. The results in this section were obtained using a simplified version of the time-dependent model described in Chapter 3. In this simplified model, the effects of planetary waves are ignored, and the transport of nitric oxide is due to vertical diffusion and/or horizontal and vertical mean winds only. As a result of these simplifications, the model is much less expensive to run, and the individual effects of zonal mean meridional winds, diffusion, and loss are more easily isolated for study.

6.2.1 *Loss Mechanisms.* In the mesosphere, the principal loss mechanism for nitric oxide is the combination of nitric oxide with atomic nitrogen in the ^4S state [SOLOMON, 1981], as follows

$$N(^4S) + NO \rightarrow N_2 + O \tag{6.5}$$

A source for $N(^4S)$ involves the photodissociation of nitric oxide,

$$NO + h\nu \rightarrow N(^4S) + O \tag{6.6}$$

Thus, N^4S is both produced and destroyed by reactions involving nitric oxide. A second sink for atomic nitrogen, and source for nitric oxide, results from the reaction of nitrogen with molecular oxygen.

$$N + O_2 \rightarrow NO + O \tag{6.7}$$

It is clear that the net charge in nitric oxide at a given point depends not only on the transport of nitric oxide into or out of the region, but also on several interrelated chemical reactions involving several chemical

species. A complete treatment of the chemistry would be complex, and is beyond the scope of this study.

In this study, we will attempt to simulate this complex chemistry by using source and sink regions for nitric oxide. We will assume that the major source of nitric oxide is the downward flux from the thermosphere, and that the major sink of nitric oxide is due to the combination of nitric oxide with $N(^4S)$. A comprehensive study of mesospheric chemistry and transport by SOLOMON [1981] indicates that the maximum in the nitrogen concentration occurs near 90 km. This maximum varies from day to night, with the concentration varying from about $3.0 \times 10^5/cm^3$ in the day time to $1.0 \times 10^4/cm^3$ night. Following SOLOMON [1981], the loss of nitric oxide due to reaction 6.5 can be expressed as

$$\frac{\partial \overline{NO}}{\partial t} = 2k\ [N]\ [NO]$$

where $k = 3.1 \times 10^{-11}/sec/cm^3$. If this is characterized as $\frac{\partial [NO]}{\partial t} = r[NO]$, the maximum value of r, (the loss coefficient) is seen to be about $2.0 \times 10^{-5}/sec$. In our study, we are not concerned with diurnal changes due to changes in incident solar radiation; we are only concerned with variations in the zonal mean nitric oxide concentration that are induced by changes in transport by winds and waves. We will assume the loss rate of nitric oxide due to combination with atomic nitrogen remains constant in time, and that the maximum average loss rate is on the order of $1.0 \times 10^{-5}/sec$.

By assuming that the loss of nitric oxide occurs in a sink region characterized by a time-independent loss coefficient, we will be able to identify the effects of changes in wind and wave amplitudes on the nitric oxide concentration. One-dimensional studies by SOLOMON [1981] indicate that the overnight change in the concentration of nitric oxide is small

and thus the use of time-independent loss rate seems to be justified. The results presented in the following sections indicates that reasonable nitric oxide profiles can be obtained by using a postulated sink region.

In the following studies, two different sink regions will be used. Each has a maximum loss rate of 1.0×10^{-5}/sec centered at $z = 11$ (90 km). The sink region extends from about 75 to 105 km, with the value of the loss coefficient decreasing linearly with distance from the maximum level. The first sink region, which will be referred to as regular loss, is constant with latitude. The second sink region, referred to as slant loss, decreases with latitude from 40° latitude and northwards. This decrease is also linear with latitude, with the loss rate at 85° being one-half of the loss rate at 40°. The amount of solar radiation decreases with latitude in the northern hemisphere, resulting in a corresponding decrease in atomic nitrogen. This effectively reduces the loss rate of nitric oxide, and the slant loss sink region is a qualitative attempt to model this phenomena. The slant loss profile is seen in Figure 6.15. Note that the loss is zero both above and below the region.

6.2.2 *Eddy diffusion.* The zonal mean nitric oxide concentration is a result of the balance between chemical loss processes and transport. On the largest scale, this transport is carried out by mean meridional motion and also by large-scale planetary waves. However, small-scale transport due to turbulence, gravity waves and tides are also important. In fact, eddy diffusion represents the major transport mechanism in the upper mesosphere, with the mean meridional circulation playing a secondary but important role.

There have been several attempts at parameterizing this transport by small-scale eddies in terms of an eddy diffusion coefficient. The study

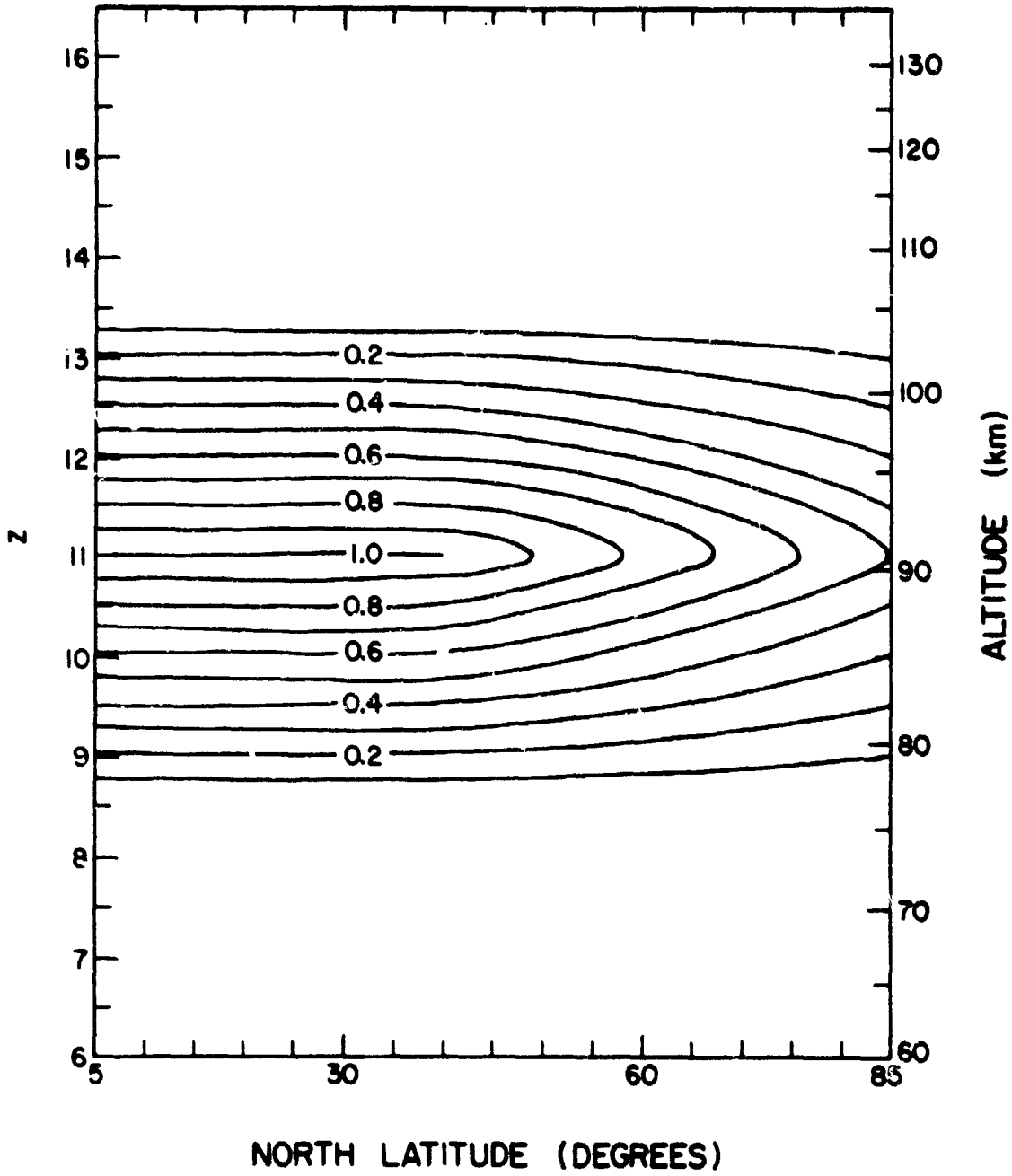

Figure 6.15 Loss profile used in model studies. Contours have units of 10^{-5} sec^{-1}.

by EBEL [1980] is the most recent and comprehensive of these, and was briefly discussed in Chapter 3. He presents coefficients for both horizontal and vertical diffusion, as well as cross terms for counter-gradient diffusion. The meridional circulation used in our study is insufficient to transport nitric oxide downwards through the sink region. Only at high latitudes where the vertical wind is strongest does nitric oxide penetrate the sink region in appreciable quantities. The addition of an eddy diffusion transport term allows for a realistic concentration of NO at all latitudes throughout the sink region.

The eddy diffusion coefficients presented in EBEL [1980] were derived from zonal mean temperature and pressure fields, and from random meridional wind estimates. They include the effects of all scales of atmospheric motion. In our model, the effects of planetary wave motions will be calculated explicitly; thus, the use of EBEL's coefficients would overestimate transport effects. The vertical diffusion coefficients exhibit a marked seasonal dependence, with the calculated coefficients for winter being larger by a factor of 5 or so than those for summer at a comparable latitude. The large winter values are partially due to the existence of large-scale winter hemisphere wave activity. The smaller coefficient values in the summer can be viewed as being representative of the background transport due to smaller scale wave activities. Thus, the value of the diffusion coefficient used in our study must be at least as large as the summer background value, but probably not as large as the calculated winter hemisphere values.

In this study, we will use vertical eddy diffusion only. Horizontal transport will be explicitly calculated from wind and wave structure. The vertical variation in the vertical eddy diffusion coefficient is similar

to that used by Ebel, and the coefficient will be assumed to be constant with latitude. Our primary concern in this study is to determine the effects of planetary wave winds and transports on the zonal mean nitric oxide concentration. By keeping the background diffusion and sink mechanisms as simple as possible, the effects of the waves and the wave mean interaction will be more clearly elucidated.

Although the vertical variation of the diffusion coefficient as presented in EBEL [1980] was used, the actual value of the coefficients needed to be determined. Ebel's coefficient values at 100 km ranged from a minimum of 8.0×10^5 cm^2/sec at the summer hemisphere pole to a maximum of about 1.1×10^7 cm^2/sec in the winter hemisphere at 30°N. Using our simplified time-dependent model, we performed a series of one-dimensional studies using various values of the diffusion coefficient and upper boundary flux. The model was run until an equilibrium was reached, which required runs of about 60 model days in most cases. A one-dimensional sink region similar to the "regular" profile discussed in the previous section was used. Three values of the coefficient were used, 2.0×10^6, 5.0×10^6, and 1.0×10^7 cm^2/sec. These were coupled with vertical diffusive fluxes of 1.0×10^8 $molec/cm^2/sec$ and 3.0×10^8 $molec/cm^2/sec$ at the upper boundary. These coefficients and fluxes are on the same order of magnitude as those used in the previously-mentioned studies by SOLOMON [1981].

Future references to the above test cases will be made using the notation as follows. (2,1) will indicate the test run using a diffusion coefficient of 2.0×10^6 cm^2/sec and an upper boundary downwards flux of 1.0×10^8 $molec/cm^2/sec$. For example, (10,2) indicates a diffusion coefficient of 10.0×10^6 cm^2/sec, and flux of 2.0×10^8 $molec/cm^2/sec$.

The results of the one-dimensional studies are shown in Figure 6.16. The first index represents the value of the diffusion coefficient, while the second index represents the downwards flux at the top of the model (here set at 120 km). Shown for comparison are vertical profiles obtained from MEIRA [1971] and TOHMATSU and IWAGAMI [1976] which were both taken from winter measurements around 40°N latitude. The vertical profile appears to be quite sensitive to both the coefficient value and the flux at the upper boundary. This sensitivity to boundary flux has also been seen by SOLOMON [1981]. For a given coefficient value, a tripling of the flux results in a tripling of the equilibrium concentration in upper levels. Even at much lower levels, the effect is still large. Thus, a change in the downward flux at the upper boundary could have a significant effect throughout the region. For a given flux, decreasing the diffusion coefficient causes an increase in concentration at upper levels, and a corresponding decrease in concentration in the middle of the region, near z = 10 or 11. The minimum concentration level also moves downward. With the smaller coefficient, transport out of the region due to diffusion has decreased. This causes the nitric oxide to pile up in the upper regions. Similarly, the minimum concentration deepens because of less efficient transport into the region from above. A readjustment in the equilibrium between transport and loss occurs, causing the downward shift of the level of minimum concentrations.

The test profiles which most closely resemble the experimental profiles seem to be those with a vertical diffusion coefficient of 2.0×10^6 cm^2/sec. The (2,1) and (2,3) profiles closely approximate the slope of the experimental profiles at the z = 9 to z = 13 region. Also, the (2,1) and (2,3) minima occur near the same level as the MEIRA [1971]

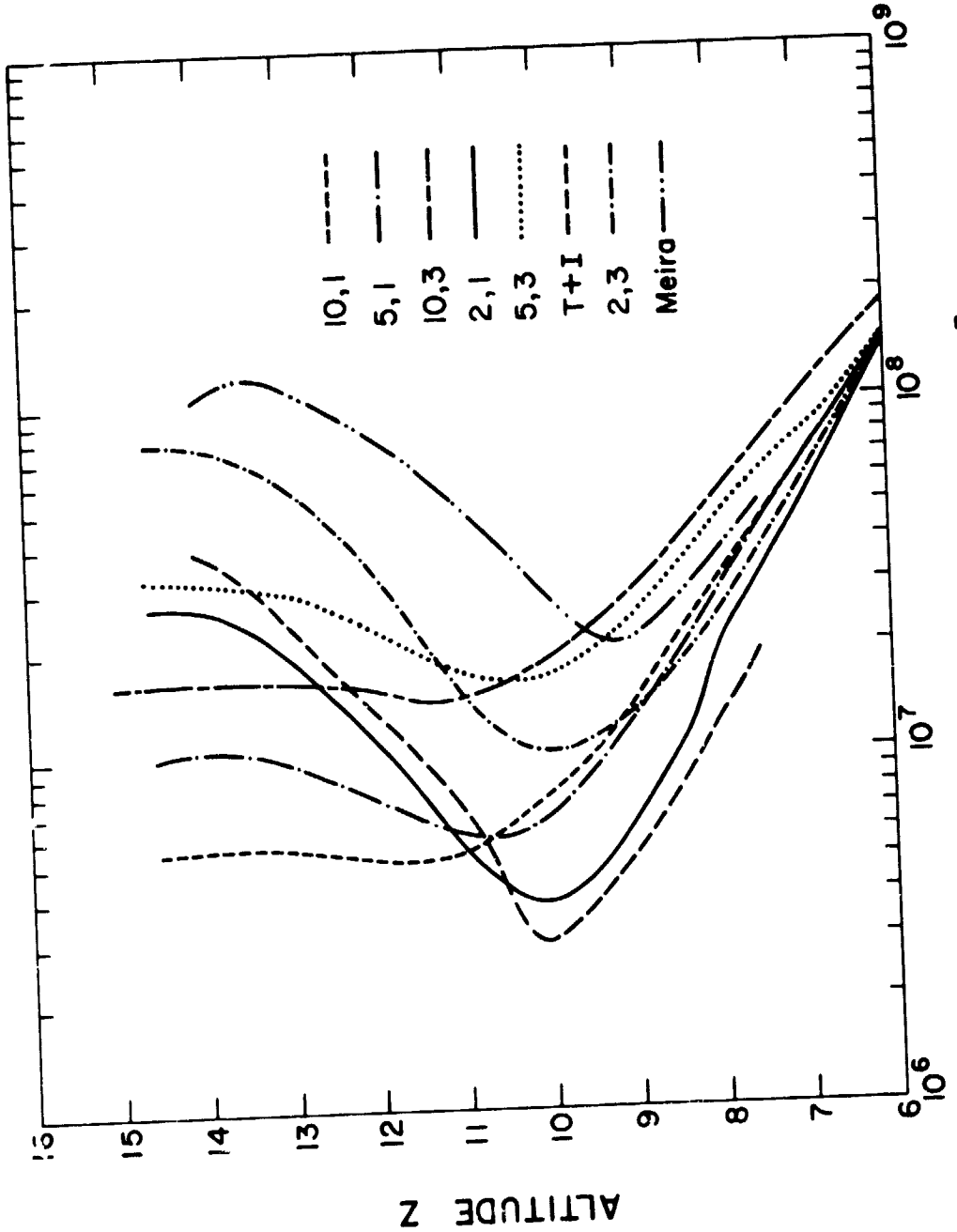

Figure 6.16 Calculated vertical nitric oxide profiles due to diffusion only, compared to the observations of MEIRA [1971] and TOMATSU and IWAGAMI [1976] (abbreviated T+I in the figure).

and TOHMATSU and IWAGAMI [1976] profiles. The (10,1) and (10,3) profiles have very little slope in the z = 11 to z = 14 region. Also, the minima in the profiles occur too high. Although the (5,1) and (5,3) profiles are a little better, they still don't approximate the experimental data as closely as the (2,1) or (2,3) profiles.

The value of 2.0×10^6 cm^2/sec falls within the acceptable range for vertical coefficients as discussed earlier in this section. While not as large as the maximum value at 100 km as presented by EBEL [1980], it is of the same order of magnitude of the coefficients at that level. Also, this value provides the best agreement with the experimentally obtained profiles as presented in Figure 6.16. From this point on, all the studies discussed will use a vertical diffusion coefficient having a value of 2.0×10^6 cm^2/sec at 100 km, and varying with height according to the EBEL [1980] profile. Also, we will assume no latitudinal variation in the diffusion coefficient.

6.2.3 *Meridional winds.* In this section, the effects of mean meridional and vertical winds on the zonal mean nitric oxide concentration will be examined. First, the calculated concentration at 105 km will be compared to experimental results, and a choice will be made between the "regular" and "slant" loss profiles. Then, the effects of horizontal and vertical winds on the equilibrium NO concentration will be explained.

The results in this section were again obtained using the simplified time-dependent model. In this and all future studies, the vertical diffusion coefficient was set to 2.0×10^6 cm^2/sec at 100 km, and the flux at the upper boundary was set at 1.0×10^8 $molec/cm^2/sec$. The model was run until equilibrium was achieved, a process which typically took about 60 model days. Planetary wave effects were ignored in these calculations.

Figures 6.17a,b contain the equilibrium distributions of $\overline{NO}$ obtained with the regular and slant loss distributions. Above $z = 13.5$, there is little difference in the two profiles. However, below this region, the effect of a reduced loss north of 40° latitude results in high nitric oxide concentrations there. The concentration minimum in both distributions occurs near $z = 10.0$. However, the minimum values in the polar regions in Figure 6.17b are much larger than those in Figure 6.17a. This is a result of the decreased importance of the loss mechanism in that region. The concentrations at low level high latitudes are also markedly larger in the slant loss case. This would indicate that transport of NO from high levels occurs most efficiently at high latitudes, where vertical winds are strongest, and the loss mechanisms are weakest. Since there is a physical basis for the slant loss profile, we will use it exclusively in the remaining studies. It should be noted that these profiles were calculated without the effects of planetary wave winds. The steep latitudinal nitric oxide gradients may be reduced greatly by the inclusion of planetary wave transports. This will be discussed in greater detail in later sections.

Figure 6.18 shows the profile obtained by using vertical winds only. Comparison of this figure with Figure 6.17b shows the effect of the addition of meridional winds. The meridional winds are northward throughout the region, and have the effect of transporting nitric oxide from the low latitudes to the polar latitudes. Thus, the nitric oxide concentrations in low and midlatitudes are reduced by the addition of meridional winds. This nitric oxide, which is brought to the polar regions by the northward transport, is then carried downwards out of the region by the strong vertical winds that exist there. The overall effect of the meridional

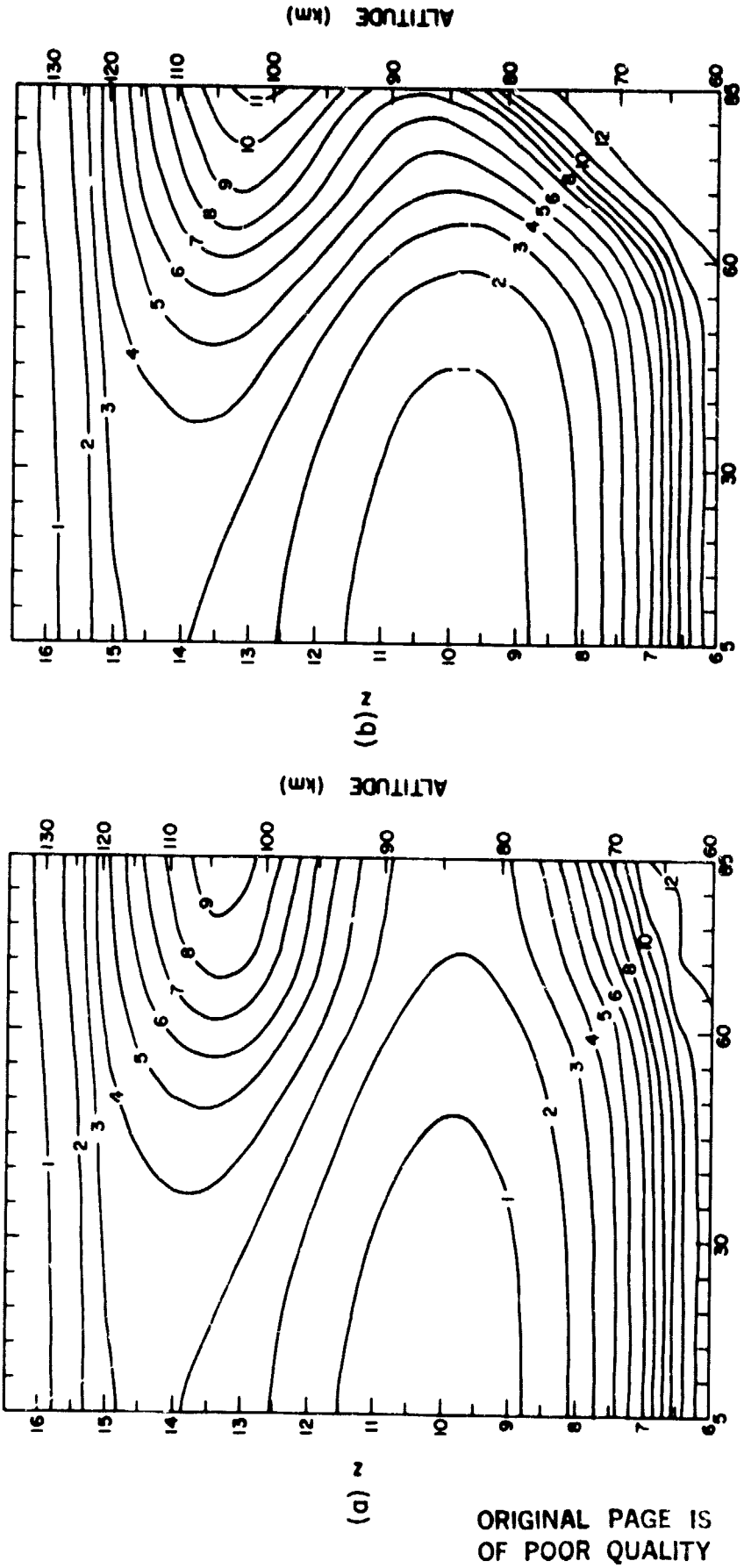

Figure 6.17 Equilibrium distributions of $\overline{NO}$ obtained with (a) regular loss and (b) slant loss. Contours have units of 10^7 molec/cm^3.

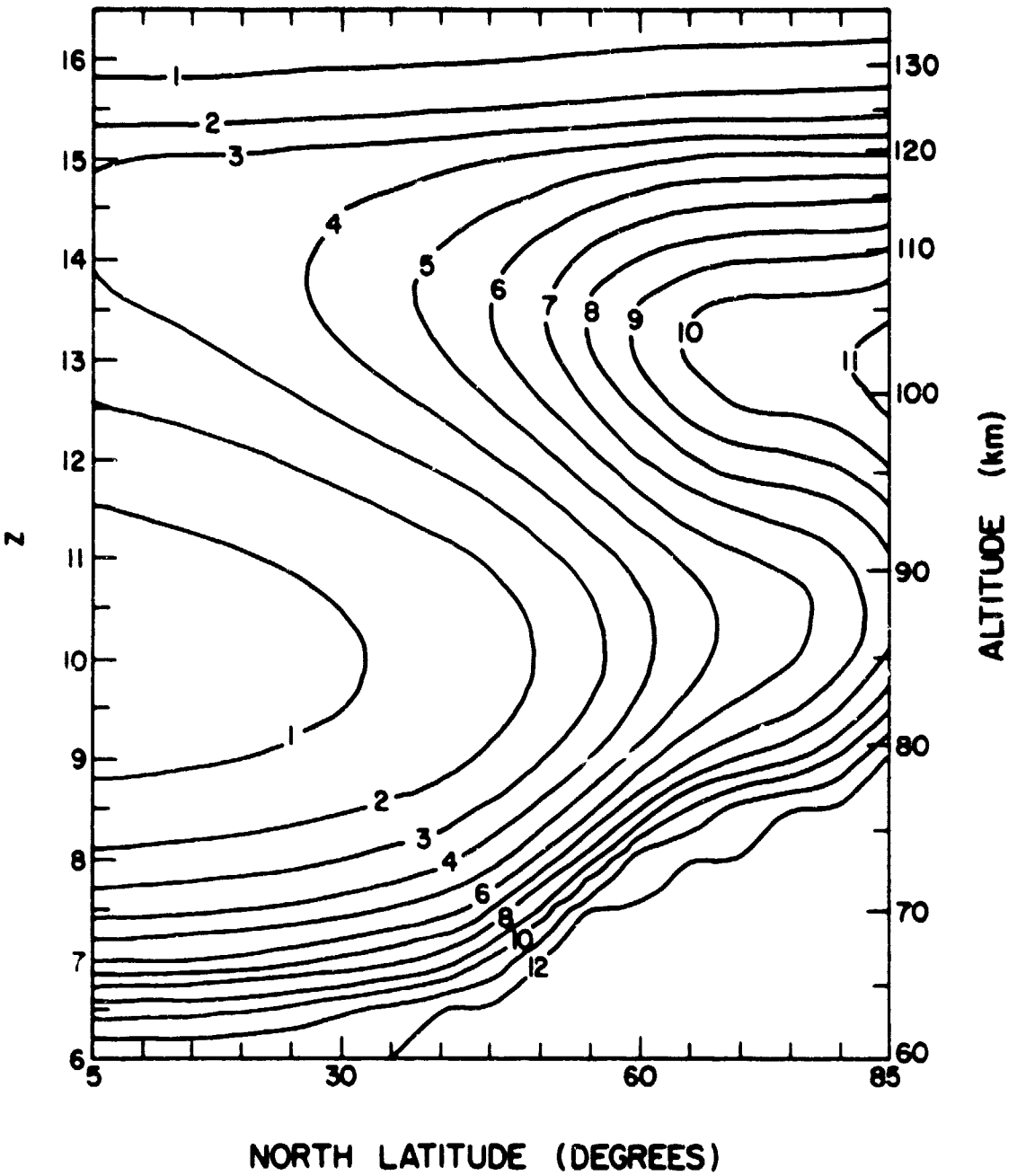

Figure 6.18 Equilibrium distribution of $\overline{NO}$ obtained using slant loss and no horizontal winds. Contours have units of 10^7 molec/cm^3.

winds is to decrease the concentration in low and middle latitudes, which in turn causes an increase in the meridional gradient of nitric oxide in the high latitude regions. This increase in gradient can be seen in comparing Figure 6.18 (no horizontal winds) with Figure 6.17b. This effect it especially pronounced in the lower levels. As before, the inclusion of planetary wave transports may modify this result.

In Figure 6.19, model results at 105 km are compared to the nitric oxide distrbution obtained from the AE satellite data, as presented in Chapter 4. Shown are model results calculated using vertical winds only, and using vertical and horizontal winds. Here again the addition of horizontal winds reduces the nitric oxide concentration at low latitudes and increases the latitudinal NO gradient at high latitudes. The model calculations provide reasonable agreement with the observational profile, especially considering the wide variation in upper atmosphere nitric oxide measurements.

Figure 6.20 shows the effect of vertical and horizontal winds on the vertical nitric oxide profile. Shown is a comparison of model results at 40° with two observational profiles due to MEIRA [1971] and TOHMATSU and IWAGAMA [1976] which were taken at the same general latitude. The smallest nitric oxide concentrations occur in the absence of winds. Adding in vertical winds effectively increases the flux of nitric oxide at the upper boundary, thus increasing the amount of nitric oxide at all levels. As before, the addition of horizontal winds causes a decrease in nitric oxide at 40°N. The calculated concentration at 40°N (vertical and horizontal winds) lies between the two observed profiles, and increases in the $z = 10$ to $z = 14$ region at about the same rate as the experimental values. Also, the location of the minimum in the calculated profile is

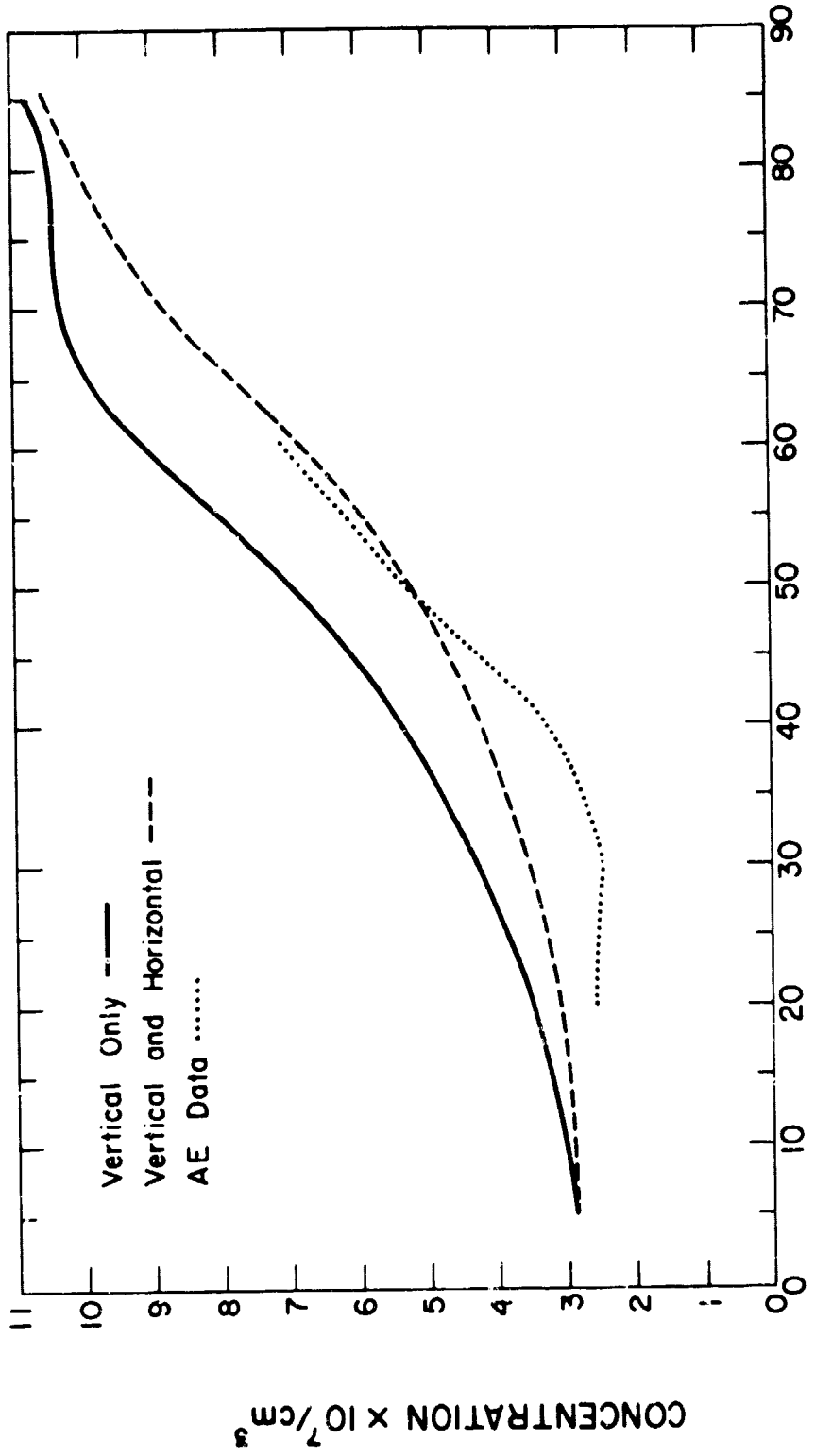

Figure 6.19 Nitric oxide distribution at 105 km. Comparison of model results with results obtained from the Atmospheric Explorer Satellite data [CRAVENS and STEWART, 1978].

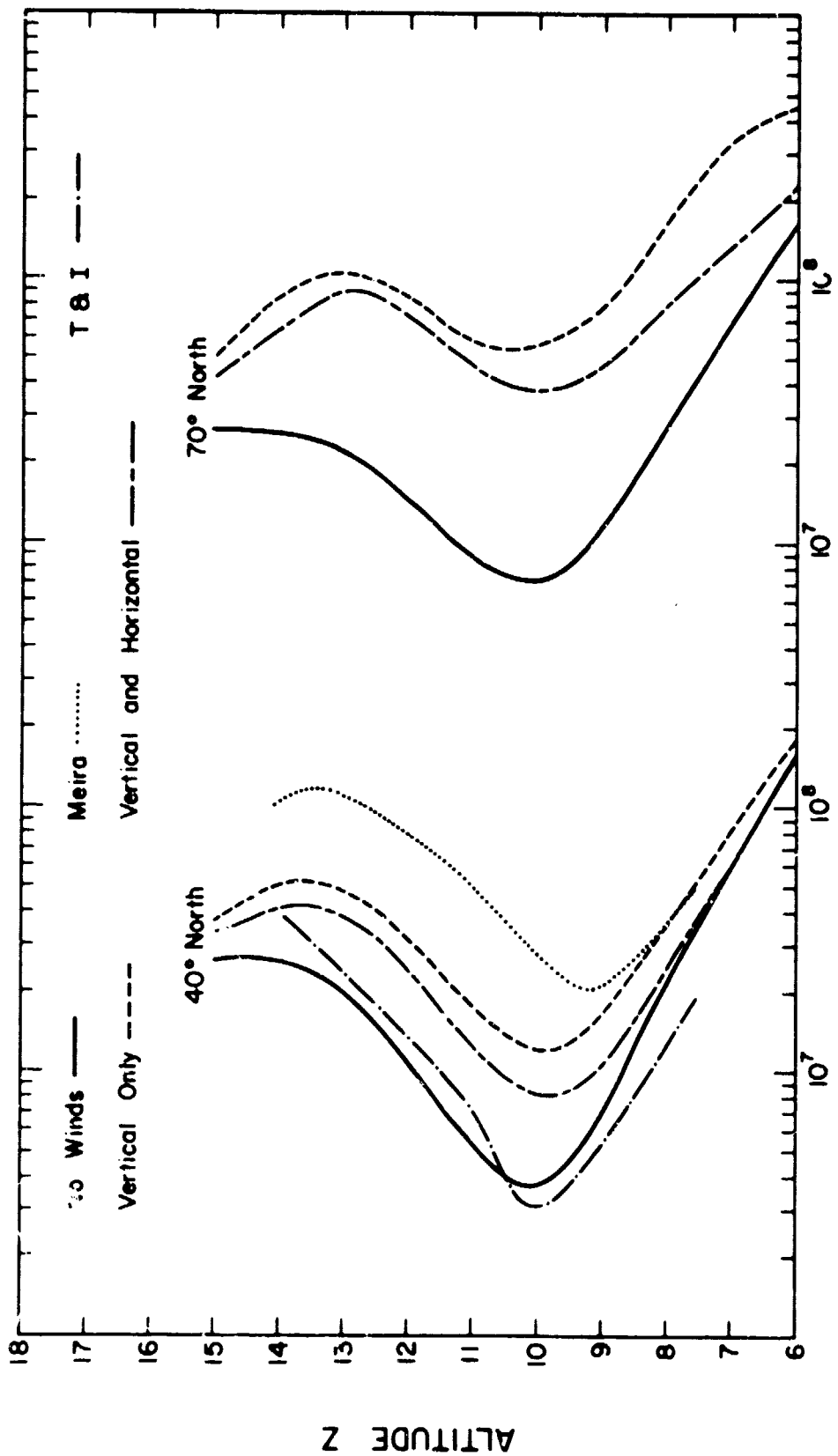

Figure 6.20 Model nitric oxide results at 40° north compared with observed profiles of MEIRA [1971] and TOHMATSU and IWAGAMI [1976] (abbreviated T&I), and model results at 70°N.

located at the correct height. Also shown are the results of the addition of winds at 70°N. An increase in the nitric oxide concentration occurred at all levels, and was much larger than that which occurred at 40°N. This is because the vertical winds are strongest at high latitudes, and hence their effect is greatest in that region.

6.3 *Planetary Wave Effects on the Nitric Oxide Distribution*

In this section, the effects of planetary waves on the mean and perturbation nitric oxide concentrations will be discussed. Vertically propagating waves act to decelerate the zonal mean circulation, and the effects of this reduction in mean winds is discussed in Section 6.3.1. In Section 6.3.2, the wave-induced perturbation nitric oxide concentration is studied, and model results are compared to observations. Section 6.3.3 discusses the transport of nitric oxide by planetary wave winds, and Section 6.3.4 draws some conclusions about the net effect of planetary waves on the zonal mean nitric oxide concentration.

6.3.1 *Changes due to zonal mean deceleration.* The effects of planetary waves on the zonal mean flow were discussed in Section 6.1.3. A vertically-propagating planetary wave tends to decelerate the mean zonal wind, causing a similar reduction in the mean meridional circulation. As a result, the amount of nitric oxide transported northwards by meridional winds is decreased, and high latitude concentrations are reduced.

In Section 6.1.3, the change in the zonal mean circulation produced by two different planetary wave forcings were considered. The final zonal mean wind states from those studies are used in this section to calculate the effect of the wind reduction on the zonal mean nitric oxide concentration. In order to isolate the effects of wind deceleration, planetary wave transports are neglected in this section; however, they will be added

later. Thus, this section discusses the effects of planetary waves on the zonal mean nitric oxide concentration only through the mechanism of mean wind deceleration.

Changes in the nitric oxide concentration will be expressed as a percent change from the mean concentration which results from the diabatic circulation only. The diabatically driven circulation was shown in Figures 6.2 and 6.3, and the resulting reference distribution of $\overline{NO}$ is shown in Figure 6.21. At high levels, the $\overline{NO}$ concentration reaches a maximum of $1.2 \times 10^8/cm^3$ near $z = 13$ in the polar regions. The loss in the sink region causes a relative minimum near $z = 10$ or 11 at all latitudes, and below the loss region, $\overline{NO}$ increases rapidly (although γ is nearly constant). In all of the runs in this section, the simplified time-dependent model was used along with meridional and vertical winds to calculate a mean nitric oxide concentration. The model was typically run for 30 to 40 days until an equilibrium for the particular wind distribution was obtained.

In Section 6.1.3, equilibrium winds were obtained using two different planetary wave boundary forcings, FEBAVE and FEBAVE*2. In the FEBAVE case, the calculated planetary waves resulted in a moderate reduction in the meridional circulation. Hence, the northward flow was reduced, particularly at high levels, and the downward flow at high latitudes was also reduced (see Figure 6.6a,b). The effect of these changes on the zonal mean nitric oxide concentration are shown in Figure 6.22a. The decrease in northward velocity results in less nitric oxide transport to high latitudes, especially at high levels. This effect, coupled with the reduction in downward winds, causes a reduction of nitric oxide at all levels in the polar regions. Since less $\overline{NO}$ is being transported out of the midlatitudes

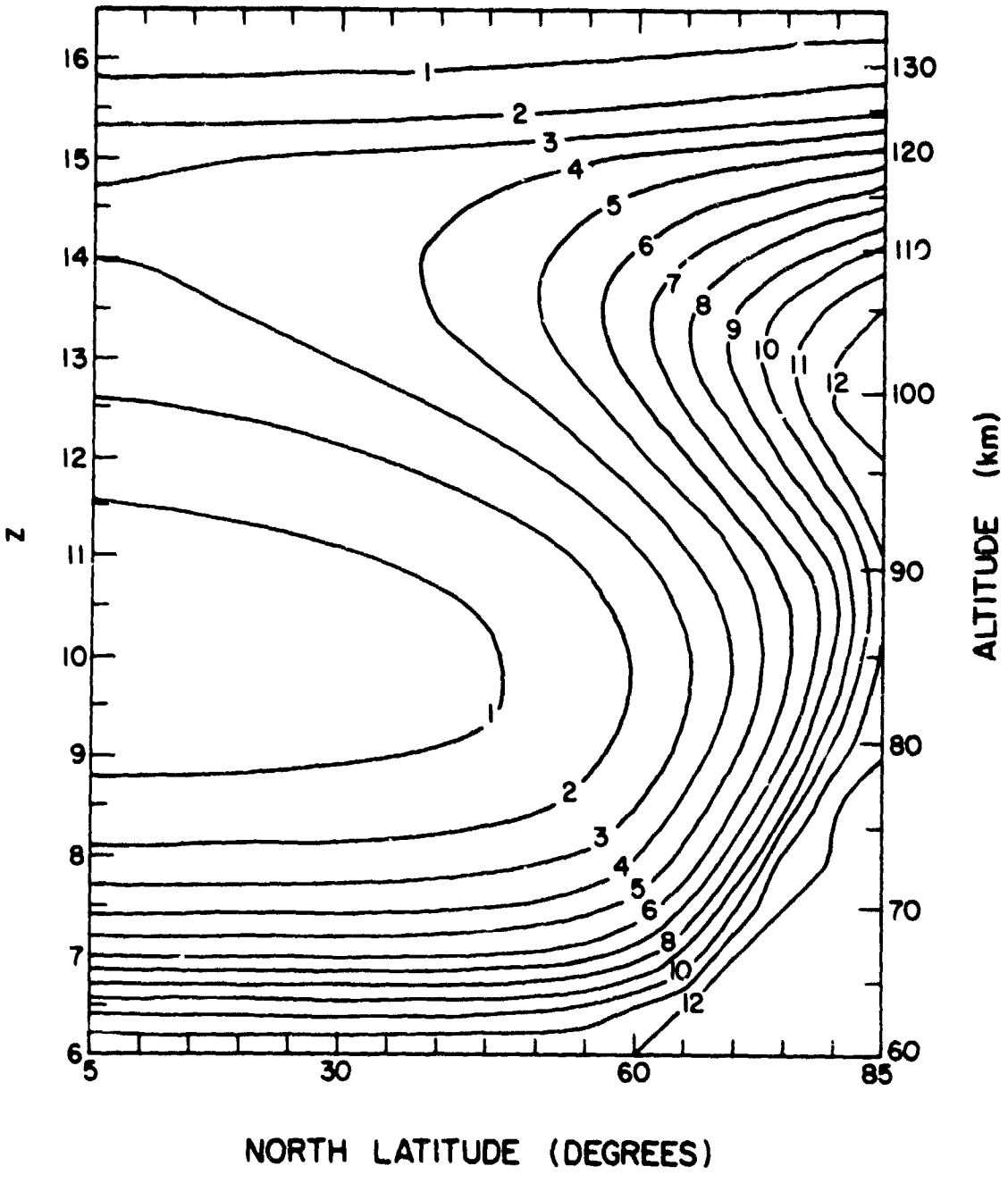

Figure 6.21 Reference distribution of $\overline{NO}$ resulting from diabatic circulation only. Contours have units of 10^7 molec/cm^3.

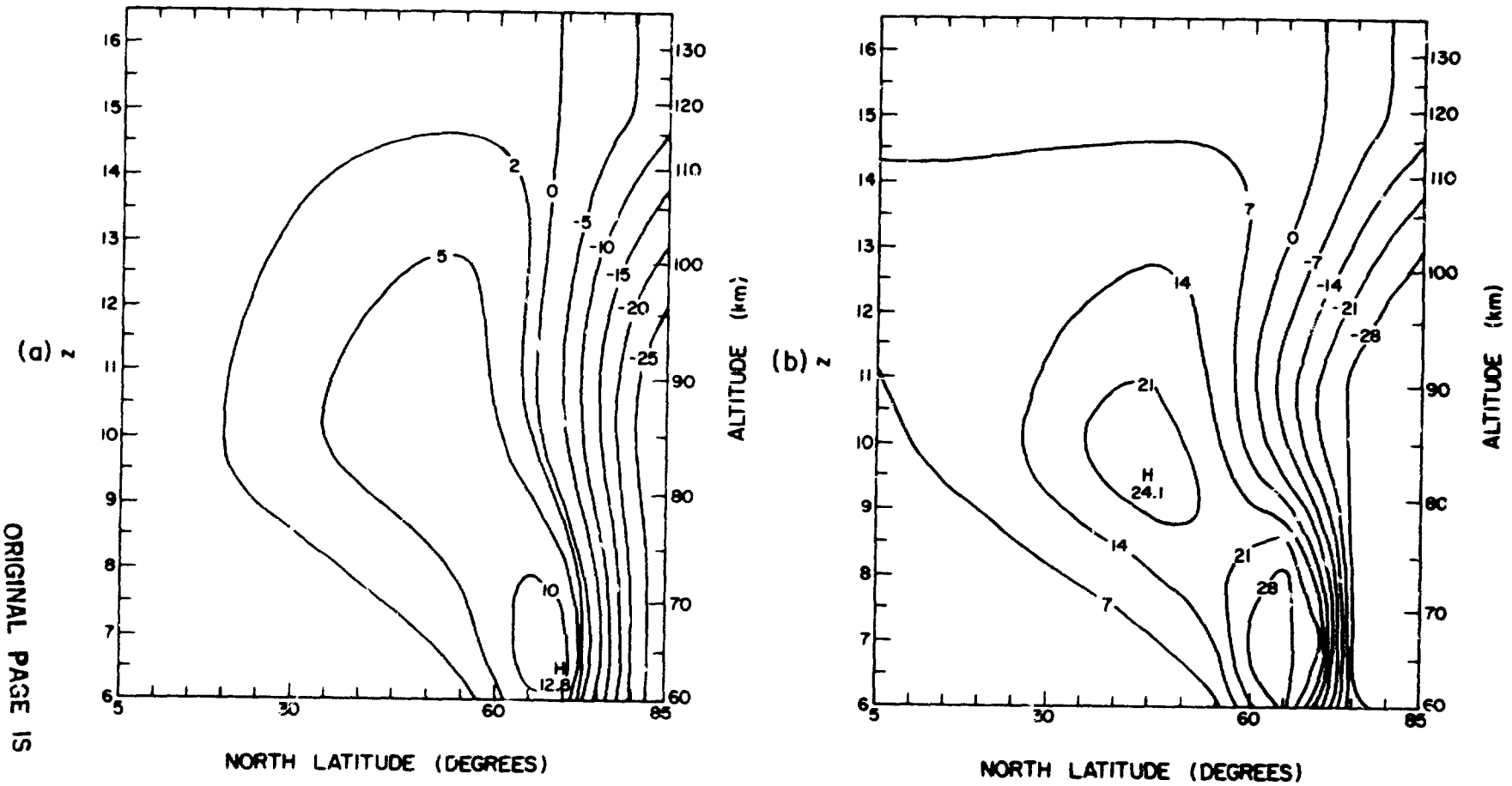

Figure 6.22 Percent change in $\overline{NO}$ as a result of zonal mean deceleration by (a) FEBAVE wave forcing and (b) FEBAVE*2 wave forcing. Contours are expressed as a percent change from the equilibrium distribution.

by northward winds, the concentration increases in that region. This increase is evident at all levels, due to downward diffusive transport. Thus, the effect of the wind reductions resulting from the FEBAVE wave is an increase of nitric oxide in midlatitudes, and a corresponding decrease at high latitudes. The midlatitude increase maximizes at about 67°N and 65 km, where the increase is about 13% over the initial state. The reduction in the polar region reaches 20% at 80°N and 65 km.

In the FEBAVE*2 case, the reduction in the meridional circulation was much more pronounced than in the FEBAVE case (see Figure 6.11a,b). The planetary wave fluxes were strong enough to cause a zonal mean wind reversal in a small localized region near z = 11 and 65°N. The meridional flow poleward of 70°N and below z = 10.5 also reversed from northward to southward, and the vertical velocity became positive in this region. At 60°N latitude, the meridional wind was reduced by 1.36 m/sec at z = 11.5 from its original value of about 1.5 m/sec. The downward wind was reduced in the polar regions by nearly 50% at z = 12.0, and was increased by almost 50% at z = 11.0 and 35°.

The results of these large changes in meridional circulation are shown in Figure 6.22b. As before, the reduction in northward wind causes a buildup of NO in midlatitudes and a depletion in the polar regions. An increase of 24% over the initial concentration occurs near z = 10 (85 km) and 45°N latitude. The weak northward wind velocities drastically reduce the amount of nitric oxide transported to the polar regions. At lower levels, the reversed meridional wind velocity transports nitric oxide out of the polar regions. This coupled with the reduction of downward transport due to vertical winds causes a depletion in the low level polar regions by as much as 30% of the original concentration. The buildup

which occurs near 65°N and $z = 7$ is due to the convergence of horizontal nitric oxide fluxes.

In summary, the changes in the mean nitric oxide concentration due only to the deceleration of the zonal mean flow were investigated in this section. The effects depend on the amount of reduction in the wind field, with a greater reduction being associated with the larger wave forcing. The effects of the FEBAVE and FEBAVE*2 forcings on the $\overline{NO}$ concentration differ mainly in magnitude. Both cases exhibit an increase in $\overline{NO}$ around $z = 10$ and 45°N, with the magnitude of the increase varying from 14% to 24% over the initial state.

Corresponding to this increase in midlatitudes is a decrease in the polar regions, with a maximum depletion of over 30% occurring at low levels in the FEBAVE*2 case. The decrease in northward wind velocity is responsible for the buildup in midlatitudes and decrease in the polar regions. The decrease in nitric oxide being brought into the polar regions, coupled with the decrease in downward velocity, results in a large reduction in nitric oxide concentrations in low level polar regions.

The effects of planetary waves, other than as input in the zonal mean wind equations, have been ignored in this section in order to isolate the effect of wind reductions. Transports due to waves may cancel or nearly cancel some of the changes just presented. The transport of nitric oxide due to planetary wave winds will be investigated in a later section.

6.3.2 *Wave-induced nitric oxide concentrations.* In this section, the planetary wave induced perturbation nitric oxide concentration will be discussed. The equations for the perturbation nitric oxide concentration were developed in Chapter 3. The equation for γ' is as follows

$$\frac{\partial \gamma'}{\partial t} + \frac{\overline{u}}{a\cos\theta}\frac{\partial \gamma'}{\partial \lambda} + \frac{\overline{v}}{a}\frac{\partial \gamma'}{\partial \theta} + \omega'\frac{\partial \overline{\gamma}}{\partial z} + \overline{\omega}\frac{\partial \gamma'}{\partial z} + r\gamma' = 0 \qquad (6.8)$$

where r is the loss coefficient. This equation is similar to the one used by PLUMB [1979] in his study of tracer transport by small amplitude waves.

To a rough approximation, the third, fifth, and sixth terms can be considered small. This leaves

$$\frac{\partial \gamma'}{\partial t} + \frac{\bar{u}}{a\cos\theta}\frac{\partial \gamma'}{\partial t} + \frac{\gamma'}{a}\frac{\partial \bar{\gamma}}{\partial \theta} + r\gamma' = 0 \tag{6.9}$$

If we assume a steady state, and expand the $\frac{\partial \gamma'}{\partial \lambda}$ term, we have

$$\gamma' = \frac{-\frac{v'}{a}\frac{\partial \gamma}{\partial \theta}}{\frac{im\bar{u}}{a\cos\theta} + r} = \frac{-\frac{v'}{a}\frac{\partial \bar{\gamma}}{\partial \theta}\left(r - \frac{im\bar{u}}{a\cos\theta}\right)}{\left(\frac{m\bar{u}}{a\cos\theta}\right)^2 + r^2} \tag{6.10}$$

For regions outside of the sink region we have $r = 0$, giving

$$\gamma' = \frac{w'\cos\theta}{m\bar{u}}\frac{\partial \gamma}{\partial \theta} \tag{6.11}$$

This, γ' is roughly 90° out of phase with v' (90° to the west) outside of the sink region. In this case, the contribution of the wave to the mean distribution, as determined by $\overline{v'NO'}$, is small, since v' and NO′ are nearly out of phase. For heights within the sink region, especially where $\bar{u}$ is small, γ' can be approximated as $\gamma' = -\frac{rv'}{a}\frac{\partial \bar{\gamma}}{\partial \theta}$. Here, γ' and v' are approximately 180° out of phase, which maximizes the $\overline{v'NO'}$ flux term. Thus, at all levels, the γ' distribution is roughly proportional to the latitudinal gradient of $\bar{\gamma}$, with a phase between 90° and 180° to the west of v'. In the sink region, (80 to 100 km) the effect of loss is to shift the phase from 90° towards 180° west of v'. Outside of the loss region, the phase is approximately 90° west of v'.

In the actual model calculation, all of the terms in equation 6.8 are included. However, the terms just discussed are the dominant ones, and the above analysis is only slightly modified by the addition of the neglected terms. To a good first approximation, the amplitude of γ' is a

function of $\partial\bar{\gamma}/\partial\theta$, and the phase is dependent on the relative magnitudes of $\bar{mu}/a\cos\theta$ and r.

Equilibrium NO′ concentrations were calculated for each of the two cases previously discussed, the FEBAVE and the FEBAVE*2. In addition, a third case was considered, FEBAVE*1.5, in which the boundary forcing was 1.5 times the FEBAVE forcing. In order to obtain these results, the full time-dependent model was run for 20 model days. The initial $\overline{NO}$ used in each run had been previously obtained using the simplified model in order to reduce the amount of time needed to reach equilibrium.

The results obtained using the FEBAVE and FEBAVE*1.5 forcings are shown in Figure 6.23a,b. The NO′ concentration gradually increases from equator to pole, due to the gradual increase in the gradient of $\overline{NO}$. The NO gradient also increases near the lower levels of the model, hence the large $\overline{NO}$ amplitude values there. In Figure 6.23a, for FEBAVE, a relative maximum amplitude of $3.85 \times 10^7/cm^3$ occurs at about $z = 12$ and about 75°N latitude. For the FEBAVE*1.5 case, a relative maximum of $4.36 \times 10^7/cm$ occurs near $z = 12.5$ and 70°N. This increase in amplitude reflects the increased wave amplitude (and hence the increased v') at that level.

Figure 6.24a,b shows the phase of the NO′ distribution resulting from each forcing. Note that the phase in each case exhibits a westward tilt with height. This is because the phase of NO′ is closely associated with the phase of v', and for a vertically propagating wave, the phase of ϕ' and hence v' exhibits a westward tilt with height. The phase for each case is similar near the lower boundary, since the phase of all three wave forcings are identical there. However, the phase in Figure 6.24b changes more rapidly with height, consistent with the fact that the FEBAVE*1.5 wave is propagating a greater amount of energy vertically. The vertical phase

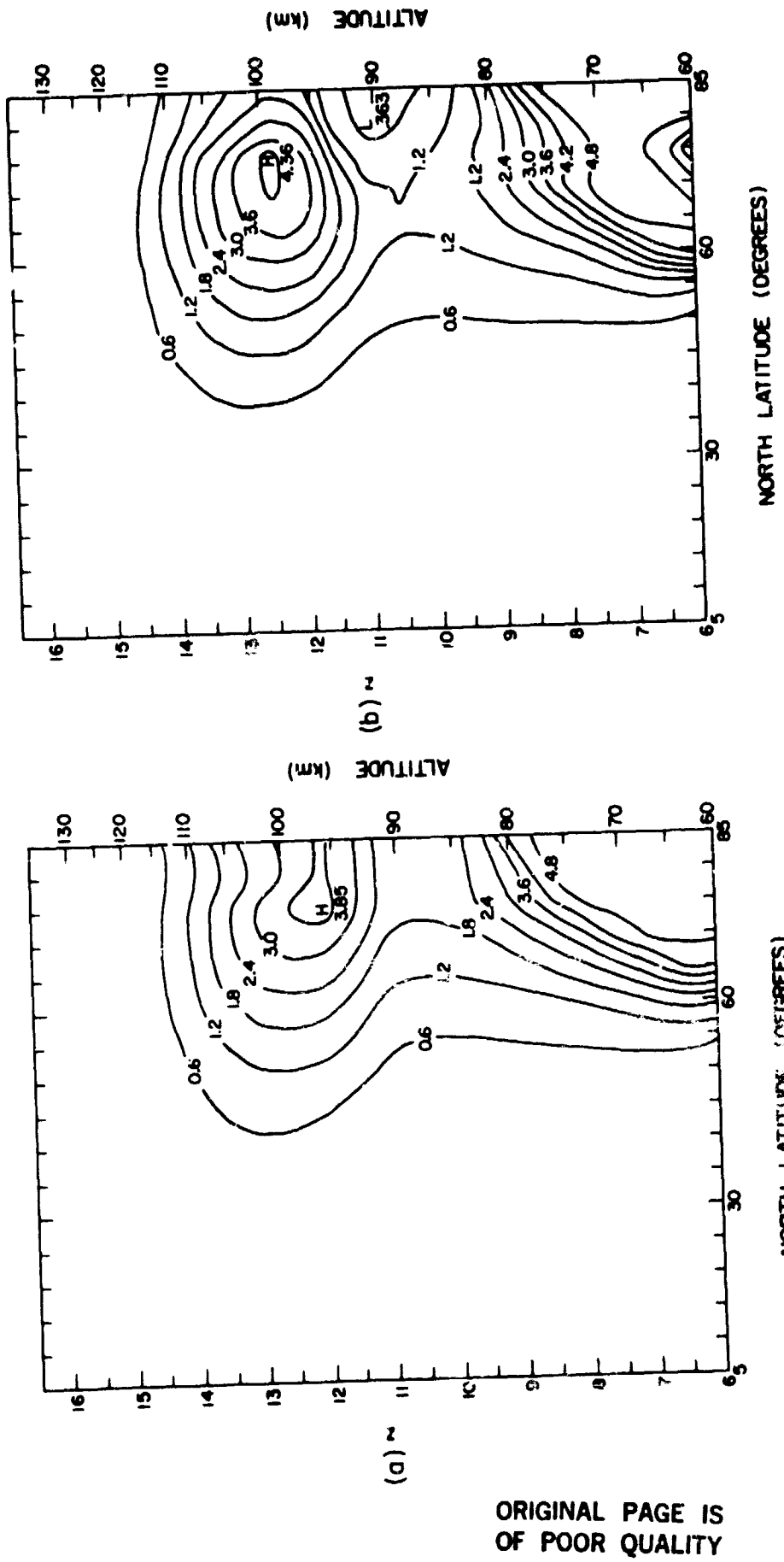

Figure 6.23 Amplitude of the perturbation nitric oxide concentration resulting from (a) FEBAVE wave and (b) FEBAVE*1.5 wave. Contours have units of 10^7 molec/cm^3.

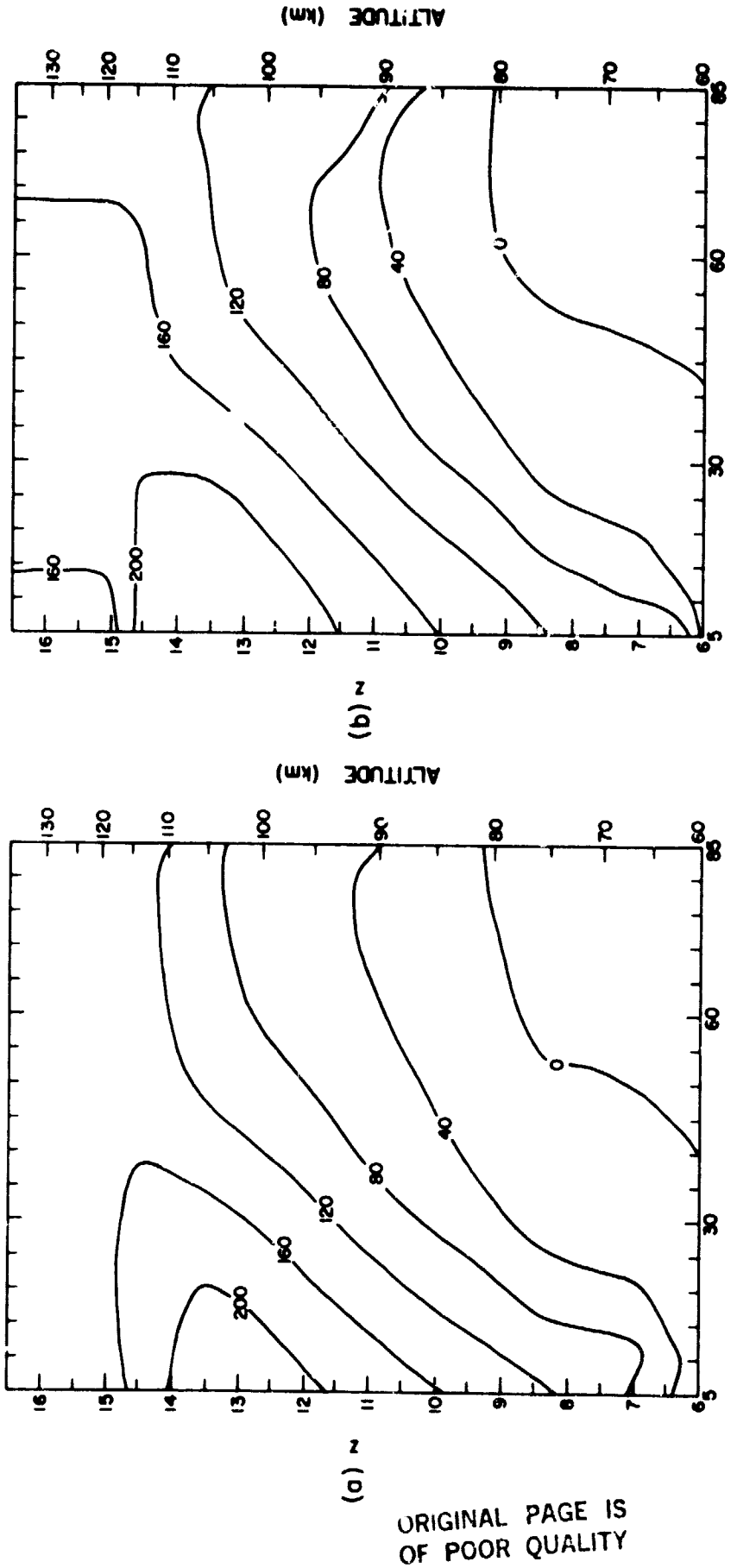

Figure 6.24 Phase of the perturbation nitric oxide concentration resulting from (a) FEBAVE wave and (b) FEBAVE*1.5 wave. Contours have units of degrees west longitude.

structures in Figure 6.24a,b are similar to the phases of v' in each case, except shifted anywhere from 90° to 180° to the west of v', as previously discussed.

A perturbation NO concentration was also obtained using the FEBAVE*2 forcing and these results are presented in Figure 6.25a,b. This case was interesting in that a critical level had developed at high latitudes near $z = 12$. This situation is treated numerically by increasing the damping near the critical level so as to simulate the inability of the wave to penetrate the level. As a result of this damping, the wave amplitude is strongly damped in the critical region.

Although the critical region in this case was small, the effect on NO is noticeable in the upper levels. The maximum amplitude of NO′ at $z = 12.5$ is reduced from the previous cases, even though the wave forcing is much larger at the lower boundary. This is due to the strong attenuation of the wave and the associated reduction in v' in the upper regions. The phase lines in Figure 6.25b exhibit a rapid phase shift with height, indicating strong absorption of the wave energy. At $z = 12.0$ and 65° N, the phase lines are nearly vertical, indicating that the wave is evanescent throughout the critical region. Future studies will include a more detailed study of the critical layer phenomenon.

In Figure 6.26a,b, model calculations of perturbation nitric oxide concentration at 105 km are compared with those results as obtained from CRAVENS and STEWART [1978]. These observational results were discussed in Chapter 4. Figure 6.26a shows the amplitude of the perturbation nitric oxide concentration NO′ obtained using three different sets of planetary wave forcings. Although the wave forcing varied by a factor of two at the lower boundary, adjustments in the zonal mean circulation caused the wave

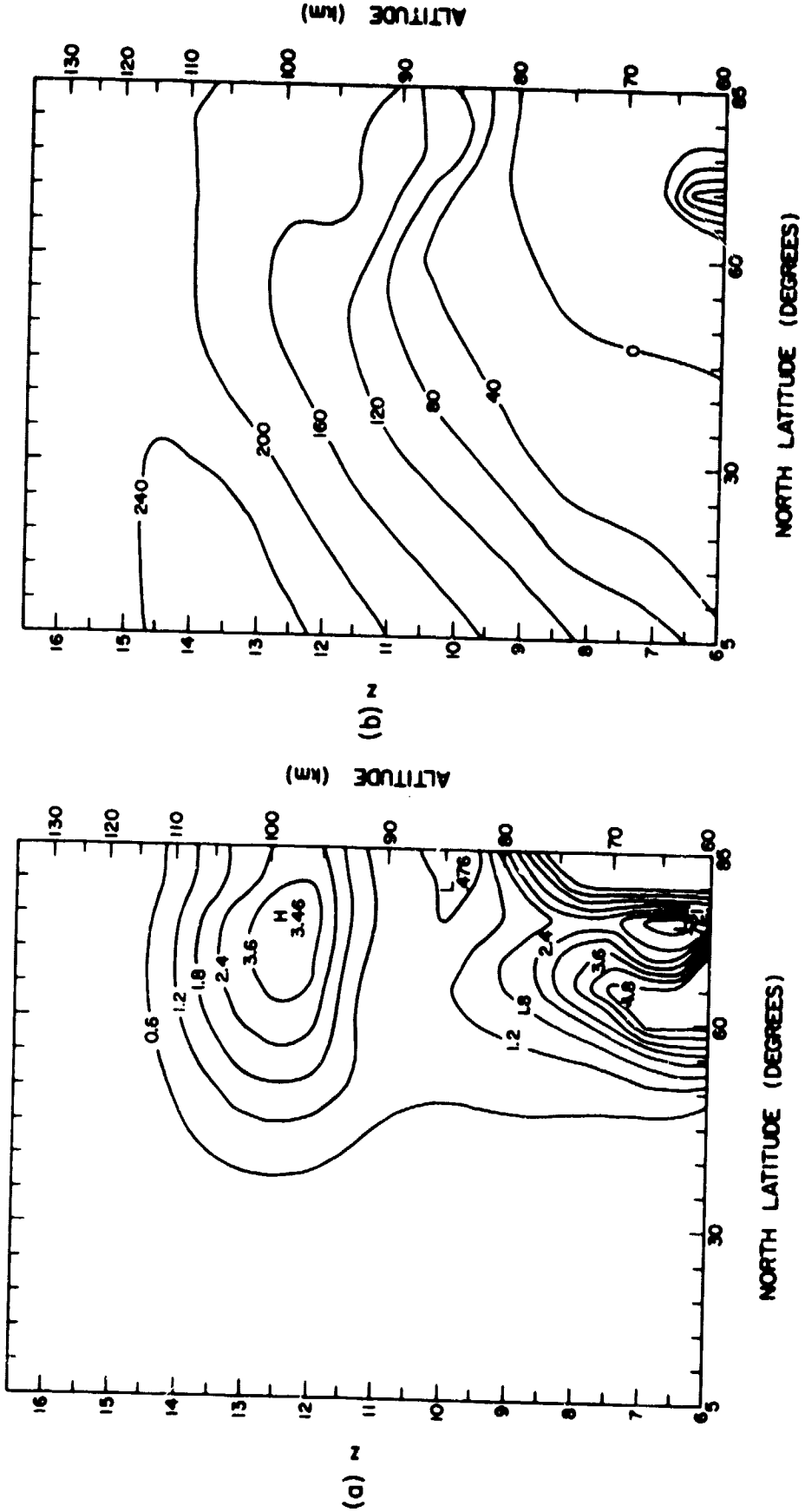

Figure 6.25 Perturbation nitric oxide concentration obtained using FEBAVE*2 forcing: (a) amplitude in units of $10^7/cm^3$, (b) phase in degrees west longitude.

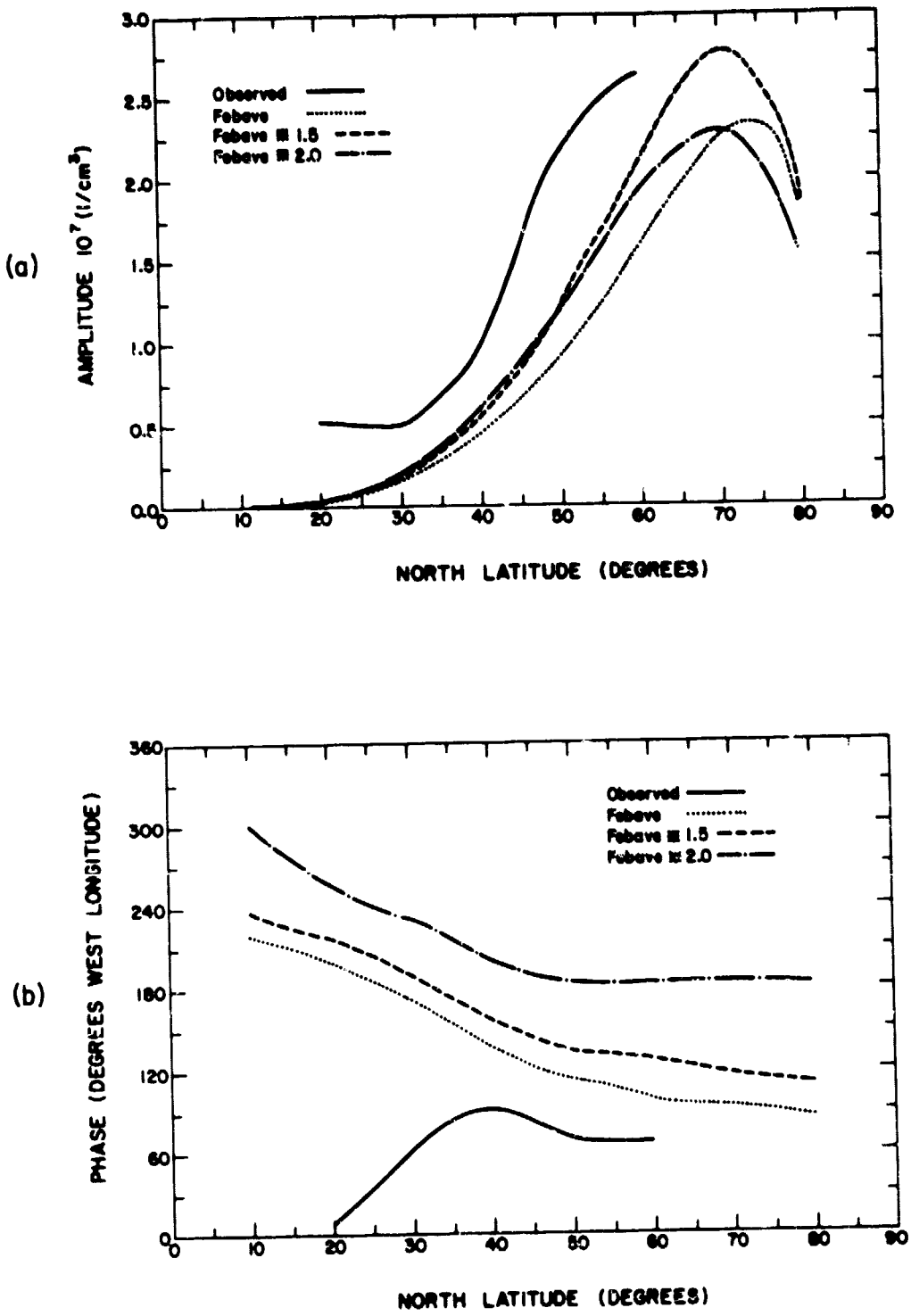

Figure 6.26 Comparison of model results to perturbation nitric oxide concentration as obtained from CRAVENS and STEWART [1978]: (a) amplitude and (b) phase.

amplitude to be constant at 105 km for the three cases. Consequently, the amplitudes of the wave-induced NO' are similar for each case. The largest amplitude occurs for the FEBAVE*1.5 case. In the FEBAVE*2 case, a critical layer has developed, and thus the wave amplitude and hence γ' are reduced. The FEBAVE forcing was taken from observations which covered the same period of time as the nitric oxide observations. The FEBAVE results provide a reasonable approximation to the NO observations, and exhibit the same general shape as the observed profile.

The fact that all three profiles are smaller than observations could be due to modeling approximations concerning upper boundary nitric oxide fluxes, diffusion coefficients, or loss coefficients. Other reasons for the discrepancy include the lack of knowledge of the actual zonal mean wind profile for that time period, which could result in differences between the calculated and actual planetary wave structures. However, CRAVENS and STEWART [1978] state that individual measurements of nitric oxide at 105 km are significantly affected by variations in magnetic activities. RUSCH et al. [1981] also indicate particle precipitation events can have an important influence on nitric oxide chemistry. These studies imply that the inclusion of an asymmetric nitric oxide source may be required to produce better agreement with observations. In our studies, we have neglected this longitudinally asymmetric source, and this may have resulted in smaller than normal perturbation concentrations. Given these limitations, the numerical model provides a reasonable qualitative agreement with observations.

The FEBAVE phase lines, Figure 6.26b, also show reasonable agreement with the observations north of 40° latitude. Notice that as the boundary forcing increases, the phase of the calculated nitric oxide distribution

shifts westward, due to the increasing amount of wave energy propagating upwards and the corresponding westward shift in phase of v'. The discrepancy between observed and calcula ed phases south of 40°N can be attributed to the poor resolution in the nitric oxide map at those latitudes.

6.3.3 *Planetary wave fluxes and transports of nitric oxide.* In this section, the role of planetary wave winds in the establishment of the nitric oxide distribution will be discussed. Planetary waves affect the zonal mean distribution of nitric oxide not only through the deceleration of the mean flow as discussed in Section 6.3.1, but also through the $\overline{v'\gamma'}$ and $\overline{\omega'\gamma'}$ terms in the nitric oxide continuity equations. In this section, we will compare the effects of two of the wave forcing cases mentioned earlier, FEBAVE and FEBAVE*1.5. The horizontal and vertical fluxes of nitric oxide due to planetary waves, as well as the changes induced in the zonal mean distribution, will be discussed.

The results presented in this section were taken from the last day of model runs which used various wave boundary forcings. In these runs, all terms in the continuity equation were calculated, and the model was run for 20 model days, which was sufficiently long to reach equilibrium. Thus, the fluxes and transports presented here represent steady state values, obtained when $\overline{NO}$ and NO' were changing less than .1% per day. Thus at the time of the calculations, the wave, mean, and $\overline{NO}$ and NO' have reached a self-consistent equilibrium state.

Figure 6.27 compares the horizontal equilibrium fluxes obtained using the FEBAVE and FEBAVE*1.5 boundary forcings. The horizontal flux $\overline{v'\gamma'}$ is shown at two heights, z = 13.5 (105 km) and z = 10.5 (87 km). These two levels correspond roughly to the heights of the maximum and minimum in the nitric oxide distribution. In the figures, an upward pointing arrow

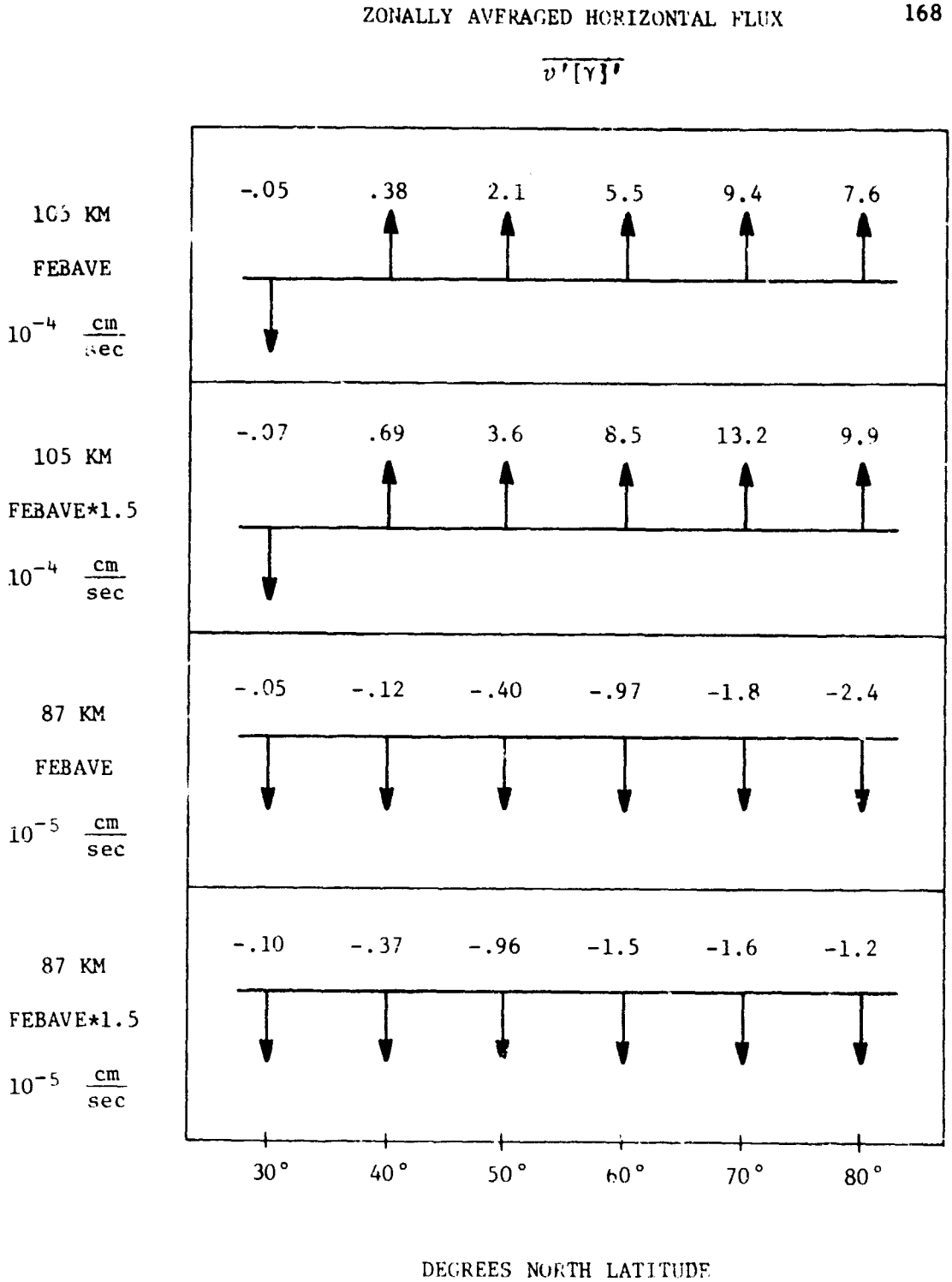

Figure 6.27 Zonally averaged horizontal nitric oxide flux due to FEBAVE and FEBAVE *1.5 waves.

indicates a northward flux, and a downwards pointing arrow represents a southward flux. The magnitude of the fluxes are also indicated.

At 105 km, the flux for both cases is northward at most latitudes. The magnitudes for the FEBAVE*1.5 case are larger, however, due to the larger values of wave velocity at that level. In Section 6.3.1, it was shown that the deceleration of the mean flow caused by planetary wave momentum and heat fluxes caused a reduction in the northward transport of nitric oxide by the mean meridional flow. The planetary wave nitric oxide fluxes at 105 km tend to oppose this reduction, thus lessening the effect of the reduction in the northward mean wind.

At 87 km, however, the situation is different. Here, the fluxes due to the waves are reversed, becoming southward at all latitudes. Again, the stronger forcing is associated with stronger southward planetary wave nitric oxide fluxes. The $z^* = 10.5$ level is near the center of the loss region. Hence, as discussed in Section 6.3.2, the dominance of the loss term results in a phase difference between v' and NO′ of greater than 90°, which in turn results in southward fluxes throughout this region. At higher levels, where the loss term is small or zero, the phase difference between v' and the wave induced NO′ distribution is less than 90°, resulting in northward fluxes. Thus, the horizontal transport of nitric oxide depends on the level under consideration. At high levels, the planetary wave transport compensates for the deceleration of the zonal mean flow; in the loss region, the wave transports tend to reinforce the effect of the reduced meridional circulation.

Figure [illegible],b shows the effect of the horizontal planetary wave fluxes on the zonal mean concentration of nitric oxide in terms of a percent change per day. At 105 km, the horizontal transport due to the waves

(a)

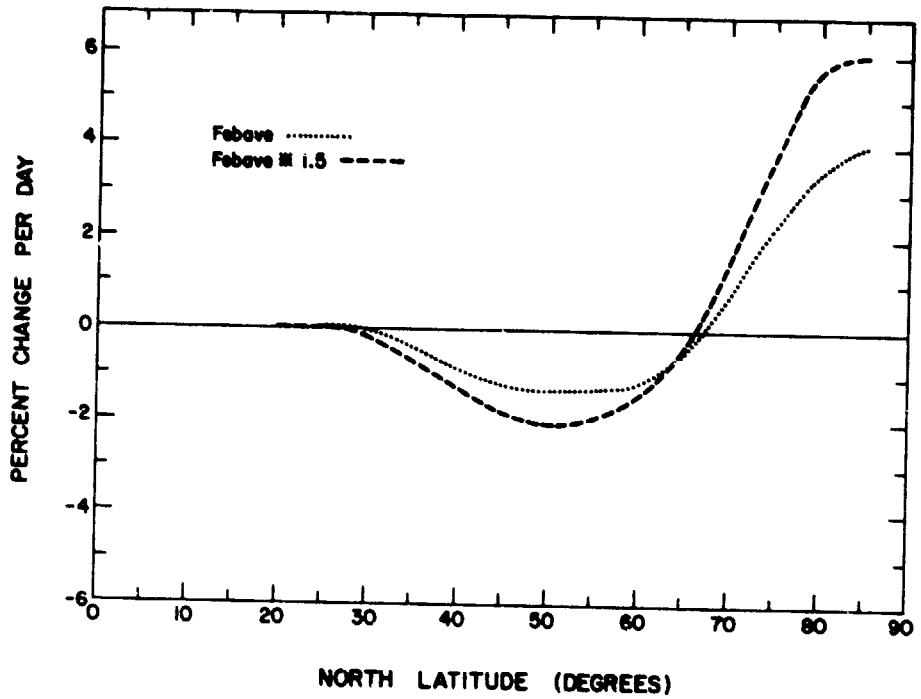

(b)

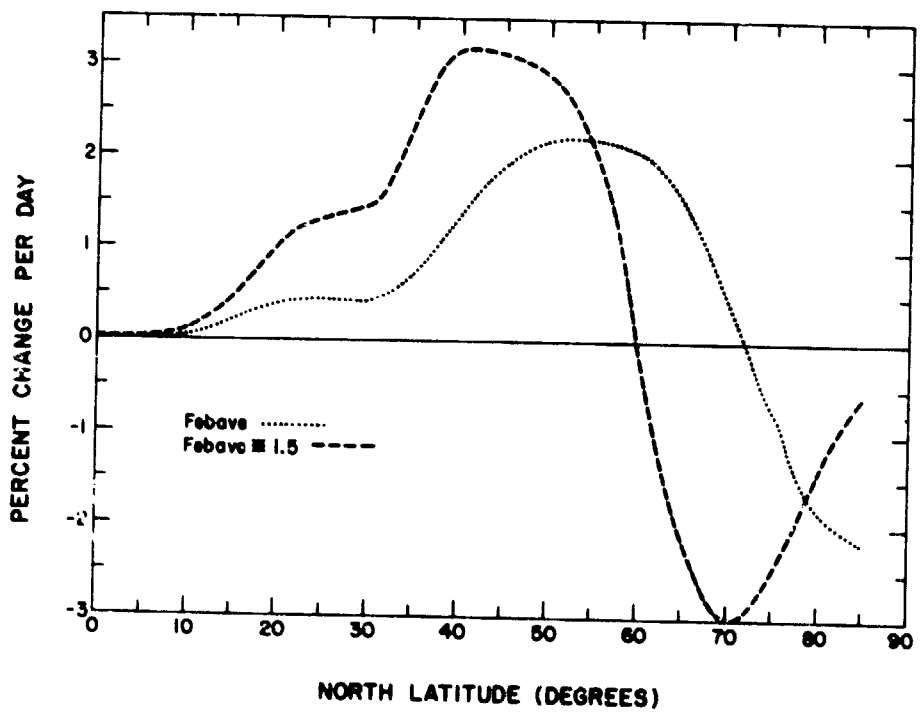

Figure 6.28 Changes in the zonal mean nitric oxide concentration due to horizontal transport by (a) FEBAVE wave and (b) FEBAVE*1.5 wave.

results in a decrease in $\overline{NO}$ in midlatitudes, and an increase in the polar regions. Again, these changes tend to counteract the effect of the zonal mean flow deceleration. The changes associated with the FEBAVE*1.5 wave are greatest, occurring at a rate which would reduce the $\overline{NO}$ concentration by 2% per day at 50°N latitude and increase it by 6% per day in the polar regions.

At lower levels the effect is reversed, with the waves causing a reduction of $\overline{NO}$ in the polar regions, and an increase at midlatitudes, reinforcing the effect of the zonal mean deceleration. Again, the effect of the FEBAVE*1.5 wave is the greatest, causing changes which would reduce the concentration at 70° by 3% per day and increase the concentration in midlatitudes by a little more than 3% per day.

The vertical fluxes obtained in the equilibrium runs are shown in Figure 6.29. The vertical flux at all heights and latitudes was downward, as represented by a downward arrow. The vertical fluxes are considerably smaller than the horizontal fluxes, due to the small amplitude of ω', which is on the order of cm/sec (Figures 6.27 and 6.29 can be approximately compared by multiplying the values in Figure 6.27 by one scale height, about 7.0×10^5 cm.) The downward flux for the FEBAVE*1.5 case is again the largest, and the maximum downward flux appears to be centered at 60° or 70°N latitude for all cases. The downward fluxes appear to counteract somewhat the effect of the reduced downward mean velocity which results from the deceleration of the mean flow.

In Figure 6.30, the changes in $\overline{NO}$ associated with the vertical fluxes are shown. Notice that the changes are considerably smaller in magnitude than those induced by horizontal motions. At 105 km, the net effect is a reduction of the $\overline{NO}$ concentration due to transport downward out of the

ZONALLY AVERAGED VERTICAL FLUX

$\overline{w'[\gamma]'}$

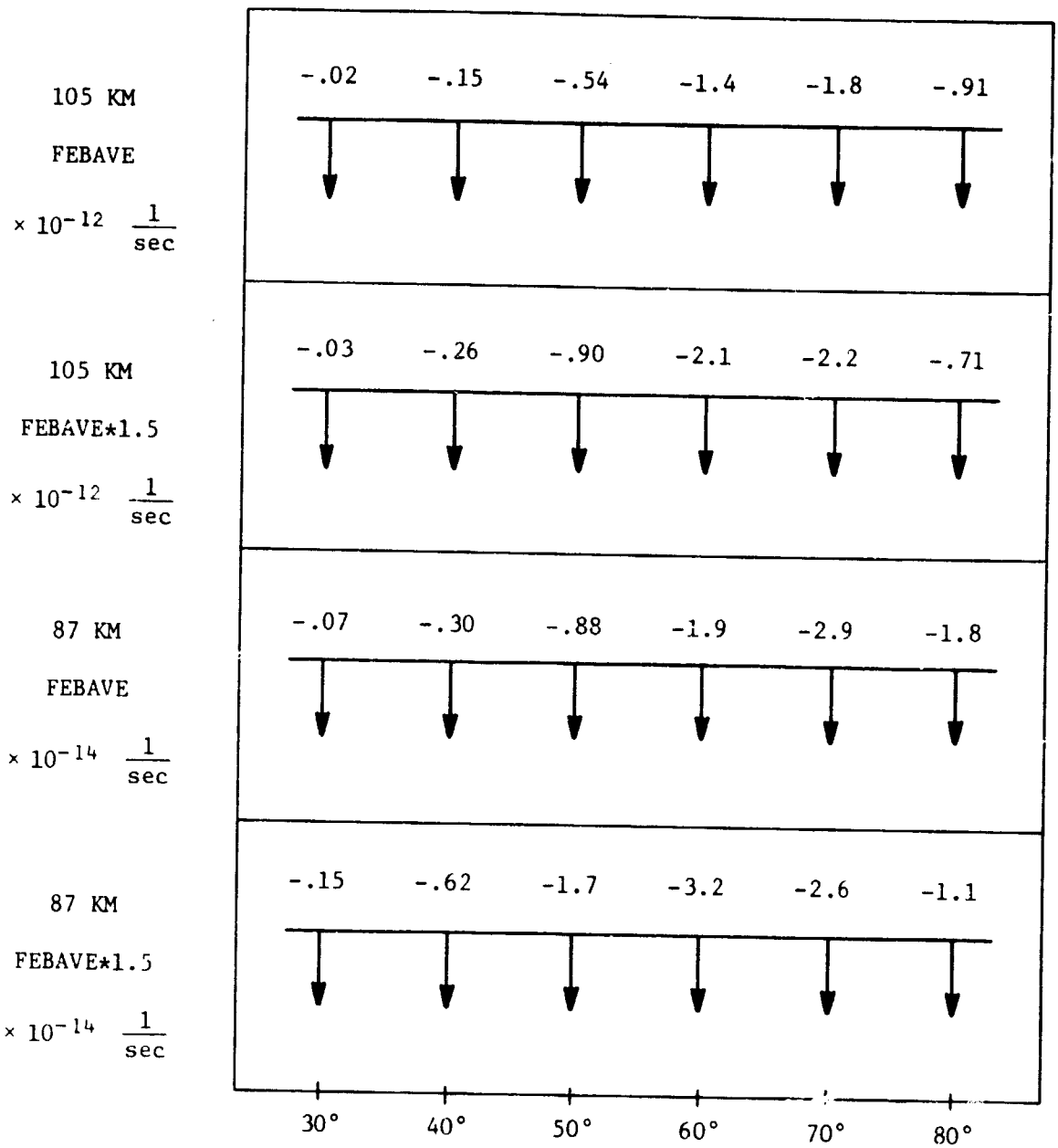

Figure 6.29 Zonally averaged vertical nitric oxide flux due to FEBAVE and FEBAVE *1.5 waves.

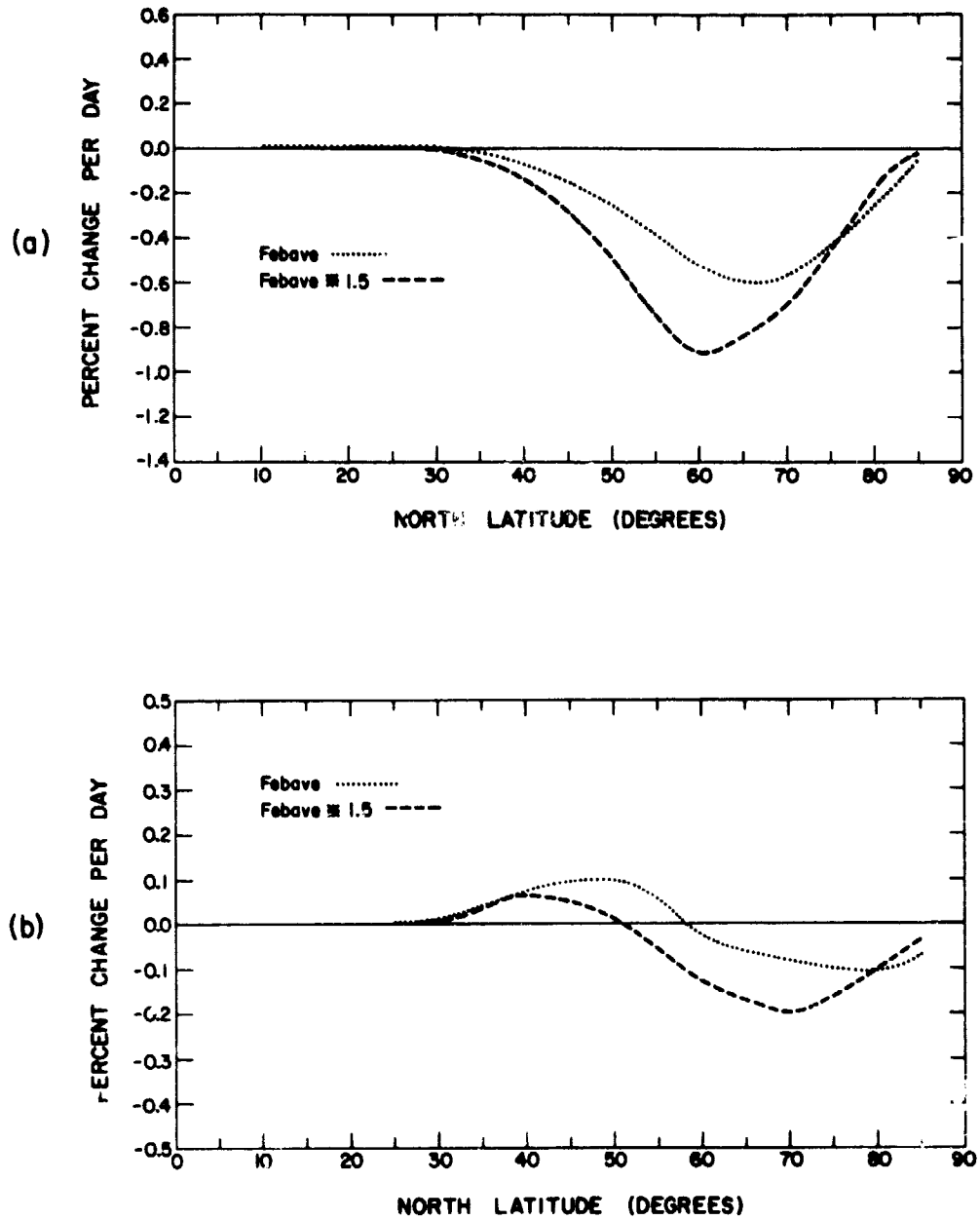

Figure 6.30 Changes in the zonal mean nitric oxide concentration due to vertical transport by (a) FEBAVE wave and (b) FEBAVE*1.5 wave.

region. The maximum change that would occur is not quite 1% per day, in the FEBAVE*1.5 case. At 87 km, the changes are even smaller, indicating that the downward nitric oxide flux due to the waves is nearly constant in this region. The maximum change is a reduction of only .2% occurring at 70°for the FEBAVE*1.5 case.

Although the results of the FEBAVE*2 case were not presented here, the effects of FEBAVE*2 wave transports are similar but slightly larger than the FEBAVE*1.5 case. The main features of the wave transport are unchanged; i.e., northward transport at high levels and southward transport in the loss region. The net effect of the FEBAVE*2 wave transports will be shown below.

In Section 6.3.1, the change in the zonal mean nitric oxide concentration due to the deceleration of the zonal mean flow was shown. Although planetary waves were calculated in that study and used to change the zonal mean circulation, the effect of the waves on the mean nitric oxide distribution were not included. Thus, Figure 6.22a,b includes the effects of planetary waves only through the deceleration mechanism.

The next step is to include the effects of planetary wave fluxes on the nitric oxide concentration. These results will be presented in two ways. First, in Figure 6.31a,b, the changes due to the addition of planetary wave fluxes are expressed as a percent change from the distribution obtained with the decelerated mean circulation only (Figure 6.22a,b). Presenting the results in this way clearly shows the effect of the wave transports, which at certain levels compensate for the reduction in mean circulation caused by the wave momentum and heat convergences. Secondly, in Section 6.3.4, the results will be presented as a percent change from the original reference nitric oxide distribution which resulted from the

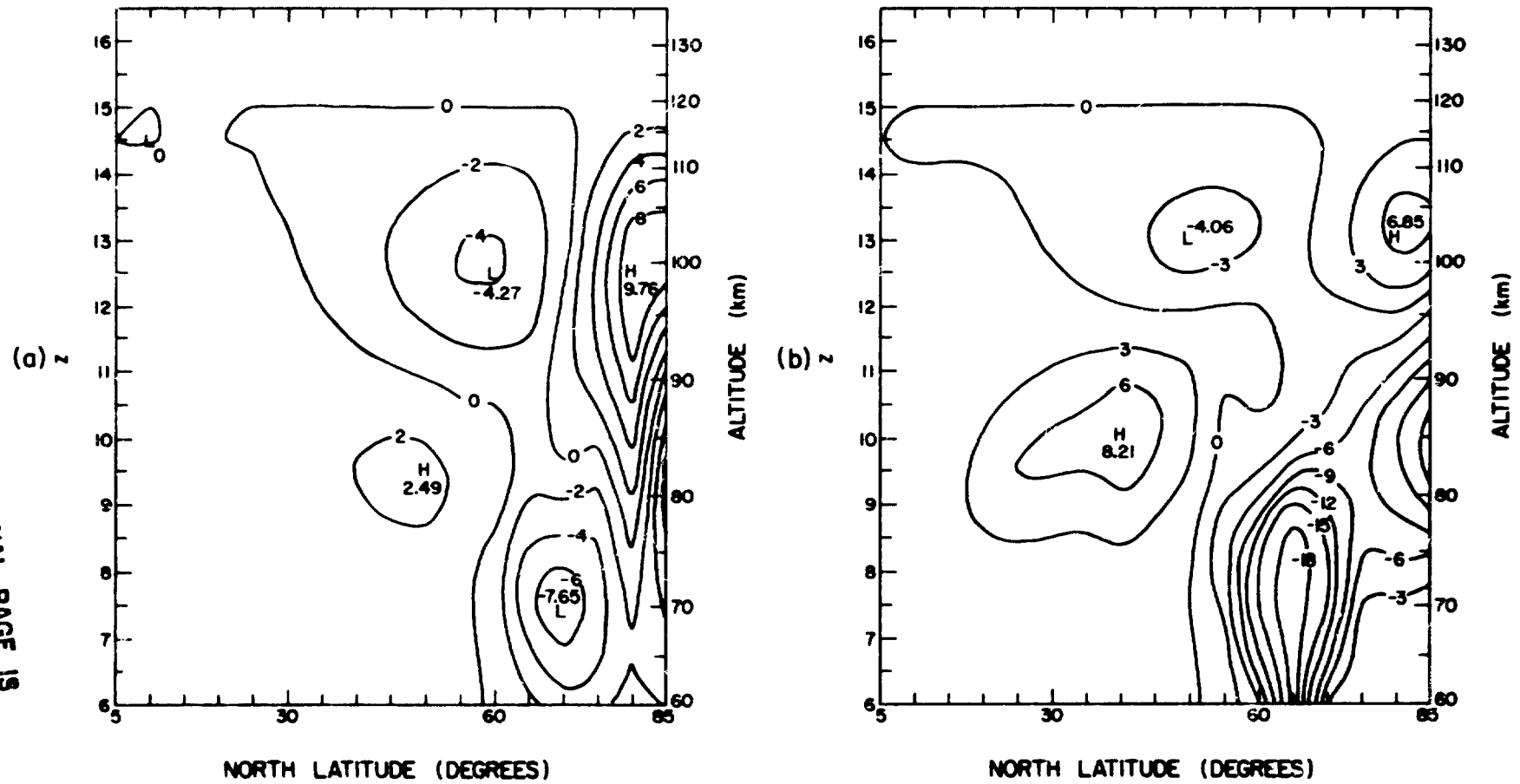

Figure 6.31 Percent change in the zonal mean nitric oxide distribution due to the addition of planetary wave transports: (a) FEBAVE wave and (b) FEBAVE*2 wave. Contours express percent change from the NO concentration obtained with the decelerated mean circulation only.

diabatic circulation only (see Figure 6.21). Presenting the results in this fashion will show the net result of turning on the planetary wave, i.e., the combined effect of transports by the decelerated mean circulation and planetary wave winds on the original nitric oxide equilibrium distribution.

Figure 6.31a shows the changes in the zonal mean nitric oxide distribution which occur due to the addition of transports by the FEBAVE wave winds. As mentioned above, the results are expressed as a percent change from the results obtained with the decelerated mean circulation only. The effect of the northward transport at high levels and southward transport at low levels is clearly seen. In the upper levels, the waves attempt to compensate for the reduction in the mean circulation, causing a decrease in $\overline{NO}$ of over 4% in midlatitudes and a corresponding increase of almost 10% in the polar regions. At lower levels, the effect of the wave is a decrease in $\overline{NO}$ by almost 8% at high latitudes, coupled with an increase in NO by 2.5% in midlatitudes near $z = 9.0$.

Figure 6.31b contains similar results only for the FEBAVE*2 case. Again, at high levels, the effect of wave transport is to reduce the $\overline{NO}$ concentration by 4% near $z = 13.0$ and 50°N, coupled with an increase in $\overline{NO}$ by 8% in the polar regions at that height. In the lower altitude regions, a decrease near 75°N of nearly 20% is coupled with a corresponding increase of 8% near $z = 10$ (85 km) and 40° latitude.

6.3.4 *Combined effects of wave and mean.* In the previous three sections, we have considered the effects of the planetary waves and zonal mean circulation on the $\overline{NO}$ concentration individually. In this section, the net effect of both wave and mean fluxes and transports will be examined for the equilibrium situation. The combined effects of zonal

mean deceleration and planetary wave transports will be presented.

Figure 6.32a shows the net change from the initial zonal mean nitric oxide state (see Figure 6.21) that occurs as a result of the FEBAVE wave. In the upper regions, the main effect is a reduction of $\overline{NO}$ in the polar regions. Above $z = 13.0$, the changes that occur in midlatitudes are small, indicating that the effects of the reduced transport by the mean flow and increased transport by planetary waves are nearly equal and opposite. At lower levels, the reduction of nitric oxide in the polar regions is more pronounced, with a reduction of over 20% occurring poleward of 80°N and below $z = 9$. The combined effects of mean deceleration and wave transport result in a region of increased $\overline{NO}$ centered at 50° latitude and about 83 km. The maximum increase is 9% over the initial concentration.

In Figure 6.32b, this region of increased $\overline{NO}$ is even more pronounced. This is due partly to the increased northward transport in this region by the FEBAVE*2 wave. The maximum increase in $\overline{NO}$ in this case is nearly 30% of the original value. The region of increased concentration is centered at 40°N latitude and 85 km in height. As before, the changes that occur in the upper levels are small, owing to the cancellation of wave and mean effects.

In this section, we have investigated the combined effect of wave and mean transports on the zonal mean nitric oxide distribution. It appears that at high levels, the planetary wave transports tend to cancel the effect of the reduction in meridional wind caused by momentum and heat fluxes. At lower levels, however, the effect is reversed, owing largely to the phase difference between the induced NO' circulation and v'. At these levels, centered at 85 km, the wave transports reinforce the

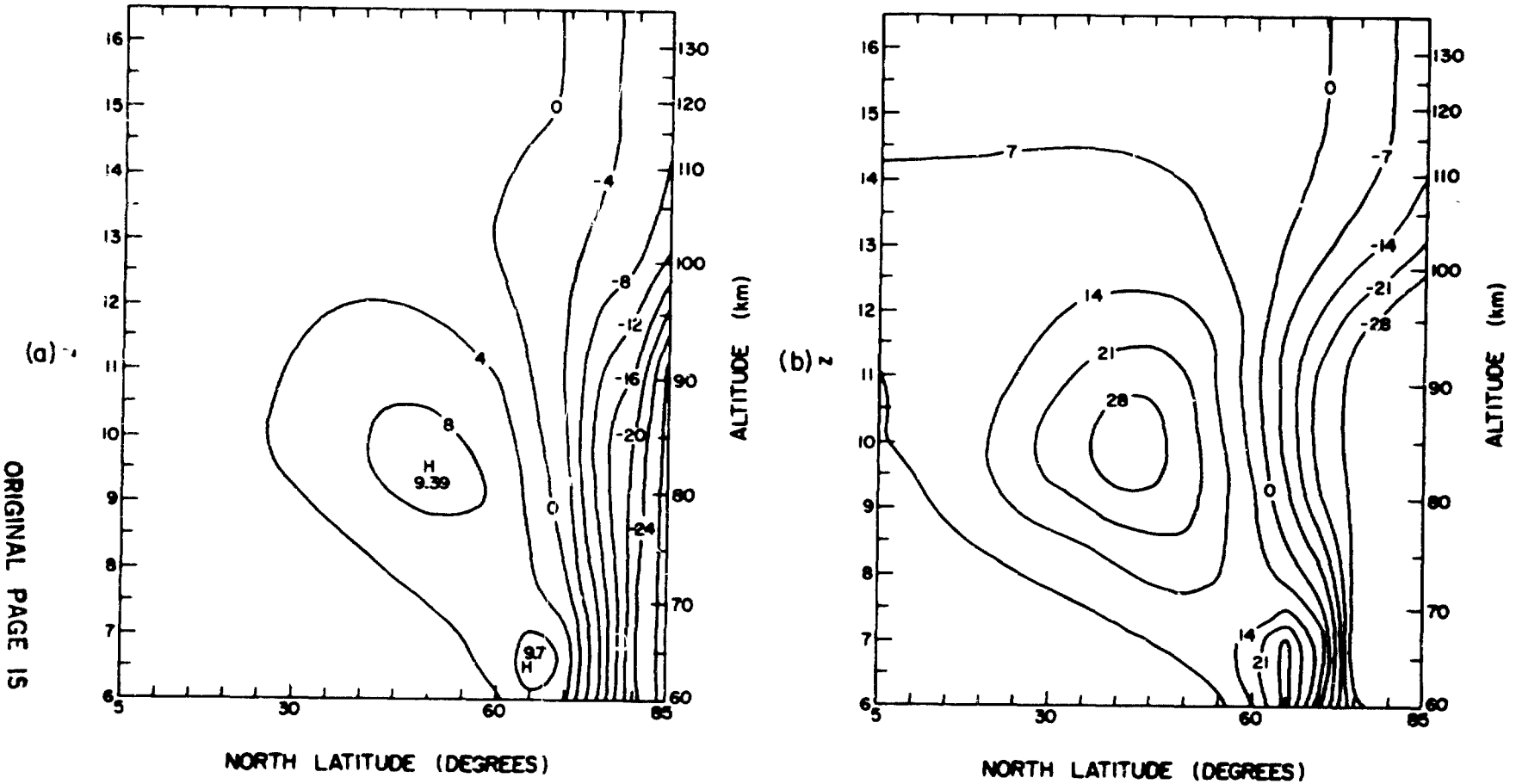

Figure 6.32 Net change in $\overline{NO}$ that results from the combined effects of zonal mean deceleration and wave transport: (a) FEBAVE wave and (b) FEBAVE*2 wave. Contours express percent change from the $\overline{NO}$ concentration obtained with the diabatic circulation only.

increase of $\overline{NO}$ in midlatitudes due to the mean circulation deceleration, resulting in a cell of increased $\overline{NO}$. The amount of this increase is dependent on the magnitude of the wave with an increase of 9% occurring in the FEBAVE case, 20% in the FEBAVE*1.5 case (not shown), and nearly 30% in the FEBAVE*2.0 case. These results indicate that the effects of wave and mean transports do not always cancel, but can at certain levels combine to produce large changes in the initial $\overline{NO}$ distribution.

The small changes in $\overline{NO}$ which occur at upper levels are consistent with the small changes which were seen to occur in the reduced Eulerian circulation above 100 km (see Section 6.1.4). Since the loss mechanism is zero at and above this level, the nitric oxide can be considered to be a conservative tracer in the region. Since transport of a conservative tracer can be viewed as simple advection by the reduced Eulerian circulation [DUNKERTON, 1978], a small change in the reduced Eulerian circulation would result in only a small change in the $\overline{NO}$ concentration. The model calculations are performed in the Eulerian framework, and agreement of model results with the reduced-Eulerian arguments indicates that the model is working properly.

At lower levels, nitric oxide cannot be treated as a conservative tracer, since a sink mechanism for nitric oxide is present. PLUMB [1979] treated the problem of a weakly nonconserved tracer for the case of steady waves and found that the effect of the wave was to transport the tracer downgradient in the sink region. This agrees with our results, in which nitric oxide was transported southward (downgradient) from the polar regions to the midlatitudes in the levels of the model which corresponded to the sink region.

6.4 *Traveling Wave Studies*

In this section, the results of a very brief study of the effects of traveling planetary waves on the nitric oxide concentration in the middle atmosphere are presented. Observational and theoretical evidence for traveling waves in this region was presented in Chapter 2. MADDEN [1978] in a study of nine years of upper level pressure data reported the existence of large-scale zonal wave number 1 disturbances which moved westward around the globe with periods averaging 5 days and 16 days. The highest level considered in the Madden study was 30 mb; for the 16-day wave, Madden indicates an amplitude of about 120 meters at that height. There is some doubt as to whether the observed traveling waves represent forced wave modes or natural resonant modes of the atmosphere; in either case however, the amplitude of the wave should increase with height in an exponential manner.

In the studies discussed briefly in this section, a traveling planetary wave will be superimposed on the equilibrium state obtained with the FEBAVE forcing. The amplitude of the traveling disturbance has arbitrarily been set to be one-half of that of the stationary wave, and the effect of this small amplitude traveling wave on the zonal mean circulation is assumed to be negligible. Also, any interaction between standing and traveling wave components has been neglected.

The purpose of these brief traveling wave studies was to determine what effect a traveling wave of small amplitude had on a pre-existing nitric oxide distribution. Two different wave periods corresponding to the most frequently observed waves were used, i.e., 16 days and 5 days. The same boundary forcing was used for each wave (FEBAVE/2.) although the observational evidence suggests that the 16-day wave is larger in the

winter hemisphere, at least at the 30 mb level. Although there have been few observational studies of traveling waves at the 55 km level, theoretical studies [GEISLER and DICKINSON, 1976] indicate that traveling wave amplitudes can be appreciable at that height. Also, preliminary calculations using .4 mb geopotential height data from satellite measurements indicates at 60°N and 55 km, that 16-day wave amplitudes of 250 m regularly occur. The 5-day wave amplitude is generally around 100 m at this latitude and height, although the 5-day amplitude appears to reach as high as 250 m at certain times. Thus, the use of the FEBAVE/2 forcing (about 250 gpm at 60°N) should provide a reasonable estimate of the effects of the 16-day wave, and an upper limit for 5-day wave effects. Since the waves currently being used have somewhat arbitrary amplitudes however, the results presented in this section can be given only qualitative significance.

The traveling wave structures used in this study were calculated by assuming that the solution to equation 3.21 could be expressed as

$$\psi = \psi_0 \, e^{i\sigma t}$$

where σ represents the frequency of the traveling wave. Hence, the time derivatives in 3.21 can be expanded as

$$\frac{\partial}{\partial t} \psi = i\sigma\psi, \text{ etc}$$

If σ is real, the solution will be oscillatory in time with a period equal to $2\pi/\sigma$. The winds obtained from this oscillating solution are combined with the steady planetary wave winds obtained using the previously described FEBAVE forcing. The results are horizontal and vertical planetary wave winds which oscillate about some equilibrium value with a frequency equal to that of the traveling wave frequency. Since the traveling wave

forcing is small, the oscillation about the equilibrium wind is small, especially at higher altitudes, where the traveling wave oscillation is diminished due to viscous damping.

Figure 6.33a,b shows some typical north-south planetary wave winds which result from the superposition of the traveling and stationary waves. In Figure 6.33a, the sum of the 16-day and stationary components are shown at heights of z = 10.5 (87 km) and z = 13.5 (105 km) for 45° latitude. The traveling wave structure shows a slight westward phase shift with height for the 16-day wave; hence, the rotating wind component at 105 km leads the component at 87 km by about 60° longitude. The 16-day wave travels 22.5° longitude per day; thus, at a given longitude, the traveling wave maximum occurs at z = 13.5, a little more than 2 1/2 days before the maximum occurs at z = 10.5. For the 16-day wave, the amplitude oscillation is nearly 50% of the stationary value, with the phase varying as much as $\pm$ 20° longitude at z = 10.5.

Figure 6.33b shows the rotating components at z = 10.5, 13.5 and 45°N for the 5-day wave. Notice that the magnitude of the 5-day rotating component is significantly smaller than the 16-day component at both heights suggesting that the higher frequency mode is more severely attenuated with height. This is a result of the CHARNEY and DRAZIN [1961] theorem, which state that a traveling wave will not propagate vertically when the Doppler shifted wind velocity it sees exceeds a certain cutoff velocity. Since the 5-day wave is traveling faster against the mean flow, the Doppler shifted velocity seen by the wave exceeds the cutoff velocity at a lower level, and hence the wave is more rapidly attenuated with height. The phase of the 5-day wave shows a small westward shift with height of about 25° between the two levels. Since the 5-day wave is traveling 72°

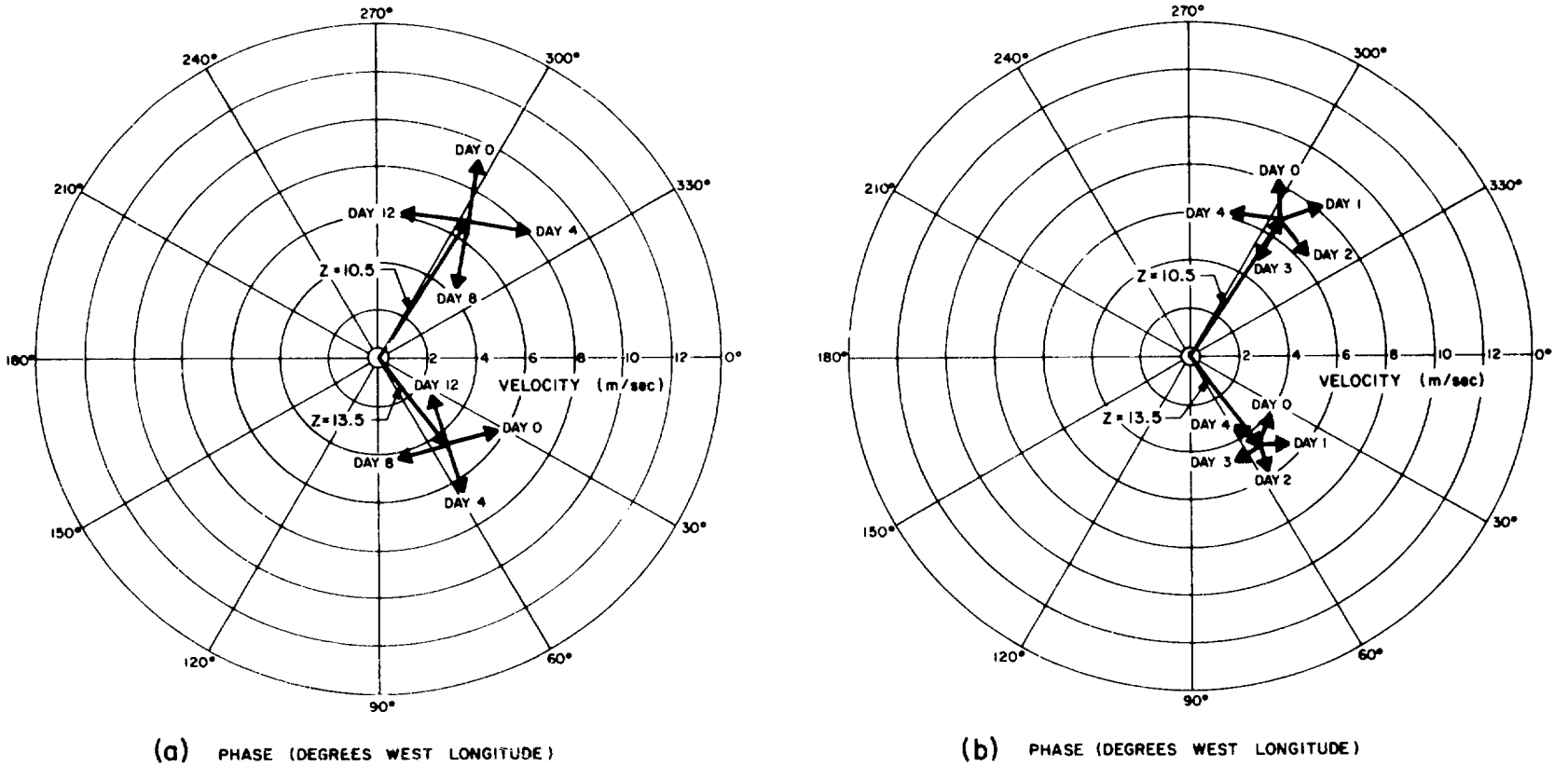

Figure 6.33 Typical north-south planetary wave winds resulting from the combination of a stationary wave and a (a) 16-day wave, (b) 5-day wave. Shown at heights of z = 10.5 (87 km) and z = 13.5 (105 km), for 45° N latitude.

longitude per day, the amplitude maximum at z = 13.5 for a given longitude occurs about 1/3 day before the amplitude maximum at z = 10.5.

The time-dependent planetary wave winds just described were used in the time-dependent model to determine the effect of these winds on the previously determined equilibrium NO concentration. The results of these studies indicate that the zonal mean nitric oxide concentration is virtually unaffected by the passage of these small amplitude waves. This was to be expected, considering that the effect of the much larger FEBAVE wave was small also. The horizontal and vertical velocities associated with the traveling wave were too small to significantly affect the zonal mean concentration.

Although the traveling wave amplitude was small, it did induce an additional component to the perturbation nitric oxide concentration. In the following figures, the concentration shown represents the sum of the mean and wave number 1 perturbation nitric oxide components at 90°W longitude. Thus, the results in the following figures represent the situation as it would be observed at 90°W. The changes with respect to time result from the variations in NO'; $\overline{NO}$ remained essentially constant throughout the model runs. The results presented will be for 60° latitude, which represents the latitude of maximum traveling wave amplitude.

Figure 6.34a shows results for the 16-day wave at z = 10.5 and 13.5 and 60°N latitude. The values shown represent the sum of the $\overline{NO}$ and NO' components at 90°W longitude as a function of time. After an initial surge, the concentration at 13.5 settles down into a regular oscillation about the original equilibrium concentrations. At z = 13.5, the change in total NO amounts to about 9% of the average NO concentration. At z = 10.5, the oscillation is relatively larger, amounting to about 14% of

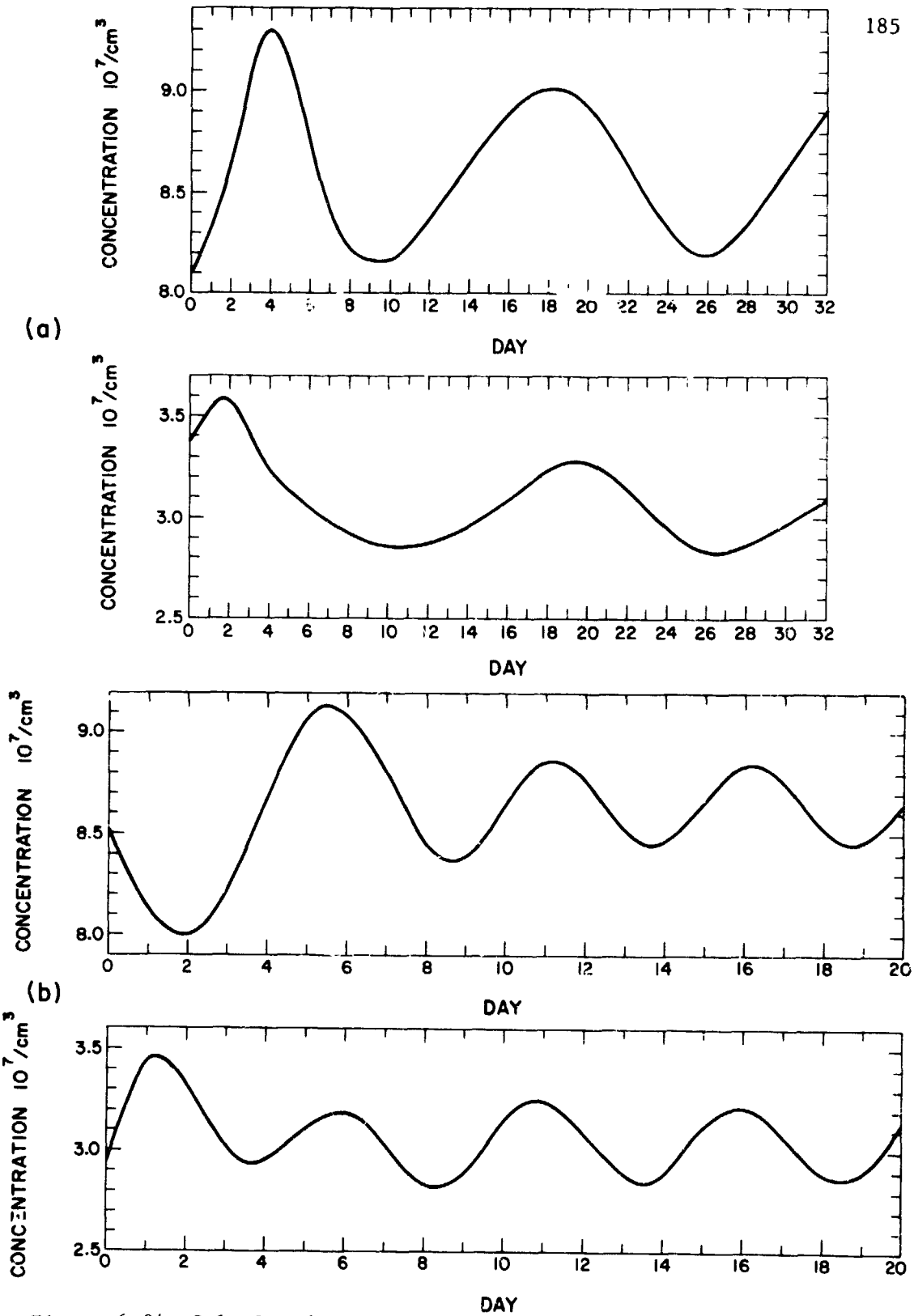

Figure 6.34 Calculated changes in total nitric oxide concentration at 90° west longitude, 60°N latitude and z = 10.5 (87 km) and z = 13.5 (105 km). Shown are the effect of the (a) 16-day wave and (b) 5-day wave.

the original equilibrium value. Thus, the 16-day wave induces a 16-day oscillation in the equilibrium concentration, with the magnitude of the oscillation being about 10% of the original concentration. Notice that the maximum amplitude at z = 13.5 leads the maximum at z = 10.5 by about a day.

The results for the 5-day wave are shown in Figure 6.34b. Again, after an initial surge, the total NO concentration undergoes a regular oscillation about the original equilibrium with a periodicity of 5 days. With the 5-day wave, the tilt in phase with height is small, and hence the observer sees peaks in the total concentration occurring nearly simultaneously at each level. The net change in total NO compared to the original equilibrium amounts to about 4% at z = 13.5 and about 10% at z = 10.5 and 60°N.

The 60°N latitude values were used because the traveling wave amplitude was largest there. The effect of the wave and hence the magnitude of the oscillation in the total nitric oxide concentration fall off poleward and equatorward of 60°. This brief traveling wave study has indicated that a traveling wave which persists for several periods can set up a regular oscillation in the total nitric oxide concentration as observed at a single ground location. An extension of this work would include a determination of the amplitude and phase structure of traveling waves in the 55 km region. These wave structures could then be used in a more complete study of the effects of traveling waves on the nitric oxide concentration. Variations in the nitric oxide concentration could then be related to changes in electron density and compared to the results of ground-based partial reflection studies.

In a study by GELLER and SECHRIST [1971], the effects of changes in

the nitric oxide concentration on the electron density were examined. They assumed that the production of electrons in the 70-90 km region was due solely to the ionization of nitric oxide by incoming Lyman-α radiation. The loss of electrons was assumed to be due to recombination of the electrons with positive molecular and hydrated ions. Assuming a steady state, they arrived at the expression

$$\frac{[NO]_{anomalous}}{[NO]_{normal}} = \frac{[e]^2_{anomalous}}{[e]^2_{normal}}$$

which implies that the electron concentration is proportional to the square root of the local NO concentration. Thus, the changes in $[e]$ induced by the traveling waves in this study would be on the order of 3-4% of the original electron concentration.

While changes of this magnitude are insufficient to cause anomalous absorption, more detailed knowledge of the structure of traveling waves in this region is needed before quantitative conclusions can be drawn concerning the relationship of traveling waves to the electron concentrations.

6.5 *Exponentially-Growing Wave*

In this section, the effects of an exponentially-growing wave on the nitric oxide concentration will be presented. The studies in Section 6.3 represented equilibrium studies in which the wave, mean, and nitric oxide concentrations were allowed to reach a steady state, a process which typically took about 20 model days. In the studies presented in this section, the effects of planetary waves on the zonal mean circulation and nitric oxide distribution will be investigated on a day-to-day basis by applying a time-dependent lower boundary forcing.

In Section 2.4, the changes in planetary wave and mean wind structure

which occur during a stratospheric warming phenomena were discussed. During some stratospheric warmings, the amplitude of planetary wave number 1 is observed to undergo a rapid increase, often doubling or tripling its average value in a period of a few days [SCHOEBERL, 1978]. This large increase in amplitude over a short period of time was also evident in the observational results presented in Chapter 4. Since the changes in wave amplitude occur so suddenly, most numerical models of the stratospheric warming perform a calculation of the waves and mean circulation once every model hour. [MATSUNO, 1971; HOLTON, 1976]. Unfortunately, cost restrictions prevented us from calculating the planetary wave structures every hour and so a study of nitric oxide transports during a major stratospheric warming was not possible.

We chose instead to study the case of a planetary wave whose amplitude increased and then decreased gradually over a two-week period. By postulating a gradual increase, we were able to perform the wave calculation only once each day, thus greatly reducing the cost of the model run. The initial basic state atmosphere was that which had resulted from the equilibrium run which used FEBAVE boundary forcing (see Figure 6.5). This lower boundary forcing was then increased by 10% per day for seven days, which had the net effect of doubling the forcing in one week. The forcing was then reduced by 10% for the next seven days, thus reaching its original value after 14 days. By increasing and then decreasing the wave amplitude over a 14-day period, we hoped to simulate at least on a reduced scale, the surge in planetary wave amplitude observed to occur during stratospheric warming events [SCHOEBERL, 1978].

In these studies, planetary wave amplitudes were calculated once each model day. The convergences of eddy heat and momentum flux used in the

calculation of the zonal mean state, were assumed to remain nearly constant over a one-day period. Changes in the nitric oxide concentration were calculated each hour, using zonal mean and planetary wave winds which were interpolated from model calculations made at the beginning and end of a given 24-hour period. In this way we hoped to minimize the effect of the once-per-day planetary wave calculation.

In order to determine the effect of the size of the time step on changes in the zonal mean circulation, two test runs were performed, one in which the wave was calculated every six hours, and one in which the wave was calculated every 24 hours. The results indicate that for small changes in lower boundary forcing (less than 10% per day), the final zonal mean state is relatively unaffected by the time step involved. After 8 days of increasing wave forcing (10% per day), the zonal mean and meridional winds obtained in each case differed by less than 5% at the end of each 8-day run. Thus, it appears that the results obtained using a once-per-day wave calculation should be equivalent to those obtained using a smaller time step, provided that the time rate of change in the boundary forcing is on the order of 10% per day or less.

The effects of planetary wave momentum and heat fluxes on the zonal mean circulation were discussed in Section 6.1. These wave fluxes serve to decelerate the mean flow, while at the same time generating a secondary meridional circulation which partially compensates for the reduction. In the studies presented in this section, the amplifying wave gradually decelerated the zonal mean flow, with the maximum deceleration occurring at the end of day 7, when the wave amplitude was at its maximum. A small reversal of the mean zonal wind occurred at the end of day 7 and persisted for about two days. After that time, the wave amplitude, which began to

decrease on day 8, became sufficiently small to allow the westerly regime to be reestablished. The wind reversal was not nearly as great in extent as that pictured in Figure 6.9, which resulted from the continuous application of FEBAVE*2 forcing. The maximum reduction that occurred amounted to about 1/3 of those shown in Figure 6.10a. For example, on day 7, the reduction in $\bar{u}$ at $z = 12.0$ and 60° N latitude was 8 m/sec, as compared to a reduction of 21 m/sec in the equilibrium case. The amplifying wave forcing was equivalent to that of the FEBAVE*2 wave only on day 7; hence, the wind reversal was not nearly as widespread, and persisted only for a few days.

This decrease in zonal mean wind was accompanied by a corresponding reduction in northward and downwards winds. In fact, the meridional wind reversed direction from northward to southward in a region poleward of 75° N at levels around $z = 12.0$. However, this change in meridional wind direction also only persisted during the few days when the planetary wave amplitude was maximized.

The planetary wave and mean winds obtained during the model run were used to calculated changes in the nitric oxide concentration which resulted from variations in the wind structure. The initial mean nitric oxide concentration was obtained from an equilibrium calculation using FEBAVE forcing at the lower boundary. The mean nitric oxide concentration resulting from the FEBAVE equilibrium run is similar to that shown in Figure 6.21a. The corresponding equilibrium perturbation concentration is shown in Figure 6.23a (amplitude) and 6.24a (phase).

Figure 6.35 summarizes the changes that occurred in the zonal mean nitric oxide concentration as a result of the amplifying boundary wave forcing. Figure 6.35a shows the changes in the zonal mean concentration

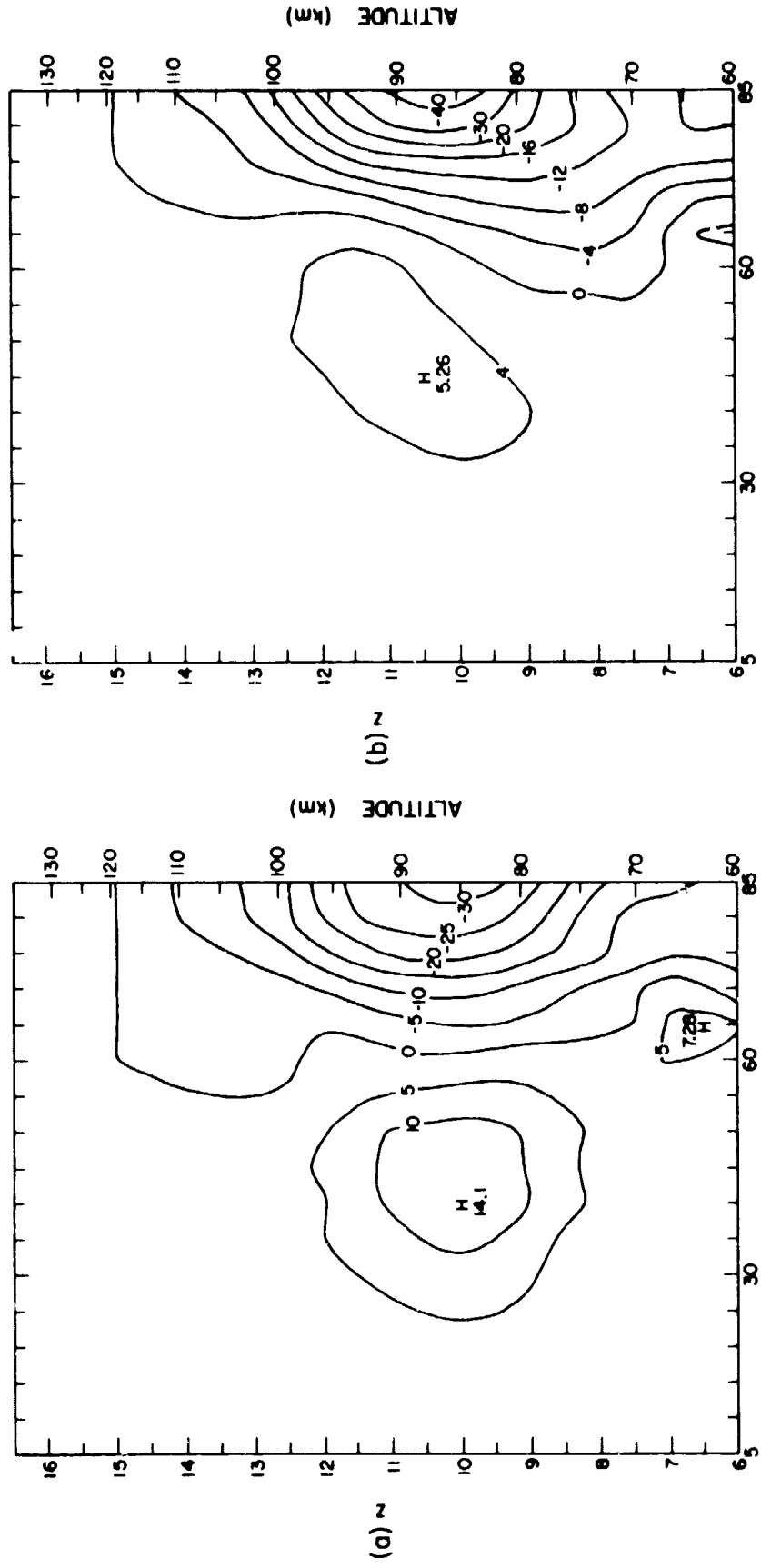

Figure 6.35 Changes in zonal mean nitric oxide concentration calculated in the amplifying wave study. Contours represent the percent change from the original distribution, calculated for (a) day 7 and (b) day 14.

at the end of day 7, expressed as a percent change from the original equilibrium distribution. The main feature is the 14% increase in midlatitudes centered at 45°N and z = 10 (85 km), with a corresponding decrease at high latitudes. This increase is partially due to the reduction in northward transport by the decelerated zonal mean meridional wind. This reduction in northward (and downward) wind, which occurs at all levels, reduces the amount of nitric oxide transported out of the midlatitude region. The result of this reduced transport is an increase in the nitric oxide concentration in midlatitudes, and a corresponding decrease at high latitudes.

Planetary wave transports also contribute to the increase of $\overline{NO}$ in midlatitudes. At high levels, where the loss coefficient is small, the wave transports tend to compensate for the reduced meridional transport by the zonal mean, and hence the changes at high levels are minimized. At lower levels, however, the large loss rate results in a wave induced perturbation concentration which is nearly 180° out of phase with v'. This effect was discussed in Section 6.3.4. This phase difference results in a mean southward flux of nitric oxide due to wave winds in the loss region, which reinforces the increase in $\overline{NO}$ in the midlatitudes and the decrease in the polar regions.

Figure 6.35b shows the percent change in $\overline{NO}$ after day 14. At this point, the planetary wave forcing has returned to its original value, and the zonal mean circulation has almost returned to its original state. The large buildup that was present on day 7 has nearly disappeared, with the concentration at midlatitudes being only 5% above its initial value. There is still a reasonably large deficit poleward of 70° latitude. Meridional winds are small at high latitudes, and hence the concentration

near the pole builds up very gradually to its original value. Fourteen days after the wave amplitude has returned to normal (day 28), the mid-latitude buildup has completely disappeared, and the deficit in the polar region is confined to the lowest height levels of the model.

Figure 6.36 shows the perturbation concentration after day 7 of the model run. Figure 6.36a,b should be compared to 6.23a and 6.24a, respectively, which show the initial perturbation concentration. Figure 6.36a shows that the perturbation amplitude has increased, mainly due to the increase in the wave amplitude. The maximum of 4.4×10^7 molec/cm^3 at $z = 12.0$ represents an increase of about 15% over the equilibrium value. This maximum value is larger than any of the maxima obtained in the equilibrium runs. Adjustments in the zonal mean circulation reduced the wave amplitude at high levels, thus limiting the maximum value of NO'. In the amplifying wave study, the boundary forcing is changing on a daily basis. Since the wave is changing so rapidly, the changes in the zonal mean state which would tend to reduce the wave amplitude, do not completely take place. Hence, the wave amplitude at a given level on a given day is larger than the amplitude of a similarly forced wave at equilibrium. This result is not unexpected, since it was noted in the equilibrium runs that the zonal mean wave system required at least 5 days to reach equilibrium.

Figure 6.36b shows the phase of the perturbation distribution on day 7. This can be compared to the initial perturbation phase state shown in Figure 6.24a. The phase lines on day 7 are more compressed at high levels than in the equilibrium case; the phase lines change more rapidly with height at upper levels on day 7. This is a result of the greater vertical wave propagation on day 7 and the corresponding increase in phase change with height. The phase above $z = 11$ on day 7 is shifted about 15° to the

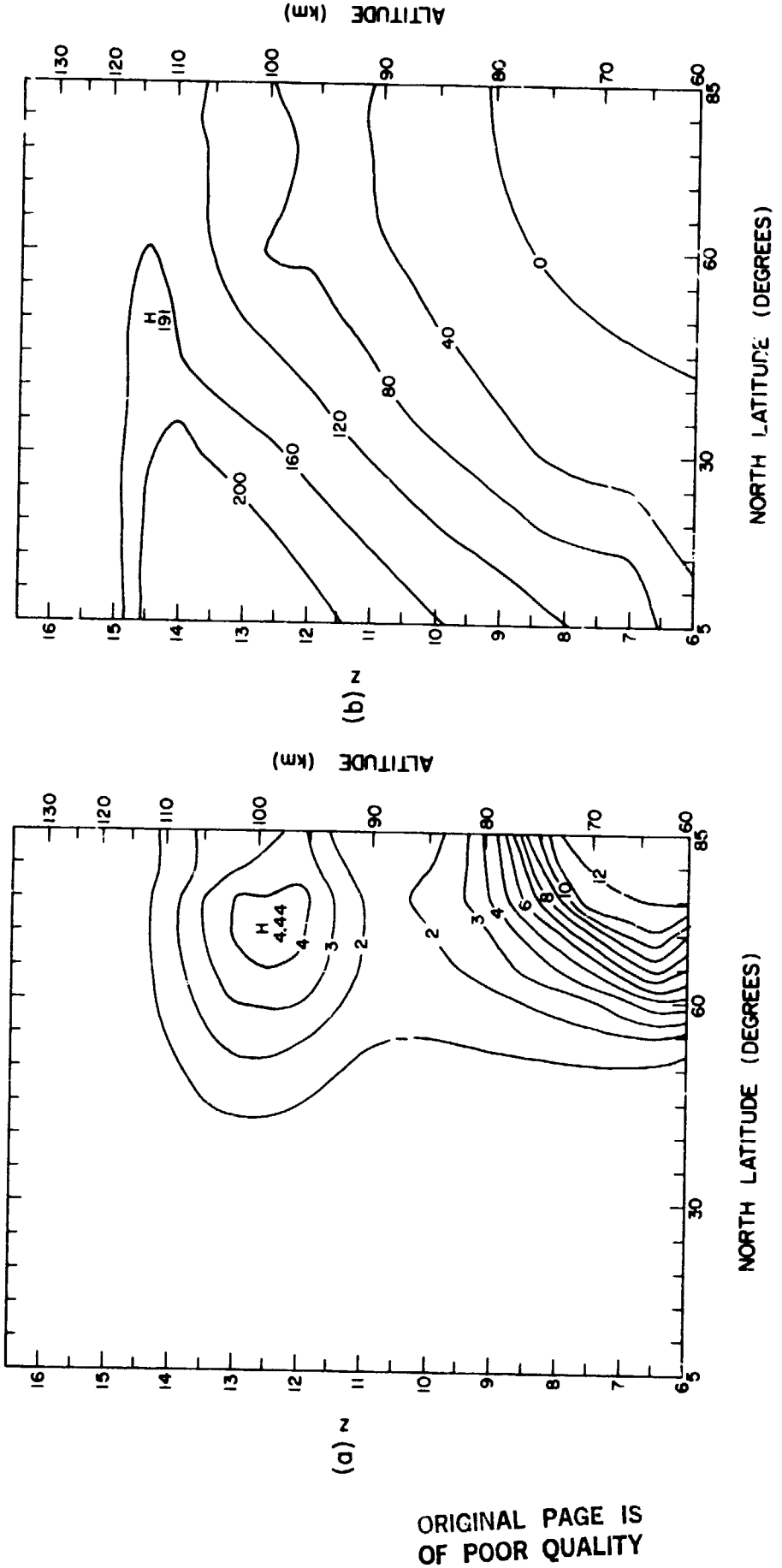

Figure 6.36 Perturbation nitric oxide concentration obtained on day 7 of amplifying wave study: (a) amplitude in units of 10^7 molec/cm^3 and (b) phase in degrees west longitude.

west of its original equilibrium position, indicating that a greater amount of wave energy is being absorbed by the zonal mean flow. As the boundary forcing is decreased after day 7, the phase of the perturbation distribution gradually returns to its equilibrium position. The amplitude decreases also, with the value at z = 12.0 and 60° falling below its original equilibrium value on day 9. This initial sharp dropoff in NO′ amplitude is again due to the fact that the adjustments in the zonal mean do not occur as rapidly as changes in the wave amplitude. As the boundary forcing is decreased (day 8), the wave amplitude is reduced. However, the zonal mean winds at this time are in a reduced state due to the effect of the large wave, on day 6 and 7. This causes a reduction in planetary wave amplitude greater than that which would result from the reduced forcing alone. This overly reduced wave amplitude results in γ' amplitudes of less than the original equilibrium value for days 8-11. After this time, the zonal mean circulation has nearly returned to normal, and the perturbation concentration gradually returns to its equilibrium value.

In this section, we have briefly discussed the results of a study in which the planetary wave boundary forcing was increased with time to double its original value in one week. The forcing was then decreased gradually for a second week, until the original forcing value was obtained. The changes in the nitric oxide concentration due to the changing wave and mean winds which resulted from this forcing variation were studied. The mean concentration had increased by 14% at 45°N latitude and z = 10 (85 km) by the end of day 7, which corresponded to the day of maximum forcing. The perturbation nitric oxide amplitude on day 7 also showed an increase of 15% over its original value at z = 12.0 and 75°N. As the boundary forcing was decreased, both $\overline{NO}$ and NO′ returned to their

equilibrium values. The time evolution of the amplitude of NO was strongly affected by the effect of the interaction between the planetary waves and the zonal mean circulation. By day 21, both $\overline{NO}$ and NO′ had nearly returned to their equilibrium values.

Due to the model restrictions and cost limitations, the time rate of change of the boundary forcing had to be severely restricted. Future studies could involve the relaxation of these restrictions, so that more rapidly changing waves could be considered. The effects of a major stratospheric warming on the nitric oxide concentration could also be investigated. However, this would involve a more complete treatment of the critical layer phenomena than is included in the present model.

The present studies indicate that an exponentially growing and decaying wave can significantly affect the $\overline{NO}$ concentration in midlatitudes. The largest change in the $\overline{NO}$ concentration occurred at midlatitudes near z = 10 (85 km), where the concentration had increased by 14% after 7 days of increasing wave forcing. Although this increase is significant, it is not on the same order of magnitude as would be required in order to produce an anomalous absorption. The limitations of the model prevented the investigation of more rapidly changing, larger amplitude waves, which would probably result in a greater effect on the zonal mean nitric oxide concentration.

7. SUMMARY AND SUGGESTIONS FOR FUTURE RESEARCH

7.1 *Summary*

The purpose of this research was to gain a better understanding of the effects of planetary waves on the nitric oxide distribution in the middle atmosphere. The factors which contribute to the structure of the nitric oxide distribution were examined, and the sensitivity of the distribution to variations in planetary wave amplitude was investigated. Wave-induced changes in the mean nitric oxide concentration were examined as a possible mechanism for the observed winter anomaly phenomena.

In Chapter 2, a review of the theoretical and observed characteristics of planetary waves was presented. Planetary waves can propagate vertically only through westerly winds, and hence they exist only during the winter months. The amplitude and phase of these waves is dependent not only on the wave forcing at the lower boundary, but also on the structure of the zonal mean wind through which the wave propagates. The interaction between the wave and the mean flow was also discussed, first on a theoretical basis and then in terms of the frequently observed stratospheric warming event.

Chapter 2 also contained a review of observational and theoretical studies of nitric oxide. Although mesospheric chemistry is quite complex, the major reactions concerning the production and loss of nitric oxide were presented. Also discussed in this chapter were the relative merits and advantages of the Eulerian and Lagrangian viewpoints. Although transport in the Lagrangian framework is conceptually simpler, the Eulerian framework is computationally easier to impose. Also, the Lagrangian picture is greatly complicated by the addition of dissipation, sources and sinks, and large amplitude waves.

In Chapter 3, the numerical model was discussed. The equations for the planetary wave and zonal mean were formulated, and the finite difference technique used to solve the equation of motion was outlined. Also presented were the equations for the time evolution of the zonal mean and perturbation nitric oxide concentrations. The iterative approach used to solve the wave, mean and nitric oxide equations simultaneously was briefly discussed.

In Chapter 4, the results of an observational analysis of geopotential height at .4 mb (55 km) were presented. Values of mean and perturbation geopotential height were obtained for the nine weeks of January 2 through February 27, 1974. The monthly averaged values of wave structure for January and February were later used as inputs for the time-dependent model. The results at the end of February were particularly interesting in that a stratospheric warming was occurring at that time. The mean and perturbation concentrations of nitric oxide at 105 km were determined by analyzing satellite data, also from the winter of 1974, as presented in CRAVENS and STEWART [1978]. The perturbation concentration was dominant in the winter months, indicating the presence of a planetary-wave-related effect. The results of this observational study were used as model inputs for the stationary wave studies in Chapter 5, and were compared to the computational results of the time-dependent model in Chapter 6.

In Chapter 5, the results of a time-independent study of transports due to planetary waves only was presented. Using a postulated perturbation nitric oxide concnetration, transports due to wave number 1 and 2 were determined for the months of January and February. The wave structures used in this study were calculated using the results of the observational geopotential height analysis as a lower boundary forcing.

It was concluded that the transports due to wave number 2 were probably not significant, but that the wave number 1 transports could, if they persisted, produce large changes in the zonal mean nitric oxide distributions. These results were somewhat artificial in that the perturbation concentration was assumed to have constant phase with height, and also to be constant in time. These restrictions were later removed by using the time-dependent model.

In Chapter 6, the effects of planetary waves on the nitric oxide concentration were investigated using a time-dependent numerical model. The model was used to calculate planetary wave and zonal mean winds, which were then used to calculate mean and perturbation nitric oxide distributions. The time-dependent model was used to determine equilibrium nitric oxide distributions resulting from steady forcing, and also time-dependent nitric oxide distributions resulting from time-dependent lower boundary planetary wave forcings.

In Section 6.1, the factors which contribute to the structure of the zonal mean circulation were discussed. The circulation in the upper atmosphere was seen to be driven primarily by the diabatic heating, in accordance with HOLTON and WEHRBEIN [1980b]. The mean circulation and temperature distribution produced by the diabatic heating were very similar to those calculated by SCHOEBERL and STROBEL [1978] with a similar model. Using the monthly averaged forcings obtained from the observational analysis presented in Chapter 4, the effects of planetary wave momentum and heat fluxes on the zonal mean circulation were determined to be small. However, a doubling of the February averaged lower boundary forcing resulted in significant changes in the zonal mean structure, including the development of a critical layer in the high altitude polar region. This

doubled forcing was well within the range of the individual weekly forcings presented in Chapter 4, and indicates that if the wave amplitude is strong enough, large changes in the zonal and meridional circulation may result.

The effect of planetary wave fluxes on the zonal mean circulation was examined in the context of the reduced Eulerian formalism, which was introduced by ANDREWS and MCINTYRE [1976]. It was seen that in the absence of dissipation and critical levels, the passage of a planetary wave produces no net acceleration of the zonal mean flow, a result which is due to CHARNEY and DRAZIN [1961] and is known as the noninteraction theorem. Even when dissipation is included, the tendency for cancellation of wave and mean effects is present, as was demonstrated by model calculations of the reduced Eulerian circulation.

In Section 6.2, the factors which contribute to the zonal mean nitric oxide concentration were examined. Nitric oxide chemistry was modeled using a simplified source-sink approach. The source was the downwards flux of nitric oxide through the top of the modeling region, and a sink region was imposed between 78 and 102 km. In order to account for transport due to gravity waves and turbulence in the upper atmosphere, a vertical eddy diffusion similar to thay presented in EBEL [1980] was included in the model. The vertical distribution of nitric oxide was seen to be sensitive to both the choice of diffusion coefficient and upper boundary flux; the final choice of coefficients and fluxes was determined by a comparison of model results to observational nitric oxide profiles.

The effects of horizontal and vertical winds on the nitric oxide distribution were also investigated in Section 6.2. In general, an increase in horizontal wind reduced the concentration in midlatitudes due

to increased transport of nitric oxide out of the region. An increase in vertical winds increased the nitric oxide at all levels, since the flux through the upper boundary was effectively increased. The zonal mean nitric oxide distribution which resulted from the combined effects of diffusion and zonal mean winds was in reasonable agreement with the limited nitric oxide observations available.

In Section 6.3, the effects of planetary waves on the nitric oxide distribution were examined. In Section 6.3.1, the effects of planetary waves on $\overline{NO}$ through the mechanism of the deceleration of the zonal mean flow by wave fluxes was examined. The reduction in mean meridional and vertical winds resulted in an increase of $\overline{NO}$ in midlatitudes and a decrease in the polar regions, mainly due to the reduced northward transport of NO by meridional circulation.

In Section 6.3.2, the perturbation nitric oxide concentration which was induced by the planetary wave and zonal mean winds was discussed. To first order, the amplitude and phase of the perturbation distribution are determined by the perturbation velocity v' and the latitudinal gradient of $\overline{NO}$, with the phase of NO' lying approximately 90° to the west of the phase of v'. This relationship is altered in the loss region, however. At heights where the loss coefficient is large, the NO' distribution can be as much as 180° out of phase with v'. The calculated values of NO' at 105 km were in reasonable agreement with observational results deduced from data presented in CRAVENS and STEWART [1978].

The implications of the phase relationship between the planetary wave winds and perturbation concentration were discussed in Sections 6.3.3 and 6.3.4. In regions where the loss coefficient was small, the mean horizontal transport of nitric oxide due to the planetary wave winds was

northward, tended to compensate for the diminished northward transport by the decelerated mean meridional wind. In regions of large loss coeffi cient, the net planetary wave transport was southward, thus enhancing the buildup of nitric oxide at midlatitudes produced by the deceleration of the mean flow. This in in agreement with the theoretical study of PLUMB [1979], who indicated that wave transports in a sink region should be downgradient relative to the mean concentration.

The effect of a small amplitude traveling wave was discussed in Section 6.4. The traveling wave solutions were superimposed on a background stationary wave solution, and the effects of the time-dependent wave winds on the nitric oxide distribution were investigated. After transient effects due to switching on the wave had vanished, the total nitric oxide at a single location underwent a regular oscillation with period equivalent to that of the imposed traveling wave. The amplitude of the oscillation was significant, but probably not large enough to be associated with an anomalous absorption event. More information on the structure and origin of traveling waves is needed before a connection between anomalous absorption and traveling planetary scale waves can be made.

In the final section of this chapter, the effects of increasing and then decreasing the planetary wave boundary forcing over a period of two weeks were discussed. The mean nitric oxide was seen to increase in midlatitudes as the wave amplitude increased, and then return to normal gradually over a period of several weeks when the wave forcing was decreased. A maximum increase of 14% was obtained on the day of maximum boundary forcing. The perturbation nitric oxide concentration also experienced a maximum increase in amplitude of 15%, and a shift in phase

of 20° to the west of the original equilibrium position. Model restrictions limited the study to waves which grew less than 10% per day; in the actual atmosphere, much larger changes can occur. Again, the calculated increase of NO in midlatitudes was probably insufficient to result in anomalous absorption, but this result could be modified by the use of more realistic rates of wave amplitude increases.

7.2 *Suggestions for Future Research*

On the basis of this work, several suggestions for future research can be made. One project would involve a detailed investigation into the observational features of traveling planatary waves in the upper atmosphere. Satellite data at high altitudes is becoming increasingly available, and such a study would provide information on the amplitude and frequency of traveling wave disturbances which could be used as input to this, the present model. The present wave and mean model could also be combined with a slightly more complicated chemical model which would allow for a better estimate of the loss coefficients in the sink region. In another project, the restrictions which limit the allowable rate of change of the planetary wave amplitude could be removed by modifying the planetary wave-zonal mean equations. This would permit the model to be used in a study of the transport of nitric oxide during a stratospheric warming event. A more ambitious project would involve extending the model boundary downwards to the 100 mb level. The model-derived time-dependent wave and mean winds could then be coupled with a photochemical model which included nitrogen and ozone chemistry. With this model, the effects of planetary waves and wave-induced changes in the zonal mean circulation on the overall distribution of various chemical constituents could be investigated.

APPENDIX

```
      PROGRAM TIMMOD(INPUT,OUTPUT,TAPE5=INPUT,TAPE6=OUTPUT,
     1S,TAPE7=S,C,TAPE8=C,PLOT,TAPE9=PLOT)
      COMMON /A/ A(17,17,45),AI(17,17,45),SRE,SIM,COUNT,IDAY,ID
     1 ,VRE(17,45),VIM(17,45),WRE(17,45),WIM(17,45)
      COMMON /B/ SNR(17),CNR(17),SNI(17),CNI(17),BDY(17),BDYI(17),
     1BASE(17),TOP(17),BOTRE(17),BOTIM(17)
      COMMON /C/ UBAR(17,45),TBAR(17,45),UFLUX(17,45),TFLUX(17,45),
     1 UINIT(17,45),VBAR(17,45),VINIT(17,45),WBAR(17,45),WINIT(17,45)
      COMMON /D/ S(45),QR(17,45),QI(17,45),QSAVE(17,45),
     1 VR(17,45),VI(17,45),WR(17,45),WI(17,45)
      COMMON /E/ QR1(17,45),QR2(17,45),QI1(17,45),QI2(17,45)
      COMMON /F/ W1(17,17),W2(17,17),W3(17,17),W4(17,17),W5(17,17),
     1W6(17,17),G1(17),G2(17),G3(17),G4(17),G5(17)
      COMMON /G/ P3(17),P4(171),BARNOX(17,45),AMPNOX(17,45),
     1PHANOX(17,45),TIMNOX(17,45),TIMAMP(17,45),TIMPHA(17,45),
     1PROMEAN(17,45),PROAMP(17,45),PROPHA(17,45)
     1 ,AIR(45),H(45),DZZ(17,45),TEST1(17,45),TEST2(17,45)
      COMMON /H/ TIME(17,45),FLUX(17,45),ANC(45),ANCZ(45),BETR(45),
     1TAU(45),SSZ(45),HEAT(17,45),HEATER(17,45)
      IWEEK=1
      IDAY=30
      ID=1
      COUNT=1.
      DTIME=3600.
C     SRE GT 0 = WESTWARD TRAVELING WAVE
C  SIM GT 0 =DECAYING WAVE,SIM LT 0 = INCREASING WAVE
C      SRE=2.*3.14159/5./8.64E4
       SRE=0.
       SI=0.
       SIM=0.
C      SIM=-.1/8.64E4
      PO=100.
      AM=1.
      DZ=.25
      MI=17
      MJ=45
       BOT=5.5
      ITHETA=5
      DTHETA=3.14159*ITHETA/180.
      CONV=3.14159/180.
      CALL INIT(PO,MI,MJ,DZ,DTHETA,CONV,AM,DTIME,BOT)
C      GO TO 92
C     GO TO 20
       DO 5 I=1,MI
       DO 5 J=1,MJ
       QSAVE(I,J)=QR(I,J)
       UINIT(I,J)=UBAR(I,J)
       VINIT(I,J)=VBAR(I,J)
 5     WINIT(I,J)=WBAR(I,J)
```

```
C       GO TO 92
        DO 90 IW=1,IWEEK
        READ(5,991)(SNR(I),I=1,MI)
        READ(5,991)(SNI(I),I=1,MI)
 991    FORMAT(5F8.2)
        READ(5,992) IFOR
 992    FORMAT(I6)
        DO 10 KK=1,MI
        I=MI+1-KK
        BOTRE(I)=SNR(KK)*EXP(-BOT/2.)*100./SQRT(.0193226)
 10     BOTIM(I)=SNI(KK)*EXP(-BOT/2.)*100./SQRT(.0193226)
        T=(COUNT-1.)*8.64E4/24.
C        GO TO 12
        DO 11 I=1,MI
        BDY(I)=(BOTRE(I)*COS(SRE*T)-BOTIM(I)*SIN(SRE*T))*EXP(-SIM*T)
 11     BDYI(I)=(BOTIM(I)*COS(SRE*T)+BOTRE(I)*SIN(SRE*T))*EXP(-SIM*T)
        CALL BASIC(MI,MJ,DZ,DTHETA,CONV,AM,DTIME,BOT)
        CALL SOLWAVE(PO,MI,MJ,DZ,DTHETA,CONV,AM,BOT)
        CALL ATWAVE(MI,MJ,DTHETA,DZ,CONV,AM,BOT,0)
        CALL FLUXX(MI,MJ,DTHETA,DZ,CONV,DTIME)
 12     CONTINUE
C       GO TO 91
C       GO TO 92
        DO 13 I=1,MI
        DO 13 J=1,MJ
        VRE(I,J)=AI(1,I,J)
        VIM(I,J)=AI(2,I,J)
        WRE(I,J)=AI(3,I,J)
 13     WIM(I,J)=AI(4,I,J)
C
C THIS SECTION READS IN STEADY WAVE
          GO TO 140
        DO 400 J=1,288
 400    READ(5,991)
        READ(5,990)((A(6,I,J),I=1,MI),J=1,MJ)
        READ(5,990)((AI(6,I,J),I=1,MI),J=1,MJ)
        READ(5,990)((A(7,I,J),I=1,MI),J=1,MJ)
        READ(5,990)((AI(7,I,J),I=1,MI),J=1,MJ)
        DO 14 I=1,MI
        DO 14 J=1,MJ
        VR(I,J)=A(6,I,J)*COS(AI(6,I,J)*CONV)
        VI(I,J)=A(6,I,J)*SIN(AI(6,I,J)*CONV)
        WR(I,J)=A(7,I,J)*COS(AI(7,I,J)*CONV)
 14     WI(I,J)=A(7,I,J)*SIN(AI(7,I,J)*CONV)
        CALL OUTPUT(2,MI,MJ,ITHETA,DZ,6)
        CALL OUTPUT(2,MI,MJ,ITHETA,DZ,7)
 140      CONTINUE
C
C  REMOVE NEXT COMMENT FOR STEADY STATE TRAVELING WAVE AND
C      INSERT COMMENT ON NEXT STATEMENT
C       GO TO 95
        DO 90 ID=1,IDAY
```

```
C       T=(COUNT+23.)*DTIME
C       SIM=-.1/8.64E4
C       T=ID*24.*DTIME
        WRITE(6,901) ID,IW,IFOR,COUNT
C  NOTE! BE CAREFUL OF COUNT HERE
        IF(ID.GE.3) SIM=-.1/8.64E4
        IF(ID.GE.10) SIM=.1/8.64E4
        IF(ID.GE.17) SIM=0.
         SIM=0.
          IF(ID.EQ.3) SI=-.1
          IF(ID.EQ.4) SI=-.2
          IF(ID.EQ.5) SI=-.3
          IF(ID.EQ.6) SI=-.4
          IF(ID.EQ.7) SI=-.5
          IF(ID.EQ.8) SI=-.6
          IF(ID.EQ.9) SI=-.7
          IF(ID.EQ.10) SI=-.6
          IF(ID.EQ.11) SI=-.5
          IF(ID.EQ.12) SI=-.4
          IF(ID.EQ.13) SI=-.3
          IF(ID.EQ.14) SI=-.2
          IF(ID.EQ.15) SI=-.1
          IF(ID.EQ.16) SI=0.
        DO 15 I=1,MI
        BDY(I)=(BOTRE(I)*COS(SRE*T)-BOTIM(I)*SIN(SRE*T))*EXP(-SI)
 15     BDYI(I)=(BOTIM(I)*COS(SRE*T)+BOTRE(I)*SIN(SRE*T))*EXP(-SI)
        JFLAG=1
C
C
C       CHANGE THIS BACK FOR NOX RUNS
C
C        JFLAG=0
        IF(ID.EQ.1) JFLAG=0
        IF(ID.EQ.9) JFLAG=0
C       IF(ID.EQ.13) JFLAG=0
        IF(ID.EQ.20) JFLAG=0
        CALL SOLMEAN(MI,MJ,DZ,DTHETA,DTIME)
        CALL ATMEAN(PO,MI,MJ,ITHETA,DZ,DTHETA,AM,DTIME,1,JFLAG)
        DO 16 I=1,MI
        DO 16 J=1,MJ
 16     QSAVE(I,J)=QR(I,J)
C        GO TO 54
        CALL BASIC(MI,MJ,DZ,DTHETA,CONV,AM,DTIME,BOT)
        CALL SOLWAVE(PO,MI,MJ,DZ,DTHETA,CONV,AM,BOT)
        CALL ATWAVE(MI,MJ,DTHETA,DZ,CONV,AM,BOT,JFLAG)
        CALL FLUXX(MI,MJ,DTHETA,DZ,CONV,DTIME)
C       GO TO 90
 95     CONTINUE
901     FORMAT(6H1 DAY=,I2,7H  WEEK=,I2,11H   FORCING=,I6,4H CT=,F3.0)
C   CHANGE THIS TO 48 OR SO FOR STEADY-STATE TRAVELING WAVE
C     SET AT 6 FOR DAY TO DAY ITERATIONS
        DO 300 ITER=1,2
```

```
      DO 300 IPRT=1,12
C     ITER=1
C     IPRT=1
      T=((ITER-1)*12+IPRT-1)*DTIME
      DO 100 I=1,MI
      DO 100 J=1,MJ
      A(15,I,J)=VRE(I,J)+(AI(1,I,J)-VRE(I,J))*T/8.64E4
C     AI(15,I,J)=VIM(I,J)+SRE*T*360./2./3.14159
     AI(15,I,J)=VIM(I,J)+(AI(2,I,J)-VIM(I,J))*T/8.64E4
C      AI(15,I,J)=VIM(I,J)
      A(14,I,J)=WRE(I,J)+(AI(3,I,J)-WRE(I,J))*T/8.64E4
C     AI(14,I,J)=WIM(I,J)+SRE*T*360./2./3.14159
      AI(14,I,J)=WIM(I,J)+(AI(4,I,J)-WIM(I,J))*T/8.64E4
C     AI(14,I,J)=WIM(I,J)
      AI(5,I,J)=UINIT(I,J)+(UINIT(I,J)-UBAR(I,J))*T/8.64E4
C  TO CHANGE TO TRAV WAVE,SWITCH COMMENTS ON AI(14),AI(15)
      IF(AI(15,I,J).GT.360.) AI(15,I,J)=AI(15,I,J)-360.
      IF(AI(14,I,J).GT.360.) AI(14,I,J)=AI(14,I,J)-360.
C
C
C      A(10,I,J)=A(15,I,J)*COS(AI(15,I,J)*CONV)
C      AI(10,I,J)=A(15,I,J)*SIN(AI(15,I,J)*CONV)
C      A(11,I,J)=A(14,I,J)*COS(AI(14,I,J)*CONV)
C      AI(11,I,J)=A(14,I,J)*SIN(AI(14,I,J)*CONV)
C      A(15,I,J)=A(10,I,J)+VR(I,J)
C      AI(15,I,J)=AI(10,I,J)+VI(I,J)
C      A(14,I,J)=A(11,I,J)+WR(I,J)
C      AI(14,I,J)=AI(11,I,J)+WR(I,J)
  100 CONTINUE
C      CALL OUTPUT(1,MI,MJ,ITHETA,DZ,14)
C      CALL OUTPUT(1,MI,MJ,ITHETA,DZ,15)
C
C
      JFLAG=1
      IF(IPRT.EQ.12) JFLAG=0
      IF(JFLAG.EQ.1) GO TO 150
      TDAY=COUNT/24.
      WRITE(6,994) TDAY,COUNT
      WRITE(6,995) TDAY
C     CALL OUTPUT(2,MI,MJ,ITHETA,DZ,15)
C     CALL OUTPUT(2,MI,MJ,ITHETA,DZ,14)
      WRITE(6,990)((A(15,9,J),J=2,44,6))
      WRITE(6,990)((AI(15,9,J),J=2,44,6))
      WRITE(6,990)((A(14,9,J),J=2,44,6))
      WRITE(6,990)((AI(14,9,J),J=2,44,6))
     WRITE(6,990)((AI(5,9,J),J=2,44,6))
  150 CONTINUE
      CALL NOX(MI,MJ,DZ,DTHETA,CONV,AM,DTIME,1,JFLAG)
      DO 200 I=1,MI
      DO 200 J=1,MJ
      A(11,I,J)=VINIT(I,J)+(VBAR(I,J)-VINIT(I,J))*T/8.64E4
      A(14,I,J)=WINIT(I,J)+(WBAR(I,J)-WINIT(I,J))*T/8.64E4
```

```
      IF(A(11,I,J).LT.0.) A(11,I,J)=0.
      IF(A(14,I,J).GT.0.) A(14,I,J)=0.
 200  CONTINUE
      IF(JFLAG.EQ.1) GO TO 250
      WRITE(6,996) TDAY
C     CALL OUTPUT(3,MI,MJ,ITHETA,DZ,11)
C     CALL OUTPUT(3,MI,MJ,ITHETA,DZ,14)
      WRITE(6,990)((A(11,9,J),J=2,44,6))
      WRITE(6,990)((A(14,9,J),J=2,44,6))
 250  CONTINUE
      CALL NOX(MI,MJ,DZ,DTHETA,CONV,AM,DTIME,0,JFLAG)
      COUNT=COUNT+1.
 300  CONTINUE
      DO 350 I=1,MI
      DO 350 J=1,MJ
      UINIT(I,J)=UBAR(I,J)
      VINIT(I,J)=VBAR(I,J)
      WINIT(I,J)=WBAR(I,J)
      VRE(I,J)=AI(1,I,J)
      VIM(I,J)=AI(2,I,J)
      A(13,I,J)=A(13,I,J)/AIR(J)
      WRE(I,J)=AI(3,I,J)
 350  WIM(I,J)=AI(4,I,J)
      WRITE(9,990)((BARNOX(I,J),I=1,MI),J=1,38)
      WRITE(9,990)((A(13,I,J),I=1,MI),J=1,38)
      WRITE(9,990)((AI(13,I,J),I=1,MI),J=1,38)
 90   CONTINUE
C     GO TO 91
 92    CONTINUE
       DO 25 I=1,MI
 25    WRITE(7,990)(QSAVE(I,J),J=1,MJ)
       WRITE(7,990)(BASE(I),I=1,MI)
       WRITE(7,990)(TOP(I),I=1,MI)
       WRITE(7,990)(BETR(J),J=1,MJ)
       WRITE(7,990)((UBAR(I,J),I=1,MI),J=1,MJ)
       WRITE(7,990)((VBAR(I,J),I=1,MI),J=1,MJ)
       WRITE(7,990)((WBAR(I,J),I=1,MI),J=1,MJ)
       WRITE(7,990)((TBAR(I,J),I=1,MI),J=1,MJ)
C      WRITE(8,990)((BARNOX(I,J),I=1,MI),J=1,MJ)
       GO TO 91
       WRITE(8,990)((UBAR(I,J),I=1,MI),J=1,MJ)
       WRITE(8,990)((VBAR(I,J),I=1,MI),J=1,MJ)
       WRITE(8,990)((WBAR(I,J),I=1,MI),J=1,MJ)
       WRITE(8,990)((AI(1,I,J),I=1,MI),J=1,MJ)
       WRITE(8,990)((AI(2,I,J),I=1,MI),J=1,MJ)
       WRITE(8,990)((AI(3,I,J),I=1,MI),J=1,MJ)
       WRITE(8,990)((AI(4,I,J),I=1,MI),J=1,MJ)
       WRITE(8,990)(TBAR(1,J),J=1,MJ)
       WRITE(8,990)(DZZ(1,J),J=1,MJ)
 990   FORMAT(8E15.9)
 994   FORMAT(24H CALCULATIONS AFTER DAY ,F6.2,7H COUNT=,F4.0)
 995   FORMAT(32H PLANETARY WAVE WINDS,UP TO DAY ,F6.2)
```

```
996   FORMAT(28H ZONAL MEAN WINDS,UP TO DAY ,F6.2)
91     CONTINUE
      STOP
      END
      SUBROUTINE INIT(PO,MI,MJ,DZ,DTHETA,CONV,AM,DTIME,BOT)
      COMMON /A/ A(17,17,45),AI(17,17,45),SRE,SIM,COUNT
      COMMON /B/ SNR(17),CNR(17),SNI(17),CNI(17),BDY(17),BDYI(17),
     1BASE(17),TOP(17)
      COMMON /C/ UBAR(17,45),TBAR(17,45),UFLUX(17,45),TFLUX(17,45),
     1 UINIT(17,45),VBAR(17,45),VINIT(17,45),WBAR(17,45),WINIT(17,45)
      COMMON /D/ SS(45),QR(17,45),QI(17,45)
      COMMON /F/ W(10,25),T(25),P(35),G1(35),G2(45),G3(35),
     1G4(35),P1(45),X(20),AN(20)
      COMMON /H/ TIME(17,45),FLUX(17,45),ANC(45),ANCZ(45),BETR(45),
     1TAU(45),SSZ(45),HEAT(17,45),HEATER(17,45)
      COMMON /G/ P3(17),P4(171),BARNOX(17,45),AMPNOX(17,45),
     1PHANOX(17,45),TIMNOX(17,45),TIMAMP(17,45),TIMPHA(17,45),
     1PROMEAN(17,45),PROAMP(17,45),PROPHA(17,45)
     1 ,AIR(45),H(45),DZZ(17.45)
       OMEGA=7.29E-5
       MJ1=MJ+1
       MJ2=MJ+2
       R=2.87E6
       ITHETA=5
       READ(5,989)(SS(J),J=1,MJ)
       READ(5,989)(SSZ(J),J=1,MJ)
       READ(5,989)(AI(3,2,J),J=1,MJ)
       READ(5,989)(ANC(J),J=1,MJ)
       READ(5,989)(ANCZ(J),J=1,MJ)
       DO 630 I=1,MI
630    READ(5,989)(HEAT(I,J),J=1,MJ)
       DO 635 I=1,MI
635    READ(5,989)(HEATER(I,J),J=1,MJ)
       READ(5,995)(DZZ(1,J),J=1,MJ)
995    FORMAT(8F10.5)
       DO 16 I=2,MI
       DO 16 J=1,MJ
16     DZZ(I,J)=DZZ(1,J)
       DO 177 I=1,MI
       DO 177 J=1,MJ
       BARNOX(I,J)=0.
       AMPNOX(I,J)=0.
       PHANOX(I,J)=0.
       PROMEAN(I,J)=0.
       DZZ(I,J)=DZZ(I,J)*2.0E5
 177   A(1,I,J)=DZZ(I,J)
       CALL OUTPUT(3,MI,MJ,ITHETA,DZ,1)
       DO 25 I=1,MI
25     READ(5,990)(QR(I,J),J=1,MJ)
       READ(5,990)(BASE(I),I=1,MI)
       READ(5,990)(TOP(I),I=1,MI)
       READ(5,990)(BETR(J),J=1,MJ)
```

```
C       GO TO 28
        READ(5,990)((UBAR(I,J),I=1,MI),J=1,MJ)
        READ(5,990)((VBAR(I,J),I=1,MI),J=1,MJ)
        READ(5,990)((WBAR(I,J),I=1,MI),J=1,MJ)
        READ(5,990)((TBAR(I,J),I=1,MI),J=1,MJ)
C       GO TO 28
        READ(5,990)((BARNOX(I,J),I=1,MI),J=1,45)
        READ(5,990)((AMPNOX(I,J),I=1,MI),J=1,45)
        READ(5,990)((PHANOX(I,J),I=1,MI),J=1,45)
        READ(5,990)((PROMEAN(I,J),I=1,MI),J=1,38)
        DO 26 I=1,MI
        DO 26 J=39,45
        BARNOX(I,J)=BARNOX(I,38)
        AMPNOX(I,J)=AMPNOX(I,38)
        PHANOX(I,J)=PHANOX(I,38)
 26     PROMEAN(I,J)=PROMEAN(I,38)
 28     CONTINUE
 990     FORMAT(8E15.9)
 991     FORMAT(5F8.2)
        DO 30 J=1,MJ
C      BETR(J)=EXP((J*DZ+BOT)/4.1)/(30.*24.*3600.)
C      ANC(J)=0.
C      ANCZ(J)=0.
C      BETR(J)=1.
 30     TAU(J)=-1.*(.75*SSZ(J)**2/(SS(J)**2)+
       1.5/SS(J)*(SSZ(J)-AI(3,2,J))+.25)
         WRITE(6,990)(BETR(J),J=1,MJ)
C       DO 31 J=19,45
C31     BETR(J)=BETR(18)
        MJM=MJ-1
        DO 640 I=1,MI
        DO 640 J=1,MJ
        A(1,I,J)=AMPNOX(I,J)*COS(PHANOX(I,J)*CONV)
        A(2,I,J)=AMPNOX(I,J)*SIN(PHANOX(I,J)*CONV)
        AMPNOX(I,J)=A(1,I,J)
        PHANOX(I,J)=A(2,I,J)
        TIMNOX(I,J)=0.
C       AMPNOX(I,J)=0.
C       PHANOX(I,J)=0.
        TIMAMP(I,J)=0.
        TIMPHA(I,J)=0.
C       BARNOX(I,J)=(BARNOX(I,32)+BARNOX(I,J))/2.
        PROAMP(I,J)=0.
        PROPHA(I,J)=0.
        A(3,I,J)=HEAT(I,J)
        HEATER(I,J)=HEATER(I,J)/(BETR(J)+1./DTIME)
        A(4,I,J)=HEATER(I,J)
C       IF(COUNT.EQ.1.) GO TO 637
        AI(7,I,J)=PROMEAN(I,J)
        A(6,I,J)=PROAMP(I,J)
        AI(6,I,J)=PROPHA(I,J)
 637    CONTINUE
```

```
      TIME(I,J)=0.
       FLUX(I,J)=0.
       TFLUX(I,J)=0.
 640  UFLUX(I,J)=0.
      CALL TIMEX(MI,MJ,DTHETA,DZ,DTIME)
C     IF(COUNT.NE.1.) GO TO 641
C     CALL ATMEAN(PO,MI,MJ,ITHETA,DZ,DTHETA,AM,DTIME,0,0)
C641  CONTINUE
      GC=1.013E-2/1.38E-23
C     READ(5,990)((BARNOX(I,J),I=1,MI),J=1,38)
      DO 17 J=1,MJ
      AIR(J)=GC*EXP(-BOT-J*DZ)/TBAR(1,J)
 17   H(J)=2.87E6*TBAR(1,J)/981.
      WRITE(6,990)(AIR(J),J=1,MJ)
      WRITE(6,990)(H(J),J=1,MJ)
      DO 650 J=1,MJ
      DO 650 I=1,MI
      AI(3,I,J)=BARNOX(I,J)*AIR(J)
      A(6,I,J)=AMPNOX(I,J)*AIR(J)
      AI(6,I,J)=PHANOX(I,J)*AIR(J)
     A(7,I,J)=QR(I,J)
     A(1,I,J)=TBAR(I,J)
     A(2,I.J)=UBAR(I,J)
     A(11,I,J)=VBAR(I,J)
     A(15,I,J)=WBAR(I,J)*7.0E5
 650  A(5,I,J)=TIME(I,J)
C     READ(5,990)((BARNOX(I,J),I=1,MI),J=1,MJ)
C      WRITE(6,990)((A(11,I,J),I=1,MI),J=1,MJ)
C      WRITE(6,990)((A(15,I,J),I=1,MI),J=1,MJ)
C    WRITE(6,990)(AI(3,I,MJ),I=1,MI)
C    WRITE(6,990)(A(1,1,J),J=1,MJ)
C    WRITE(6,990)((BARNOX(I,J),I=1,MI),J=1,MJ)
C    GO TO 999
C     CALL OUTPUT(3,MI,MJ,ITHETA,DZ,3)
C     CALL OUTPUT(3,MI,MJ,ITHETA,DZ,4)
C     CALL OUTPUT(3,MI,MJ,ITHETA,DZ,5)
      WRITE(6,998)
 998  FORMAT(24H INITIAL NO DISTRIBUTION)
      CALL OUTPUT(4,MI,MJ,ITHETA,DZ,3)
      CALL OUTPUT(0,MI,MJ,ITHETA,DZ,6)
      WRITE(6,992)
 992  FORMAT(26H PRODUCTION AND LOSS TERMS)
      CALL OUTPUT(4,MI,MJ,ITHETA,DZ,7)
C     CALL OUTPUT(0,MI,MJ,ITHETA,DZ,6)
     TI=(COUNT-1.)/24.
     WRITE(6,993) COUNT,TI
 993 FORMAT(23H INITIAL STATE,COUNT = ,F6.2,7H DAY = ,F6.2)
      CALL OUTPUT(3,MI,MJ,ITHETA,DZ,7)
      CALL OUTPUT(3,MI,MJ,ITHETA,DZ,1)
      CALL OUTPUT(3,MI,MJ,ITHETA,DZ,2)
      CALL OUTPUT(3,MI,MJ,ITHETA,DZ,11)
      CALL OUTPUT(3,MI,MJ,ITHETA,DZ,15)
```

```
 660   CONTINUE
C      WRITE(6,989)(BETR(J),J=1,MJ)
C      WRITE(6,989)(TAU(J),J=1,MJ)
 989   FORMAT(9E13.6)
C      DO 410 I=1,MI
C410   WRITE(6,990)(QR(I,J),J=1,MJ)
C      WRITE(6,990)(BASE(I),I=1,MI)
C      WRITE(6,990)(TOP(I),I=1,MI)
C      DO 411 I=1,MI
C411   WRITE(6,990)(BARNOX(I,J),J=1,MJ)
C      DO 412 I=1,MI
C412   WRITE(6,990)(AMPNOX(I,J),J=1,MJ)
C      DO 413 I=1,MI
C413   WRITE(6,990)(PHANOX(I,J),J=1,MJ)
C      WRITE(6,989)(SS(J),J=1,MJ)
C      WRITE(6,989)(SSZ(J),J=1,MJ)
C      WRITE(6,989)(AI(3,2,J),J=1,MJ)
C      WRITE(6,989)(ANC(J),J=1,MJ)
C      WRITE(6,989)(ANCZ(J),J=1,MJ)
C      WRITE(6,989)(BDY(I),I=1,MI)
C      WRITE(6,989)(BDYI(I),I=1,MI)
C      DO 4 I=1,MI
C430   WRITE(6,989)(HEAT(I,J),J=1,MJ2)
 999     CONTINUE
         RETURN
        END
       SUBROUTINE BASIC(MI,MJ,DZ,DTHETA,CONV,AM,DTIME,BOT)
       COMMON /A/ A(17,17,45),AI(17,17,45),SRE,SIM
       COMMON /C/ UBAR(17,45),TBAR(17,45),OBAR(17,45),ODER(17,45)
       COMMON /D/ SS(45),QR(17,45),QI(17,45)
       COMMON /E/ QR1(17,45),QR2(17,45),QI1(17,45),QI2(17,45)
       COMMON /F/ P(45),P1(45),G1(45),G2(45),G3(45),G4(45),T1(35),T2(35),
      1W(10,30)
       COMMON /H/ TIME(17,45),FLUX(17,45),ANC(45),ANCZ(45),BETR(45),
      1TAU(45),SSZ(45),HEAT(17,45),HEATER(17,45)
       COMPLEX Q1,Q2,Q3,Q4,Q5,Q6,Q7,Q,CMPLX
       OMEGA=7.292E-5
       KOUNT=10
       L=23
       DO 50 J=1,L
 50    P(J)=BOT+(J-1)*.5+DZ
       DO 55 J=1,L
       W(1,J)=0.
       W(10,J)=0.
       DO 55 I=2,9
       JJ=2*J-1
       II=2*I-2
 55    W(I,J)=UBAR(II,JJ)/(6.37E8*COS(CONV*(I-1)*10.))
C      DO 57 I=1,10
C      DO 57 J=14,16
C57    W(I,J)=0.
       DO 61 J=1,MJ
```

```
61    P1(J)=DZ*(J-1)+BOT+DZ
      DO 67 KK=1,KOUNT
      DO 62 J=1,L
62    G1(J)=W(KK,J)
      CALL INTER(G2,P1,MJ,G1,P,L)
      DO 63 J=1,MJ
63    A(2,KK,J)=G2(J)
      CALL DIFF(G4,G3,L,G1,P)
      CALL INTER(G2,P1,MJ,G4,G3,L)
      DO 64 J=1,MJ
64    A(3,KK,J)=G2(J)
      CALL DIFF(G1,G2,L,G4,G3)
      CALL INTER(G4,P1,MJ,G1,G2,L)
      DO 65 J=1,MJ
65    A(4,KK,J)=G4(J)
67    CONTINUE
      DO 69 I=1,KOUNT
69    P(I)=(I-1)*10.*CONV
      DO 70 I=1,MI
70    P1(I)=I*DTHETA
      DO 79 J=1,MJ
      DO 71 I=1,KOUNT
71    G1(I)=A(2,I,J)
      CALL INTER(G2,P1,MI,G1,P,KOUNT)
      DO 72 I=1,MI
72    A(2,I,J)=G2(I)
      CALL DIFF(G4,G3,KOUNT,G1,P)
      CALL INTER(G2,P1,MI,G4,G3,KOUNT)
      DO 73 I=1,MI
73    A(5,I,J)=G2(I)
      CALL DIFF(G1,G2,KOUNT,G4,G3)
      CALL INTER(G4,P1,MI,G1,G2,KOUNT)
      DO 74 I=1,MI
74    A(6,I,J)=G4(I)
      DO 79 LL=3,4
      DO 76 JJ=1,KOUNT
76    G1(JJ)=A(LL,JJ,J)
      CALL INTER(G2,P1,MI,G1,P,KOUNT)
      DO 77 JJ=1,MI
77    A(LL,JJ,J)=G2(JJ)
79    CONTINUE
C     STORE OBAR,ODER FOR USE IN ATWAVE
        DO 80 I=1,MI
        DO 80 J=1,MJ
        ODER(I,J)=A(3,I,J)
80      OBAR(I,J)=A(2,I,J)
C          GO TO 500
       DO 32 J=1,MJ
         BR=EXP((J*DZ+BOT)/4.1)/(30.*24.*3600.)
         IG=0
         IT=0
         NR1=MI-1
```

```
      DO 25 K=1,NR1
        BR1=A(2,K,J)*AM
        BR2=A(2,K+1,J)*AM
        IF (BR1.LE.0.AND.BR2.GE.0.) IT=K
25      IF (BR1.GE.0.AND.BR2.LE.0.) IG=K
      MT=IT+3
      MT2=IG-4
      ML=IT-3
      ML2=IG+3
      IF (MT.GT.MI) GO TO 26
      AP2=AM*A(2,MT,J)/3.
      GO TO 27
26    AP2=AM*A(2,ML,J)/3.
27    IF (MT2.LT.1) GO TO 28
      AP3=AM*A(2,MT2,J)/3.
      GO TO 29
28    AP3=AM*A(2,ML2,J)/3.
29    DO 31 K=1,MI
        T2(K)=0.
        T1(K)=0.
        IF (K.GE.ML.AND.K.LE.MT) T1(K)=AP2*EXP(-(K-IT)**2/8.)
        IF (IG.EQ.0) GO TO 30
        IF (K.GE.MT2.AND.K.LE.ML2) T2(K)=AP3*EXP(-(K-IG)**2/8.)
30      T1(K)=T1(K)+T2(K)
31      IF (T1(K).LT.BR) T1(K)=BR
      DO 32 I=1,MI
      AI(17,I,J)=T1(I)
32    AI(1,I,J)=T1(I)
500    CONTINUE
    DO 33 J=1,MJ
      DO 33 I=1,MI
C       CHANGE THIS FOR CRITICAL LEVELS
        Q3=(0.,1.)
        X=AM*A(2,I,J)+SRE
        Y=ANC(J)-SIM
        Z=AI(1,I,J)-SIM
      Q1=(X-Q3*Y)/(X-Q3*Z)
        Q2=-1.*Q3*ANCZ(J)/(X-Q3*Z)
        QR1(I,J)=REAL(Q1)
        QI1(I,J)=AIMAG(Q1)
        QR2(I,J)=REAL(Q2)
        QI2(I,J)=AIMAG(Q2)
        D=2.*(OMEGA+A(2,I,J))
        B=3.*TAN(I*DTHETA)*A(5,I,J)
        C=((SIN(I*DTHETA)**2)/SS(J))*(A(3,I,J)-A(4,I,J))
       F=((SIN(I*DTHETA)**2)/(SS(J)**2)*SSZ(J)*A(3,I,J))
        A(7,I,J)=D-A(6,I,J)+B+C+F
        IF (A(7,I,J).LE.0.) A(7,I,J)=1.E-7
        AI(7,I,J)=D-A(6,I,J)+B
        Q1=CMPLX(X,-Z)
        Q2=CMPLX(X,-Y)
        Q8=0.5+0.5*SSZ(J)/SS(J)
```

```
      Q4=AM*A(7,I,J)/Q1
      Q5=AM**2/COS(I*DTHETA)**2
      Q6=(SIN(I*DTHETA)**2*TAU(J)*Q2)/(Q1*SS(J))
      Q7=(Q3*SIN(I*DTHETA)**2*ANCZ(J)*Q8)/(SS(J)*Q1)
      Q=Q4-Q5+Q6-Q7
      A(8,I,J)=REAL(Q)
      AI(8,I,J)=AIMAG(Q)
      QR(I,J)=A(8,I,J)
 33   QI(I,J)=AI(8,I,J)
      RETURN
      END
      SUBROUTINE SOLWAVE(PO,MI,MJ,DZ,DTHETA,CONV,AM,BOT)
      COMMON /A/ A(17,17,45),AI(17,17,45)
      COMMON /B/ SNR(17),CNR(17),SNI(17),CNI(17),BDY(17),BDYI(17),
     1BASE(17),TOP(17)
      COMMON /D/ S(45),QR(17,45),QI(17,45)
      COMMON /E/ QR1(17,45),QR2(17,45),QI1(17,45),QI2(17,45)
      COMMON /F/ W1(17,17),G1(17),W2(17,17),G2(17),W3(17,17),W4(17,17),W
     15(17,17),G3(17),G4(17),W6(17,17),G5(17)
      COMMON /H/ TIME(17,45),FLUX(17,45),ANC(45),ANCZ(45),BETR(45),
     1TAU(45),SSZ(45),HEAT(17,45),HEATER(17,45)
      ITHETA=5
C          DO 34 KK=2,6
C34        CALL OUTPUT(3,MI,MJ,ITHETA,DZ,2)
C          CALL OUTPUT(4,MI,MJ,ITHETA,DZ,1)
      DO 1 I=1,MI
         DO 1 J=1,MJ
        DO 1 K=1,MI
        A(K,I,J)=0.
   1   AI(K,I,J)=0.
      DO 3 I=1,MI
        G1(I)=0.
        G2(I)=0.
        G3(I)=0.
        G4(I)=0.
        DO 3 J=1,MI
        W1(I,J)=0.
        W2(I,J)=0.
        W4(I,J)=0.
        W3(I,J)=0.
        W5(I,J)=0.
    3   W6(I,J)=0.
C        WRITE(6,901)(QR1(I,1),I=1,MI)
C        WRITE(6,901)(QI1(I,1),I=1,MI)
C        WRITE(6,901)(QR2(I,1),I=1,MI)
C        WRITE(6,901)(QI2(I,1),I=1,MI)
      DO 6 J=1,MI
        JJ=ITHETA*J
        P=SIN(CONV*JJ)
        Q=COS(CONV*JJ)
        G11=-1.0*(1.0+Q*Q)/(P**3*2.*Q*DTHETA)
        A1=1./(DTHETA*DTHETA*P*P)
```

```
      B1=1./(P*P)
      DO 6 K=1,MJ
      IF (J.EQ.MI) GO TO 4
      A(J,J+1,K)=(A1+G11)*S(K)*DZ*DZ
    4 IF (J.EQ.1) GO TO 5
      A(J,J-1,K)=(A1-G11)*S(K)*DZ*DZ
    5 AI(J,J,K)=QI(J,K)*B1*S(K)*DZ*DZ-2.*QI1(J,K)
      A(J,J,K)=(QR(J,K)*B1-2.*A1)*S(K)*DZ*DZ-2.*QR1(J,K)
      FA=QR1(J,K)
      FB=QI1(J,K)
      EA=QR2(J,K)*DZ/2.
      EB=QI2(J,K)*DZ/2.
      QR1(J,K)=FA+EA
      QI1(J,K)=FB+EB
      QR2(J,K)=FA-EA
      QI2(J,K)=FB-EB
    6  CONTINUE
C     WRITE(6,901)(QR1(I,1),I=1,MI)
C     WRITE(6,901)(QI1(I,1),I=1,MI)
C     WRITE(6,901)(QR2(I,1),I=1,MI)
C     WRITE(6,901)(QI2(I,1),I=1,MI)
      DO 7 J=1,MI
     G2(J)=BDY(J)
  7  G4(J)=BDYI(J)
C     WRITE(6,901)(G2(J),J=1,MI)
C     WRITE(6,901)(G4(J),J=1,MI)
      DO 12 K=1,MJ
     CALL CPY (K,1,MI)
      DO 8 I=1,MI
     DO 8 J=1,MI
     W5(I,J)=W2(I,J)
     W6(I,J)=W4(I,J)
      W2(I,J)=-1.0*(W1(I,J)+QR2(I,K)*W5(I,J)-QI2(I,K)*W6(I,J))
    8 W4(I,J)=-1.0*(W3(I,J)+QR2(I,K)*W6(I,J)+QI2(I,K)*W5(I,J))
C     IF(K.GE.2) GO TO 50
C     DO 47 I=1,MI
C47  WRITE(6,901)(W2(I,J),J=1,MI)
C     DO 48 I=1,MI
C48   WRITE(6,901)(W4(I,J),J=1,MI)
901    FORMAT(10E10.3)
 50   CALL CINV (MI,W2,W4)
C      IF(K.GE.2) GO TO 55
C     DO 51 I=1,MI
C51   WRITE(6,901)(W2(I,J),J=1,MI)
C     DO 52 I=1,MI
C52   WRITE(6,901)(W4(I,J),J=1,MI)
C55   CONTINUE
      DO 9 J=1,MI
        AAA=G4(J)
        BBB=G2(J)
          G4(J)=QI2(J,K)*BBB+QR2(J,K)*AAA
          G2(J)=QR2(J,K)*BBB-QI2(J,K)*AAA
```

```
    9      CONTINUE
C         IF(K.GE.2) GO TO 60
C         WRITE(6,901)(G2(J),J=1,MI)
C         WRITE(6,901)(G4(J),J=1,MI)
C60       CONTINUE
          DO 65 J=1,MI
            G3(J)=0.
            G1(J)=0.
            DO 10 I=1,MI
            AAA=W4(J,I)
            BBB=W2(J,I)
            G3(J)=G3(J)+W4(J,I)*G2(I)+W2(J,I)*G4(I)
            G1(J)=G1(J)+W2(J,I)*G2(I)-W4(J,I)*G4(I)
            W4(J,I)=QR1(I,K)*AAA+QI1(I,K)*BBB
   10       W2(J,I)=QR1(I,K)*BBB-QI1(I,K)*AAA
C         IF(K.GE.2) GO TO 65
C         WRITE(6,901) G1(J),G3(J)
 65       CONTINUE
          DO 11 J=1,MI
            G4(J)=G3(J)
   11       G2(J)=G1(J)
          CALL CPY (K,2,MI)
   12     CONTINUE
             DO 14 I=1,MI
            G2(I)=0.
  14        G4(I)=0.
C         WRITE(6,1000) (G2(I),I=1,MI)
C        WRITE(6,1000) (G4(I),I=1,MI)
         CALL CPY (MJ,2,MI)
         DO 24 KK=2,MJ
           K=MJ-KK+1
           CALL CPY (K,1,MI)
           DO 22 J=1,MI
             DO 22 JK=1,MI
             G1(J)=G1(J)+W1(J,JK)*G2(JK)-W3(J,JK)*G4(JK)
   22        G3(J)=G3(J)+W1(J,JK)*G4(JK)+W3(J,JK)*G2(JK)
           DO 23 J=1,MI
             G2(J)=G1(J)
   23        G4(J)=G3(J)
           CALL CPY (K,2,MI)
   24     CONTINUE
1000      FORMAT(1X,4(1X,E13.6))
70         CONTINUE
          RETURN
          END
        SUBROUTINE ATWAVE(MI,MJ,DTHETA,DZ,CONV,AM,BOT,JFLAG)
        COMMON /A/ A(17,17,45),AI(17,17,45),SRE,SIM,COUNT
       1 ,VRE(17,45),VIM(17,45),WRE(17,45),WIM(17,45)
        COMMON /B/ SNR(17),CNR(17),SNI(17),CNI(17),BDY(17),
       1BDYI(17),BASE(17),TOP(17)
         COMMON /C/ UBAR(17,45),TBAR(17,45),OBAR(17,45),ODER(17,45)
        COMMON /D/ S(45),QR(17,45),QI(17,45)
```

```
      COMMON /H/ TIME(17,45),FLUX(17,45),ANC(45),ANCZ(45),BETR(45),
     1TAU(45),SSZ(45),HEAT(17,45),HEATER(17,45)
      DT=DTHETA
       AO=6.37E8
      G=981.
      MJM=MJ-1
      MIM=MI-1
      R=2.87E6
      DO 1 J=1,MJ
       DO 1 I=1,MI
      A(8,I,J)=QR(I,J)
      AI(8,I,J)=QI(I,J)
      QR(I,J)=G*EXP((J*DZ+BOT)/2.)*QR(I,J)*SQRT(S(J))
      QI(I,J)=G*EXP((J*DZ+BOT)/2.)*QI(I,J)*SQRT(S(J))
      A(7,I,J)=QR(I,J)
 1    AI(7,I,J)=QI(I,J)
      DO 12 J=1,MJ
      A(10,1,J)=QR(2,J)/DT/2.
      AI(10,1,J)=QI(2,J)/DT/2.
       A(10,MI,J)=-QR(MIM,J)/DT/2.
      AI(10,MI,J)=-QI(MIM,J)/DT/2.
      DO 12 I=2,MIM
      A(10,I,J)=(QR(I+1,J)-QR(I-1,J))/DT/2.
12    AI(10,I,J)=(QI(I+1,J)-QI(I-1,J))/DT/2.
      DO 13 I=1,MI
      A(11,I,1)=(QR(I,2)-BDY(I)*G*EXP(BOT/2.)*SQRT(.0193))/DZ/2.
      AI(11,I,1)=(QI(I,2)-BDYI(I)*G*EXP(BOT/2.)*SQRT(.0193))/DZ/2.
      A(11,I,MJ)=-1.*QR(I,MJM)/DZ/2.
C     BDY(I)=BDY(I)*1.1
C     BDYI(I)=BDYI(I)*1.1
       AI(11,I,MJ)=-1.*QI(I,MJM)/DZ/2.
      DO 13 J=2,MJM
      A(11,I,J)=(QR(I,J+1)-QR(I,J-1))/DZ/2.
 13   AI(11,I,J)=(QI(I,J+1)-QI(I,J-1))/DZ/2.
      DO 14 I=1,MI
       F=1.458E-4*SIN(I*DTHETA)
       P=COS(I*DTHETA)
      DO 14 J=1,MJ
      A(12,I,J)=A(11,I,J)/R
      AI(12,I,J)=AI(11,I,J)/R
      A(13,I,J)=A(10,I,J)/(-1.*AO*F)
      AI(13,I,J)=AI(10,I,J)/(-1.*AO*F)
      A(15,I,J)=-AM*QI(I,J)/(AO*COS(I*DTHETA)*F)
      AI(15,I,J)=AM*QR(I,J)/(AO*COS(I*DTHETA)*F)
C     A(16,I,J)=A(15,I,J)-AM*OBAR(I,J)*AI(13,I,J)/F
C     AI(16,I,J)=AI(15,I,J)+AM*OBAR(I,J)*A(13,I,J)/F
C     A(16,I,J)=A(13,I,J)+(OBAR(I,J)*AI(15,I,J)-BETR(J)*A(15,I,J))/F
C     AI(16,I,J)=AI(13,I,J)-(OBAR(I,J)*A(15,I,J)+
C    1BETR(J)*AI(15,I,J))/F
       A(14,I,J)=((AM*OBAR(I,J)+SRE)*AI(11,I,J)+F*AO*P*A(15,I,J)
     1 *ODER(I,J)-(ANC(J)-SIM)*A(11,I,J))/(1.458E-4*AO)**2./S(J)
       AI(14,I,J)=((-AM*OBAR(I,J)-SRE)*A(11,I,J)+F*AO*P*AI(15,I,J)
```

```
     1 *ODER(I,J)-(ANC(J)-SIM)*AI(11,I,J))/(1.458E-4*AO)**2./S(J)
 14      CONTINUE
C       GO TO 45
        DO 20 J=1,MJ
        A(3,1,J)=A(15,2,J)/2./DT
        AI(3,1,J)=AI(15,2,J)/2./DT
        A(3,MI,J)=-A(15,MIM,J)/2./DT
        AI(3,MI,J)=-AI(15,MIM,J)/2./DT
        DO 20 I=2,MIM
        A(3,I,J)=(A(15,I+1,J)-A(15,I-1,J))/2./DT
 20     AI(3,I,J)=(AI(15,I+1,J)-AI(15,I-1,J))/2./DT
        DO 30 I=1,MI
        A(5,I,1)=(A(14,I,2)-A(14,I,1))/2./DZ
        AI(5,I,1)=(AI(14,I,2)-AI(14,I,1))/2./DZ
        A(5,I,MJ)=(A(14,I,MJ)-A(14,I,MJM))/2./DZ
        AI(5,I,MJ)=(AI(14,I,MJ)-AI(14,I,MJM))/2./DZ
        DO 30 J=2,MJM
        A(5,I,J)=(A(14,I,J+1)-A(14,I,J-1))/2./DZ
30      AI(5,I,J)=(AI(14,I,J+1)-AI(14,I,J-1))/2./DZ
C       DO 31 I=1,MI
C       A(4,I,J)=(QR(I,2)-2.*QR(I,1))/DZ/DZ
C       AI(4,I,1)=(QI(I,2)-2.*QI(I,1))/DZ/DZ
C       A(4,I,MJ)=(-2.*QR(I,MJ)+QR(I,MJM))/DZ/DZ
C       AI(4,I,J)=(-2.*QI(I,MJ)+QI(I,MJM))/DZ/DZ
C       DO 31 J=2,MJM
C       A(4,I,J)=(QR(I,J+1)-2.*QR(I,J)+QR(I,J-1))/DZ/DZ
C31     AI(4,I,J)=(QI(I,J+1)-2.*QI(I,J)+QI(I,J-1))/DZ/DZ
C       DO 32 I=1,MI
C       DO 32 J=1,MJ
C       A(5,I,J)=-SSZ(J)/S(J)*A(14,I,J)+(-AM*QI(I,J)*TIMPHA(I,J)-
C     1 ANCZ(J)*A(11,I,J)-ANC(J)*A(4,I,J)+AM*OBAR(I,J)*AI(4,I,J))
C     1 /(1.458E-4*AO)**2./S(J)
C       AI(5,I,J)=-SSZ(J)/S(J)*AI(14,I,J)+(AM*QR(I,J)*TIMPHA(I,J)-
C     1 ANCZ(J)*AI(11,I,J)-ANC(J)*AI(4,I,J)
C     1 -AM*OBAR(I,J)*A(4,I,J))/(1.458E-4*AO)**2./S(J)
C IN THE ABOVE CALCULATION,TIMPHA IS THE SECOND DERIVATIVE
C  WITH RESPECT TO Z OF OMEGABAR
C       A(6,I,J)=A(14,I,J)-A(5,I,J)
C32     AI(6,I,J)=AI(14,I,J)-AI(5,I,J)
        FAC=AM/1.458E-4/AO/AO
        DO 40 I=1,MI
        P=COS(I*DTHETA)
        Q=SIN(I*DTHETA)
        DO 40 J=1,MJ
        A(4,I,J)=A(15,I,J)*Q/P/AO-A(3,I,J)/AO
        AI(4,I,J)=AI(15,I,J)*Q/P/AO-AI(3,I,J)/AO
        A(6,I,J)=A(14,I,J)-A(5,I,J)
        AI(6,I,J)=AI(14,I,J)-AI(5,I,J)
C       A(1,I,J)=FAC*QR(I,J)/Q/Q
C       AI(1,I,J)=FAC*QI(I,J)/Q/Q
C       A(2,I,J)=-FAC*A(10,I,J)/P/Q
C       AI(2,I,J)=-FAC*AI(10,I,J)/P/Q
```

```
C       A(3,I,J)=A(1,I,J)+A(2,I,J)
C       AI(3,I,J)=AI(1,I,J)+AI(2,I,J)
        A(17,I,J)=(AI(4,I,J)+AI(6,I,J))*AO*COS(I*DT)/AM
 40     AI(17,I,J)=-(A(4,I,J)+A(6,I,J))*AO*COS(I*DT)/AM
 45     CONTINUE
C       WRITE(6,902)
C       CALL OUTPUT(1,MI,MJ,ITHETA,DZ,8)
        WRITE(6,903)
       CALL OUTPUT(JFLAG,MI,MJ,ITHETA,DZ,7)
C      WRITE(6,904)
       CALL OUTPUT(1,MI,MJ,ITHETA,DZ,12)
C      WRITE(6,905)
       CALL OUTPUT(1,MI,MJ,ITHETA,DZ,13)
C       DO 50 KK=3,6
C50     CALL OUTPUT(2,MI,MJ,ITHETA,DZ,K...
C      CALL OUTPUT(JFLAG,MI,MJ,ITHETA,DZ,17)
 990      FORMAT(8E15.9)
       WRITE(6,906)
       CALL OUTPUT(JFLAG,MI,MJ,ITHETA,DZ,15)
C      CALL OUTPUT(JFLAG,MI,MJ,ITHETA,DZ,16)
C      WRITE(6,908)(A(14,1,1),I=1,MI)
C      WRITE(6,908)(AI(14,I,1),I=1,MI)
 908   FORMAT(9E13.6)
        WRITE(6,907)
        CALL OUTPUT(JFLAG,MI,MJ,ITHETA,DZ,14)
C      CALL OUTPUT(2,MI,MJ,ITHETA,DZ,10)
C      CALL OUTPUT(2,MI,MJ,ITHETA,DZ,11)
       DO 100 I=1,MI
       DO 100 J=1,MJ
       AI(1,I,J)=A(15,I,J)
       AI(2,I,J)=AI(15,I,J)
       AI(3,I,J)=A(14,I,J)
 100   AI(4,I,J)=AI(14,I,J)
 902   FORMAT(6H1  PSI)
 903   FORMAT(16H  GEOPOTENTIAL  )
 904   FORMAT(19H1 TEMPERATURE DEG K)
 905   FORMAT(22H1  EASTWARD VELOCITY U)
 906   FORMAT(26H1   NORTHWARD VELOCITY   V)
 907     FORMAT(23H VERTICAL VELOCITY,ZDOT)
       RETURN
       END
       SUBROUTINE FLUXX(MI,MJ,DTHETA,DZ,CONV,DTIME)
       COMMON /A/ A(17,17,45),AI(17,17,45),SRE,SIM,COUNT,IDAY,ID
       COMMON /C/ UBAR(17,45),TBAR(17,45),UFLUX(17,45),TFLUX(17,45),
      1 UINIT(17,45),VBAR(17,45),VINIT(17,45),WBAR(17,45),WINIT(17,45)
       COMMON /D/ S(45),QR(17,45),QI(17,45)
       COMMON /H/ TIME(17,45),FLUX(17,45),ANC(45),ANCZ(45),BETR(45),
      1TAU(45),SSZ(45),HEAT(17,45),HEATER(17,45)
       DT=DTHETA
       IF(ID.NE.IDAY)  GO TO 100
C      WRITE(9,990)((A(7,I,J),I=1,MI),J=1,MJ)
C      WRITE(9,990)((AI(7,I,J),I=1,MI),J=1,MJ)
```

```
100  CONTINUE
         G=981.
      OMEGA=7.292E-5
         R=2.87E6
      MIM=MI-1
      F=1.458E-4
      MJM=MJ-1
      AO=6.37E8
      DO 1 I=1,MI
      P=COS(I*DTHETA)
      DO 1 J=1,MJ
      A(1,I,J)=A(13,I,J)*A(15,I,J)*COS(CONV*(AI(13,I,J)-AI(15,I,J)))/2.
1     A(4,I,J)=A(15,I,J)*A(12,I,J)*R*COS(CONV*
     1(AI(15,I,J)-AI(12,I,J)))/2.
      DO 2 J=1,MJ
      A(2,1,J)=A(1,2,J)/2./DT
      A(2,MI,J)=-A(1,MIM,J)/2./DT
      A(3,1,J)=(A(1,2,J)-2.*A(1,1,J))/DT/DT
901       FORMAT(10E10.3)
      A(3,MI,J)=(A(1,MIM,J)-2.*A(1,MI,J))/DT/DT
      A(5,1,J)=A(4,2,J)/2./DT
      A(5,MI,J)=-A(4,MIM,J)/2./DT
      DO 2 I=2,MIM
      A(2,I,J)=(A(1,I+1,J)-A(1,I-1,J))/2./DT
      A(3,I,J)=(A(1,I+1,J)-2.*A(1,I,J)+A(1,I-1,J))/DT/DT
2     A(5,I,J)=(A(4,I+1,J)-A(4,I-1,J))/2./DT
      DO 7 I=1,MI
      DO 7 J=1,MJ
 7    A(5,I,J)=COS(I*DT)*A(5,I,J)-SIN(I*DT)*A(4,I,J)
      DO 3 I=1,MI
      A(6,I,1)=0.
      A(6,I,MJ)=0.
      DO 3 J=2,MJM
3     A(6,I,J)=(A(5,I,J+1)-A(5,I,J-1))/2./DZ
      DO 4 I=1,MI
      P=COS(I*DTHETA)
      Q=SIN(I*DTHETA)
      DO 4 J=1,MJ
      A(7,I,J)=A(3,I,J)/Q-(1.+2.*Q*Q)*A(2,I,J)/(P*Q*Q)
      A(7,I,J)=F*A(7,I,J)*S(J)/(BETR(J)+1/DTIME)
C  DTIME SHOULD BE INCLUDED HERE
      A(8,I,J)=(A(6,I,J)-(1.+SSZ(J)/S(J))*A(5,I,J))
      A(8,I,J)=A(8,I,J)/(AO*P*(BETR(J)+1/DTIME))
C INCLUDE TIME TERM IN FLUX CALCULATION
      A(9,I,J)=A(7,I,J)-A(8,I,J)
      FLUX(I,J)=A(9,I,J)
C     FLUX(I,J)=0.
 4    CONTINUE
C     CALL OUTPUT(3,MI,MJ,ITHETA,DZ,1)
C     CALL OUTPUT(3,MI,MJ,ITHETA,DZ,4)
C         WRITE(6,902)
C       DO 10 KK=7,9
```

```
C10         CALL OUTPUT(3,MI,MJ,ITHETA,DZ,9)
C         DO 6 J=70,MJ
C          WRITE(6,901)(A(7,I,J),I=1,MI)
C          WRITE(6,901)(A(8,I,J),I=1,MI)
C6         WRITE(6,901)(A(9,I,J),I=1,MI)
           DO 5 I=1,MI
           P=COS(I*DTHETA)
           Q=SIN(I*DTHETA)
           DO 5 J=1,MJ
           UFLUX(I,J)=A(2,I,J)/AO-2.*Q*A(1,I,J)/AO/P
           A(7,I,J)=(A(2,I,J)/AO-2.*Q*A(1,I,J)/AO/P)/F/Q
           A(8,I,J)=-A(5,I,J)/R/P/AO/ANC(J)
           A(9,I,J)=-1.*(A(2,I,J)/AO-2.*Q*A(1,I,J)/AO/P)
           TFLUX(I,J)=A(5,I,J)/AO/P
5          A(10,I,J)=-A(5,I,J)/R/P/AO*86400.
           IF(ID.NE.IDAY) GO TO 30
C          WRITE(6,905)
C          CALL OUTPUT(3,MI,MJ,ITHETA,DZ,9)
 905       FORMAT(36H CONVERGENCE OF EDDY FLUX,CM/SEC/DAY)
C          WRITE(6,903)
C          CALL OUTPUT(3,MI,MJ,ITHETA,DZ,7)
C          WRITE(6,906)
C906       FORMAT(43H CONVERGENCE OF NORTHWARD HEAT FLUX,DEG/DAY)
C          CALL OUTPUT(3,MI,MJ,ITHETA,DZ,10)
C         WRITE(6,904)
C          CALL OUTPUT(3,MI,MJ,ITHETA,DZ,8)
C          WRITE(6,907)
C907       FORMAT(15H EDDY HEAT FLUX)
C          CALL OUTPUT(3,MI,MJ,ITHETA,DZ,4)
902         FORMAT(11H FLUX TERMS)
903         FORMAT(20H VBAR DUE TO FLUXXES)
 904        FORMAT(19H TEMP DUE TO FLUXES)
          GO TO 30
          FAC=F*F*AO*AO
          DO 15 I=1,MI
          A(13,I,1)=(A(4,I,2)-A(4,I,1))/DZ
          A(13,I,MJ)=(A(4,I,MJ)-A(4,I,MJM))/DZ
          DO 15 J=2,MJM
 15       A(13,I,J)=(A(4,I,J+1)-A(4,I,J-1))/2./DZ
          DO 20 I=1,MI
          Q=SIN(I*DTHETA)
          P=COS(I*DTHETA)
          DO 20 J=1,MJ
          A(10,I,J)=A(5,I,J)/FAC/AO/P/S(J)
          A(11,I,J)=WBAR(I,J)
          A(12,I,J)=WBAR(I,J)+A(10,I,J)
          A(14,I,J)=(A(4,I,J)*(1.+SSZ(J)/S(J))-A(13,I,J))/FAC/S(J)
          A(15,I,J)=VBAR(I,J)
          A(16,I,J)=VBAR(I,J)+A(14,I,J)
          AI(17,I,J)=-2.*OMEGA*Q*A(14,I,J)
 20       A(17,I,J)=-2.*OMEGA*Q*A(14,I,J)-A(2,I,J)/AO+2.*A(1,I,J)*Q/AO/P
          DO 25 KK=10,17
```

```
25      CALL OUTPUT(3,MI,MJ,ITHETA,DZ,KK)
990    FORMAT(8E15.9)
       GO TO 30
       WRITE(9,990)((A(10,I,J),I=1,MI),J=1,MJ)
       WRITE(9,990)((A(12,I,J),I=1,MI),J=1,MJ)
       WRITE(9,990)((A(14,I,J),I=1,MI),J=1,MJ)
       WRITE(9,990)((A(16,I,J),I=1,MI),J=1,MJ)
       WRITE(9,990)((A(9,I,J),I=1,MI),J=1,MJ)
       WRITE(9,990)((AI(17,I,J),I=1,MI),J=1,MJ)
       WRITE(9,990)((A(17,I,J),I=1,MI),J=1,MJ)
30     CONTINUE
       RETURN
       END
       SUBROUTINE SOLMEAN(MI,MJ,DZ,DTHETA,DTIME)
       COMMON /A/ A(17,17,45),AI(17,17,45)
       COMMON /B/ SNR(17),CNR(17),SNI(17),CNI(17),BDY(17),
      1BDYI(17),BASE(17),TOP(17)
       COMMON /D/ S(45),QR(17,45),QI(17,45)
       COMMON /F/ W1(17,17),W2(17,17),W3(17,17),W4(17,17),W5(17,17),
      1W6(17,17),G1(17),G2(17),G3(17),G4(17),G5(17)
         COMMON /G/ P3(17),P4(171)
       COMMON /H/ TIME(17,45),FLUX(17,45),ANC(45),ANCZ(45),BETR(45),
      1TAU(45),SSZ(45),HEAT(17,45),HEATER(17,45)
       MJM=MJ-1
       MIM=MI-1
       MJ1=MJ+1
       MJ2=MJ+2
          G=981.
          ITHETA=5
          T=240.
          ZTOP=18.25
          R=2.87E6
          DO 3 I=1,MI
          G3(I)=0.
          DO 3 K=1,MI
          W3(I,K)=0.
          DO 3 J=1,MJ
          A(I,K,J)=0.
3         AI(I,K,J)=0.
       DO 10 I=1,MI
       P=COS(I*DTHETA)
       Q=SIN(I*DTHETA)
       G11=-1.0*(1.0+P*P)/(P*Q**3*2.*DTHETA)
       A1=1./(Q*Q*DTHETA*DTHETA)
       B1=1./(Q*Q)
       DO 10 J=1,MJ
       IF(I.EQ.1) GO TO 4
       A(I,I-1,J)=(A1-G11)*S(J)*DZ*DZ
4      IF(I.EQ.MI) GO TO 5
       A(I,I+1,J)=(A1+G11)*S(J)*DZ*DZ
5      A(I,I,J)=-2.*A1*S(J)*DZ*DZ-2.*(ANC(J)+1./DTIME)
      1/(BETR(J)+1./DTIME)
```

```
10        CONTINUE
        DT=DTHETA
        P=COS(DT)
        Q=SIN(DT)
        G11=-1.*(1.+P*P)/(P*Q**3*2.*DT)
        A1=1./(Q*Q*DT*DT)
        DO 500 J=1,MJ
 500    A(1,1,J)=A(1,1,J)+(A1-G11)*S(J)*DZ*DZ
        P=COS(MI*DT)
         Q=SIN(MI*DT)
        G11=-1.*(1.+P*P)/(P*Q**3*2.*DT)
        A1=1./(Q*Q*DT*DT)
        DO 510 J=1,MJ
 510    A(MI,MI,J)=A(MI,MI,J)+(A1+G11)*S(J)*DZ*DZ
       DO 20 J=1,MJ
       QI(1,J)=((ANC(J)+1./DTIME)*(1.-DZ/2.-DZ/2./S(J)*SSZ(J))
      1+DZ/2.*ANCZ(J))/(BETR(J)+1./DTIME)
       QI(2,J)=((ANC(J)+1./DTIME)*(1.+DZ/2.+DZ*SSZ(J)/2./S(J))
      1-DZ/2.*ANCZ(J))/(BETR(J)+1./DTIME)
C  REMOVE AO AND BR DEPENDENCE HERE
C      QI(1,J)=1.
C      QI(2,J)=1.
       DO 8 I=1,MI
       DO 8 K=1,MI
       W2(I,K)=QI(2,J)*W3(I,K)
       W4(I,K)=-1.*(A(I,K,J)+W2(I,K))
8         W1(I,K)=W4(I,K)
C          IF(J.GE.4) GO TO 52
C         WRITE(6,903)
C         DO 51 I=1,MI
C51       WRITE(6,901)(W2(I,K),K=1,MI)
C         WRITE(6,904)
C          DO 60 I=1,MI
C         WRITE(6,901)(W4(I,K),K=1,MI)
C         WRITE(6,901)(W1(I,K),K=1,MI)
C60       CONTINUE
C52       CONTINUE
        CALL BRT4Z1(W4,MI,P3,P4,MI)
C         IF(J.GE.4) GO TO 54
C         WRITE(6,905)
C          DO 53 I=1,MI
C53       WRITE(6,901)(W4(I,K),K=1,MI)
C54       CONTINUE
C         IF(J.GE.4) GO TO 110
C         CALL MULT(MI,W3,W1,W4)
C         WRITE(6,906)
C         DO 100 I=1,MI
C100      WRITE(6,901)(W3(I,K),K=1,MI)
C         CALL MULT(MI,W3,W4,W1)
C         DO 105 I=1,MI
C105      WRITE(6,901)(W3(I,K),K=1,MI)
C110      CONTINUE
```

```
         DO 9 I=1,MI
         DO 9 K=1,MI
      AI(I,K,J)=W4(I,K)
      W3(I,K)=W4(I,K)*QI(1,J)
9     A(I,K,J)=W3(I,K)
C         IF(J.GE.4.AND.J.LE.69) GO TO 20
C        WRITE(6,907) J
C        DO 63 I=1,MI
C63         WRITE(6,901)(W3(I,K),K=1,MI)
20    CONTINUE
 901       FORMAT(10E10.3)
C        WRITE(6,908)
C        WRITE(6,901)(QI(1,J),J=1,MJ)
C        WRITE(6,901)(QI(2,J),J=1,MJ)
C        DO 81 J=41,MJ
C        WRITE(6,909) J
C        WRITE(6,901)(TIME(I,J),I=1,MI)
C81        WRITE(6,901)(FLUX(I,J),I=1,MI)
C
C
C     SET TIME ITERATION HERE
        DO 80 IT=1,24
C         WRITE(6,950) IT
C950      FORMAT(13H ITERATION = ,I3)
C   CALCULATE INITIAL GAMMA HERE
      DO 21 I=1,MI
 21   G3(I)=BASE(I)
C        WRITE(6,910)
C        WRITE(6,901)(BASE(I),I=1,MI)
C       WRITE(6,901)(G3(I),I=1,MI)
         DO 6 I=1,MI
         DO 6 J=1,MJ
6        TIME(I,J)=TIME(I,J)*DZ*DZ
      DO 25 J=1,MJ
      DO 22 I=1,MI
      G1(I)=TIME(I,J)+(FLUX(I,J)+HEATER(I,J))*DZ*DZ
      G2(I)=QI(2,J)*G3(I)-G1(I)
22    G3(I)=0.
      DO 24 I=1,MI
      DO 23 K=1,MI
      G3(I)=G3(I)+AI(I,K,J)*G2(K)
23       G4(K)=G3(I)
C        IF(J.GE.4.AND.J.LE.41) GO TO 24
C        WRITE(6,920) J,I
C       WRITE(6,901)(G4(K),K=1,MI)
24    QR(I,J)=G3(I)
C         IF(J.GE.4.AND.J.LE.41) GO TO 25
C        WRITE(6,911) J
C        WRITE(6,912)
C         WRITE(6,901)(G1(I),I=1,MI)
C        WRITE(6,913)
C            WRITE(6,901)(G2(I),I=1,MI)
```

```
C         WRITE(6,914)
C             WRITE(6,901)(G3(I),I=1,MI)
25         CONTINUE
C         WRITE(6,915)
          DO 270 I=1,MI
          G3(I)=TOP(I)
270       G4(I)=0.
C         WRITE(6,901)(TOP(K),K=1,MI)
C          WRITE(6,901)(G3(K),K=1,MI)
C          WRITE(6,901)(G4(K),K=1,MI)
       DO 40 JJ=1,MJ
       J=MJ-JJ+1
       DO 30 I=1,MI
       DO 30 K=1,MI
30     G4(I)=G4(I)+A(I,K,J)*G3(K)
C          IF(JJ.GE.4) GO TO 70
C         WRITE(6,916) J
C         WRITE(6,901)(G4(I),I=1,MI)
C70           CONTINUE
       DO 31 I=1,MI
       G3(I,=G4(I)+QR(I,J)
       QR(I,J)=G3(I)
31     G4(I)=0.
C          IF(JJ.GE.4) GO TO 40
C         WRITE(6,917) J
C          WRITE(6,901)(G3(I),I=1,MI)
40     CONTINUE
       CALL TIMEX(MI,MJ,DTHETA,DZ,DTIME)
80     CONTINUE
C           DO 90 I=1,MI
C90        WRITE(6,989)(QR(I,J),J=1,M1)
902       FORMAT(17H INITIAL A MATRIX)
        DO 280 I=1,MI
        DO 280 J=1,MJ
 280    A(7,I,J)=TIME(I,J)
C         WRITE(6,930)
 930      FORMAT(27H1TIME TERMS,AFTER ITERATION)
C 90      CALL OUTPUT(3,MI,MJ,ITHETA,DZ,7)
903       FORMAT(20H (A-DZ*B/2)*OMEGA=W2)
904       FORMAT(25H W4=MATRIX TO BE INVERTED)
905       FORMAT(29H INVERTED MATRIX,STORED IN W4)
906       FORMAT(37H MULTIPLICATION OF MATRIX AND INVERSE)
907       FORMAT(18H OMEGA,END OF LOOP,I3)
908       FORMAT(12H A+OR-DZ*B/2)
909       FORMAT(21H TIME AND FLUX,LEVEL=,I3)
910       FORMAT(11H BASE VALUE)
911       FORMAT(16H J LEVEL INDEX =,I3)
912       FORMAT(19H G1=TIME+FLUX/DZ/DZ)
913       FORMAT(19H G2=QI(2,J)*BETA-G1)
914       FORMAT(19H G3=INVERSE*G2=BETA)
915       FORMAT(21H UPPER BOUNDARY VALUE)
916         FORMAT(17H OMEGA*PSI,LEVEL=,I3)
```

```
920          FORMAT(21H BETA,LEVEL AND INDEX,2I5)
917        FORMAT(15H NEW PSI,LEVEL=,I3)
989        FORMAT(9E13.6)
           RETURN
          END
       SUBROUTINE TIMEX(MI,MJ,DTHETA,DZ,DTIME)
        COMMON /B/ SNR(17),CNR(17),SNI(17),CNI(17),BDY(17),
      1BDYI(17),BASE(17),TOP(17)
       COMMON /D/ S(45),QR(17,45),QI(17,45)
        COMMON /E/ QR1(17,45),QR2(17,45),QI1(17,45),QI2(17,45)
       COMMON /H/ TIME(17,45),FLUX(17,45),ANC(45),ANCZ(45),BETR(45),
      1TAU(45),SSZ(45),HEAT(17,45),HEATER(17,45)
       DT=DTHETA
       MIM=MI-1
       MJM=MJ-1
       DO 10 J=1,MJ
       QR1(1,J)=(QR(2,J)-QR(1,J))/DT/2.
       QR1(MI,J)=(QR(MI,J)-QR(MIM,J))/DT/2.
       QR2(1,J)=(QR(2,J)-2.*QR(1,J)+QR(1,J))/DT/DT
       QR2(MI,J)=(QR(MI,J)-2.*QR(MI,J)+QR(MIM,J))/DT/DT
       DO 10 I=2,MIM
       QR1(I,J)=(QR(I+1,J)-QR(I-1,J))/2./DT
  10   QR2(I,J)=(QR(I+1,J)-2.*QR(I,J)+QR(I-1,J))/DT/DT
       DO 11 I=1,MI
       QI1(I,1)=(QR(I,2)-BASE(I))/2./DZ
       QI1(I,MJ)=(TOP(I)-QR(I,MJM))/2./DZ
       QI2(I,1)=(QR(I,2)-2.*QR(I,1)+BASE(I))/DZ/DZ
       QI2(I,MJ)=(TOP(I)-2.*QR(I,MJ)+QR(I,MJM))/DZ/DZ
       DO 11 J=2,MJM
       QI1(I,J)=(QR(I,J+1)-QR(I,J-1))/2./DZ
  11   QI2(I,J)=(QR(I,J+1)-2.*QR(I,J)+QR(I,J-1))/DZ/DZ
       DO 12 I=1,MI
       P=COS(I*DTHETA)
       Q=SIN(I*DTHETA)
       DO 12 J=1,MJ
       QR1(I,J)=(1.+P**2)*S(J)*QR1(I,J)/P/Q**3.
       QR2(I,J)=S(J)*QR2(I,J)/Q/Q
       QI1(I,J)=(1.+SSZ(J)/S(J))*QI1(I,J)
  12   TIME(I,J)=(QR2(I,J)-QR1(I,J)+QI2(I,J)-QI1(I,J))
      1/DTIME/(BETR(J)+1./DTIME)
C12          TIME(I,J)=0.
C12        TIME(I,J)=(QI2(I,J)+TAU(J)*QR(I,J)+QI1(I,J))
C    BR DEPENDENCE REMOVED HERE
           RETURN
       END
       SUBROUTINE ATMEAN(PO,MI,MJ,ITHETA,D2,DTHETA,AM,DTIME,IFLAG,JFLAG)
       COMMON /A/ A(17,17,45),AI(17,17,45)
       COMMON /B/ SNR(17),CNR(17),SNI(17),CNI(17),BDY(17),
      1BDYI(17),BASE(17),TOP(17)
       COMMON /C/ UBAR(17,45),TBAR(17,45),UFLUX(17,45),TFLUX(17,45),
      1 UINIT(17,45),VBAR(17,45),VINIT(17,45),WBAR(17,45),WINIT(17,45)
       COMMON /D/ S(45),QR(17,45),QI(17,45)
```

```
      COMMON /H/ TIME(17,45),FLUX(17,45),ANC(45),ANCZ(45),BETR(45),
     1TAU(45),SSZ(45),HEAT(17,45),HEATER(17,45)
      DT=DTHETA
      AO=6.37E8
      MJM=MJ-1
      MIM=MI-1
      G=981.
      R=2.87E6
      F=1.458E-4
      DO 1 J=1,MJ
      DO 1 I=1,MI
C     A(8,I,J)=QR(I,J)
C     QR(I,J)=G*EXP(J*DZ/2.)*QR(I,J)*SQRT(S(J))
1     A(7,I,J)=QR(I,J)
      DO 12 J=1,MJ
      A(2,1,J)=(QR(1,J)-QR(2,J))/(DT*2.*F*SIN(DTHETA)*AO)
      A(2,MI,J)=(QR(MIM,J)-QR(MI,J))/(DT*2.*F*SIN(MI*DTHETA)*AO)
      DO 12 I=2,MIM
      FAC=1.458E-4*SIN(I*DT)
12    A(2,I,J)=-(QR(I+1,J)-QR(I-1,J))/(DT*2.*AO*FAC)
      DO 13 I=1,MI
      A(1,I,1)=(QR(I,2)-BASE(I))/(DZ*2.*R)
         PHITOP=TOP(I)
C        WRITE(6,901) PHITOP
      A(1,I,MJ)=(PHITOP-QR(I,MJM))/(DZ*2.*R)
      DO 13 J=2,MJM
13    A(1,I,J)=(QR(I,J+1)-QR(I,J-1))/(DZ*2.*R)
 901      FORMAT(10E10.3)
        IF(JFLAG.EQ.1) GO TO 70
        CALL OUTPUT(3,MI,MJ,ITHETA,DZ,7)
        CALL OUTPUT(3,MI,MJ,ITHETA,DZ,1)
        CALL OUTPUT(3,MI,MJ,ITHETA,DZ,2)
 70     CONTINUE
          DO 15 I=1,MI
          DO 15 J=1,MJ
          IF(IFLAG.EQ.0) GO TO 100
          A(9,I,J)=(A(2,I,J)-UBAR(I,J))/24./DTIME
          A(12,I,J)=(A(1,I,J)-TBAR(I,J))/24./DTIME
          GO TO 110
 100      A(9,I,J)=0.
          A(12,I,J)=0.
 110      A(10,I,J)=UFLUX(I,J)
          A(11,I,J)=(A(9,I,J)+A(10,I,J)+BETR(J)*A(2,I,J))/F/SIN(I*DT)
          A(13,I,J)=TFLUX(I,J)
       A(14,I,J)=(HEAT(I,J)-R*(A(12,I,J)
     1+ANC(J)*A(1,I,J))-A(13,I,J))/S(J)/(F*AO)**2.
        A(15,I,J)=A(14,I,J)*7.0E5
        VBAR(I,J)=A(11,I,J)
        WBAR(I,J)=A(14,I,J)
         UBAR(I,J)=A(2,I,J)
15       TBAR(I,J)=A(1,I,J)
       IF(IFLAG.EQ.0.) GO TO 55
```

```
          GO TO 55
C  CONTINUITY EQN CALCULATIONS
          DO 20 I=1,MI
          DO 20 J=1,MJ
 20       A(3,I,J)=A(11,I,J)*SIN(I*DT)/COS(I*DT)/AO
          DO 30 J=1,MJ
          A(15,1,J)=(A(11,2,J)-A(11,1,J))/AO/DT
          A(15,MI,J)=(A(11,MI,J)-A(11,MIM,J))/AO/DT
          DO 30 I=2,MIM
 30       A(15,I,J)=(A(11,I+1,J)-A(11,I-1,J))/AO/DT
          DO 40 I=1,MI
          A(16,I,1)=A(14,I,2)/2./DZ-A(14,I,1)
          A(16,I,MJ)=-A(14,I,MJM)/2./DZ-A(14,I,MJ)
          DO 40 J=2,MJM
40        A(16,I,J)=(A(14,I,J+1)-A(14,I,J-1))/2./DZ-A(14,I,J)
          DO 50 I=1,MI
          DO 50 J=1,MJ
          A(15,I,J)=A(15,I,J)-A(3,I,J)
 50       A(17,I,J)=A(15,I,J)+A(16,I,J)
 55         CONTINUE
            IF(JFLAG.EQ.1) GO TO 60
            WRITE(6,902)
902         FORMAT(36H MERIDIONAL CIRCULATION CALCULATIONS)
C           DO 17 KK=9,14
C 17        CALL OUTPUT(3,MI,MJ,ITHETA,DZ,KK)
            CALL OUTPUT(3,MI,MJ,ITHETA,DZ,11)
C           DO 14 KK=14,17
 14         CALL OUTPUT(3,MI,MJ,ITHETA,DZ,15)
 60         CONTINUE
            GO TO 140
          DO 61 J=1,MJ
 61       A(16,17,J)=A(11,17,J)
          DO 62 I=1,MI
          A(12,I,1)=-(A(14,I,2)-A(14,I,1))/DZ+A(14,I,1)
          A(12,I,MJ)=-(A(14,I,MJ)-A(14,I,MJM))/DZ+A(14,I,MJ)
          DO 62 J=2,MJM
 62       A(12,I,J)=-(A(14,I,J+1)-A(14,I,J-1))/2./DZ+A(14,I,J)
          DO 67 J=1,MJ
          A(16,16,J)=-2.*DT*(SIN(17.*DT)/COS(17.*DT)*A(11,17,J)
     1   +A(12,17,J)*AO)
          DO 65 KK=1,15
          I=MI-KK-1
 65       A(16,I,J)=-2.*DT*(TAN((I+1)*DT)*A(16,I+1,J)
     1   +A(12,I+1,J)*AO)+A(16,I+2,J)
 67        CONTINUE
C         IF(JFLAG.EQ.1) GO TO 140
C         CALL OUTPUT(3,MI,MJ,ITHETA,DZ,12)
C         CALL OUTPUT(3,MI,MJ,ITHETA,DZ,11)
C         CALL OUTPUT(3,MI,MJ,ITHETA,DZ,16)
 140      CONTINUE
              RETURN
              END
```

```
      SUBROUTINE DIFF (G2,G1,L1,Y,X)
      DIMENSION G2(L1), G1(L1), Y(L1), X(L1)
       MIM=L1-1
       G1(1)=(X(2)-X(1))/2.+X(1)
       G2(1)=(Y(2)-Y(1))/(X(2)-X(1))
        G1(L1)=(X(L1)-X(MIM))/2. +X(MIM)
       G2(L1)=(Y(L1)-Y(MIM))/(X(L1)-X(MIM))
      DO 3 J=2,MIM
        J1=J-1
        J2=J+1
        G1(J)=(X(J2)-X(J1))/2.+X(J1)
    3   G2(J)=(Y(J2)-Y(J1))/(X(J2)-X(J1))
      RETURN
      END
      SUBROUTINE INTER (A,B,M,Y,X,N)
      DIMENSION A(M), B(M), X(N), Y(N), Q(4), R(4), S(3), T(2), E(3)
      DO 7 J=1,M
        DO 1 K=1,N
          IF (B(J).LE.X(K)) GO TO 2
    1     CONTINUE
    2   LQ=K-2
        IF (LQ.LE.1) LQ=1
        IR=N-3
        IF (LQ.GE.IR) LQ=N-3
        DO 3 L=1,4
          LN=L+LQ-1
          Q(L)=X(LN)
    3     R(L)=Y(LN)
        DO 4 L=1,3
    4     S(L)=(R(L+1)-R(L))/(Q(L+1)-Q(L))
        DO 5 L=1,2
    5     T(L)=(S(L+1)-S(L))/(Q(L+2)-Q(L))
        D=(T(2)-T(1))/(Q(4)-Q(1))
        DO 6 L=1,3
    6     E(L)=B(J)-Q(L)
    7   A(J)=R(1)+S(1)*E(1)+T(1)*E(1)*E(2)+D*E(1)*E(2)*E(3)
      RETURN
      END
      SUBROUTINE CPY (K,M,MI)
      COMMON /D/ S(45),QR(17,45),QI(17,45)
      COMMON /A/ A(17,17,45),AI(17,17,45)
      COMMON /F/ W1(17,17),G1(17),W2(17,17),G2(17),W3(17,17),W4(17,17),W
     15(17,17),G3(17),G4(17),W6(17,17),G5(17)
      IF (M.EQ.1) GO TO 2
      DO 1 I=1,MI
        QR(I,K)=G2(I)
        QI(I,K)=G4(I)
        DO 1 J=1,MI
        AI(I,J,K)=W4(I,J)
    1   A(I,J,K)=W2(I,J)
         GO TO 10
         IF(K.GE.2) GO TO 10
```

```
      WRITE(6,901)(QR(I,K),I=1,MI)
      WRITE(6,901)(QI(I,K),I=1,MI)
      DO 4 I=1,MI
4     WRITE(6,901)(A(I,J,K),J=1,MI)
      DO 5 I=1,MI
5     WRITE(6,901)(AI(I,J,K),J=1,MI)
10    CONTINUE
901   FORMAT(10E10.3)
      RETURN
    2 DO 3 I=1,MI
      G1(I)=QR(I,K)
      G3(I)=QI(I,K)
      DO 3 J=1,MI
      W3(I,J)=AI(I,J,K)
    3 W1(I,J)=A(I,J,K)
      GO TO 20
      IF(K.GE.2) GO TO 20
      WRITE(6,901)(G1(I),I=1,MI)
      WRITE(6,901)(G3(I),I=1,MI)
      DO 15 I=1,MI
15    WRITE(6,901)(W1(I,J),J=1,MI)
      DO 16 I=1,MI
16    WRITE(6,901)(W3(I,J),J=1,MI)
20    CONTINUE
      RETURN
      END
      SUBROUTINE CINV (MI,SR,SI)
C
C....   THIS SUBROUTINE TAKES THE INVERSE OF A COMPLEX MATRIX S
C....   WHOSE REAL AND IMAGINARY PARTS ARE LABELED SR AND SI
C....   THE INVERSE IS RETURNED INTO THE SAME MATRIX AND THE
C....   INITIAL MATRIX IS DESTROYED.
C
      DIMENSION SR(17,17), SI(17,17), SC1(17,17), SC2(17,17), SC3(17,17)
      COMMON /G/ P3(17),P4(171)
      DO 1 J=1,MI
        DO 1 K=1,MI
    1   SC1(J,K)=SR(J,K)
      CALL BRT4Z1 (SC1,MI,P3,P4,MI)
      CALL MULT (MI,SC2,SC1,SI)
      CALL MULT (MI,SC3,SI,SC2)
      DO 2 I=1,MI
        DO 2 J=1,MI
        SI(I,J)=-1.*SI(I,J)
    2   SR(I,J)=SC3(I,J)+SR(I,J)
      CALL BRT4Z1 (SR,MI,P3,P4,MI)
      CALL MULT (MI,SC2,SI,SR)
      CALL MULT (MI,SI,SC1,SC2)
      RETURN
      END
      SUBROUTINE MULT (MI,A,B,C)
C
```

```
C....   THIS SUBROUTINE MULTIPLIES B*C YIELDING A
C....   WHERE ALL ARE MATRICES.
C
      DIMENSION A(MI,MI), B(MI,MI), C(MI,MI)
      DO 1 I=1,MI
        DO 1 J=1,MI
        A(I,J)=0.
        DO 1 K=1,MI
    1   A(I,J)=A(I,J)+B(I,K)*C(K,J)
      RETURN
      END
      SUBROUTINE BRT4Z1 (Y,N,Z,W,NX)
C
C....    IMPLICIT REAL*8(A-H,O-V,X)
C
      DIMENSION A(17,17), P(17), Q(171)
      DIMENSION Y(NX,N), Z(N), W(1)
      FLG(X)=ALOG10(ABS(X))
      MXL=FLG(Y(1,1))
      MXH=MXL
      DO 1 J=1,NX
        DO 1 I=1,N
        IF (Y(I,J).EQ.0.) GO TO 1
        MX1=FLG(Y(I,J))
        IF (MX1.GE.MXH) MXH=MX1
        IF (MX1.LE.MXL) MXL=MX1
    1   CONTINUE
      MXM=MXH-MXL
      IF (MXM.GT.75) WRITE (6,901)
      XF=10.**(-1.*(MXL+MXM/2.))
      DO 2 J=1,NX
        DO 2 I=1,N
    2   A(I,J)=Y(I,J)*XF
      NM1=N-1
      L=0
      DO 6 I=1,N
        IP1=I+1
        S=0.0
        L=L+1
        DO 3 J=1,N
          T=A(J,I)
          P(J)=T
C
C....       P HAS I'TH COLUMN OF U(I-1)
C
    3     S=S+T*T
C
C....     S HAS (COL I)OF U(I-1))'*COL I)OF U(I-1))
C
        Q(L)=S
C
C....     Q(L) HAS R(I,I)
```

```
C
        IF (I.EQ.N) GO TO 6
        DO 5 IG=IP1,N
          T=0.0
          DO 4 J=1,N
    4       T=T+P(J)*A(J,IG)
C
C....       T HAS (COL I OF U(I-1))'*(COL IG OF U(I-1))
C....            =IG ELEMENT OF ROW I OF U'A
C
          L=L+1
          Q(L)=T
C
C....       Q(L) HAS R(I,IG)
C
          T=T/S
C
C....       STORE IG'TH COLUMN OF U(I) IN A
C
          DO 5 J=1,N
    5     A(J,IG)=A(J,IG)-P(J)*T
    6   CONTINUE
      NN=N+2
      DO 10 II=1,N
        I=N+1-II
        IP1=I+1
        IH=I-I
        T=Q(L)
        DO 9 J=1,N
          S=A(J,I)
          IF (I.EQ.N) GO TO 8
          DO 7 IG=IP1,N
    7       S=S-Q(IG+IH)*A(J,IG)
C
C....       CALCULATE V' INSTEAD OF V BECAUSE U AND V ARE BOTH
C....       STORED IN A.
C
    8     A(J,I)=S/T
    9     CONTINUE
C
C....     RESET TO DIAGONAL ELEMENT ONE ROW UP TO GET A PROPER R
C...      ELEMENT
C
   10   L=L+I-NN
      DO 11 I=1,NM1
        IP1=I+1
        DO 11 J=IP1,N
        S=A(I,J)
        A(I,J)=A(J,I)
   11   A(J,I)=S
      DO 12 I=1,NX
        DO 12 J=1,N
```

```
   12   Y(I,J)=A(I,J)*XF
        RETURN
C
  901 FORMAT (12H RANGE ERROR)
        END
         SUBROUTINE OUTPUT(KD,MI,MJ,ITHETA,DZ,LAP)
        COMMON /A/ A(17,17,45),AI(17,17,45)
        COMMON /B/ SNR(17),CNR(17),SNI(17),CNI(17),BDY(17),
       1BDYI(17),BASE(17),TOP(17)
        COMMON /D/ S(45),QR(17,45),QI(17,45)
        KO=KD
        BOT=5.5
        ITHETA=5
        IF(KO.GE.2.) GO TO 4
        DO 3 J=1,45
        DO 3 I=1,MI
        XXY=SQRT(A(LAP,I,J)**2+AI(LAP,I,J)**2)
        IF(A(LAP,I,J).EQ.0.) GO TO 1
        XYY=180.*ATAN2(AI(LAP,I,J),A(LAP,I,J))/3.14159
        IF(XYY.LT.0.) XYY=XYY+360.
        GO TO 2
1       XYY=90.
2       A(LAP,I,J)=XXY
         AI(LAP,I,J)=XYY
3       CONTINUE
        IF(KO.EQ.0) GO TO 4
        RETURN
4       CONTINUE
        IR=MJ/8
        DO 5 I=1,MI
5       CNR(I)=5.*I
        IF(KO.GE.2) GO TO 6
C        0 PRINTS OUT AMP AND PHASE
C        1 CALCULATES AMP AND PHASE,BUT DOESN'T PRINT OUT
C        2 PRINTS OUT A AND AI
C        3 PRINTS A ONLY
C        4 PRINTS AI ONLY
C       THIS IS A STRANGE PLACE FOR COMMENTS,ISN'T IT?
        WRITE(6,907) LAP
          GO TO 7
6       CONTINUE
        IF(KO.EQ.4) GO TO 8
        WRITE(6,903) LAP
7       CONTINUE
C       DO 36 J=1,IR
CC      DO 36 J=1,3
        DO 36 J=1
C       KL=(J-1)*8+1
CC      KL=(J-1)*16+2
        KL=2
C        KU=KL+7
CC       KU=KL+14
```

```
       KU=44
       DO 35 K=1,8
CC35   SNR(K)=(J-1)*16.*DZ+K*DZ*2.+BOT
  35   SNR(K)=BOT+.5+(K-1)*DZ*6.
C35    SNR(K)=(J-1)*8.*DZ +K*DZ
       WRITE(6,904)(SNR(K),K=1,8)
CC36    WRITE(6,905)(CNR(JJ),(A(LAP,JJ,K),K=KL,KU,2),CNR(JJ),JJ=1,MI)
  36    WRITE(6,905)(CNR(JJ),(A(LAP,JJ,K),K=KL,KU,6),CNR(JJ),JJ=1,MI)
C36    WRITE(6,905)(CNR(JJ),(A(LAP,JJ,K),K=KL,KU),JJ=1,MI)
       IF(KO.EQ.3)GO TO 10
       IF(KO.EQ.2) GO TO 8
       WRITE(6,908)
       GO TO 9
8      WRITE(6,906) LAP
9      CONTINUE
C      DO 38 J=1,IR
CC     DO 38 J=1,3
       DO 38 J=1
C      KL=(J-1)*8+1
CC     KL=(J-1)*16+2
       KL=2
C      KU=KL+7
CC     KU=KL+14
       KU=44
       DO 37 K=1,8
CC37    SNR(K)=(J-1)*16.*DZ+K*DZ*2.+BOT
 37     SNR(K)=BOT+.5+(K-1)*DZ*6.
C37     SNR(K)=(J-1)*8.*DZ+K*DZ
       WRITE(6,904)(SNR(K),K=1,8)
CC38     WRITE(6,905)(CNR(JJ),(AI(LAP,JJ,K),K=KL,KU,2),CNR(JJ),JJ=1,MI)
 38      WRITE(6,905)(CNR(JJ),(AI(LAP,JJ,K),K=KL,KU,6),CNR(JJ),JJ=1,MI)
C38      WRITE(6,905)(CNR(JJ),(AI(LAP,JJ,K),K=KL,KU),JJ=1,MI)
10     CONTINUE
903    FORMAT(14H1 INDEX (1)  =,I4)
904    FORMAT(1H0,14X,8(F6.2,7X))
905    FORMAT(2X,0PF6.0,2X,1PE13.3,1PE13.3,1PE13.3,1PE13.3,1PE
      113.3,1PE13.3,1PE13.3,1PE13.3,2X,0PF6.0)
906    FORMAT(14H1 INDEX (2)  =,I4)
907    FORMAT(23H    AMPLITUDE ,INDEX = ,I4)
908    FORMAT(9H    PHASE)
       RETURN
       END
       SUBROUTINE NOX(MI,MJ,DZ,DTHETA,CONV,AM,DTIME,IFLAG,JFLAG)
       COMMON /A/ A(17,17,45),AI(17,17,45),SRE,SIM,COUNT
       COMMON /C/ UBAR(17,45),TBAR(17,45),UFLUX(17,45),TFLUX(17,45)
      1,UINIT(17,45),VBAR(17,45),VINIT(17,45),WBAR(17,45),WINIT(17,45)
       COMMON /G/ P3(17),P4(45),P5(45),P6(81),BARNOX(17,45),
      1AMPNOX(17,45),PHANOX(17,45),TIMNOX(17,45),TIMAMP(17,45),
      1TIMPHA(17,45),PROMEAN(17,45),PROAMP(17,45),PROPHA(17,45)
      1 ,AIR(45),H(45),DZZ(17,45),TEST1(17,45),TEST2(17,45)
       AO=6.37E8
       MJ=38
```

```
      BOT=5.5
      GC=1.013E-2/1.38E-23
      TDAY=COUNT/24.
      MJM=MJ-1
      MIM=MI-1
      C=CONV
      DT=DTHETA
      IF(IFLAG.EQ.0) GO TO 70
      DO 7 I=1,MI
      DO 7 J=1,MJ
      A(17,I,J)=AMPNOX(I,J)
 7    AI(17,I,J)=PHANOX(I,J)
      CALL OUTPUT(1,MI,MJ,ITHETA,DZ,17)
      DO 10 J=1,MJ
      DO 10 I=1,MI
      A(1,I,J)=A(17,I,J)*A(15,I,J)*COS(C*(AI(17,I,J)-AI(15,I,J)))/2.
10    A(4,I,J)=A(17,I,J)*A(14,I,J)*COS(C*(AI(17,I,J)-AI(14,I,J)))/2.
      DO 20 J=1,MJ
      A(2,1,J)=(A(1,2,J)-A(1,1,J))/DT
      A(2,MI,J)=(A(1,MI,J)-A(1,MIM,J))/DT
      A(8,1,J)=(BARNOX(2,J)-BARNOX(1,J))/DT
      A(8,MI,J)=(BARNOX(MI,J)-BARNOX(MIM,J))/DT
      DO 20 I=2,MIM
      A(2,I,J)=(A(1,I+1,J)-A(1,I-1,J))/2./DT
 20   A(8,I,J)=(BARNOX(I+1,J)-BARNOX(I-1,J))/2./DT
      DO 30 I=1,MI
      A(5,I,1)=(A(4,I,2)-A(4,I,1))/DZ
      A(5,I,MJ)=(A(4,I,MJ)-A(4,I,MJM))/DZ
      A(9,I,1)=(BARNOX(I,2)-BARNOX(I,1))/DZ
      A(9,I,MJ)=(BARNOX(I,MJ)-BARNOX(I,MJM))/DZ
      DO 30 J=2,MJM
      A(5,I,J)=(A(4,I,J+1)-A(4,I,J-1))/2./DZ
30    A(9,I,J)=(BARNOX(I,J+1)-BARNOX(I,J-1))/2./DZ
      DO 40 I=1,MI
      P=COS(I*DT)
      Q=SIN(I*DT)
      DO 40 J=1,MJ
      A(3,I,J)=-A(2,I,J)/AO+Q*A(1,I,J)/P/AO
      A(6,I,J)=-A(5,I,J)+A(4,I,J)
      A(7,I,J)=A(3,I,J)+A(6,I,J)
      TIMNOX(I,J)=A(7,I,J)
      A(10,I,J)=-A(15,I,J)*COS(AI(15,I,J)*C)*A(8,I,J)/AO
      AI(10,I,J)=-A(15,I,J)*SIN(AI(15,I,J)*C)*A(8,I,J)/AO
      A(11,I,J)=-A(14,I,J)*COS(AI(14,I,J)*C)*A(9,I,J)
      AI(11,I,J)=-A(14,I,J)*SIN(AI(14,I,J)*C)*A(9,I,J)
      A(12,I,J)=A(10,I,J)+A(11,I,J)
      AI(12,I,J)=AI(10,I,J)+AI(11,I,J)
C     IF(COUNT.NE.1.) GO TO 40
      TIMAMP(I,J)=A(12,I,J)
      TIMPHA(I,J)=AI(12,I,J)
 40   CONTINUE
C     IF(JFLAG.EQ.1) GO TO 65
```

```
      GO TO 65
      IF(COUNT.NE.1.AND.COUNT.NE.480.) GO TO 65
      WRITE(6,900) IFLAG,TDAY
      CALL OUTPUT(3,MI,MJ,ITHETA,DZ,1)
      CALL OUTPUT(3,MI,MJ,ITHETA,DZ,3)
      CALL OUTPUT(3,MI,MJ,ITHETA,DZ,4)
      CALL OUTPUT(3,MI,MJ,ITHETA,DZ,6)
      CALL OUTPUT(3,MI,MJ,ITHETA,DZ,7)
C     DO 50 KK=8,9
C50   CALL OUTPUT(3,MI,MJ,ITHETA,DZ,KK)
C     DO 60 KK=10,12
C60   CALL OUTPUT(2,MI,MJ,ITHETA,DZ,KK)
 65   CONTINUE
      GO TO 220
 70   CONTINUE
      GO TO 78
C     IF(COUNT.NE.1) GO TO 78
      DO 71 I=1,MI
      B=AM*AI(5,I,MJ)/AO/COS(I*DT)
      AMPNOX(I,MJ)=TIMPHA(I,MJ)/B
 71   PHANOX(I,MJ)=-TIMAMP(I,MJ)/B
      GO TO 78
      CALL OUTPUT(0,MI,MJ,ITHETA,DZ,17)
C     DO 74 J=1,MJ
C     DO 72 I=1,5
C72   A(17,I,J)=A(17,6,J)
C     AI(17,6,J)=AI(17,8,J)+2.*DT*AM*AI(5,7,J)/C/VBAR(7,J)/COS(7.*DT)
C     AI(17,4,J)=AI(17,6,J)+2.*DT*AM*AI(5,5,J)/C/VBAR(5,J)/COS(5.*DT)
C74   AI(17,2,J)=AI(17,4,J)+2.*DT*AM*AI(5,3,J)/C/VBAR(3,J)/COS(3.*DT)
      DO 76 I=1,MI
      DO 76 J=1,MJ
      A(13,I,J)=A(17,I,J)
 76   AI(13,I,J)=AI(17,I,J)
      CALL OUTPUT(2,MI,MJ,ITHETA,DZ,13)
      DO 75 I=1,MI
      DO 75 J=1,MJ
      AMPNOX(I,J)=A(13,I,J)
      PHANOX(I,J)=AI(13,I,J)
 75     A(13,I,J)=A(13,I,J)*AIR(J)
        CALL OUTPUT(2,MI,MJ,ITHETA,DZ,13)
 78   CONTINUE
      DO 80 I=1,MI
      DO 80 J=1,MJ
      A(1,I,J)=A(11,I,J)*BARNOX(I,J)
      A(4,I,J)=A(14,I,J)*BARNOX(I,J)
      A(17,I,J)=AMPNOX(I,J)
 80   AI(17,I,J)=PHANOX(I,J)
      DO 90 J=1,MJ
      A(2,1,J)=(BARNOX(2,J)-BARNOX(1,J))/DT
      A(2,MI,J)=(BARNOX(MI,J)-BARNOX(MIM,J))/DT
C     A(8,1,J)=(A(17,2,J)-A(17,1,J))/DT
      A(8,1,J)=0.
```

```
      A(8,MI,J)=(A(17,MI,J)-A(17,MIM,J))/DT
C     AI(8,1,J)=(AI(17,2,J)-AI(17,1,J))/DT
      AI(8,MI,J)=(AI(17,MI,J)-AI(17,MIM,J))/DT
      AI(8,1,J)=0.
      DO 90 I=2,MIM
      A(2,I,J)=(BARNOX(I,J)-BARNOX(I-1,J))/DT
      A(8,I,J)=(A(17,I,J)-A(17,I-1,J))/DT
 90   AI(8,I,J)=(AI(17,I,J)-AI(17,I-1,J))/DT
      DO 100 I=1,MI
      A(5,I,1)=(BARNOX(I,2)-BARNOX(I,1))/DZ
      A(5,I,MJ)=(BARNOX(I,MJ)-BARNOX(I,MJM))/DZ
      A(9,I,1)=(A(17,I,2)-A(17,I,1))/DZ
C     A(9,I,MJ)=(A(17,I,MJ)-A(17,I,MJM))/DZ
      A(9,I,MJ)=0.
      AI(9,I,1)=(AI(17,I,2)-AI(17,I,1))/DZ
C     AI(9,I,MJ)=(AI(17,I,MJ)-AI(17,I,MJM))/DZ
      AI(9,I,MJ)=0.
      DO 100 J=2,MJM
      A(5,I,J)=(BARNOX(I,J+1)-BARNOX(I,J))/DZ
      A(9,I,J)=(A(17,I,J+1)-A(17,I,J))/DZ
 100  AI(9,I,J)=(AI(17,I,J+1)-AI(17,I,J))/DZ
      DO 110 I=1,MI
      DO 110 J=1,MJ
      A(3,I,J)=-A(11,I,J)*A(2,I,J)/AO
      A(6,I,J)=-A(14,I,J)*A(5,I,J)
      A(7,I,J)=A(3,I,J)+A(6,I,J)
      A(10,I,J)=-A(11,I,J)*A(8,I,J)/AO
      AI(10,I,J)=-A(11,I,J)*AI(8,I,J)/AO
      A(11,I,J)=-A(14,I,J)*A(9,I,J)
      AI(11,I,J)=-A(14,I,J)*AI(9,I,J)
      A(12,I,J)=A(10,I,J)+A(11,I,J)
      AI(12,I,J)=AI(10,I,J)+AI(11,I,J)
C     IF(COUNT.NE.1.) GO TO 110
C     PROAMP(I,J)=A(12,I,J)
C     PROPHA(I,J)=AI(12,I,J)
 110  CONTINUE
       DO 114 I=1,MI
       A(13,I,1)=0.
      A(13,I,MJ)=-1.0E8
       DO 114 J=2,MJM
 114   A(13,I,J)=-(DZZ(I,J-1)*AIR(J-1)/H(J-1)+DZZ(I,J)
     1 *AIR(J)/H(J))/2./DZ*(BARNOX(I,J)-BARNOX(I,J-1))
      DO 117 I=1,MI
      A(14,I,MJ)=0.
      DO 117 J=1,MJM
 117  A(14,I,J)=-(A(13,I,J+1)-A(13,I,J))/DZ/AIR(J)/H(J)
C     IF(JFLAG.EQ.1) GO TO 135
      GO TO 512
      IF(COUNT.NE.1.AND.COUNT.NE.480.) GO TO 135
      WRITE(6,900) IFLAG,TDAY
      CALL OUTPUT(3,MI,MJ,ITHETA,DZ,13)
      CALL OUTPUT(3,MI,MJ,ITHETA,DZ,14)
```

```
      CALL OUTPUT(3,MI,MJ,ITHETA,DZ,1)
      CALL OUTPUT(3,MI,MJ,ITHETA,DZ,3)
      CALL OUTPUT(3,MI,MJ,ITHETA,DZ,4)
      CALL OUTPUT(3,MI,MJ,ITHETA,DZ,6)
      CALL OUTPUT(3,MI,MJ,ITHETA,DZ,7)
C     DO 120 KK=1,7
C120  CALL OUTPUT(3,MI,MJ,ITHETA,DZ,KK)
C     CALL OUTPUT(2,MI,MJ,ITHETA,DZ,17)
C     DO 130 KK=8,12
C130  CALL OUTPUT(2,MI,MJ,ITHETA,DZ,KK)
C     DO 131 KK=13,14
C131  CALL OUTPUT(3,MI,MJ,ITHETA,DZ,KK)
 135  CONTINUE
      IF(COUNT.NE.1) GO TO 512
      DO 511 KK=13,14
 511  CALL OUTPUT(3,MI,MJ,ITHETA,DZ,KK)
 512  CONTINUE
      DO 138 J=1,MJ
      DO 138 I=1,MI
      A(1,I,J)=A(14,I,J)*DTIME
      A(2,I,J)=TIMNOX(I,J)*DTIME
      IF(J.LT.8) A(2,I,J)=0.
      A(3,I,J)=A(7,I,J)*DTIME
C     IF(COUNT.GT.1.) GO TO 136
C     A(4,I,J)=-A(2,I,J)-A(3,I,J)-A(1,I,J)
C     PROMEAN(I,J)=A(4,I,J)/BARNOX(I,J)/DTIME
C     PROMEAN(I,J)=-4.0E-6*DTIME
C     IF(J.LT.20) PROMEAN(I,J)=0.
C136  CONTINUE
      A(4,I,J)=-PROMEAN(I,J)*BARNOX(I,J)*DTIME
 138  A(5,I,J)=A(1,I,J)+A(2,I,J)+A(3,I,J)+A(4,I,J)
      DO 139 I=2,MI
      DO 139 J=2,37
      A(6,I,J)=BARNOX(I,J)+A(5,I,J)
      BARNOX(I,J)=A(6,I,J)
 139  IF(BARNOX(I,J).LT.0.) BARNOX(I,J)=0.
      DO 140 I=1,MI
      P=COS(I*DT)
      DO 140 J=1,MJM
      A(7,I,J)=TIMAMP(I,J)
      AI(7,I,J)=TIMPHA(I,J)
      A(8,I,J)=A(12,I,J)
C     A(8,I,J)=PROAMP(I,J)
      AI(8,I,J)=AI(12,I,J)
C     AI(8,I,J)=PROPHA(I,J)
      A(9,I,J)=A(7,I,J)+A(8,I,J)
      AI(9,I,J)=AI(7,I,J)+AI(8,I,J)
C     A(10,I,J)=A(9,I,J)-TIMNOX(I,J)
      A(10,I,J)=A(9,I,J)
      AI(10,I,J)=AI(9,I,J)
      B=AM*AI(5,I,J)/AO/P
C     IF(COUNT.NE.1.) GO TO 137
```

```
C       A(11,I,J)=-A(10,I,J)-AI(17,I,J)*B
C       AI(11,I,J)=-AI(10,I,J)+A(17,I,J)*B
C       PROAMP(I,J)=A(11,I,J)
C       PROPHA(I,J)=AI(11,I,J)
C       PROAMP(I,J)=0.
C       PROPHA(I,J)=0.
C       A(17,I,J)=AI(10,I,J)/B
C        AI(17,I,J)=-A(10,I,J)/B
  137   CONTINUE
        A(11,I,J)=-PROMEAN(I,J)*A(17,I,J)
        AI(11,I,J)=-PROMEAN(I,J)*AI(17,I,J)
        A(12,I,J)=A(10,I,J)+A(11,I,J)
        AI(12,I,J)=AI(10,I,J)+AI(    ,J)
C       IF(COUNT.NE.1.) GO TO 1000
C       TEST1(I,J)=A(12,I,J)
C       TEST2(I,J)=AI(12,I,J)
C1000   CONTINUE
C       A(12,I,J)=A(7,I,J)
C       AI(12,I,J)=AI(7,I,J)
        A(15,I,J)=AI(10,I,J)/B
        AI(15,I,J)=-A(10,I,J)/B
        A(16,I,J)=B
        A(13,I,J)=A(17,I,J)*COS(B*DTIME)+AI(17,I,J)*SIN(B*DTIME)
     1 -AI(12,I,J)*(COS(B*DTIME)-1.)/B+A(12,I,J)*SIN(B*DTIME)/B
        AI(13,I,J)=AI(17,I,J)*COS(B*DTIME)-A(17,I,J)*SIN(B*DTIME)
     1 +A(12,I,J)*(COS(B*DTIME)-1.)/B+AI(12,I,J)*SIN(B*DTIME)/B
C       A(13,I,J)=A(17,I,J)+(AI(17,I,J)*B+A(12,I,J))*DTIME
C       AI(13,I,J)=AI(17,I,J)+(-A(17,I,J)*B+AI(12,I,J))*DTIME
        A(14,I,J)=(A(17,I,J)-AI(10,I,J)/B)*(1.-COS(B*DTIME))
     1 -(AI(17,I,J)+A(10,I,J)/B)*SIN(B*DTIME)
  140   AI(14,I,J)=(A(17,I,J)-AI(10,I,J)/B)*SIN(B*DTIME)
     1 +(AI(17,I,J)+A(10,I,J)/B)*(1.-COS(B*DTIME))
C       DO 145 J=1,MJ
C       BARNOX(MI,J)=2.*BARNOX(MIM,J)-BARNOX(MI-2,J)
C       A(13,1,J)=A(13,2,J)
C       AI(13,1,J)=AI(13,2,J)
C       A(13,MI,J)=A(13,MIM,J)
C145    AI(13,MI,J)=AI(13,MIM,J)
C        DO 146 I=1,MI
C        DO 146 J=42,MJ
C        A(13,I,J)=A(17,I,J)
C  THIS SECTION PINS DOWN CONCENTRATION AT TOP
C146     AI(13,I,J)=AI(17,I,J)
C         IF(COUNT.NE.1.) GO TO 149
C        DO 142 J=1,MJ
C        DO 142 I=1,5
C        A(13,I,J)=A(13,6,J)
C142     AI(13,I,J)=AI(13,6,J)
  149    CONTINUE
         GO TO 147
        IF(COUNT.NE.1.AND.COUNT.NE.480.) GO TO 147
         DO 152 KK=1,6
```

```
 152    CALL OUTPUT(3,MI,MJ,ITHETA,DZ,KK)
       WRITE(6,904)
C      CALL OUTPUT(3,MI,MJ,ITHETA,DZ,4)
       CALL OUTPUT(0,MI,MJ,ITHETA,DZ,11)
C      CALL OUTPUT(0,MI,MJ,ITHETA,DZ,15)
C      CALL OUTPUT(3,MI,MJ,ITHETA,DZ,16)
 147   CONTINUE
C      DO 150 KK=4,5
C150   CALL OUTPUT(3,MI,MJ,ITHETA,DZ,5)
C      DO 155 J=1,MJ
C      DO 154 I=14,17
C154   BARNOX(I,J)=A(1,I,J)
C      A(13,MI,J)=A(13,MIM,J)
C      AI(13,MI,J)=AI(13,MIM,J)
C      DO 155 I=1,5
C      BARNOX(I,J)=A(1,I,J)
C      A(13,I,J)=A(13,6,J)
C      AI(13,I,J)=AI(13,6,J)
 155   CONTINUE
C        DO 156 I=1,MI
C      DO 156 J=1,3
C      A(13,I,J)=A(13,I,4)
C156   AI(13,I,J)=AI(13,I,4)
        DO 157 I=1,MI
        DO 157 J=1,MJM
        AMPNOX(I,J)=A(13,I,J)
 157    PHANOX(I,J)=AI(13,I,J)
        DO 158 I=1,MI
        DO 158 J=1,MJ
        A(13,I,J)=AMPNOX(I,J)*AIR(J)
        AI(13,I,J)=PHANOX(I,J)*AIR(J)
 158    A(6,I,J)=BARNOX(I,J)*AIR(J)
       IF(JFLAG.EQ.1) GO TO 165
       WRITE(6,902) TDAY
       CALL OUTPUT(3,MI,MJ,ITHETA,DZ,6)
C      DO 160 KK=7,10
C160   CALL OUTPUT(2,MI,MJ,ITHETA,DZ,KK)
 165   CONTINUE
C      IF(JFLAG.EQ.1) GO TO 167
C      WRITE(6,901) TDAY
 167   CONTINUE
C      DO 170 KK=11,12
C170   CALL OUTPUT(JFLAG,MI,MJ,ITHETA,DZ,12)
       IF(JFLAG.EQ.1) GO TO 168
       WRITE(6,903) TDAY
 168   CONTINUE
       CALL OUTPUT(JFLAG,MI,MJ,ITHETA,DZ,13)
C      CALL OUTPUT(JFLAG,MI,MJ,ITHETA,DZ,15)
       IF(JFLAG.EQ.1) GO TO 175
       DO 169 I=1,MI
       DO 169 J=1,MJ
 169   A(6,I,J)=A(6,I,J)+A(13,I,J)*COS((270.+AI(13,I,J))*CONV)
```

```
C       CALL OUTPUT(3,MI,MJ,ITHETA,DZ,6)
 175    CONTINUE
C       DO 190 I=1,MI
C190    WRITE(6,990)(PROMEAN(I,J),J=1,MJ)
C       DO 200 I=1,MI
C200    WRITE(6,990)(PROAMP(I,J),J=1,MJ)
C       DO 210 I=1,MI
C210    WRITE(6,990)(PROPHA(I,J),J=1,MJ)
 220    CONTINUE
        MJ=45
 990    FORMAT(8E15.9)
 900    FORMAT(43H NOX FLUX AND TRANSPORT CALCULATIONS,INDEX=,I5,
     1 11H AFTER DAY ,F6.2)
 901    FORMAT(22H NOXPRIME CALCULATIONS,11H AFTER DAY ,F6.2)
 902    FORMAT(18H NOXBAR AFTER DAY ,F6.2)
 903    FORMAT(20H NOXPRIME AFTER DAY ,F6.2)
 904    FORMAT(26H PRODUCTION AND LOSS TERMS)
        RETURN
        END
```

REFERENCES

ANDREWS, D. G., and M. E. MCINTYRE [1976], Planetary waves in horizontal and vertical shear: The generalized Eliassen-Palm relation and the mean zonal acceleration, J. Atmos. Sci., 33, 2031-2048.

ANDREWS, D. G., and M. E. MCINTYRE [1978a], Generalized Eliassen-Palm and Charney-Drazin theorems for waves on axisymmetric mean flows in compressible atmospheres, J. Atmos. Sci., 35, 175-185.

ANDREWS, D. G., and M. E. MCINTYRE [1978b], An exact theory of nonlinear waves on a Lagrangian mean flow, J. Fluid. Mech., 89, 609-646.

AVERY, S. K. [1978], The tropospheric forcing and vertical propagation of stationary planetary waves in the atmosphere, Ph.D. Thesis, Dept. Atmos. Sci., Univ. Ill., Urbana-Champaign.

BAKER, K. D., A. F. NAGY, R O. OLSEN, E. S. ORAN, J. RANDHAWA, D. F. STROBEL, and T. TOHMATSU [1977], Measurement of the nitric oxide altitude distribution in the midlatitude mesosphere, J. Geophys. Res., 82, 3281-3286.

BALSLEY, B. B., and K. S. GAGE [1980], The M.S.T. radar technique: potential for middle atmospheric studies, Pure Appl. Geophys., 118, 452-493.

BARNES, A. A. [1972], Status report on radar meteor wind and density measurements, Bull. Am. Meteor. Soc., 54, 900-910.

BARTH, C. A. [1956a], Nitric oxide in the upper atmosphere, Ann. Geophys., 22, 198-207.

BARTH, C. A. [1966b], Rocket measurement of nitric oxide in the upper atmosphere, Planet. Space Sci., 14, 623-630.

BARTH, C. A., D. W. RUSCH, and A. I. STEWART [1973], The UV nitric-oxide experiment for Atmospheric Explorer, Radio Sci., 8, 379-385.

BATES, J. R. [1977], Dynamics of stationary ultra-long waves in middle latitudes, Quart. J. R. Meteor. Soc., 103, 397-430.

BELMONT, A. D., D. G. DARTT and G. D. NASTROM [1975], Variations of stratospheric zonal winds, 20-65 km, 1961-1971, J. Appl. Met., 14, 585-594.

BOYD, J. P. [1976], The noninteraction of waves with zonally averaged flow on a spherical Earth and the interrelationships of eddy fluxes of energy, heat, and momentum, J. Atmos. Sci., 33, 2285-2291.

BROWN, G. M. and D. C. WILLIAMS [1971], Pressure variations in the stratosphere and ionosphere, J. Atmos. Terr. Phys., 33, 1321-1328.

CAVALIERI, D. J., R. J. DELAND, T. A. POTEMRA, and R. F. GAVIN [1974], The correlation of ULF propagation variations with atmospheric planetary-scale waves, J. Atmos. Terr. Phys., 36, 561-574.

CHARNEY, J. G., and P. G. DRAZIN [1961], Propagation of planetary scale disturbances from the lower into the upper atmosphere, J. Geophys. Res., 66, 83-109.

CHARNEY, J. G., and A. ELIASSEN [1949], A numerical method for predicting the perturbations of the middle latitude westerlies, Tellus, 2, 184-195.

CHRISTIE, A. D. [1970], D region winter anomaly and transport near the mesopause, J. Atmos. Terr. Phys., 32, 35-56.

CLARK, J. and T. ROGERS [1979], The transport of conservative trace gases by planetary waves, J. Atmos. Terr., 35, 2232-2235.

CIRA [1972], Cospar International Reference Atmosphere.

CIRA [1975], Cospar International Reference Atmosphere.

COUNTRYMAN, I. D., and S. A. BOWHILL [1979], Wind and wave observations in the mesosphere using coherent-scatter radar, Aeron. Rep. 89, Aeron.

Lab., Dept. Elec. Eng., Univ. Ill., Urbana-Champaign.

CRAVENS, T. R., and A. I. STEWART [1978], Global morphology of nitric oxide in the lower E region, J. Geophys. Res., 83, 2446-2452.

CRUTZEN, P. J. [1970], The influence of nitrogen oxides on the atmospheric ozone content, Quart J. Roy. Meteor. Soc., 96, 320-325.

CRUTZEN, P. J. [1971] Ozone production rates in an oxygen-hydrogen-nitrogen atmosphere, J. Geophys. Res., 76, 7311-7327.

DELAND, R. J. [1964], Traveling planetary scale waves, Tellus, 16, 271-273.

DELAND, R. J. [1973], Spectral analysis of traveling planetary scale waves: vertical structure in midlatitudes of northern hemisphere, Tellus, 15, 355-373.

DICKINSON, R. E. [1968a], On the exact and approximate linear theory of vertically propagating planetary Rossby waves forced at a spherical lower boundary, Mon. Weather Rev., 96, 405-415.

DICKINSON, R. E. [1968b], Planetary Rossby waves propagating vertically through weak westerly wave guides, J. Atmos. Sci., 25, 984-1002.

DICKINSON, R. E. [1969a], Vertical propagation of planetary Rossby waves through an atmosphere with Newtonian Cooling, J. Geophys. Res., 74, 929-938.

DICKINSON R. E. [1969b], Theory of planetary wave zonal flow interaction, J. Atmos. Sci., 26, 73-81.

DICKINSON R. E. [1973], Method of parameterization for infrared cooling between altitudes of 30 and 70 kilometers, J. Geophys. Res., 78, 4451-4457.

DICKINSON R. E., E. C. RIDLEY and R. G. ROBLE [1977], Meridional circulation in the thermosphere. II. Solstice conditions, J. Atmos. Sci.,

34, 178-192.

DOPPLICK, T. G. [1971], The energetics of the lower stratosphere including radiative effects, Quart. J. Roy Meteor. Soc., 97, 209-237.

DUNKERTON, T. [1978], On the mean neridional mass motions of the stratosphere and mesosphere, J. Atmos. Sci., 35, 2325-2333.

DUNKERTON, T. [1980], A Lagrangian mean theory of wave, mean-flow interaction with applications to nonacceleration and its break down, Rev. Geophys. Space Phys., 18, 387-400.

EBEL, A. [1980], Eddy diffusion models for the mesophere and lower thermosphere, J. Atmos. Terr. Phys., 42, 617-628.

ELIASSEN, E., and B. MACHENHAUER [1969], On the observed large scale atmospheric wave motions, Tellus, 21, 149-165.

ELIASSEN, A, and E. PALM [1961], On the transfer of energy in stationary mountain waves, Geofysiske Publikajnoner, 12, 1-23.

GAGE, K. S. [1981], Wind measurement techniques available for the middle atmosphere program, Middle Atmosphere Program, Handbook for MAP, Vol. 2, S. Avery, Ed., 21-29.

GEISLER, J. E., and DICKINSON, R. E. [1968], Vertical motions and nitric oxide in the upper mesosphere, J. Atmos. Terr. Phys., 30, 1501-1521.

GEISLER, J. E., and DICKINSON, R. E. [1976], The five day wave on a sphere with realistic zonal winds, J. Atmos. Sci., 33, 632-641.

GELLER, M. A., G. C. HESS, and D. WRATT [1976], Simultaneous partial reflection and meteor radar wind observations at Urbana, Illinois, during the winter of 1974-1975, J. Atmos. Terr. Phys., 38, 287-290.

GELLER, M. A., AND C. F. SECRIST, JR. [1971], Coordinated rocket measurements on the D region winter anomaly - II. Same implications, J. Atmos. Terr. Phys., 33, 1027-1040.

GERARD J. C., and D. W. RUSCH [1979], The auroral ionosphere: Comparison of a line dependent model with composition measurements, J. Geophys. Res., 84, 4335-4340.

GILLE, J. C., W. J. KOHRI, and P.L. BAILEY [1977], LRIR observations of planetary wave variations in the stratosphere and mesosphere, Paper presented at IAGA/IAMAP Joint Assembly, Seattle, WA.

GREGORY, J. B. [1965], The influence of atmospheric circulation on mesospheric electron densities in winter, J. Atmos. Sci., 22, 18-23.

GREGORY, J. B., C. E. MEEK, A. H. MANSON, and D. G. STEPHENSON [1979], Developments in the radiowave drifts technique for measurement of high-altitude winds, J. Appl. Meteorol., 18, 682-691.

HARTMANN, D. L., and R. R. GARCIA [1979], A mechanistic model of ozone transport by planetary waves in the stratosphere, J. Atmos. Sci., 36, 350-364.

HESS, G. C., and M. A. GELLER [1978], Urbana meteor radar observations during GRMWSP/CTOP periods, J. Atmos. Terr. Phys., 40, 895-903.

HIROTA, I. [1968], Planetary waves in the upper stratosphere in early 1966, J. Meteor. Soc. Japan 46, 418-430.

HIROTA, I. [1971], Excitation of planetary Rossby waves in the winter stratosphere by periodic forcing, J. Meteor. Soc. Japan 49, 439-449.

HIROTA, I., and J. J. BARNETT [1977], Planetary waves in the winter mesosphere - preliminary analysis of Nimbus 6 PMR results, Quart. J. R. Meteor. Soc., 103, 487-498.

HIROTA, I., and Y. SATO [1969], Periodic variation of the winter stratospheric circulation and intermittent vertical propagation of planetary waves, J. Meteor. Soc. Japan 47, 390-402.

HOLTON, J. R. [1972], An Introduction to Dynamic Meteorology, Academic

Press, Inc.

HOLTON, J. R. [1974], Forcing of mean flows by stationary waves, J. Atmos. Sci., 31, 942-945.

HOLTON, J. R. [1975], The dynamical meteorology of the stratosphere and mesosphere, Meteor. Mon., 37, 216.

HOLTON, J. R. [1976], A semi-spectral numerical model for wave-mean flow interactions in the stratosphere: Application to sudden stratospheric warmings, J. Atmos. Sci., 33, 1639-1649.

HOLTON, J. R. [1980a], The dynamics of sudden stratospheric warmings, Ann. Rev. Earth Planet. Sci., 8, 169-190.

HOLTON, J. R. [1980b], Wave propagation and transport in the middle atmosphere, Phil. Trans. Roy. Soc. London, A 296, 73-85.

HOLTON J. R., and C. MASS [1976], Stratospheric vacillation cycles, J. Atmos. Sci., 33, 2218-2225.

HOLTON, J. R., and W. M. WEHRBEIN [1980a], A numerical model of the zonal mean circulation of the middle atmosphere, Pure Appl. Geophys., 118, 284-306.

HOLTON, J. R., and W. M. WEHRBEIN [1980b], The role of forced planetary waves in annual cycle of the zonal mean circulation of the middle atmosphere, J. Atmos. Sci., 37, 1968-1980.

HUNT, B. G. [1978], Atmospheric vacillations in a general circulation model - II. Tropospheric-stratospheric coupling and stratospheric variability, J. Atmos. Sci., 35, 2052-2067.

JOHNSTON, H. S. [1971], Reduction of stratospheric ozone by nitrogen oxide catalysts from SST exhaust, Science, 173, 517-522.

JONES, W. L., and D. D. HOUGHTON [1971], The coupling of momentum between internal gravity waves and the mean flow: a numerical study, J.

Atmos. Sci., 28, 604-608.

KURZEJA, R. J. [1981], The transport of trace chemicals by planetary waves in the stratosphere, Part 1: Steady waves, J. Atmos. Sci., 38, 2779-2788.

LABITZKE, K. [1977], Interannual variabilities of the winter stratosphere in northern hemisphere, Mon, Weather Rev., 105, 762-770.

LABITZKE, K., K. PETZOLOT, and H. SCHWENTAK [1979], Planetary waves in the strato- and mesosphere during the western European winter anomaly campaign 1975/76 and their relation to ionospheric absorption, J. Atmos. Terr. Phys., 41, 1149-1162.

LEOVY, C. B. [1964], Simple models of thermally driven mesospheric conditions, J. Atmos. Sci., 21, 327-341.

LINDZEN, R., and R. GOODY [1965], Radiative and photochemical processes in mesospheric dynamics: Part 1. Models for radiative and photochemical processes, J. Atmos. Sci., 22, 341-348.

LINDZEN, R. S., and H. L KUO [1969], A reliable method for the numerical solution of a large class of ordinary and partial differentail equations, Mon. Weather Rev., 97, 732-734.

LINDZEN R. S., and D. I. WILL [1973], An analytic formula for heating due to ozone absorption, J. Atmos. Sci., 30, 513-515.

MADDEN, R. A. [1978], Further evidence of traveling planetary waves, J. Atmos. Sci., 35, 1606-1618.

MADDEN, R., and P. JULIAN [1972], Further evidence of global-scale 5-day pressure waves, J. Atmos. Sci., 29, 1464-1469.

MAHLMAN, J. D., and W. J. MOXIM [1978], Tracer simulation using a global general circulation model: Results from a midlatitude instantaneous source experiment, J. Atmos. Sci., 35, 1340-1374.

MANSON, A. M. [1971], The concentration and transport of minor constituents in the mesosphere and lower thermosphere (70-110 km) during periods of anomalous absorption, J. Atmos. Terr. Phys., 33, 715-721.

MATSUNO, T. [1970], Vertical propagation of stationary planetary waves in the winter northern hemisphere, J. Atmos. Sci., 27, 388-393.

MATSUNO, T. [1971], A dynamical model of the stratospheric sudden warming, J. Atmos. Sci., 28, 1479-1494.

MATSUNO, T. [1980], Lagrangian motion of air parcels in the stratosphere in the presence of planetary waves, Pure and Appl. Geophys., 118, 189-216.

MATSUNO, T., and K. NAKAMURA [1979], The Eulerian and Lagrangian-mean meridional circulations in the stratosphere at the time of a sudden warming, J. Atmos. Sci., 36, 640-654.

MCGUIRK, J. P., and E. R. REITER [1976], A vacillation in atmospheric energy parameters, J. Atmos. Sci., 33, 2079-2093.

MCINTYRE, M. E. [1980], An introduction to the generalized Lagrangian-mean description of wave, mean-flow interaction, Pure Appl. Geophys., 118, 152-176.

MEEK, C. E., and A. H. MANSON [1978], Comparisons between time variations in D-region winds and electron densities at Saskatoon, Canada (52°N, 106°W), J. Atmos. Terr. Phys., 40, 1267-1274.

MEIRA, C. G., JR. [1971], Rocket measurements of upper atmospheric nitric oxide and their consequences to the lower ionosphere, J. Geophys. Res., 76, 202-212.

MUENCH, H. S. [1965], On the dynamics of the wintertime stratosphere circulation, J. Atmos. Sci., 22, 349-360.

MURGATROYD, R. J. [1969], The structure and dynamics of the stratosphere,

The Global Circulation of the Atmosphere, G. A. Corby, Ed., London Roy. Meteor. Soc., 159-195.

NASTROM, G. D., B. B. BALSLEY, and D. A. CARTER [1982], Mean meridional winds in the mid- and high-latitude summer mesosphere, Geophys. Res. Lett., 9, 139-142.

OFFERMANN, D. [1979], Recent advances in the study of the D-region winter anomaly, J. Atmos. Terr. Phys., 41, 735-752.

OGAWA, T., and SHIMAZAKI, T. [1975], Diurnal variations of odd nitrogen and ionic densities in the mesosphere and lower thermosphere: simultaneous solution of photochemical-diffusive equations, J. Geophys. Res., 80, 3945-3960.

OORT, A. H., and E. M. RASMUSSON [1971], Atmospheric circulation statistics, NOAA Prof. Paper 5, U. S. Dept. Commerce, Rockville, MD, 1-323.

ORAN, E. S., P. S. JULIENNE, and D. F. STROBEL [1975], The aeronomy of odd nitrogen in the thermosphere, J. Geophys. Res., 80, 3068-3076.

PARK, J. H., and J. LONDON [1974], Ozone photochemistry and radiative heating of the middle atmosphere, J. Atmos. Sci., 31, 1898-1916.

PLUMB, R. A. [1979], Eddy fluxes of conserved quantities by small-amplitude waves, J. Atmos. Sci., 36, 1699-1704.

QUIROZ, R. S., A. J. MILLER, and R. M. NAGATANI [1975], A comparison of observed and simulated properties of sudden stratospheric warmings, J. Atmos. Sci., 32, 1723-1736.

REED, R. J., and K. E. GERMAN [1965], A contribution to the problem of stratospheric diffusion by large-scale mixing, Mon. Weather Rev., 93, 313-321.

REES, M. H., and R. G. ROBLE [1979], The morphology of N and NO in auroral

substorms, Planet. Space Sci., 27, 453-462.

ROBLE, R. G., and J. M. GARY [1979], The effect of horizontal transport on auroral NO densities, Geophys. Res. Lett., 6, 703-706.

ROBLE, R. G., and M. H. REES [1977], Time-dependent studies of the aurora: Effects of particle precipitation on the dynamic morphology of ionospheric and atmospheric properties, Planet. Space Sci., 25, 991-1010.

RODGERS, C. D. [1976], Evidence for the 5-day wave in the upper stratosphere, J. Atmos. Sci., 33, 710-711.

RUSCH, D. W. [1973], Satellite ultraviolet measurements of nitric oxide fluorescence with a diffusive transport model, J. Geophys. Res., 78, 5676-5686.

RUSCH, D. W., and C. A. BARTH [1975], Satellite measurements of nitric oxide in the polar region, J. Geophys. Res., 80, 3719-3721.

RUSCH, D. W., J.-C. GERARD, S. SOLOMON, P. J. CRUTZEN, and G. C. REID [1981], The effect of particle precipitation events on the neutral and ion chemistry of the middle atmosphere, I. Odd nitrogen, Planet. Space Sci., 29, 767-774.

SALTZMAN, B. [1965], On the theory of the winter average perturbations in the troposphere and stratosphere, Mon. Weath. Rev., 93, 195-211.

SATO, Y. [1974], Vertical structure of quasi-stationary planetary waves in several winters, J. Meteor. Soc. Japan, 52, 272-281.

SATO, Y. [1977], Transient planetary waves in the winter stratosphere, J. Meteor. Soc. Japan, 55, 89-105.

SCHOEBERL, M. R. [1978], Stratospheric warmings: Observations and theory, Rev. Geophys. Space Phys., 16, 521-538.

SCHOEBERL, M. R. [1981], A simple model of the Lagrangian-mean flow pro-

duced by dissipating planetary waves, J. Atmos. Sci., 38, 1841-1855.

SCHOEBERL, M. R., and J. CLARK [1980], Resonant planetary waves in a spherical atmosphere, J. Atmos. Sci., 37, 20-28.

SCHOEBERL, M. R., and M. A. GELLER [1976], The propagation of planetary scale waves into the upper atmosphere, Aeron. Rep. No. 70, Dep. Elec. Eng., Univ. Ill., Urbana-Champaign.

SCHOEBERL, M. R., and M. A. GELLER [1977], A calculation of the structure of stationary planetary wvaes in winter, J. Atmos. Sci., 34, 1235-1255.

SCHOEBERL, M. R., and D. F. STROBEL [1978], The zonally averaged circulation of the middle atmosphere, J. Atmos. Sci., 35, 577-591.

SCHWENTEK, H. [1971], Regular and irregular behaviour of the winter anomaly in ionospheric absorption, J. Atmos. Terr. Phys., 33, 1647-1650.

SCHWENTEK, H. [1974], Wave-like structures in the variation of ionospheric absorption, J. Atmos. Terr. Phys., 36, 1173-1178.

SECHRIST, C. F., JR. [1967], A theory of the winter absorption anomaly at middle latitudes, J. Atmos. Terr. Phys., 29, 113-136.

SECHRIST, C. F., JR., E. A. MECHTLY, J. S. SHIRKE, and J.S. THEON [1969], Coordinated rocket measurements on the D-region winter anomaly. I. Experimental results, J. Atmos. Terr. Phys., 31, 145-153.

SMAGORINSKY, J. [1953], The dynamical influence of large scale heat sources and sinks on the quasi-stationary mean motions of the atmosphere, Quart. J. Roy. Meteor. Soc., 79, 342-366.

SOLOMON, S. [1981], One- and two-dimensional photochemical modeling of the chemical interactions in the middle atmosphere, 0-120 km, Cooperative Thesis No. 62, Univ. California and NCAR.

STROBEL, D. F. [1971a], Diurnal variation of nitric oxide in the upper atmosphere, J. Geophys. Res., 76, 2441-2452.

STROBEL, D. F. [1971b], Odd nitrogen in the mesosphere, J. Geophys. Res., 76, 8384-8393.

STROBEL, D. F. [1972], Minor neutral constituents in the mesosphere and lower thermosphere, Radio Sci., 7, 1-21.

STROBEL, D. F., D. M. HUNTEN, and M. B. MCELROY [1970], Production and diffusion of nitric oxide, J. Geophys. Res., 75, 4307-4321.

SWIDER, W., and R. S. NARCISI [1977], Auroral E region: Ion composition and nitric oxide, Planet. Space Sci., 25, 103-116.

TOHMATSU, T., and N. IWAGAMI [1976], Measurement of nitric oxide abundance in the equatorial upper atmosphere, J. Geomag. Geoelec., 28, 343-358.

URYU, M. [1974], Mean zonal flows induced by a vertically propagating Rossby wave packet, J. Meteor. Soc. Japan 52, 481-490.

VAN LOON, H., R. L. JENNE, and K. LABITZKE [1973], Zonal harmonic standing waves, J. Geophys. Res., 78, 4463-4471.

WALTERSCHEID, R. L. [1980], Traveling planetary waves in the stratosphere, Pure Appl. Geophys., 118, 239-260.

WEBSTER, P. J., and J. L. KELLER [1975], Atmospheric variations: vacillations and index cycles, J. Atmos. Sci., 32, 1283-1300.